UNIVERSIDAD NACIONAL DE GENERAL SAN MARTÍN
COMISIÓN NACIONAL DE ENERGÍA ATÓMICA
INSTITUTO DE TECNOLOGÍA
"Prof. Jorge A. Sabato"

Precisión en producción de Higgs en el LHC (*)

por Mg. Ignacio Fabre

Directores

Dr. Daniel de Florian
Dr. Massimiliano Grazzini

(*) Tesis para optar al título de Doctor en Ciencia y Tecnología, mención Física

República Argentina

2020

UNIVERSIDAD NACIONAL DE GENERAL SAN MARTÍN
COMISIÓN NACIONAL DE ENERGÍA ATÓMICA
INSTITUTO DE TECNOLOGÍA
"Prof. Jorge A. Sabato"

Precision in Higgs production at the LHC (*)

Ignacio Fabre

Supervisors

Dr. Daniel de Florian
Dr. Massimiliano Grazzini

(*) Thesis submitted for the degree of Doctor in Science and Technology, Physics

República Argentina

2020

Para Guada.

RESUMEN

A diez años del encendido del LHC, los resultados obtenidos por las colaboraciones de ATLAS y CMS no han mostrado evidencia de física más allá del modelo estándar. A medida que los esfuerzos para encontrar física nueva migran de las búsquedas resonantes hacia los experimentos de precisión, se hacen necesarias predicciones teóricas de mayor precisión. Un interés particular yace en los auto-acoplamientos del bosón de Higgs, ya que estos están directamente ligados al potencial escalar que conduce la ruptura espontánea de simetría electrodébil. En este contexto, el quark top juega un rol importante al ser la partícula fundamental más pesada conocida y aquella con el mayor acoplamiento al bosón de Higgs. El valor del acoplamiento Yukawa del top determina la evolución del auto-acoplamiento del bosón de Higgs y tiene un gran impacto en la sección eficaz de producción de Higgs en colisionadores hadrónicos, donde el principal canal de producción es la fusión de gluones mediada por un quark top virtual.

La forma más directa de acceder al auto-acoplamiento del bosón de Higgs es mediante su producción múltiple. En la primera parte de esta tesis, calcularemos las correcciones de QCD a segundo orden en la constante de acoplamiento fuerte (NNLO) para la producción múltiple de Higgs en la aproximación de top pesado. En el caso de producción de pares de Higgs, extenderemos los resultados ya conocidos al tener en cuenta efectos de nueva física, los cuales son parametrizados por operadores de dimensión seis en el contexto de la teoría efectiva del modelo estándar. Esta es una forma consistente de parametrizar nueva física pesada, siendo a la vez agnóstico a la teoría ultravioleta que la describe. En el caso de producción triple de bosones de Higgs, calcularemos las correcciones de QCD a NNLO para el proceso en el límite de top pesado del modelo estándar, y la combinaremos con la mejor aproximación disponible para los efectos de masa finita del top, obteniendo así nuestra mejor predicción para su sección eficaz.

A diferencia de otras partículas, el decaimiento del bosón de Higgs a pares de tops está cinemáticamente prohibido. Sin embargo, es posible observar directamente el acoplamiento de Yukawa del quark top en la producción asociada de un par de ellos con un bosón de Higgs. En un contexto en que la precisión experimental se acerca a la incerteza teórica actual, necesitamos un formalismo para calcular las correcciones de QCD a NNLO para este proceso. En la segunda parte de esta tesis extenderemos el formalismo de substracción q_T, que ha sido implementado para estados finales sin color y para producción de $t\bar{t}$, al proceso de producción de $t\bar{t}h$. Presentaremos una implementación completa para la sección eficaz a NLO, así como los contratérminos necesarios para cancelar las divergencias infrarrojas a NNLO. Estos resultados abren paso al cálculo completo de correcciones de QCD a NNLO para la producción de $t\bar{t}h$ en colisionadores hadrónicos.

ABSTRACT

About ten years after the start of the LHC the results obtained by the ATLAS and CMS collaborations have not shown evidence of physics beyond the Standard Model (BSM). As the experimental efforts to find BSM physics move from resonant searches to precision measurements, accurate theory predictions are needed. Particular interest lies in the Higgs boson self couplings, as they are directly connected to the scalar potential that drives ElectroWeak Symmetry Breaking. An important role in this context is played by the top quark, which is the heaviest known fundamental particle and the one with the largest coupling with the Higgs boson. The value of the top Yukawa coupling drives the evolution of the Higgs boson self coupling, and has a great impact in the Higgs boson production cross section at hadronic colliders, where the main production channel is gluon fusion mediated by a top-quark loop.

The most direct way to access the Higgs boson self couplings is through multiple Higgs boson production. In the first part of this thesis, we will compute the Next-to-Next-to-Leading Order QCD corrections to its production cross section in the heavy-top approximation. In the case of double Higgs production, we will extend the known NNLO results to the SM cross section to include new physics effects, which are parametrised by six-dimensional operators in the context of the standard model effective field theory. This is a way to consistently parametrise heavy new physics, while being agnostic to the UV complete theory that underlies it. In the case of triple Higgs production, we will compute the NNLO QCD corrections to the SM process in the heavy-top limit, and combine it with the current best approximation to the top-quark mass effects, thus obtaining our best prediction for its cross section.

Unlike other quarks, the decay of a Higgs boson into a pair of top-quarks is kinematically forbidden, but a direct observation of the top-quark Yukawa coupling is possible in the associated production of a top quark pair and a Higgs boson. In a context in which the experimental accuracy is getting closer to the current theory uncertainty, we need a framework to compute the NNLO QCD corrections to this process. In the second part of this thesis we will extend the q_T-subtraction framework, which currently has been implemented for colourless and $t\bar{t}$ final states, to the $t\bar{t}h$ process. We will present a full implementation for the NLO cross section and for the NNLO counter-terms, needed to regulate the divergences appearing in the real emission cross sections. These results pave the way to the full computation of NNLO QCD corrections to $t\bar{t}h$ hadroproduction.

ZUSAMMENFASSUNG

Etwa zehn Jahre nach dem Start des LHC haben die Ergebnisse der ATLAS- und CMS-Kollaborationen keine Hinweise auf Physik jenseits des Standardmodells (BSM) gezeigt. Da die experimentellen Bemühungen, die BSM-Physik zu finden, von der Resonanzsuche zu Präzisionsmessungen übergehen, sind genaue theoretische Vorhersagen erforderlich. Von besonderem Interesse sind die Selbstkopplungen des Higgs-Bosons, da sie direkt mit dem skalaren Potential verbunden sind, das die elektroschwache Symmetriebrechung antreibt. Eine wichtige Rolle spielt in diesem Zusammenhang das Top-Quark, das schwerste bekannte Elementarteilchen und dasjenige mit der größten Kopplung an das Higgs-Boson. Der Wert der Top-Yukawa-Kopplung dominiert die Skalenabhängigkeit der Selbstkopplung des Higgs-Bosons und hat einen großen Einfluss auf den Produktionsquerschnitt des Higgs-Bosons an hadronischen Collidern, wo der Hauptproduktionskanal die durch eine Top-Quark-Schleife vermittelte Gluonenfusion ist.

Der direkteste Weg der Messung der Higgs-Boson-Selbstkopplungen führt über die Produktion mehrerer Higgs-Bosonen. Im ersten Teil dieser Arbeit werden wir die QCD-Korrekturen der nächst-nach-nächsten-führenden (NNLO) Ordnung für ihren Produktionsquerschnitt in der Heavy-Top-Approximation berechnen. Im Falle der doppelten Higgs-Produktion werden wir die bekannten NNLO-Ergebnisse für den SM-Querschnitt erweitern, um neue physikalische Effekte einzubeziehen, die durch sechsdimensionale Operatoren im Kontext des Standardmodells der effektiven Feldtheorie parametrisiert werden. Dies ist eine Möglichkeit, schwere neue Physik konsistent zu parametrisieren und gleichzeitig der ihr zugrundeliegenden vollständigen UV-Theorie gegenüber agnostisch zu sein. Im Falle der dreifachen Higgs-Produktion werden wir die NNLO-QCD-Korrekturen des SM-Prozesses im Heavy-Top-Limit berechnen und mit der derzeit besten Näherung der Top-Quark-Masseneffekte kombinieren, um so unsere beste Vorhersage für seinen Querschnitt zu erhalten.

Im Gegensatz zu anderen Quarks ist der Zerfall eines Higgs-Bosons in ein Paar von Top-Quarks kinematisch verboten, aber eine direkte Beobachtung der Top-Quark-Yukawa-Kopplung ist bei der damit verbundenen Erzeugung eines Top-Quark-Paares und eines Higgs-Bosons möglich. In einem Kontext in dem sich die experimentelle Genauigkeit der aktuellen theoretischen Unsicherheit annähert, brauchen wir einen Rahmen, um die NNLO-QCD-Korrekturen zu diesem Prozess zu berechnen. Im zweiten Teil dieser Arbeit werden wir den q_T-Subtraktionsformalismus, der gegenwärtig für farbneutrale und $t\bar{t}$ Endzustände implementiert wurde, auf den $t\bar{t}h$ Prozess erweitern. Wir werden eine vollständige Implementierung für den NLO Querschnitt und die NNLO Beiträge vorstellen, die erforderlich sind, um die in den realen Emissionsquerschnitten auftretenden Divergen-

zen zu regulieren. Diese Ergebnisse bereiten den Weg zur vollständigen Berechnung der NNLO-QCD-Korrekturen für die $t\bar{t}h$ Hadroproduktion vor.

CONTENTS

1

INTRODUCTION

The standard model of particle physics (SM) represents one of the greatest achievements of the past century. Developed during the 60's, it has since accumulated a number of experimental checks and successful predictions.The SM is a gauge theory that describes the dynamics of 12 spin $\frac{1}{2}$ fermions and their corresponding anti-particles, which are charged under the SM symmetry group $U(1) \times SU(2) \times SU(3)$, and of the spin 1 gauge bosons that mediate the three fundamental forces: The photon for electromagnetism, eight gluons for the strong force and the three massive weak bosons $W^{\pm}$ and Z for the weak force. Because explicit mass terms can't be added to the Lagrangian of the theory without breaking the symmetries of the SM, a mechanism was developed [1–3] to break the $U(1) \times SU(2)$ symmetry of the SM at low energies into the electromagnetic and weak interactions, a process known as Electroweak Symmetry Breaking (EWSB), which also provides masses to the $W^{\pm}$ and Z bosons through an interaction with a new scalar field charged under $U(1) \times SU(2)$. This new field would also generate masses for the fermions through Yukawa interactions, making the SM fully compatible with the experimental observations. Nevertheless, the EWSB mechanism gave a crucial prediction: The excitations of the scalar field would give rise to a new 0-spin particle. After 50 years of experimental search for this particle, now known as the Higgs boson, its discovery was announced in 2012 by the ATLAS and CMS experiments at CERN [4–6].

Despite its overall success, the SM is known to be incomplete as there are a few unresolved issues, such as the mass of neutrinos, the existence of Dark Matter and the hierarchy problem, to name a few. The knowledge of the existence of new physics beyond the SM (BSM) has inspired a number of theories that intend to solve some of these issues, but so far the Large Hadron Collider (LHC) at CERN has found no evidence for such theories, putting bounds on the scales at which they should appear to be above the few TeV. In this scenario of a gap between the scales of the SM and the scales of new physics, differences respect to the SM can only be spotted as small deviations from the SM predictions, making the discovery of BSM physics likely to hide in precision experiments.

Since its discovery in 2012, the experimental community of high energy physics has been devoted to characterise the properties of the Higgs boson, as well as its coupling with other particles and with itself. In the SM, the Higgs self-couplings are uniquely fixed

in the EWSB potential via the preservation of the corresponding gauge symmetries and renormalizability [7, 8], and the Yukawa coupling can be directly inferred from a fermion's mass. Therefore, a direct measurement of these couplings is a non-trivial test of the SM consistency and any deviation found would be a sign of BSM physics. This poses two challenges for the theory community: On one hand, we need to be able to provide precise predictions for these processes, while on the other we need to be able to parametrise the shape of deviations from the SM in a consistent framework. The first of these challenges is being continuously put forward through the computation of perturbative corrections, in particular the current state of the art corresponds to the computation of Next-to-Next-to-Leading order (NNLO) corrections in a perturbative expansion on the power of the strong coupling constant α_s. The second of these challenges, is currently being lead in the context of Effective Field Theories which consists in considering the SM as the renormalizable piece of a low energy effective theory, and any interaction with the heavier BSM degrees of freedom manifests as non-renormalizable operators of higher mass-dimension in the Lagrangian of the theory.

Among the different possibilities to search for deviations of the SM, most of the effort is focused on the top quark and the Higgs boson. These two particles are the heaviest of the SM spectrum, and are intimately related. The top quark, being the most massive particle in the SM, has the largest coupling to the Higgs boson and therefore it drives the evolution of the Higgs boson self-coupling. In this way, the precise value of the Yukawa of the top affects the stability of the EW vacuum, and is possible that it plays a role in the EWSB. The Higgs boson, being a scalar particle, is a good candidate to act as a portal to BSM physics as it would couple to anything charged under the SM $U(1) \times SU(2)$ symmetry group. Its main production channel in the LHC is gluon fusion, mediated by a top-quark loop. In this way, the search for deviations from the SM in the self couplings of the Higgs boson will be intertwined with the Yukawa coupling of the top quark.

We begin this thesis by providing a brief overview on the computation of radiative corrections to processes in hadron colliders, such as the LHC, in chapter 2. In part I we focus on Multiple Higgs production as a direct way to access the Higgs self couplings. In chapter 3 we extend the NNLO computation for double Higgs production in the heavy-top limit of the SM (HTL), to include dimension 6 operators in the context of EFTs. In chapter 4 we switch to the process of triple Higgs production in the SM, we compute the full NNLO cross section in the HTL and then combine it with the current state of the art predictions. Then we move to the part II of this thesis, where we focus on the direct measurement of the Yukawa of the top quark in the associated production of a top-quark pair and a Higgs boson. In this context, we address the extension of the q_T-subtraction framework for the computation of fully differential NNLO cross sections to processes in which a $t\bar{t}$ pair is produced together with a colourless particle. We will present the results of a full implementation at NLO in 7 and the partial results of a NNLO implementation in 8. Then, we will close this thesis by presenting our conclusions in chapter 9.

2

PRECISION PHYSICS AT HADRON COLLIDERS

In this chapter we will review some basic theoretical background regarding the computation of higher order corrections in hadron colliders. In section 2.1 we sketch the procedure of perturbation theory, and present the factorization properties of the amplitudes in the soft and collinear limits. In section 2.2 we refer to hadronic collisions, describing the long and short range factorization in the naive parton model, and how infrared singularities lead to the renormalization of parton distribution functions. Finally, in section 2.3 we describe the FKS method for the computation of NLO QCD corrections of a colourless final state, which we will use in part I of this thesis.

2.1 RADIATIVE CORRECTIONS AND INFRARED DIVERGENCES

The standard procedure to obtain theoretical predictions in Quantum Field Theories, such as a cross section, is to perform a perturbative expansion in powers of the coupling constant. In hadronic colliders, where the hard scattering originates from the collision of two colored partons, the largest contributions come from the QCD corrections, that is from the expansion on the strong coupling constant $\alpha_s = g_S^2/(4\pi)$, as this one is typically about an order of magnitude larger that the fine-structure constant $\alpha = e^2/(4\pi)$[1]. In a generic process of two incoming partons, each with momenta k_1 and k_2, this expansion in α_s can be written as

$$\sigma(k_1,k_1;\{p_i\};\alpha_s) = \alpha_s^k\Big[\sigma^{(LO)}(k_1,k_2;\{p_i\}) + \alpha_s\sigma^{(NLO)}(k_1,k_2;\{p_i\}) + \alpha_s^2\sigma^{(NNLO)}(k_1,k_2;\{p_i\}) + \mathcal{O}(\alpha_s^3)\Big], \tag{2.1}$$

where k is the power of α_s of the first non-vanishing term of the series expansion, and $\{p_i\}$ are the momenta of the final state particles. If the α_s coupling constant is small, the first estimate for the value of the cross-section is given by the Leading Order (LO) cross section

$$\alpha_s^k\sigma^{(LO)}(k_1,k_2;\{p_i\}) = \int_n \mathrm{d}\sigma^B\,, \tag{2.2}$$

1 At the scale of the Z boson mass, $\alpha_s(m_Z) \approx 0.118$ while $\alpha(m_Z) \approx 1/127 \sim 0.008$

where the Born cross section $\mathrm{d}\sigma^B$ is given by the tree level matrix element $\mathcal{M}_n^{(0)}(\{p_i\})$ squared times the phase space measure $\mathrm{d}\Phi_n$ of the n final state particles, a flux factor and a measurement function $\mathcal{J}_n(\{p_i\})$

$$\mathrm{d}\sigma^B = \frac{\mathrm{d}\Phi_n}{2\sqrt{(k_1+k_2)^2}} \left|\mathcal{M}_n^{(0)}(\{p_i\})\right|^2 \mathcal{J}_n(\{p_i\}), \tag{2.3}$$

$$\mathrm{d}\Phi_n = (2\pi)^4\delta^4\left(k_1+k_2-\sum_{i=1}^n p_i\right)\prod_{i=1}^n \frac{\mathrm{d}^4 p_i}{(2\pi)^3}\delta_+(p_i^2). \tag{2.4}$$

The matrix element $\mathcal{M}_n^{(0)}(\{p_i\})$ is computed as usual from the Feynman Rules, while the measurement function $\mathcal{J}_n(\{p_i\})$ defines the observable we want to compute.

While the LO cross section can give us an estimate for the observable, in most cases it only provides a qualitative description. For a reliable calculation, higher order terms of the perturbative expansion have to be taken into account. At Next-To Leading Order (NLO) we find two different kinds of contributions: The virtual corrections which have the same final state as the Born cross section, and the real emissions which contain one more parton in the final state. Explicitly,

$$\begin{aligned}\sigma^{(NLO)}(k_1,k_2;\{p_i\}) &= \int_{n+1}\mathrm{d}\sigma^R + \int_n \mathrm{d}\sigma^V \\ &= \int_{n+1}\frac{\mathrm{d}\Phi_{n+1}}{2\sqrt{(k_1+k_2)^2}}\left|\mathcal{M}_{n+1}^{(0)}\right|^2\mathcal{J}_{n+1} \\ &\quad + \int_n \frac{\mathrm{d}\Phi_n}{2\sqrt{(k_1+k_2)^2}}\left[\mathcal{M}_n^{(1)\dagger}\mathcal{M}_n^{(0)} + \mathcal{M}_n^{(0)\dagger}\mathcal{M}_n^{(1)}\right]\mathcal{J}_n.\end{aligned} \tag{2.5}$$

The virtual amplitude $\mathcal{M}_n^{(1)}$ contains integrals on unconstrained loop momenta ℓ, which lead to ultraviolet (UV) divergences arising from the region where $\ell \to \infty$, as well as infrared (IR) divergences from the soft region where $\ell \to 0$, whenever the propagator carrying the momenta ℓ is massless. The UV divergences can be handled as usual by absorbing them in a redefinition of the fields, couplings and masses. This renormalization leads to a dependence of the physical coupling (as well as the masses the particles involved) on a renormalization scale μ_R. As for the IR singularities, the Kinoshita-Lee-Nauenberg (KLN) theorem [9–11] guarantees that for sufficiently inclusive observables $\mathcal{J}$ they will cancel against analogous terms coming from the real emission contribution $\int_{n+1}\mathrm{d}\sigma^R$ (more details will be given in sec. 2.3).

The real emission amplitude $\mathcal{M}_{n+1}^{(0)}$ is a tree level amplitude which contains one extra unobserved parton in the final state, of momenta p_{n+1}. The integration over the phase space of this parton will generically lead to a singular behaviour whenever it becomes soft ($p_{n+1} \to 0$) or collinear to another parton. To illustrate this, let us consider the emission

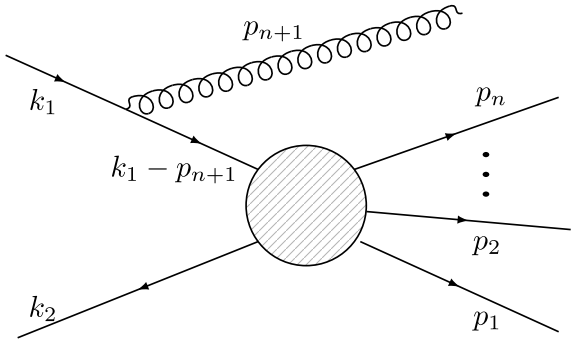

Figure 2.1: Diagram corresponding to the gluon emission of an initial state parton.

of a gluon from an initial leg. The corresponding diagram is shown in Figure 2.1. The emission of such a gluon generates a new propagator in the amplitude of the form

$$\frac{1}{(k_1 - p_{n+1})^2 - m^2} = \frac{-1}{2k_1 \cdot p_{n+1}} = \frac{1}{2|\mathbf{k}_1||\mathbf{p}_{n+1}|(\cos\theta - \sqrt{1 + m^2/|k_1|^2})}, \tag{2.6}$$

where θ is the angle of between the vectors $\mathbf{k}_1$ and $\mathbf{p}_{n+1}$ and m is the mass of the initial leg, $k_1^2 = m^2$. We see that, as we integrate over the phase-space of the emitted gluon, there is a singularity in the region where it becomes soft, $p_{n+1}^0 \to 0$. As we anticipated before, this soft singularity will cancel the IR singularities in the virtual amplitude for a sufficiently inclusive observable. In the case that the emitter is massless, i. e. $k_1^2 = m^2 = 0$, another singularity arises when the two particles become collinear to one another, i. e. $\cos\theta \to 1$. This collinear singularity will also cancel for well defined asymptotic states, and in the case of emission from initial state hadrons it will be absorbed, as we explain section 2.2, in a redefinition of the parton distribution functions.

The structure of real emission amplitudes in the soft and collinear limits is well understood, and it shows some universal factorization properties. In the following subsections we will present the infrared factorization of amplitudes at the lowest order of QCD.

2.1.1 *Factorization in the soft limit*

Let us consider a generic tree-level matrix element $\mathcal{M}_{n+1}^{c_1,\ldots,c_n;c}(p_1,\ldots,p_n;q)$ of n external QCD partons with momenta and colour p_i, c_i, respectively, and a gluon of colour c and momenta q in the limit in which the latter becomes soft, $q \to 0$. We note that neither the emission of a quark nor a gluon attached to an internal offshell line are singular in the soft limit, so we restrict ourselves to consider the gluon as being emitted from the i external line with momenta p_i and colour c_i.

We first consider the case in which the emitter is a final state quark of colour α, that is $c_i = \alpha$. To keep notation clean, we omit the dependence on the momenta and colour of the other particles. The matrix element can be generically written in $D = 4 - 2\varepsilon$ dimensions as

$$\mathcal{M}^{\alpha;c}_{n+1}(p_i;q) = g_S \mu^\epsilon \bar{u}(p_i)(t^c)_{\alpha\beta}\epsilon_\mu(q)\gamma^\mu \frac{\not{p}_i + \not{q}}{(p_i+q)^2}\widetilde{\mathcal{M}}^\beta_n, \tag{2.7}$$

where g_S is the $SU(3)$ coupling ($\alpha_s = g_S^2/(4\pi)$), μ is the dimensional-regularization scale introduced to keep g_S dimensionless, $\bar{u}$ is the Dirac spinor of quark i, t^c is the colour-charge matrix in the fundamental representation of $SU(3)$, $\epsilon_\mu(q)$ is the polarization vector of the emitted gluon, γ^μ are the Dirac matrices in four-vector notation and the Feynman slash notation is used, $\not{p} = p_\mu\gamma^\mu$. $\widetilde{\mathcal{M}}^\beta_n$ is the n-particles matrix element with the on-shell quark i replaced by an off-shell quark, i. e. $M^\beta_n = \bar{u}(p_i)\widetilde{\mathcal{M}}^\beta_n$.

In the $q \to 0$ limit, Eq. (2.7) takes the following form

$$\mathcal{M}^{\alpha;c}_{n+1}(p_i;q) \overset{q\to 0}{\approx} g_S\mu^\epsilon \bar{u}(p_i)(t^c)_{\alpha\beta}\epsilon_\mu(q)\gamma^\mu\frac{\not{p}_i}{2p_i\cdot q}\widetilde{\mathcal{M}}^\beta_n = g_S\mu^\epsilon\epsilon_\mu(q)\left[\frac{p_i^\mu}{p_i\cdot q}\right](t^c)_{\alpha\beta}\mathcal{M}^\beta_n, \tag{2.8}$$

where the Clifford algebra and the Dirac equation for a massless quark $\bar{u}(p_i)\not{p}_i = 0$ were used. We see that the $(n+1)$-particles matrix element factorizes into an onshell n-particles matrix element, contracted with a colour matrix.

The factorization formula (2.8) derived for the gluon emission from a final state quark takes the same form in the case of an initial state anti-quark, while for initial state quarks and final state anti-quarks the analogous expression can be obtained by replacing the colour-charge matrix $(t^c)_{\alpha\beta}$ by the conjugate one $(\bar{t}^c)_{\alpha\beta} = -(t^c)_{\beta\alpha}$.

Let us proceed to the case in which the soft gluon is emitted from an external gluon of colour $c_i = a$. In this case, the matrix element takes the form

$$\mathcal{M}^{a;c}_{n+1}(p_i;q) = \mu^\epsilon\epsilon^\lambda(p_i)\epsilon^\nu(q)\frac{id^\mu_\sigma(p_i+q)}{(p_i+q)^2}V^{abc}_{\mu\nu\lambda}(p+q,-q,-p)\widetilde{\mathcal{M}}^{b,\sigma}_n, \tag{2.9}$$

where $d_{\mu\sigma}(p_i+q)$ is the gluon polarization tensor, and $\widetilde{M}^\sigma_m$ is the n-particles matrix element with the i leg exchanged by an of-shell gluon, analogous to the quark case, that is $\mathcal{M}^a_n = \epsilon_\sigma(p_i)\widetilde{\mathcal{M}}^{a,\sigma}_n$. The tensor $V^{\mu\nu\lambda}$ arises from the gluon triple vertex, and reads

$$V^{abc}_{\mu\nu\lambda} = -g_S f^{abc}\left[g_{\mu\lambda}(2p_i+q)_\nu + g_{\lambda\nu}(q-p_i)_\mu + g_{\mu\nu}(-p_i-2q)_\lambda\right], \tag{2.10}$$

where f^{abc} is the colour-charge matrix in the adjoint representation of $SU(3)$.

In the soft limit, $q \to 0$, Eq. (2.9) simplifies to

$$\mathcal{M}^{a;c}_{n+1}(p_i;q) \overset{q\to 0}{\approx} -g_S\mu^\epsilon f^{abc}\epsilon_\lambda(p_i)\epsilon_\nu(q)\frac{id_{\mu\sigma}(p_i)}{2p_i\cdot q}\left[2g^{\mu\lambda}p_i^\nu - g^{\lambda\nu}p_i^\mu - g^{\mu\nu}p_i^\lambda\right]\widetilde{\mathcal{M}}^{b,\sigma}_n$$

$$= g_S \mu^\epsilon \epsilon_\nu(q) \left[\frac{p_i^\nu}{p_i \cdot q} \right] (i f^{abc}) \mathcal{M}_n^b. \tag{2.11}$$

The simplification from the first to the second line can be easily performed in a physical gauge, where given a light-like four vector n^μ orthogonal to the polarization of the gluon, i. e. $n \cdot \epsilon(p_i) = 0$, the gluon polarization tensor takes the form

$$d^{\mu\nu} = -g^{\mu\nu} + \frac{p_i^\mu n^\nu + n^\mu p_i^\nu}{p_i \cdot n}. \tag{2.12}$$

Equations (2.8) and (2.11) show the factorization of QCD amplitudes in the soft limit, and we see that the only difference between them is in the colour factor. This allow us to write more generally the factorization formula, in terms of operators in colour-space. To this end, we define a colour-basis formed by vectors $|c_1, \ldots, c_n\rangle$[2]. The n-particles amplitude with colours $c_1, \ldots, c_n$, and its squared modulus summed over colour and spin configurations, can then be written as

$$\mathcal{M}_n^{c_1,\ldots,c_n}(p_1, \ldots, p_n) = \langle c_1, \ldots, c_n | \, \mathcal{M}(p_1, \ldots, p_n) \rangle \,, \tag{2.13}$$

$$|\mathcal{M}_n(p_1, \ldots, p_n)|^2 = \langle \mathcal{M}(p_1, \ldots, p_n) | \, \mathcal{M}(p_1, \ldots, p_n) \rangle \,. \tag{2.14}$$

Next, we define the colour operator $\mathbf{T}_i$ associated with the soft emission of a gluon of colour a from leg i as

$$\mathbf{T}_i = \langle a | \, T_i^a, \tag{2.15}$$

which acts into colour-space vectors as

$$\langle b_1, \ldots, b_n | \, \mathbf{T}_i \, | c_1, \ldots, c_n, a \rangle = \delta_{b_1 c_1} \ldots (T_i^a)_{b_i c_i} \ldots \delta_{b_n, c_n}, \tag{2.16}$$

$$(T_i^a)_{bc} = \begin{cases} (t^c)_{bc} & \text{if leg } i \text{ is a final-state quark or initial-state anti-quark,} \\ -(t^c)_{cb} & \text{if leg } i \text{ is a final-state anti-quark or initial-state quark,} \\ i f^{bac} & \text{if leg } i \text{ is a gluon.} \end{cases} \tag{2.17}$$

Some properties of the colour operator $\mathbf{T}_i$ are

$$\sum_{i=1}^{n} \mathbf{T}_i \, |\mathcal{M}(p_1, \ldots, p_n)\rangle = 0, \tag{2.18}$$

$$\mathbf{T}_i \cdot \mathbf{T}_j = \mathbf{T}_j \cdot \mathbf{T}_i = T_i^a T_j^a, \tag{2.19}$$

$$\mathbf{T}_i \cdot \mathbf{T}_i = C_i = \begin{cases} C_A & \text{if leg } i \text{ is a quark or anti-quark,} \\ C_A & \text{if leg } i \text{ is a gluon,} \end{cases} \tag{2.20}$$

2 The colour basis is defined in the same way as in Ref. [12].

where the first identity follows from colour conservation and the fact that the vector $|\mathcal{M}(p_1,\dots,p_n)\rangle$ is by definition a colour-singlet, and in the last equation we introduce the Casimir invariants of $SU(3)$: $C_A = N_c = 3$ being the number of colours, and $C_F = T_F(N_c^2-1)/N_c = 4/3$.

Now, we can write equations (2.8) and (2.11) in a single line

$$\langle a|\,\mathcal{M}(p_1,\dots,p_n;q)\rangle \overset{q\to 0}{\approx} g_S\mu^\epsilon \epsilon_\mu(q)\mathbf{J}^\mu(q)\,|\mathcal{M}(p_1,\dots,p_n)\rangle\,, \tag{2.21}$$

where the tree-level eikonal current $\mathbf{J}^\mu$ is given by

$$\mathbf{J}^\mu(q) = \sum_{i=1}^{n} \mathbf{T}_i \frac{p_i^\mu}{p_i\cdot q}. \tag{2.22}$$

Due to colour-conservation, the eikonal-current is conserved: $q_\mu \mathbf{J}^\mu\,|\mathcal{M}(p_1,\dots,p_n;q)\rangle = 0$, which also implies that Eq. (2.22) is gauge invariant.

With these expressions, we can also write the factorization equation for the amplitude squared (summed over colours and gluon polarizations):

$$|M(p_1,\dots,p_n;q)|^2 \overset{q\to 0}{\approx} -g_S^2\mu^{2\epsilon}\,2\sum_{i,j=1}^{n}\mathcal{S}_{ij}(q)\left|M_{(ij)}(p_1,\dots,p_n)\right|^2, \tag{2.23}$$

where we defined the eikonal function $\mathcal{S}_{ij}$ and the squared colour-correlated tree-level amplitude $\mathcal{M}_{(ij)}$ as

$$\mathcal{S}_{(ij)}(q) = \frac{p_i\cdot p_j}{2(p_i\cdot q)(p_j\cdot q)}, \tag{2.24}$$

$$\left|M_{(ij)}(p_1,\dots,p_n)\right|^2 = \langle M(p_1,\dots,p_n)|\,\mathbf{T}_i\cdot\mathbf{T}_j\,|M(p_1,\dots,p_n)\rangle\,. \tag{2.25}$$

2.1.2 *Factorization in the collinear limit*

Let us consider now the collinear limit of a n-particles tree level amplitude

$$\mathcal{M}^{c_1,\dots,c_n;s_1,\dots,s_n}_{a_1,\dots,a_n}(p_1,\dots,p_n), \tag{2.26}$$

where c_i, s_i and a_i label the colour, spin and flavour of the external particle i with momenta p_i. Without loss of generality, let us call p_1 and p_2 the partons that become collinear to one another, so that in the collinear limit $p_1 \parallel p_2$. To formally define such limit, we parametrise the momenta as follows

$$\begin{aligned} p_1^\mu &= z p^\mu + k_\perp^\mu - \frac{k_\perp^2}{z}\frac{n^\mu}{2p\cdot n}, \\ p_2^\mu &= (1-z)p^\mu - k_\perp^\mu - \frac{k_\perp^2}{1-z}\frac{n^\mu}{2p\cdot n}, \end{aligned} \tag{2.27}$$

where we used a light-like vector p^μ to indicate the collinear direction, n^μ is an auxiliary light-like vector which specifies the plane in which the collinear limit is approached, and $k_\perp^\mu$ is a vector perpendicular to p^μ and n^μ such that the collinear limit corresponds to $k_\perp^\mu \to 0$. To see this, we can note that

$$2p_1 \cdot p_2 = -\frac{k_\perp^2}{z(1-z)}, \tag{2.28}$$

so that $k_\perp^2 \to 0$ corresponds to $p_1 \cdot p_2 \to 0$.

The squared amplitude, summed over colours and polarizations, factorizes in the following way in the limit $k_\perp^2 \to 0$:

$$|\mathcal{M}_{a_1,\dots,a_n}(p_1,\dots,p_n)|^2 \xrightarrow{k_\perp^2 \to 0} \frac{g_S^2 \mu^{2\varepsilon}}{p_1 \cdot p_2} \hat{P}^{ss'}_{a_1 a_2}(z, k_\perp; \varepsilon) \mathcal{T}^{ss'}_{a,\dots,a_n}((p_1+p_2),\dots,p_n), \tag{2.29}$$

where g_S is the d-dimensional strong coupling and the spin-polarization tensor is defined as

$$\mathcal{T}^{s_1 s_1'}_{a_1,a_2,\dots,a_n} = \sum_{s_2,\dots,s_n} \sum_{c_1,c_2,\dots,c_n} \mathcal{M}^{c_1,\dots,c_n;s_1,\dots,s_n}_{a_1,\dots,a_n} \left(\mathcal{M}^{c_1,\dots,c_n;s_1',\dots,s_n}_{a_1,\dots,a_n}\right)^\dagger, \tag{2.30}$$

and it enters the expression with the legs 1 and 2 replaced by a new leg $(1+2)$ with momenta (p_1+p_2) and flavour $a = (a_1 + a_2)$ according to the rule *quark + antiquark = gluon*, *gluon + anything = anything*.

The kernel $P^{ss'}_{a_1 a_2}(z, k_\perp; \varepsilon)$ is the d-dimensional spin dependent Altarelli-Parisi splitting function, in $d = 4 - 2\varepsilon$. Its expression for the different channels is given by [13]

$$\hat{P}^{ss'}_{qg}(z, k_\perp; \varepsilon) = \hat{P}^{ss'}_{\bar{q}g}(z, k_\perp; \varepsilon) = \delta_{ss'} C_F \left[\frac{1+z^2}{1-z} - \varepsilon(1-z)\right], \tag{2.31}$$

$$\hat{P}^{ss'}_{gq}(z, k_\perp; \varepsilon) = \hat{P}^{ss'}_{g\bar{q}}(z, k_\perp; \varepsilon) = \delta_{ss'} C_F \left[\frac{1+(1-z)^2}{z} - \varepsilon z\right], \tag{2.32}$$

$$\hat{P}^{\mu\nu}_{q\bar{q}}(z, k_\perp; \varepsilon) = \hat{P}^{\mu\nu}_{\bar{q}q}(z, k_\perp; \varepsilon) = T_R \left[-g^{\mu\nu} + 4z(1-z)\frac{k_\perp^\mu k_\perp^\nu}{k_\perp^2}\right], \tag{2.33}$$

$$\hat{P}^{\mu\nu}_{gg}(z, k_\perp; \varepsilon) = 2C_A \left[-g^{\mu\nu}\left(\frac{z}{1-z} + \frac{1-z}{z}\right) - 2(1-\varepsilon)z(1-z)\frac{k_\perp^\mu k_\perp^\nu}{k_\perp^2}\right]. \tag{2.34}$$

These kernels are matrices in the spin space of particle a, which for the case of $a \neq$ gluon turn out to be proportional to the identity due to helicity conservation of the quark-gluon vertex. For the case of $a =$gluon, the spin indices s, s' are Lorentz indices μ, ν which lead to spin-correlations that make impossible to factorize the spin averaged amplitude $\mathcal{M}_{a,\dots,a_n}(p,\dots,p_n)$ from Eq. (2.29).

The spin average of the kernels $\hat{P}^{ss'}_{a_1 a_2}$ in (2.29) (which corresponds to contract them with $\delta_{ss'}/2$ for the case of $a \neq$ gluon and $-g_{\mu\nu}/2$ for the case of $a =$gluon) provides the regular

part of the unpolarized Altarelli-Parisi splitting kernels $P^{(1)}_{a_1 a}$[3] at leading order in α_s, which drive the LO evolution of the hadronic structure functions, as we will see in section 2.2. The corresponding expressions for them are [13]

$$P^{(1)}_{qq}(z) = C_F \left[\frac{1+z^2}{1-z}\right]_+, \tag{2.35}$$

$$P^{(1)}_{qg}(z) = T_R \left[z^2 + (1-z)^2\right], \tag{2.36}$$

$$P^{(1)}_{gq}(z) = C_F \left[\frac{1+(1-z)^2}{z}\right], \tag{2.37}$$

$$P^{(1)}_{gg}(z) = 2C_A \left[\frac{z}{(1-z)_+ + \frac{1-z}{z} + z(1-z)}\right] + \delta(1-z)\beta_0, \tag{2.38}$$

where β_0 is the first coefficient of the perturbative expansion of the QCD beta function, which will be defined in Eq.(2.41) of the next section, and the following definition for the *plus* prescription is used:

$$\int_0^1 \mathrm{d}z\, f(z) g(z)_+ = \int_0^1 (f(z) - f(1)) g(z), \tag{2.39}$$

for any given function $f(z)$ that is regular at $z = 1$. The *plus* prescription makes these functions regular upon integration in z and it is originated, as well as the one in the delta term in P_{gg}, from the cancellation with IR singularities in the virtual amplitude (located at $z = 1$).

2.2 HADRONIC COLLISIONS

The theory of QCD that describes the strong force between quarks and gluons has a number of important properties. The first one we will mention is *colour confinement*, which means that at low energies the interaction is so strong that all coloured particles will form colour-singlet bound states, known as *hadrons*. A direct consequence of colour confinement is that the asymptotic states of the theory at low energies are no longer quarks and gluons, but hadrons instead. Another important property is that QCD is *asymptotically free*, which refers to the fact that at high energies the strong coupling constant becomes small, and the individual quark and gluons that compose the hadron, that we will call *partons*, can be treated as if they were free. This also implies that at high energies, we can rely on perturbation theory to compute observables.

One of the consequences of asymptotic freedom can be observed in the running behaviour of the strong coupling constant with the energy scale. To compute this, one

3 Note the difference in the labeling of flavours, the splitting kernels label the *parent* flavour $a = a_1 + a_2$ instead of a_2.

has to consider loop-corrections to the vertex interactions and, after performing the UV-renormalization of the charge, one gets a relation between the value of the strong coupling α_s at the energy scale of the process Q^2 and a reference scale μ_0. At LO, it reads

$$\alpha_s(Q^2) = \frac{\alpha_s(\mu_0^2)}{1 + \alpha_s(\mu_0^2)\frac{\beta_0}{\pi}\ln(Q^2/\mu_0^2)}, \tag{2.40}$$

where the QCD β function and the first coefficients of its perturbative expansion are

$$\beta(\alpha_s(Q^2)) = \frac{\mathrm{d}\ln\alpha_s(Q^2)}{\mathrm{d}\ln Q^2} = -\sum_{n=0}^{\infty}\left(\frac{\alpha_s}{\pi}\right)^{n+1}\beta_n, \tag{2.41}$$

$$\beta_0 = \frac{11C_A - 2n_f}{12}, \qquad \beta_1 = \frac{1}{24}\left(17C_A^2 - 5C_A n_f - 3C_F n_f\right), \tag{2.42}$$

and n_f is the number of active light quark flavours in the theory.

As we can see from Eq. (2.40), $\alpha_s(Q^2) \xrightarrow{Q^2\to\infty} 0$ allowing for a perturbative expansion at high energies, while for $Q^2 \to \mu_0^2 e^{-\pi/(\beta_0\alpha_s(\mu_0^2))} \sim \Lambda_{QCD}$ the formula predicts the divergent behaviour $\alpha_s(Q^2) \to \infty$. Of course, the calculation performed at LO is not reliable for low values of Q^2, for which $\alpha_s(Q^2) \sim 1$, as perturbation theory breaks down and the non-perturbative phenomenon of *hadronization* takes place. The scale at which this transition happens can be estimated from Eq. (2.40) using any measurement of $\alpha_s(\mu_0)$ at a reference scale μ_0, and its order of magnitude is found to be around $\Lambda_{QCD} \sim 200$ MeV.

Let us consider the collision between two hadrons in a high energy experiment. The running behaviour of the strong coupling in Eq.(2.40) allows us to distinguish between two regimes: On one hand, there is a long distance (low energy) regime, in which two hadrons collide towards each other, and on the other hand there is a short range (high energy) interaction between the constituents of the two hadrons, the *partons*. While the former is governed by non-perturbative physics, the latter is tractable in perturbation theory. To compute a given observable in the collision of two hadrons h_1 and h_2 with momenta P_1 and P_2 respectively, the *naive parton model* proposes to factorize the cross section $\sigma_{h_1h_2\to F}$, characterised by a hard scale Q, in the following way

$$\sigma_{h_1h_2}(P_1,P_2) = \sum_{a_1,a_2}\iint_0^1 \mathrm{d}x_1\,\mathrm{d}x_1\, f_{a_1/h_1}(x_1) f_{a_2/h_2}(x_2)\,\hat{\sigma}_{a_1a_2}(x_1P_1, x_2P_2) + \mathcal{O}\left(\frac{\Lambda_{QCD}}{Q}\right)^p, \tag{2.43}$$

where the sum runs over all possible parton flavours a_1 and a_2, the *parton distribution function* (PDF) $f_{a/h}(x)$ represents the probability density of finding a parton inside h with flavour a and momentum fraction x, $\hat{\sigma}_{a_1a_2}$ is the *partonic* cross section for the collision of partons a_1 and a_2, and p is an integer which depends on the process and the observable (e. g. $p = 2$ for inclusive Drell-Yan production). While the partonic cross section encodes all the short-distance interactions and is therefore computable in perturbation theory, the

PDFs encode all the long-distance behaviour, are process independent and have to be fitted from experimental data. The last term in Eq. (2.43) represents all the non-factorizable effects due to process-dependent non-perturbative physics, which are parametrised by the quotient of the scales Λ_{QCD}, at which non-perturbative effects take place, and Q, which characterises the hard process and is typically of the same order of magnitude as the centre of mass energy of the partonic system $Q^2 \sim (x_1 P_1 + x_2 P_2)^2$.

2.2.1 *Evolution of parton distribution functions*

While the naive parton model works perfectly for Leading Order calculations, it breaks down as one tries to include radiative corrections. As discussed in the previous section 2.1, when we compute the partonic cross section $\hat{\sigma}_{a_1 a_2}$ at higher orders in perturbation theory we have to include virtual corrections to the born configuration as well as real emission radiation corrections where an extra parton b is emitted. The KLN theorem guarantees that for sufficiently inclusive observables, the IR singularities arising in the virtual corrections (after regularization of UV divergences through the renormalization procedure at a renormalization scale μ_R) will cancel against the soft singularities described by Eq. (2.22). Nevertheless, there are still remaining singularities in the real emission amplitudes when the parton b becomes collinear with the one of the initial partons a_1 or a_2, as described by Eq. (2.29). Because the physical cross section $\sigma_{h_1 h_2 \to F}$ is finite, all remaining singularities in $\hat{\sigma}_{a_1 a_2 \to F}$ have to cancel order by order in perturbation theory with analogous factors coming from the $f_{a/h}$ functions.

The physical origin of this can be interpreted as follows: The collinear emission of a parton b with momentum fraction z from an initial leg a can be considered either as a real emission correction to the hard process, or as a correction to the PDF itself where, instead of finding in the hadron a parton a with momentum fraction x, we find a parton b with momentum fraction $\xi = zx$ (see Figure 2.2). The separation between the two cases induces the introduction of a technical *factorization scale* μ_F.

Thanks to the factorization properties of collinear amplitudes, we can formally redefine our cross section to be of the form

$$\hat{\sigma}_{a_1 a_2 \to F}(p_1, p_2) = \sum_{b_1, b_2} \iint_0^1 \bar{\sigma}_{b_1 b_2 \to F}(z_1 p_1, z_2 p_2; \mu_F) \Gamma_{b_1 a_1}(z_1; \mu_F) \Gamma_{b_2 a_2}(z_2; \mu_F) \mathrm{d}z_1 \, \mathrm{d}z_2 \,, \tag{2.44}$$

where the factorized partonic cross section $\bar{\sigma}_{b_1 b_2 \to F}$ is finite, while transition functions $\Gamma_{ba}(z)$ characterize the collinear emission process of partons carrying a momentum fraction of $(1 - z)$. This way, all singular terms are absorbed in the transition functions. Next, we can redefine our PDFs in the following way

$$\bar{f}_{b/h}(\xi; \mu_F) = \sum_a \iint_0^1 \mathrm{d}x \, \mathrm{d}z \, f_{a/h}(x) \Gamma_{ba}(z) (\xi - xz) = \int_\xi^1 \frac{\mathrm{d}z}{z} f_{a/h}\left(\frac{\xi}{z}\right) \Gamma_{ba}(z; \mu_F)$$

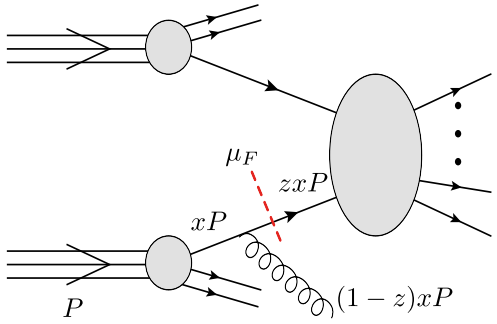

(a) The collinear emission as a correction to the PDF

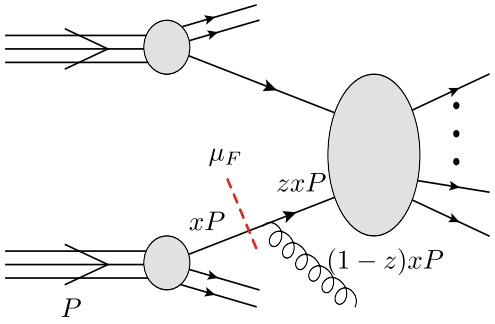

(b) The collinear emission as a real emission correction to the hard process

Figure 2.2: Diagram corresponding to the collinear emission of gluon from an initial state parton. Depending on the factorization scale μ_F, the process can be considered a correction to the PDF or as a real emission correction of the hard process.

$$= (f_{a/h} \otimes \Gamma_{ba})(\xi), \tag{2.45}$$

where the symbol $\otimes$ denotes a convolution, such that the hadronic cross section takes the simple form

$$\sigma_{h_1h_2}(P_1, P_2) = \sum_{a_1,a_2} \int\int_0^1 \mathrm{d}x_1\, \mathrm{d}x_1\, \bar{f}_{a_1/h_1}(x_1;\mu_F) f_{a_2/h_2}(x_2;\mu_F)\; \bar{\sigma}_{a_1a_2}(x_1P_1, x_2P_2;\mu_F). \tag{2.46}$$

The transition functions are computable order by order in perturbation theory, and using the results of the previous section, in particular of Eq.(2.29), we can compute them at NLO using dimensional regularization in the $\overline{MS}$ scheme, and they read

$$\Gamma_{ab}(z) = \delta_{ab}\delta(1-z) - \frac{1}{\varepsilon}\frac{\alpha_s}{2\pi}P^{(1)}_{ab}(z) + \mathcal{O}(\alpha_s^2), \tag{2.47}$$

where we the first order AP splitting kernel $P^{(1)}_{ab}(z)$ was defined in Eqs.(2.35) - (2.38).

If we expand Eq.(2.44) in powers of $\alpha_s/(2\pi)$, we can invert the relation:

$$\bar{\sigma}^{(0)}_{a_1a_2\to F}(p_1,p_2) = \hat{\sigma}^{(0)}_{b_1b_2\to F}(p_1,p_2;\mu_F) \tag{2.48}$$

$$\bar{\sigma}^{(1)}_{a_1a_2\to F}(p_1,p_2) = \hat{\sigma}^{(1)}_{a_1a_2\to F}(p_1,p_2) + \sigma^{(ct+)} + \sigma^{(ct-)}, \tag{2.49}$$

with

$$\sigma^{(ct+)} = \frac{1}{\varepsilon}\sum_b \int_0^1 \mathrm{d}z\, \hat{\sigma}^{(0)}_{ba_2\to F}(zp_1,p_2)P^{(1)}_{ba_1}(z), \tag{2.50}$$

$$\sigma^{(ct-)} = \frac{1}{\varepsilon} \sum_b \int_0^1 \mathrm{d}z\, \hat{\sigma}^{(0)}_{a_1 b \to F}(p_1, z p_2) P^{(1)}_{b a_2}(z). \tag{2.51}$$

We see that the finite NLO factorized cross section can be found in terms of the partonic cross section through the inclusion of counter terms $\sigma^{(ct\pm)}$ which are proportional to the LO partonic cross section, with legs convoluted with the unpolarized AP kernel. For simplicity, in the following chapters of this work we will loose the overline and just denote the factorized partonic cross section $\bar{\sigma}$ as $\hat{\sigma}$.

2.3 THE FKS METHOD FOR THE COMPUTATION OF NLO CORRECTIONS

As we have seen in section 2.1, radiative corrections introduce several IR divergences which, although they all cancel among each other, make the calculation intractable for a numerical computation. In order to automatize the numerical integration of phase space integrals, that could work for a general observable $\mathcal{J}$, one has to perform analytical manipulations to explicitly cancel all IR divergences and achieve the finite result as a sum of finite integrals, which can then be handled numerically.

In this section we will sketch a general method developed by Frixione, Kunszt and Signer [14, 15], generally known as FKS, to handle IR divergences appearing in NLO calculations. We will present a simplified description which only considers the case of colourless final states. This will be later used for the calculations in part I of this thesis.

Let us consider the process $h_1 + h_2 \to F + X$, which denotes the inclusive production of a colourless massive final state F composed of n particles, whose momenta we generally denote by Φ_n. In general, we will be interested in the expectation value of some observable $\mathcal{J}$. The formal expression of the LO contribution can be written as

$$\langle \mathcal{J} \rangle_{\mathrm{LO}} = \sum_{a_1, a_2} \int_0^1 \mathrm{d}x_1\, \mathrm{d}x_2\, f_{a_1/h_1}(x_1) f_{a_2/h_2}(x_2) \int \mathrm{d}\Phi_n\, \mathcal{J}_n(\Phi_n) \mathcal{B}(\Phi_n), \tag{2.52}$$

where $\mathcal{B}$ is the squared renormalized Born amplitude of $a_1 + a_2 \to F$, including all flux, colour, and statistical factors. Special cases for the observable are $\mathcal{J}_n = 1$, that corresponds to the inclusive cross-section, and $\mathcal{J}_n = \delta(\Phi_n - \Phi_{n,0})$ which provides the fully differential cross section in the phase-space point $\Phi_{n,0}$.

When computing radiative corrections at NLO we have to consider virtual corrections $\mathcal{V}$ and real-emission corrections $\mathcal{R}$. $\mathcal{V}$ corresponds to the interference between one-loop and the born renormalized amplitudes and therefore is defined in the same phase-space volume as $\mathcal{B}$, Φ_n. On the other hand, $\mathcal{R}$ corresponds to the squared tree-level renormalized amplitude of the production of the final state F plus an unobserved coloured particle, and therefore is defined in the phase-space domain of $n+1$ particles, Φ_{n+1}. The expression for the NLO correction to the expectation value of our observable $\mathcal{J}$ is given by

$$\langle \mathcal{J} \rangle_{\text{NLO}} = \sum_{a_1,a_2} \int_0^1 \mathrm{d}x_1\, \mathrm{d}x_2\, f_{a_1/H_1}(x_1) f_{a_2/H_2}(x_2) \left[\int \mathrm{d}\Phi_n\, \mathcal{J}_n(\Phi_n)\, (\mathcal{B}(\Phi_n) + \mathcal{V}(\Phi_n)) + \int \mathrm{d}\Phi_{n+1}\, \mathcal{J}_{n+1} \mathcal{R}(\Phi_{n+1}) \right]. \tag{2.53}$$

The two terms of this expression will, in general, be independently divergent in four dimensions. For the real-emission amplitude, this divergences are located in the phase-space region where the the emitted particle becomes unresolved. If we label this particle i and its momentum p_i, the particle will become unresolved when $p_i \to 0$ (*soft* region) or when the particle i becomes collinear, and therefore indistinguishable, to some other particles momentum p_j, i. e. $p_i \parallel p_j$ and therefore indistinguishable from j (*collinear* region). In the case that we're considering, $a_1 + a_2 \to F + X$ with F colourless, the unresolved emission can only be originated from one of the initial particles a_1 or a_2. As seen in section 2.2, initial particles can only be found in nature as partons inside hadronic bound states, which means that the singular behaviour in $\mathcal{R}$ due to the collinear emission of initial state legs is regulated with the counter-terms introduced in (2.49). All remaining divergences that appear when integrating $\mathcal{R}$ are of soft origin and cancel the IR singular terms in $\mathcal{V}$, making the final result finite.

According to the KLN theorem, soft divergences in $\mathcal{R}$ and IR divergences in $\mathcal{V}$ cancel out, making the expectation value $< \mathcal{J} >$ finite, whenever the observable $\mathcal{J}$ under consideration is *sufficiently inclusive* or *infrared-safe*. What this means is that $\mathcal{J}_{n+1}(\Phi_{n+1})$ reduces to $\mathcal{J}_n(\tilde{\Phi}_n)$ in the unresolved regions. Here $\tilde{\Phi}_n$ is a mapping of the Φ_{n+1} kinematics into the LO one, which is defined as

$$\mathcal{J}_{n+1}(\dots, p_{i-1}, p_i, p_{i+1}, \dots) \xrightarrow{p_i \to 0} \mathcal{J}_n(\dots, p_{i-1}, p_{i+1}, \dots) \tag{2.54}$$

$$\mathcal{J}_{n+1}(\dots, p_i, p_j, \dots) \xrightarrow{p_i \parallel p_j} \mathcal{J}_n(\dots, p_i + p_j, \dots). \tag{2.55}$$

When considering a NLO calculation, any such infrared-safe observable will have to be independent of the momentum of the emitted particle, and therefore we will be most interested in computing the cross section fully differential in Φ_n, as this can be afterwards convoluted with any $\mathcal{J}$ such that $\mathcal{J}_{n+1}(\Phi_{n+1}) = \mathcal{J}_n(\Phi_n)$. For the purpose of this section, we will restrict ourselves to the differential cross section

$$\mathrm{d}\sigma_{H_1,H_2} = \sum_{\substack{a_1 \in H_1 \\ a_2 \in H_2}} \int_0^1 \mathrm{d}x_1\, \mathrm{d}x_2\, f_{a_1/H_1}(x_1) f_{a_2/H_2}(x_2) \mathrm{d}\hat{\sigma}_{a_1,a_2}\,, \tag{2.56}$$

$$\mathrm{d}\hat{\sigma}_{a_1,a_2} = \mathrm{d}\Phi_n\, [\mathcal{B} + \mathcal{V}] + \int_1 \mathrm{d}\Phi_{n+1}\, \mathcal{R}, \tag{2.57}$$

where the last integral is over the phase space of the extra emitted particle, and we don't integrate over the n-particle phase space Φ_n.

The FKS method allow us to compute this quantity in four dimensions, providing a way to make the convolutions with generic observables numerically. This is achieved by dividing the NLO phase $\mathrm{d}\Phi_{n+1}$ into non-singular regions, which can be evaluated in four-dimensions, and singular regions, which are then analytically cancelled. Let us show how this works:

The first thing to do is to divide the phase-space into different non-overlapping regions that contain at most one particle becoming unresolved or two particles becoming collinear. In the case of a colourless final state, the emitted parton can only become collinear to the initial partons, which are colliding. Therefore, the two singular regions are naturally separated.

Let us label the initial partons momentum as p_1 and p_2, and the one of the emitted particle as k. Without loss of generality, we put our reference system in the partonic centre of mass frame and parametrize these momenta as

$$p_1^\mu = \frac{\sqrt{\hat{s}}}{2}(1,0,0,1) \tag{2.58}$$

$$p_2^\mu = \frac{\sqrt{\hat{s}}}{2}(1,0,0,-1) \tag{2.59}$$

$$k^\mu = \xi\frac{\sqrt{\hat{s}}}{2}(1,\sqrt{1-y^2}\epsilon_T^{(D-2)},y), \tag{2.60}$$

where $\hat{s}$ is the squared partonic centre of mass energy, ξ is it's fraction taken by the emitted particle, $y \in [-1,1]$ and $\epsilon_T^{(D-2)}$ is the $(D-2)$ dimensional unit vector pointing in the direction of momentum transversal to $p_{1,2}$. If the final-state system is composed of massive particles such that $m_F^2 = \sum_{i\in F} m_i^2 \neq 0$ then ξ is bounded to be in the range $\xi \in \left[0,(1-m_F^2/\hat{s})\right]$.

With this parametrization, we see that in the limit $y \to \pm 1$ the emitted particle becomes collinear to either p_1 or p_2, and that the soft limit of vanishing k is mapped to $\xi \to 0$. Let us proceed to the decomposition of the NLO phase space

$$\mathrm{d}\Phi_{n+1} = \frac{\mathrm{d}^{D-1}k}{2k_0(2\pi)^{D-1}}\,\mathrm{d}\widetilde{\Phi}_n\,, \tag{2.61}$$

where $k_0 = \xi\frac{\sqrt{\hat{s}}}{2}$ is the energy of the emitted particle, and $\mathrm{d}\widetilde{\Phi}_n$ is the n-particles phase space measure in the boosted frame $p_1+p_2 \to p_1+p_2-k$, that is

$$\mathrm{d}\widetilde{\Phi}_n = (2\pi)^4\delta^4\left((p_1+p_2-k)-\sum_{i\geq 3}p_i\right)\prod_{i\geq 3}\frac{\mathrm{d}^4p_i}{(2\pi)^3}\delta_+(p_i^2). \tag{2.62}$$

If we write $\mathrm{d}^{D-1}k$ in polar coordinates, and integrate over the $D-4$ extra dimensions, in which the amplitude is symmetric, we get

$$\mathrm{d}^{D-1}k = k_0^{D-2}\mathrm{d}k_0\,(1-y^2)^{\frac{(D-4)}{2}}\mathrm{d}y\,\sin(\phi)^{D-4}\mathrm{d}\phi\,\Omega^{D-3}, \tag{2.63}$$

where Ω^d is the total solid angle in d dimensions

$$\Omega^d = 2^d \pi^{(d-1)/2} \frac{\Gamma(\frac{1+d}{2})}{\Gamma(d)}. \tag{2.64}$$

Setting $D = 4 - 2\varepsilon$, we get for the phase space differential of the emitted particle

$$\frac{\mathrm{d}\Phi_{n+1}}{\mathrm{d}\widetilde{\Phi}_n} = \frac{(4\pi)^\varepsilon}{\Gamma(1-\varepsilon)} \frac{\Gamma(1-\varepsilon)^2}{\Gamma(1-2\varepsilon)} \frac{\hat{s}^{1-\varepsilon}}{4} \xi^{1-2\varepsilon} (1-y^2)^{-\varepsilon} \sin(\phi)^{-2\varepsilon} \frac{\mathrm{d}\phi \mathrm{d}y \mathrm{d}\xi}{(2\pi)^3}. \tag{2.65}$$

The universality of the infrared singularities, expressed in the Eqs. (2.22) and (2.29), tells us that the quantity $\xi^2(1-y)(1+y)\mathcal{R} = \xi^2(1-y^2)\mathcal{R}$ is free of singularities, and therefore regular in the soft ($\xi \to 0$) and collinear ($y \to \pm 1$) limits. Using this, we can isolate the infrared divergences of the real amplitude in the integration measure of ξ and y

$$\int \mathrm{d}\xi \, \mathrm{d}y \, \xi^{-1-2\varepsilon} (1-y^2)^{-1-\varepsilon} \left(\xi^2 (1-y^2)\mathcal{R}\right). \tag{2.66}$$

As the factor $(\xi^2(1-y^2)\mathcal{R})$ is regular in the integration domain, we can explicitly write the divergences by expanding the factor $\xi^{-1-2\varepsilon}(1-y^2)^{-1-\varepsilon}$ in ε using the following distribution identities

$$\xi^{-1-2\varepsilon} = -\frac{1}{2\varepsilon}\delta(\xi) + \left(\frac{1}{\xi}\right)_+ - 2\varepsilon \left(\frac{\log(\xi)}{\xi}\right)_+ + \mathcal{O}(\varepsilon^2), \tag{2.67}$$

$$\begin{aligned}(1-y^2)^{-1-\varepsilon} = &-\frac{4^{-\varepsilon}}{2\varepsilon}(\delta(1-y)+\delta(1+y)) \\ &+ \frac{1}{2}\left(\left(\frac{1}{1-y}\right)_+ + \left(\frac{1}{1+y}\right)_+\right) + \mathcal{O}(\varepsilon),\end{aligned} \tag{2.68}$$

where the plus-prescriptions used here[4] are defined as

$$\int_0^1 \mathrm{d}\xi \, G(1-\xi)_+ f(\xi) = \int_0^1 \mathrm{d}\xi \, G(1-\xi)\left(f(\xi) - f(0)\right), \tag{2.69}$$

$$\int_{-1}^1 \mathrm{d}y \left(\frac{1}{1\pm y}\right)_+ f(y) = \int_{-1}^1 \mathrm{d}y \, \frac{f(y) - f(\mp 1)}{1 \pm y}. \tag{2.70}$$

This results in the following separation of singular regions

$$\begin{aligned}\iint \mathrm{d}\xi \, \mathrm{d}y \, \xi^{-1-2\varepsilon}(1-y^2)^{-1-\varepsilon} f(\xi, y) = &-\frac{1}{2\varepsilon}\int \mathrm{d}y \, f(0,y)(1-y^2)^{-1-\varepsilon} \\ &- \frac{4^{-\varepsilon}}{2\varepsilon}\int \mathrm{d}\xi \left(\left(\frac{1}{\xi}\right)_+ - 2\varepsilon\left(\frac{\log(\xi)}{\xi}\right)_+\right)\left(f(\xi,1) + f(\xi,-1)\right)\end{aligned}$$

4 Note that that (2.69) corresponds to (2.39) with the mapping $\xi \to (1-z)$.

$$+\iint \mathrm{d}\xi\,\mathrm{d}y\,\frac{1}{2}\left(\left(\frac{1}{1-y}\right)_+ + \left(\frac{1}{1+y}\right)_+\right)\left(\frac{1}{\xi}\right)_+ f(\xi,y)$$
$$+\mathcal{O}(\varepsilon), \tag{2.71}$$

where the auxiliary function $f(\xi,y) = \left(\xi^2(1-y^2)\mathcal{R}\right)\mathrm{d}\widetilde{\Phi}_n$ is regular in the entire integration domain. The first term in the expression corresponds to the limit of vanishing k^μ, i. e. the soft limit $\xi \to 0$, while the second term corresponds to the limit of $k \parallel p_{1,2}$, i. e. the collinear limits $y \to \pm 1$. Because of the universal singular behaviour of QCD amplitudes, using the soft and collinear factorization formulas in Eqs.(2.22) and (2.29), the functions $f(0,y)$ and $f(\xi,\pm 1)$ can be computed directly from the Born amplitude $\mathcal{B}$. Their poles will cancel the ones originating from the virtual amplitudes $\mathcal{V}$ as well as the counter terms in (2.49) arising from the evolution of the PDFs, leaving a finite remainder dependent on the factorization scale μ_F. The third line on the other hand is completely regular, which allow us to take the limit of $\varepsilon \to 0$ and compute the integrals numerically in four dimensions.

Let us proceed to show that the separation above leads to an explicit cancellation of singularities. Using the factorization properties of the amplitude in the soft and collinear regions (see Eqs. (2.22) and (2.29)) and using colour conservation ($\mathbf{T}_1 + \mathbf{T}_2 = 0$), we can compute the limits of the regular function $f(x,y)$ in terms of the Born amplitude as

$$f(0,y) = \lim_{x\to 0}\left(\xi^2(1-y^2)\mathcal{R}\right)\mathrm{d}\widetilde{\Phi}_n = 4\pi\alpha_s\mu^{2\varepsilon}8\hat{s}^{-1}(\mathbf{T}_1^2+\mathbf{T}_2^2)\left(\mathrm{d}\Phi_n\,\mathcal{B}\right), \tag{2.72}$$

$$\begin{aligned} f(x,1) &= \lim_{x\to 1}\left(\xi^2(1-y^2)\mathcal{R}\right)\mathrm{d}\widetilde{\Phi}_n \\ &= 4\pi\alpha_s\mu^{2\varepsilon}8\hat{s}^{-1}\xi\left[\sum_b P_{bg}^{ss'}((1-\xi,\phi,\varepsilon))\mathcal{T}_{b,a_2}^{ss'}((1-\xi)p_1,p_2)\right]\mathrm{d}\Phi_n\,|_{p_1\to(1-\xi)p_1} \\ &= 4\pi\alpha_s\mu^{2\varepsilon}8\hat{s}^{-1}\xi\left[P_{ba_1}^{<}(1-\xi,\varepsilon)\mathcal{B}_{b,a_2}((1-\xi)p_1,p_2)+\Delta\right]\mathrm{d}\widetilde{\Phi}_n\,, \end{aligned} \tag{2.73}$$

where we used that $\lim_{\xi\to 0}\mathrm{d}\widetilde{\Phi}_n = \mathrm{d}\Phi_n$, and the $f(\xi,-1)$ limit is analogous to $f(\xi,1)$.

In Eq. (2.73) we wrote the explicit dependence of the splitting kernel on the azimuthal angle ϕ of the emitted particle (which defines the auxiliary momentum $k_\perp$ in Eq. (2.29)), and in the last line we divided the spin contraction between the kernel and the $\mathcal{T}$ tensor in a diagonal part $P_{ba_1}^{<}(z,\varepsilon) = \frac{\delta_{ss'}}{2}P_{bg}^{ss'}(z,\varepsilon)$ (which doesn't depend on ϕ), and a spin correlation term Δ. The diagonal piece is proportional to the Born amplitude, in which we explicitly wrote the change in the flavour of the initial partons, and to the spin average $P_{ba_1}^{<}(z,\varepsilon)$, which when $\varepsilon = 0$ and $z < 1$ corresponds to the unpolarized AP splitting kernel introduced in Eqs. (2.35) - (2.38). As for the spin correlation term Δ, it can be shown that at NLO it vanishes upon azimuthal integration

$$\int_0^\pi \mathrm{d}\phi\,\sin(\phi)^{-2\varepsilon}\Delta = 0. \tag{2.74}$$

As we will briefly mention in part II, at NNLO this is no longer true and there is a finite contribution arising from spin correlations.

Using the expression in Eq. (2.72), we can write explicitly the soft part of the cross section $\mathrm{d}\sigma^{(s)}$, which arises from the first line of Eq. (2.71). We notice that $f(0,y)$ doesn't depend on the variables y and ϕ, so they can be integrated out

$$\int_0^\pi \mathrm{d}\phi\, \sin(\phi)^{-2\varepsilon} = \sqrt{\pi}\frac{\Gamma(\frac{1-2\varepsilon}{2})}{\Gamma(1-\varepsilon)}, \tag{2.75}$$

$$\int_{-1}^1 \mathrm{d}y\, (1-y^2)^{-1-\varepsilon} = \sqrt{\pi}\frac{\Gamma(-\varepsilon)}{\Gamma(\frac{1-2\varepsilon}{2})}. \tag{2.76}$$

Considering all normalization factors and expanding in ε, we obtain the following expression for the soft part

$$\begin{aligned}\mathrm{d}\sigma^{(s)} =& \frac{\alpha_s}{2\pi}\frac{(4\pi)^\varepsilon}{\Gamma(1-\varepsilon)}\left(\frac{\mu^2}{\hat{s}}\right)^\varepsilon (\mathbf{T}_1^2+\mathbf{T}_2^2)\left[\frac{-1}{\varepsilon}\frac{\Gamma(1-\varepsilon)\Gamma(-\varepsilon)}{\Gamma(1-2\varepsilon)}\right]\mathrm{d}\sigma^{(0)} \\ =& \frac{\alpha_s}{2\pi}\frac{(4\pi)^\varepsilon}{\Gamma(1-\varepsilon)}\left(\frac{\mu^2}{\hat{s}}\right)^\varepsilon (\mathbf{T}_1^2+\mathbf{T}_2^2)\left[\frac{1}{\varepsilon^2}-\frac{\pi^2}{6}\right]\mathrm{d}\sigma^{(0)} + \mathcal{O}(\varepsilon),\end{aligned} \tag{2.77}$$

where we defined the LO cross section $\mathrm{d}\sigma^{(0)} = \mathrm{d}\Phi_n\, \mathcal{B}$.

Similarly, we can define the collinear cross sections $\mathrm{d}\sigma^{(\pm)}$ as the contributions arising from the second line of Eq. (2.71) which depend on $f(\xi,\pm 1)$, respectively. Using Eq. (2.73) and integrating over the azimuthal angle ϕ, we expand it in ε to get the following result for $\mathrm{d}\sigma^{(+)}$ ($\mathrm{d}\sigma^{(-)}$ is analogous)

$$\begin{aligned}\mathrm{d}\sigma^{(+)} =& \frac{\alpha_s}{2\pi}\left(\frac{\mu^2}{\hat{s}}\right)^\varepsilon\left[\frac{-1}{\varepsilon}(\pi)^{\varepsilon-1/2}\frac{\Gamma(\frac{1-2\varepsilon}{2})}{\Gamma(1-2\varepsilon)}\right] \\ &\times\sum_b\int \mathrm{d}\xi\left(\frac{1}{\xi}\right)_+ \xi P^<_{ba_1}(1-\xi,0)\mathrm{d}\sigma^{(0)}_{ba_2}((1-\xi)p_1,p_2) \\ &+\frac{\alpha_s}{2\pi}\sum_b\int \mathrm{d}\xi\,\xi\left[2\left(\frac{\log(\xi)}{\xi}\right)_+ P^<_{ba_1}(1-\xi,0)\right. \\ &\left.-\left(\frac{1}{\xi}\right)_+ P'^<_{ba_1}(1-\xi,0)\right]\mathrm{d}\sigma^{(0)}_{ba_2}((1-\xi)p_1,p_2)+\mathcal{O}(\varepsilon),\end{aligned} \tag{2.78}$$

where we Taylor expanded in ε the function $P^<_{ba_1}(z,\varepsilon)$, and $\mathrm{d}\sigma^{(0)}_{ba_2}((1-\xi)p_1,p_2)$ is the LO cross section with the flavour and momentum of the first leg replaced as $(a_1,p_1)\to(b,(1-\xi)p_1)$, that is

$$P^<_{ba_1}(z,\varepsilon) = P^<_{ba_1}(z,0)+\varepsilon P'^<_{ba_1}(z,0)+\mathcal{O}(\varepsilon) \tag{2.79}$$

$$\mathrm{d}\sigma^{(0)}_{ba_2}((1-\xi)p_1,p_2) = \mathrm{d}\Phi_n\,|_{p_1\to(1-\xi)p_1}\,\mathcal{B}_{ba_2}. \tag{2.80}$$

We can see that expression for the soft cross section in Eq. (2.77) contains a double pole in ε, while the collinear cross section in Eq. (2.79) contains only a single pole given by

$$\begin{aligned}
\mathrm{d}\sigma^{(+)} &= -\frac{1}{\varepsilon}\frac{\alpha_s}{2\pi}\sum_b \int \mathrm{d}\xi \left(\frac{1}{\xi}\right)_+ \xi P^{<}_{ba_1}((1-\xi),0)\mathrm{d}\sigma^{(0)}_{ba_2}((1-\xi)p_1,p_2) + \mathcal{O}(\varepsilon^0) \\
&= -\frac{1}{\varepsilon}\frac{\alpha_s}{2\pi}\sum_b \int \mathrm{d}z \left(\frac{1}{1-z}\right)_+ (1-z)P_{ba_1}(z)\mathrm{d}\sigma^{(0)}_{ba_2}((1-\xi)p_1,p_2) \\
&\quad + \frac{1}{\varepsilon}\frac{\alpha_s}{2\pi}\gamma(a_1)\mathrm{d}\sigma^{(0)} + \mathcal{O}(\varepsilon^0),
\end{aligned} \tag{2.81}$$

where in the last line we changed the integration variable to $z = 1-\xi$, and used the identity

$$P_{ba_1}(z) = \left(\frac{1}{1-z}\right)_+ (1-z)P^{<}_{ba_1}(z,0) + \delta_{ba_1}\delta(1-z)\gamma(a_1) \tag{2.82}$$

to introduce the AP splitting kernels defined in Eqs. (2.35) - (2.38). The coefficients $\gamma(a)$ are given by

$$\gamma(g) = \frac{11C_A - 2n_F}{6}, \qquad \gamma(q) = \gamma(\bar{q}) = \frac{3}{2}C_F. \tag{2.83}$$

We see that the first term exactly cancels against the corresponding pole in Eq. (2.50), which arises from the evolution of PDF as discussed in section 2.2. An analogous result is obtained for $\mathrm{d}\sigma^{(+)}$. The remaining pole is proportional to the Born cross section, and together with the double pole in Eq. (2.77) will cancel the ones coming from the virtual amplitudes. The counter terms arising form the PDF are uniquely defined modulo finite terms, which define the *subtraction scheme*. In Eq. (2.49) we used the MS scheme, while if we change $\frac{1}{\varepsilon} \to (\frac{1}{\varepsilon} - \gamma_E + \ln 4\pi)$ we get the expressions in the $\overline{\text{MS}}$ scheme. Such changes will introduce differences in the finite part of $\mathrm{d}\sigma^{(\pm)}$, which we label $\mathrm{d}\sigma^{(c\pm)}$ and define such that

$$\mathrm{d}\sigma^{(+)} + \mathrm{d}\sigma^{(ct+)} = \frac{\alpha_s}{2\pi}\frac{(4\pi)^\varepsilon}{\Gamma(1-\varepsilon)}\left(\frac{\mu^2}{\hat{s}}\right)^\varepsilon \frac{1}{\varepsilon}\gamma(a_1)\mathrm{d}\sigma^{(0)} + \mathrm{d}\sigma^{(c+)} + \mathcal{O}(\varepsilon), \tag{2.84}$$

$$\mathrm{d}\sigma^{(-)} + \mathrm{d}\sigma^{(ct-)} = \frac{\alpha_s}{2\pi}\frac{(4\pi)^\varepsilon}{\Gamma(1-\varepsilon)}\left(\frac{\mu^2}{\hat{s}}\right)^\varepsilon \frac{1}{\varepsilon}\gamma(a_2)\mathrm{d}\sigma^{(0)} + \mathrm{d}\sigma^{(c-)} + \mathcal{O}(\varepsilon). \tag{2.85}$$

We can factorize the virtual amplitude $\mathcal{V}$ in the following way

$$\mathcal{V} = \frac{\alpha_s}{2\pi}\frac{(4\pi)^\varepsilon}{\Gamma(1-\varepsilon)}\left(\frac{\mu^2}{\hat{s}}\right)^\varepsilon \left[-\left(\frac{1}{\varepsilon^2}(\mathbf{T}_1^2 + \mathbf{T}_2^2) + \frac{1}{\varepsilon}(\gamma(a_1) + \gamma(a_2))\right)\mathcal{B} + \mathcal{V}_{fin}\right], \tag{2.86}$$

where $\mathcal{V}_{fin}$ is free of divergences, so that the poles match exactly (except for a sign difference) those in $\mathrm{d}\sigma^{(s)}$ and $\mathrm{d}\sigma^{(\pm)}$. The finite remainder in $\sigma^{(s)}$ together with the contribution coming from $\mathcal{V}_{fin}$ define the soft-virtual amplitude $\mathrm{d}\sigma^{(sv)}$.

Using all the results presented above, we can finally rewrite the partonic cross section in Eq. (2.57) as a sum of finite pieces

$$\begin{aligned} \mathrm{d}\hat{\sigma}_{a_1,a_2} =& \mathrm{d}\Phi_n \left[\mathcal{B}_{a_1,a_2} + \mathcal{V}_{a_1,a_2}\right] + \int_1 \mathrm{d}\Phi_{n+1}\, \mathcal{R}_{a_1,a_2} \\ =& \mathrm{d}\sigma^{(sv)}_{a_1,a_2} + \mathrm{d}\sigma^{(c+)}_{a_1,a_2} + \mathrm{d}\sigma^{(c-)}_{a_1,a_2} + \mathrm{d}\sigma^{(f)}_{a_1,a_2} \end{aligned} \tag{2.87}$$

where the expressions for the finite terms in the $\overline{\text{MS}}$ scheme are given by

$$\mathrm{d}\sigma^{(sv)}_{a_1,a_2} = \frac{\alpha_s}{2\pi}\left[-\frac{\pi^2}{6}(\mathbf{T}_1^2 + \mathbf{T}_2^2)\mathrm{d}\sigma^{(0)}_{a_1,a_2} + \mathcal{V}_{fin}\mathrm{d}\Phi_n\right], \tag{2.88}$$

$$\begin{aligned} \mathrm{d}\sigma^{(c+)}_{a_1,a_2} =& -\frac{\alpha_s}{2\pi}\ln\left(\frac{\mu^2}{\hat{s}}\right)\gamma(a_1)\mathrm{d}\sigma^{(0)}_{a_1,a_2} \\ &+\frac{\alpha_s}{2\pi}\sum_b \int \mathrm{d}\xi\, \xi \left[2\left(\frac{\log(\xi)}{\xi}\right)_+ P^{<}_{ba_1}(1-\xi,0)\right. \\ &\left. - \left(\frac{1}{\xi}\right)_+ P'^{<}_{ba_1}(1-\xi,0)\right]\mathrm{d}\sigma^{(0)}_{ba_2}((1-\xi)p_1,p_2), \end{aligned} \tag{2.89}$$

$$\begin{aligned} \mathrm{d}\sigma^{(c-)}_{a_1,a_2} =& -\frac{\alpha_s}{2\pi}\ln\left(\frac{\mu^2}{\hat{s}}\right)\gamma(a_2)\mathrm{d}\sigma^{(0)}_{a_1,a_2} \\ &+\frac{\alpha_s}{2\pi}\sum_b \int \mathrm{d}\xi\, \xi \left[2\left(\frac{\log(\xi)}{\xi}\right)_+ P^{<}_{ba_2}(1-\xi,0)\right. \\ &\left. - \left(\frac{1}{\xi}\right)_+ P'^{<}_{ba_1}(1-\xi,0)\right]\mathrm{d}\sigma^{(0)}_{a_1 b}(p_1,(1-\xi)p_2), \end{aligned} \tag{2.90}$$

$$\begin{aligned} \mathrm{d}\sigma^{(f)}_{a_1,a_2} =& \frac{\alpha_s}{2\pi}\iiint \frac{\mathrm{d}\phi\,\mathrm{d}\xi\,\mathrm{d}y}{(2\pi)^3}\frac{\hat{s}}{4} \\ & \frac{1}{2}\left[\left(\frac{1}{1-y}\right)_+ + \left(\frac{1}{1+y}\right)_+\right]\left(\frac{1}{\xi}\right)_+ \left[\xi^2(1-y^2)\mathcal{R}_{a_1a_2}\mathrm{d}\widetilde{\Phi}_n\right] \end{aligned} \tag{2.91}$$

and we wrote explicitly the flavour of the initial state legs in the amplitudes involved.

All of the terms presented in Eqs. (2.88) - (2.91) are finite and can be convoluted numerically with any given measurement function $\mathcal{J}$. The coefficient $\mathrm{d}\sigma^{(f)}_{a_1,a_2}$, that arises from the third line of Eq. (2.71), is the only one that depends on the full NLO phase space.

The method described above, that corresponds to FKS applied to the production of a colourless final state, introduces the ingredients of any NLO computation, and we will make use of this in part I of this thesis in the context of multiple Higgs production.

Part I

MULTIPLE HIGGS PRODUCTION

The production of two and three Higgs bosons is sensitive to its triple and quartic self couplings, respectively, already at the lowest order of perturbation theory. In this part we will first discuss how the double Higgs production cross section is modified when we consider deviations from the SM. We will do this in the context of the SM EFT, and at NNLO of perturbation theory on the strong coupling constant. Then, we will move to triple Higgs production and compute the NNLO QCD corrections to provide our best estimate on its inclusive cross section.

3

DOUBLE HIGGS BOSON PRODUCTION

The production of Higgs boson pairs provides a direct way to test the Higgs trilinear coupling (see Refs. [16–18] for an alternative approach), and as it happens for single Higgs boson production cross section, the dominant production channel proceeds at hadron colliders via gluon fusion mediated by heavy-quark loops [19–21]. This means that BSM physics can be realized in two distinct ways, either through a resonance due to a reasonably light field that acts as a mediator, or through heavier fields that participate in the loop thus modifying the effective couplings between the SM particles. In the former, a direct detection can be achieved by looking at the invariant mass spectrum of the final state, but in the latter a precision measurement has to be performed in order to search for deviations from the SM. A model-independent approach to parametrize BSM effects consists in considering the low energy effective field theory (EFT) that remains after integrating out the heavy fields of new physics (NP), introducing higher dimensional operators suppressed by the NP scale (Λ). In principle one could consider to add all possible higher order operators to the SM Lagrangian that are compatible with its symmetries, up to some power of Λ [22–25]. Expanding up to dimension 6 (Λ^{-2}), 2499 of such operators are found [26]. However, if we consider only those that vanish in the absence of the Higgs boson, and therefore, those that only contribute to observables when at least one Higgs boson participates in the process, the number reduces to 5, which can be written in several different basis.

Given that the leading order (LO) contribution to Higgs pair production occurs at loop level, higher orders in QCD perturbation theory are extremely difficult to calculate. Recently, a complete next-to-leading order (NLO) computation became available [27–29] that evaluates numerically the integrals of the required multi-scale two-loop amplitudes. In the heavy-top limit (HTL), where the top quark is considered heavy and the rest massless, NLO corrections have been presented in Ref. [30] and a rescaling with the exact Born cross section was performed. The NLO corrections represent an increase of about 100%, and the HTL result is only about 14% bigger than the exact result from Ref. [27]. While the computation of the three-loop virtual corrections is presently out of reach, working within the HTL it is possible to compute corrections beyond NLO, like the ones derived in Refs. [31, 32], which allowed for the next-to-next-to-leading order (NNLO) result presented in Ref. [33]. This calculation allows to compute not only the

inclusive cross section (resulting in an increase of about 20% at this order), but also the differential invariant mass distribution of the produced pair of Higgs bosons. Within the same heavy-top limit, a fully exclusive calculation at NNLO was presented in Ref. [34], and very recently N^{3}LO QCD corrections became available as well [35, 36]. With respect to computations that include dimension 6 operators in the SM EFT approach [37], bounds for the Wilson coefficients of the new operators have been obtained from the data collected by the LHC and earlier experiments by different groups [38–43], a NLO calculation for Higgs pair production in the HTL was performed in Ref. [44] and recently in Ref. [45] was presented with the full top-mass dependence.

In this chapter we present the computation of the Higgs bosons pair production cross section at NNLO in QCD, including the relevant dimension 6 operators of the SM EFT, as published in Ref. [46]. In section 3.1 we provide the details of the calculation, including two popular basis for the EFT. In section 3.2 we present the phenomenological results, discussing the dependence of the K-factor on the higher dimensional couplings and the degeneracy of the inclusive cross section on them. Recently, these NNLO results in the HTL have been combined with the full NLO (with exact top-mass dependence) [47], providing the most accurate predictions so far for the Higgs pair production with EFT effects.

3.1 DETAILS OF THE CALCULATION

3.1.1 *EFT basis*

Heavy states of NP can be integrated out to obtain a low energy effective Lagrangian, with new contact interactions that would be otherwise mediated by the NP states. The coupling constant of the effective interaction is therefore suppressed by the mass scale Λ of the new heavy state, making the operator of dimension higher than four, and therefore non-renormalizable. In this context, in order to parametrize all possible BSM theories that are free of new light states, one should include in the SM Lagrangian all higher dimensional terms that are consistent with the SM symmetries. There are 1350 CP-even and 1149 CP-odd of such dimension 6 ($\mathcal{O}(\Lambda^{-2})$) operators [26]. Nevertheless, we will focus only on the operators that vanish in the absence of the scalar boson, as the others can be better constrained by other observables. This includes for instance the chromomagnetic operator, that introduces a coupling between gluons, the top quark and the Higgs doublet, which in recent studies [48] has been shown to mix with other operators. Nevertheless, the effects arising from this operator also appear in the absence of the Higgs boson (from the term proportional to the Higgs vacuum expectation value) and therefore introduce corrections to *pure* QCD processes, in particular to the top pair production cross section that can set a better constraint on the corresponding anomalous coupling [49]. Formally, this operator introduces corrections of order $\mathcal{O}(y_t^2)$ to the results of this work, where y_t is the top Yukawa coupling, and therefore is not considered herein.

In this work we will neglect the mass of all fermions (thus their couplings to the Higgs) except for the top quark, since their contributions to Higgs pair production through gluon fusion accounts for less than 1% of the LO cross section in the SM [50]. Due to this suppression, these contributions were not considered in the present work, although in principle they could be enhanced in some BSM scenarios.

If one considers the Higgs boson h as a singlet of the custodial symmetry, and not necessarily part of an $SU(2)_L$ doublet, the relevant dimension 6 operators can be written as [51]

$$\begin{aligned}\mathcal{L}_{\text{non-lin}} \supset & - m_t\, \bar{t}t \left(c_t \frac{h}{v} + c_{tt} \frac{h^2}{2v^2} \right) - c_3 \frac{1}{6} \left(\frac{3m_H^3}{v} \right) h^3 \\ & + \frac{\alpha_s}{\pi} G^{a\,\mu\nu} G^a_{\mu\nu} \left(c_g \frac{h}{v} + c_{gg} \frac{h^2}{2v^2} \right), \end{aligned} \tag{3.1}$$

where $\alpha_s = g_s^2/(4\pi)$, g_s is the strong coupling constant, t represents the top quark with mass m_t, $v \approx 246$ GeV is the SM Higgs field vacuum expectation value, m_H is the mass of the Higgs boson h, $G^a_{\mu\nu}$ is the gluon field strength tensor, and $c_{i=t,tt,3,g,gg}$ are the Wilson coefficients, after a canonical normalization of the Lagrangian. The operators parametrized by c_t and c_3 modify the ones already present in the SM, namely the coupling between the Higgs boson and the top, and the Higgs boson self-coupling, respectively. The rest of the operators are new, c_g and c_{gg} parametrizing the contact interaction between gluons and one and two Higgs bosons, respectively, and c_{tt} the one between the top quark and a pair of Higgs bosons. In this Lagrangian, the $SU(2)_L \times U(1)_Y$ symmetry is non-linearly realized, and the SM corresponds to the point in parameter space given by $c_3 = c_t = 1$ and $c_{tt} = c_g = c_{gg} = 0$.

Using a different approach, one could assume that the Higgs boson is part of an $SU(2)_L$ doublet H. This particular extension of the SM is included in the so-called SILH basis [52], and is given by the operators

$$\begin{aligned}\mathcal{L}_6^{\text{SILH}} \supset & \frac{\bar{c}_H}{2v^2} \partial_\mu (H^\dagger H) \partial^\mu (H^\dagger H) + \frac{\bar{c}_u}{v^2} y_t (H^\dagger H \bar{q}_L H^c t_R + h.c.) \\ & - \frac{\bar{c}_6}{6v^2} \frac{3m_H^2}{v^2} (H^\dagger H)^3 + \bar{c}_g \frac{g_s^2}{m_W^2} H^\dagger H G^{a\,\mu\nu} G^a_{\mu\nu}, \end{aligned} \tag{3.2}$$

where m_W is the mass of the W boson, and $\bar{c}_{i=H,u,6,g}$ are 4 free parameters (the SM corresponding to $\bar{c}_i = 0$ for all i). Expanding H around v in the physical gauge, one finds that it corresponds to $\mathcal{L}_{\text{non-lin}}$ with

$$c_t = 1 - \frac{\bar{c}_H}{2} - \bar{c}_u, \quad c_{tt} = -\frac{1}{2}(\bar{c}_H + 3\bar{c}_u), \quad c_3 = 1 - \frac{3}{2}\bar{c}_H + \bar{c}_6, \quad c_g = c_{gg} = \bar{c}_g \left(\frac{4\pi^2 v^2}{m_W^2} \right). \tag{3.3}$$

Bounds for the SILH coefficients can be found in Ref. [53]. In this work we will use the more general extension of the SM, $\mathcal{L}_{\text{non-lin}}$.

3.1.2 *NNLO results*

Performing higher order QCD calculations for Higgs boson pair production has been probed to be quite complicated. Even within the SM, the NLO computation could be obtained only very recently [27–29]. Therefore, an approach that is widely used consists in integrating out the top quark of the SM Lagrangian and work with the remaining effective theory that is valid for energy scales smaller than $\sim 2m_t$, in what is called the heavy-top limit (HTL).

In the HTL approximation one considers the top-quark too heavy to be excited, and therefore it can be integrated out from the Lagrangian. This induces a series of higher dimensional effective operators in the Lagrangian, that couple the remaining light degrees of freedom of the SM and can be thought of as an expansion on the inverse mass squared of the top quark. In particular, a coupling between the Higgs boson and the gluon field is induced

$$\mathcal{L}_{\text{SM}}^{\text{HTL}} = \frac{\alpha_s}{12\pi} G^a_{\mu\nu} G_a^{\mu\nu} \left(C_H \frac{h}{v} - C_{HH} \frac{h^2}{2v^2} + C_{HHH} \frac{h^3}{3v^3} + \dots \right), \tag{3.4}$$

where the matching coefficients can be expanded in powers of the strong coupling constant α_s as

$$C_X = \sum_{n \geq 0} C_X^{(n)} \left(\frac{\alpha_s}{\pi} \right)^n . \tag{3.5}$$

and the expansion is known up to fourth order for $X = H, HH, HHH$ [32, 54–59]. Up to NNLO, the relevant coefficients for double Higgs production are

$$C_H = 1 + \frac{11}{4} \frac{\alpha_s}{\pi} + \left(\frac{\alpha_s}{\pi} \right)^2 \left[\frac{2777}{288} + \frac{19}{16} \log \frac{\mu_R^2}{m_t^2} + n_f \left(-\frac{67}{96} + \frac{1}{3} \log \frac{\mu_R^2}{m_t^2} \right) \right] + \mathcal{O}(\alpha_s^3) , \tag{3.6}$$

$$C_{HH} = C_H + \left(\frac{\alpha_s}{\pi} \right)^2 \Delta C_{HH}^{(2)} + \mathcal{O}(\alpha_s^3) , \tag{3.7}$$

$$\Delta C_{HH}^{(2)} = \frac{35}{24} + \frac{2}{3} n_f . \tag{3.8}$$

In recent higher order calculations [33], the QCD corrections were computed in the HTL, and then multiplied by the LO exact result, providing a rescaling (known as *Born-improved HTL* or simply *Bi HTL*) that improves the accuracy of this approach [30]. The exact NLO order calculation has shown that –despite the fact that the bulk of the cross section comes from di-Higgs invariant masses larger than the threshold $2m_t$– this procedure is a rather good approximation at NLO, being the exact result for the inclusive cross section at NLO only a 14% smaller than the Bi HTL one [28], to be compared to the radiative correction of about 100%. Of course, the situation is in general different for kinematic

distributions, finding –for some of them– large discrepancies between the full NLO and the aforementioned approximation (see Ref. [27] for a detailed comparison). However, the differences in the shape of the Higgs-pair invariant mass distribution, which is the only one considered in this work, are moderate, being always below 25% in the whole mass range under analysis for the SM. It is worth to mention, though, that the size of the NNLO corrections in the HTL is of the same magnitude of the top-mass effects at NLO. For this reason, an EFT analysis has been recently performed in Ref. [47] that combines the full NLO with the HTL NNLO corrections presented in this chapter.

In this work we follow a similar scheme as in Ref. [33]: We compute the QCD corrections within the effective theory where the top quark has been integrated out, and then we rescale the result in such a way that the exact LO cross section is recovered.

After integrating the top quark field in Eq. (3.1), the effective Lagrangian reads

$$\begin{aligned}\mathcal{L}^{\text{HTL}}_{\text{non-lin}} \supset & \frac{\alpha_s}{\pi} G^{a\,\mu\nu} G^a_{\mu\nu} \left\{ \frac{h}{v} \left[\frac{c_t}{12} C_H + c_g \right] + \frac{h^2}{2v^2} \left[-\frac{c_t^2}{12} C_{HH} + \frac{c_{tt}}{12} C_H + c_{gg} \right] \right\} \\ & - c_3 \frac{1}{6} \left(\frac{3 m_H^3}{v} \right) h^3 . \end{aligned} \tag{3.9}$$

We can see in Eq. (3.9) that the coefficients c_i only modify the effective couplings between the Higgs and gluons present in Eq. (3.4) for the SM HTL. This simplification provides a straightforward way of generalizing the SM result to the EFT that includes dimension 6 operators.

We follow the approach described in Ref. [33], where we distinguish between (a) contributions to the squared matrix element that have only two effective vertices between Higgs boson(s) and gluons (σ^a), and (b) those with more than two effective vertices (σ^b). Thus the partonic cross section, differential in the invariant mass of the di-Higgs system Q, can be written as

$$Q^2 \frac{\mathrm{d}\hat{\sigma}}{\mathrm{d}Q^2} = \hat{\sigma}^a + \hat{\sigma}^b, \tag{3.10}$$

where $\hat{\sigma}^a$ receives the same corrections than those for single Higgs production, due to the similarity of the amplitudes involved. We found that for each partonic subprocess $ij \to HH + X$, and for factorization and renormalization scales $\mu_R = \mu_F = Q$, the result is

$$\begin{aligned}\hat{\sigma}^a_{ij} = & \hat{\sigma}_{\text{LO}} \left[\eta^{(0)}_{ij} + \left(\frac{\alpha_S}{2\pi} \right) 2\eta^{(1)}_{ij} + \left(\frac{\alpha_S}{2\pi} \right)^2 4\eta^{(2)}_{ij} \right] \\ & - \int_{t_-}^{t_+} dt \frac{G_F^2 \alpha_s^2}{512(2\pi)^3} \left\{ \left(\frac{\alpha_S}{2\pi} \right) \delta_{ig}\, \delta_{jg} \delta(1-x) 4\, C_H^{(1)} \mathrm{Re}(A^* C_{LO}) \right. \\ & + \left(\frac{\alpha_S}{2\pi} \right)^2 \delta_{ig}\, \delta_{jg} \delta(1-x)\, 4 \left[2\,\mathrm{Re}(C^*_{LO}\, F_{box})\, c_t^2\, \Delta C^{(2)}_{HH} - (C_H^{(1)})^2 |A|^2 + C_H^{(2)}\, 2\,\mathrm{Re}(A^* C_{LO}) \right] \\ & \left. + \left(\frac{\alpha_S}{2\pi} \right)^2 8 \mathrm{Re}(A^* C_{LO})\, C_H^{(1)} \eta^{(1)}_{ij} \right\}, \end{aligned} \tag{3.11}$$

where the coefficients η_{ij} are those expressed in Ref. [60] (which also agree with the results presented in Refs. [61, 62]), A and C_{LO} are defined as

$$A = \frac{2}{3}\left[c_3 C_\triangle\, 12\, c_g + 12\, c_{gg}\right] , \tag{3.12}$$

$$C_{LO} = c_3\, C_\triangle \left(c_t\, F_\triangle + \frac{2}{3} 12\, c_g\right) + c_t^2\, F_{box} + c_{tt}\, F_\triangle + \frac{2}{3} 12\, c_{gg} , \tag{3.13}$$

$F_\triangle$, F_{box} and G_{box} are the usual triangle and box form factors and can be found in Ref. [21], $C_\triangle$ includes the Higgs propagator

$$C_\triangle = \frac{3 m_H^2}{Q^2 - m_H^2 + i m_H \Gamma_H} \tag{3.14}$$

where Γ_H is the Higgs total width, and $\hat{\sigma}_{\text{LO}}$ is the LO partonic cross section for $gg \to HH$

$$\hat{\sigma}_{\text{LO}} = \int_{t_-}^{t_+} dt \frac{G_F^2\, \alpha_s^2}{512 (2\pi)^3} \left\{ \left| C_{LO} \right|^2 + \left| c_t^2 G_{box} \right|^2 \right\} . \tag{3.15}$$

The integration variable is

$$t = -\frac{1}{2}\left(Q^2 - 2 m_H^2 - Q\sqrt{Q^2 - 4 m_H^2}\cos\theta_1\right) , \tag{3.16}$$

where θ_1 is the scattering angle in the Higgs centre-of-mass system. The limits of integration correspond to $t_\pm = t\,(\cos\theta_1 = \pm 1)$.

The effective vertex between gluons and Higgs is proportional to α_s, which implies that $\hat{\sigma}^b$ is NLO at tree-level, and at NNLO there are one-loop virtual and single real emission corrections (see chapter 2). The SM result from Ref. [31] uses the FKS approach described in section 2.3 to compute σ^b, which is split into different pieces making it possible to keep track of the different amplitudes contributing to each of them, and thus to adapt this result to our EFT by inserting the appropriate factors. The renormalized result (for $\mu_F = \mu_R = Q$) can be written for the different channels as

$$\hat{\sigma}^b_{gg} = \hat{\sigma}^{(sv)}_{gg} + \hat{\sigma}^{(c+)}_{gg} + \hat{\sigma}^{(c-)}_{gg} + \hat{\sigma}^{(f)}_{gg} , \tag{3.17}$$

$$\begin{aligned}\hat{\sigma}^{(sv)}_{gg} = \int_{t_-}^{t_+} dt \frac{G_F^2\, \alpha_s^2}{512 (2\pi)^3}\, \delta(1-x) \Bigg\{ & \left(\frac{\alpha_s}{2\pi}\right) \frac{4}{3} \operatorname{Re}\left(C_{LO}^*\, V_{\text{eff}}^2\right) \\ & + \left(\frac{\alpha_s}{2\pi}\right)^2 \Bigg[\operatorname{Re}\left(C_{LO}^*\, V_{\text{eff}}^2\right) \left(\frac{8\pi^2}{3} + \mathcal{R}^{(2)} - 8\, \Delta C_{HH}^{(2)}\right) + \operatorname{Im}\left(C_{LO}^*\, V_{\text{eff}}^2\right) \mathcal{I}^{(2)} \\ & + |V_{\text{eff}}|^4\, \mathcal{V}^{(2)} - \frac{22}{3} \left(2 \operatorname{Re}\left(C_{LO}^* V_{\text{eff}}\right) \frac{2}{3} 12\, c_g + \operatorname{Re}\left(A^* V_{\text{eff}}^2\right)\right) \Bigg] \Bigg\} ,\end{aligned} \tag{3.18}$$

$$\hat{\sigma}^b_{qg} = \hat{\sigma}^{(c+)}_{qg} + \hat{\sigma}^{(f)}_{qg} , \tag{3.19}$$

$$\hat{\sigma}^b_{gq} = \hat{\sigma}^{(c-)}_{gq} + \hat{\sigma}^{(f)}_{gq}\,, \tag{3.20}$$

$$\hat{\sigma}^b_{q\bar{q}} = \hat{\sigma}^{(f)}_{q\bar{q}}\,, \tag{3.21}$$

where the expressions for $\mathcal{R}^{(2)}$, $\mathcal{I}^{(2)}$, and $\mathcal{V}^{(2)}$ can be found in Ref. [31]. The factor V_{eff} accounts for the effective vertex between gluons and the (on-shell) Higgs boson appearing in $\hat{\sigma}^b$, and is given by

$$V_{\text{eff}} = c_t\, F_\triangle(Q/2) + \frac{2}{3}\, 12\, c_g, \tag{3.22}$$

where the form factor $F_\triangle$ is evaluated at half the invariant mass of the produced Higgs pair ($Q/2$). At variance with all other contributions, where $F_\triangle$ arises from the triangle diagram originated (at LO) from on-shell gluons and, therefore, is evaluated at the off-shell Higgs (invariant) mass Q, in this effective vertex the outgoing Higgs is on-shell while the exchanged gluon is off-shell. As a consequence, evaluating this vertex either at the fixed scale m_H or the invariant mass Q is not fully satisfactory, and a dynamical scale appears as a more sensible choice. We use the same scale as the one chosen for the renormalization and factorization scales, $Q/2$, which also takes the value m_H at the production threshold.

The expressions for $\sigma^{(c+)}_{ij}$, $\sigma^{(c-)}_{ij}$ and $\sigma^{(f)}_{ij}$ are given in Appendix A, and correspond to the renormalized real emission corrections defined in Ref. [33], with a modification to properly account for the V_{eff} contribution.

Replacing these expressions into Eq. (3.10) provides the result for the differential cross section for Higgs pair production in the EFT as a function of the invariant mass of the pair, including the radiative corrections up to NNLO in QCD.

A comment is in order regarding the rescaling of the HTL result with the exact LO result. In previous work [33], the final result has been reweighted with the quotient between the Born cross sections, schematically

$$\mathrm{d}\sigma = \frac{\mathrm{d}\sigma^{\text{Exact}}_{LO}}{\mathrm{d}\sigma^{\text{HTL}}_{LO}} \mathrm{d}\sigma^{\text{HTL}}, \tag{3.23}$$

which is known as the *Born-improved* or Bi cross section. However, this method can fail if at some point of the phase space the Born cross section in the HTL vanishes and the exact does not. This is not a problem in the SM, for which the LO partonic cross section in the HTL only vanishes at the production threshold, but it is in the EFT, where particular combinations of the coefficients c_i can produce vanishing cross sections in the HTL for certain values of $Q > 2m_H$, while they remain different from zero for the exact result (as seen in section 3.3 of Ref. [28]). In order to surpass this issue, in this work we directly rescale the individual vertices that appear at the amplitude level, to get what we call the *dynamically Born-improved* (or dBi) cross section. To be precise, in those matrix elements for which the QCD corrections factorize from the Born cross section, the full LO cross section is introduced by using the exact expression for C_{LO}. This is the case for the amplitudes that

contribute to $\sigma^{(a)}$. In the terms arising from the new topology that appears at NLO, the reweighting of the two corresponding gluon-Higgs effective vertices is taken into account by the factor V_{eff} defined in Eq. (3.22). This factor is introduced in the terms extracted from Ref. [31] either as its square modulus, or as the real and imaginary parts of $C^*_{LO}\, V^2_{\text{eff}}$ in the interference terms. In particular, in the real emission contributions presented in Appendix A, it is the real part of $C^*_{LO}\, V^2_{\text{eff}}$ that is taken into account.

As mentioned before, the dBi prescription for rescaling the HTL result is different from the Bi used in Ref. [33], and it allows to generalize it to BSM scenarios in which the HTL Born cross section can vanish for a certain invariant mass of the Higgs boson pair. The difference in the inclusive cross section at NNLO between these two prescriptions is less than 0.4% (compared to the scale uncertainties of the order of 8%-10%). In Ref. [44] a similar prescription was tacitly used, but the effective vertex for the new topology amplitudes V_{eff} was introduced in the HTL, as $\frac{2}{3}(c_t + 12c_g)$. The difference between the rescaling used in Ref. [44] and the one presented herein, results in a slightly stronger dependence of the K-factor on the anomalous couplings c_i when using the latter, as we will see in section 3.2.1. More details on the dBi prescription will be given in the next chapter, section 4.2.1, in the context of triple Higgs production.

3.2 PHENOMENOLOGY

We present here the numerical predictions for the Higgs boson pair production cross section at the LHC, based on the results presented in the previous section. For parton densities and strong coupling constant scaling we used the PDF4LHC15 distribution [63–68] interpolated with the LHAPDF package [69]. The integration was performed using the CUBA implementation of the VEGAS algorithm [70]. We fixed the collider c.m. energy to $\sqrt{s} = 14$ TeV, the mass of the Higgs and of the top quark were set to the values $m_H = 125$ GeV and $m_t = 172.5$ GeV respectively, and the Higgs width $\Gamma_h = 4.07$ MeV. The factorization and renormalization scales are set to $\mu_R = \mu_F = Q/2$ where Q is the invariant mass of the Higgs boson pair.

The anomalous couplings c_3 and c_t belong to operators already present in the SM. In fact, c_3 modifies the Higgs boson self-coupling and can take values ranging from $c_3 = -10$ to 10 [71], and c_t modifies the top Yukawa coupling, with allowed values in the interval $0.65 \leq c_t \leq 1.15$ [72]. The normalization is such that the SM corresponds to $c_3 = c_t = 1$, with all the other new couplings set to zero. The rest of the couplings are not present in the SM and only arise due to BSM effects. The parameter c_{tt} corresponds to a new contact interaction between a top-anti-top pair and two Higgs bosons, and is varied from -1.5 to 1.5 [71]. New contact interactions between gluons and one and two Higgs bosons are parametrized through the c_g and c_{gg} couplings, respectively, and both were varied in the range $[-0.15, 0.15]$ [71]. This interval was chosen mostly for illustrative purposes, despite

the fact that the current experimental limit obtained for c_g under certain assumptions is smaller [71, 72].

A comment on the validity of the result is in order. The Lagrangian used here is a low energy expansion in powers of Λ, so the new couplings c_i are expected to show deviations from the SM of order $(v/\Lambda)^2$. With this into account, we can notice that only interferences between the BSM and the SM are of order Λ^{-2}, whilst quadratic terms in c_i, together with the interference between the SM and dimension 8 operators (not considered here), are of order Λ^{-4}. In principle, one should expand the result linearly in the anomalous couplings and constrain their values to the region where this linear approximation is valid.

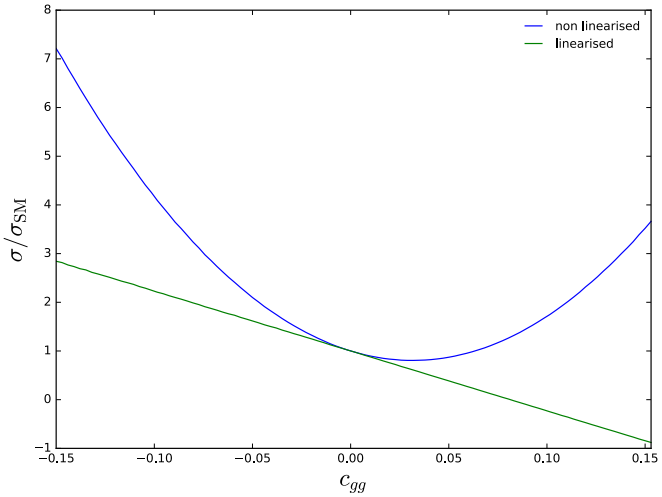

Figure 3.1: Total cross section for Higgs boson pair production at LO as a function of c_{gg}, both for the linearised and non-linearised cases.

In this chapter we vary the coefficients c_i in the whole range so far experimentally allowed, far beyond the region where the linear approximation is valid. This is illustrated in Figure 3.1, where we show the LO total cross section for Higgs pair production as a function of c_{gg}, both for the linearised and non-linearised cases. It is clear that we are exploring regions which are far beyond the linear regime; in particular we can observe that the linear approximation vanishes at $c_{gg} \approx 0.08$ and continues to negative values. Nevertheless, in the absence of results for operators up to dimension 8, it has been shown that in some cases it is better to keep the non linear terms [73]. In particular, in scenarios where the dimension 8 operators do not interfere with the SM (e.g. due to different total helicity) or where the dimension 6 couplings are enhanced (e.g. strongly coupled theories) the current analysis is justified.

3.2.1 *K-factors*

We compute the *K*-factors, as the ratios between the NNLO and LO cross sections. It is interesting to see if the change introduced by the new couplings factorizes from the radiative corrections or if, on the contrary, there is a significant dependence of the *K*-factors on the anomalous couplings. To compare dependencies of the *K*-factor as a function of the different anomalous couplings, we parametrize their departure from the SM with the variable ξ. In this computation only one anomalous coupling at a time is left free, and the rest are set to their SM values ($\xi = 0$). The coefficients c_i are parametrized as follow (note that for illustrative purposes, c_3 is varied from -9 to 11),

$$c_3 = 1 + 10\,\xi\,, \tag{3.24}$$
$$c_t = 1 + 0.35\,\xi\,, \tag{3.25}$$
$$c_{tt} = 1.5\,\xi\,, \tag{3.26}$$
$$c_g = 0.15\,\xi\,, \tag{3.27}$$
$$c_{gg} = 0.15\,\xi\,. \tag{3.28}$$

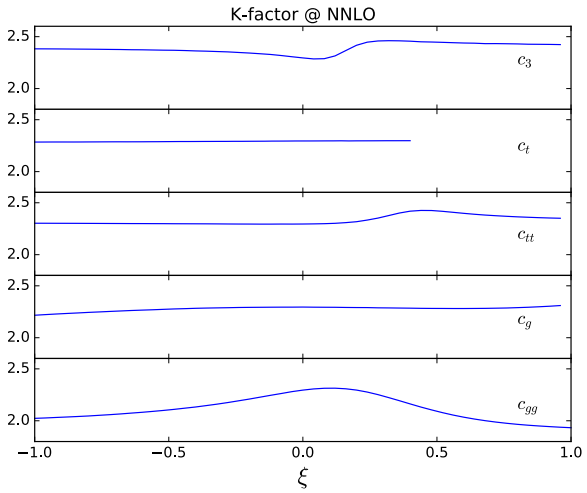

Figure 3.2: *K*-factor for total production of Higgs boson pairs as a function of each anomalous coupling, whilst leaving the others set to their SM value. The SM corresponds to $\xi = 0$ in all cases, and the parametrization in terms of ξ is given by Eqs. (3.24) – (3.28).

We can observe from Figure 3.2 that the dependence of the *K*-factor on each anomalous coupling, aside for a small bump in some cases, is rather flat. The origin of the bump can be understood on a simple basis: the dependence of the cross section (both at LO as NNLO) on the anomalous couplings is shaped as a parabola with a minimum near the SM. The *K*-factor is then a quotient of two parabola-like functions, thus has a single

extreme (either a maximum or a minimum) in ξ_0 if the parabolas share a minimum in ξ_0, or a maximum next to a minimum if the minima of the parabolas are separated from one another (as is the case of c_3). From this kind of analysis, we see that the radiative corrections change the position of the minimnum of the cross section as a function of c_3. In the case of c_t, the minimum lies outside the allowed values for the anomalous coupling, resulting in a rather flat dependence of the K-factor.

The maximum deviation of the K-factor from the SM case, when varying one anomalous coupling at a time, is achieved by c_{gg} with a departure of

$$\Delta K^{c_{gg}} = \frac{\max \left| K(c_{gg}) - K_{SM} \right|}{K_{SM}} \approx 15.8\% \qquad \text{at } c_{gg} = 0.15\,. \tag{3.29}$$

The rest of the parameters show the following maximum departure:

$$\Delta K^{c_3} \approx 7.2\% \qquad \text{at } c_3 = 4.20\,, \tag{3.30}$$
$$\Delta K^{c_{tt}} \approx 5.7\% \qquad \text{at } c_{tt} = 0.66\,, \tag{3.31}$$
$$\Delta K^{c_g} \approx 3.4\% \qquad \text{at } c_g = -0.15\,, \tag{3.32}$$
$$\Delta K^{c_t} \approx 0.5\% \qquad \text{at } c_t = 0.65\,. \tag{3.33}$$

Nevertheless, when we allow the five anomalous couplings to vary at the same time, larger deviations from the SM K-factor can be found. When sampling the five dimensional parameter space[1], the maximum deviation observed is

$$\Delta K^{\max} \approx 84\% \tag{3.34}$$

at the point of parameter space $c_3 = 7.0$, $c_t = 1.15$, $c_{tt} = 0.1$, $c_g = -0.09$, $c_{gg} = 0.02$. At this point, the K-factor is as high as 4.07, and if we modify the value of c_g to $c_g = -0.11$ we get a value as low as 0.80 (36% of the SM value). This shows a strong dependence on c_g on this region of parameter space, with a similar shape as the dependence shown for c_3 in Figure 3.2. The reason is also clear: at the maximum K-factor, the LO cross section has a minimum of 2.46 fb (12.5% of the SM value), whilst at the minimum of the K-factor (lowering c_g) it is the NNLO cross section that gets minimized to 4.84 fb (10.7% of the SM value). Because the cross section is near a minimum, any variation in the radiative corrections amounts for a significant relative change, resulting in this behaviour of the K-factor. It is also worth noting that in this region of parameter space where the K-factor reaches a minimum of 0.76, the radiative corrections are negative, thus resulting in a decrease of the total cross section with respect to the LO one. Also, the NLO K-factor at that point is 1.01, still greater than one, which means that the negative corrections that decrease the cross section below its LO value are a purely NNLO effect. The change of

1 Clustering algorithms that are sensitive to the kinematics of the process have been derived in [74] that could improve the choice of the benchmark points when sampling high-dimensional parameter spaces.

sign of the NNLO corrections while varying the value c_g from -0.09 to -0.11 at this point of parameter space is driven by the sign of the contributions proportional to $\mathrm{Re}\,(A^* C_{LO})$ in $\hat{\sigma}^a$ (Eq. (3.11)), which happen to be dominant in this particular region.

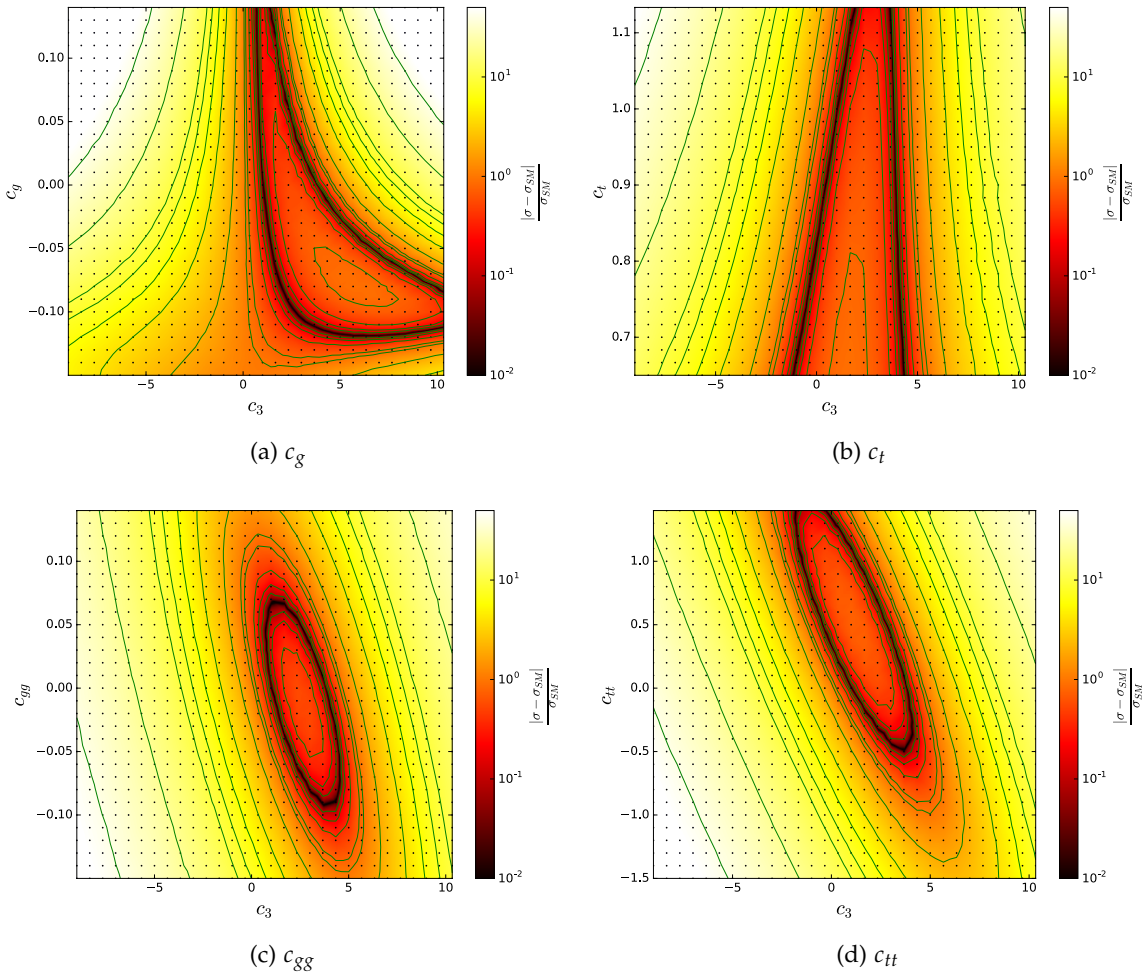

Figure 3.3: Heatmaps showing the total cross section in a coloured logarithmic scale as a function of pairs of anomalous couplings. The degenerate directions are drawn in green lines, in particular the black region of the heatmaps shows some combination of parameters degenerate with the SM. The points mark the grid in which the cross section was computed, and a cubic interpolation was done elsewhere for illustrative purposes.

From this analysis we conclude that, while the K-factor can be approximated by a constant (up to a 16% variation) when moving one coupling at a time away from its SM value, that no longer holds true if we allow a general deviation from the SM. When considering situations in which the cross section is small, the shape of the K-factor plays an important role and should be taken into account. Of course, the dependence of the

K-factor on the EFT parameters presented here are subject to modifications once the full top-mass effects are included at NLO (see Ref. [28]).

3.2.2 *Degeneracy of the parameters*

One important question that arises when considering several parameters is that of their degeneracy. The partonic cross section at LO in the HTL can be written as

$$\frac{\mathrm{d}\sigma_{LO}}{\mathrm{d}Q} = \frac{\mathrm{d}\sigma_{SM}}{\mathrm{d}Q} \frac{\left|\left[c_3(c_t + 12\,c_g)\right] C_\triangle + \left[-c_t^2 + c_{tt} + 12\,c_{gg}\right]\right|^2}{\left|C_\triangle - 1\right|^2}, \tag{3.35}$$

where $C_\triangle$ is defined in Eq. (3.14) and does not depend on the anomalous couplings. We see that the total cross section depends only on two linear combinations of the couplings, the ones inside the squared brackets.

In order to see the structure of the degeneracy at NNLO, we present in Figure 3.3 heatmaps of the relative deviation of the total Higgs pair production cross section from its SM value in four different two-dimensional slices of the parameter space. These slices correspond to the variation of the anomalous Higgs boson self-coupling together with the other four anomalous couplings separately.

We can see in Figure 3.3 that the structure of the degeneracy presented at LO in the HTL is preserved after including radiative corrections and reweighting by the exact Born cross section. In the two lower plots we see an elliptic pattern of degeneracies, which is related to the fact that the two couplings varied (c_3 and the couplings of gluons and top quarks to a pair of Higgs bosons) modify two different topologies of diagrams (triangle and box-like) and thus enter in two different terms in the amplitude. If we expand the square in Eq. (3.35) setting all other couplings to their SM values, we see that the expression is quadratic in the previously mentioned couplings, leading to an elliptic pattern of degeneracies. In the two upper plots, the two couplings varied modify the same diagram and enter in the final expression multiplicatively, resulting in a deformed pattern with respect to the two lower plots. It is easy, for example, to recognize in the first plot the family of parameters degenerated with the SM arising from the relation $c_3(1 + 12\,c_g) = 1$.

A consequence of the present degeneracies on the anomalous couplings is that, even in the case of a measurement for the total cross section compatible with the SM prediction, it would be possible to accommodate significant departures from the SM couplings (the dark bands on the heatmaps of Figure 3.3) without affecting the corresponding theoretical prediction. This means that the total cross section is not enough to distinguish between different scenarios and more observables are needed, e.g. differential distributions (see Refs. [75, 76]).

3.2.3 *Invariant mass distributions*

As we could see from section 3.2.2, the total cross section is not enough to discriminate between the effects of the different EFT parameters, and therefore differential distributions are needed. Our calculation allows us to compute the invariant mass distribution of the produced Higgs boson pair, thus providing a tool for breaking these degeneracies. In fact, because of the scalar character of the Higgs boson, there is no reason to expect strong angular dependencies and most of the information of the process can be extracted from the invariant mass and transverse-momentum distributions (see Ref. [75]).

In the SM, an almost exact destructive interference between the box and triangle diagrams occurs at the production threshold [77], resulting in an overall small cross section. At tree-level in the SM, because the triangle and box amplitudes are independently gauge invariant, we can write the cross section in terms of their contributions $\mathcal{M}_\triangle$ and $\mathcal{M}_{box}$ as

$$\mathrm{d}\sigma_{SM} \propto \left|\mathcal{M}_\triangle\right|^2 + \left|\mathcal{M}_{box}\right|^2 + 2\mathrm{Re}\left(\mathcal{M}_\triangle^* \mathcal{M}_{box}\right) \tag{3.36}$$

When changing the Higgs boson triple self-coupling, the cancellation is still destructive [78] but the balance between the triangle (which is affected by the self-coupling) and box (independent of the self-coupling) contributions changes, resulting in a fast increase in the cross section [77]. Also, when new (scalar or vector-like fermions) particles that couple to the Higgs boson are taken into account inside the loop (which corresponds to modifications of c_g and c_{gg} in the EFT), the cancellation between contributions also breaks down and the cross section grows [77]. This makes the threshold region very sensitive to BSM physics.

In Figure 3.4(a) we show the invariant mass distributions for different values of the Higgs boson anomalous self-coupling (c_3). As mentioned before, varying the self-coupling changes the balance between amplitudes in Eq. (3.36), resulting in more involved escenarios. When the self-coupling runs to large values, either positive or negative, the triangle amplitude dominates and we observe a boost of the cross section at threshold due to the Higgs boson propagator in the triangle contribution.

In Figure 3.4(b) we show combinations of anomalous couplings that render inclusive cross sections similar to the one of the SM (their relative deviations from the SM are shown between brackets on the label). They correspond to points of parameter space inside the black bands in Figure 3.3. Nevertheless, we can identify rather different behaviours for each of their invariant mass distributions. For instance for the green curve in Figure 3.4(b), when choosing $c_g = -0.8 \approx -\frac{1}{12}$, there is an almost exact cancelation between this term and the one proportional to $F_\triangle$ at LO in the HTL (see Eq. (3.13)), and thus $\mathcal{M}_\triangle \approx 0$. The resulting invariant mass distribution is given mostly by the box contribution ($|\mathcal{M}_{box}(Q)|^2$). In the other case, for the red curve, the value $c_{tt} = 1$ sets $\mathcal{M}_{box}$ to zero in the HTL, and this results in a distribution given primary by the triangle contribution ($\left|\mathcal{M}_\triangle(Q)\right|^2$), which shows the two peaks that arise from the pole on the Higgs propagator, the first one, and from the maximum of $\left|F_\triangle(Q)\right|$, the second one.

The substantial differences that we observe for these particular points in the parameter space in the shape of the invariant mass distributions shown in Figure 3.4 illustrate the fact that this observable can definitely help to disentangle the contributions from different operators which otherwise would be degenerated.

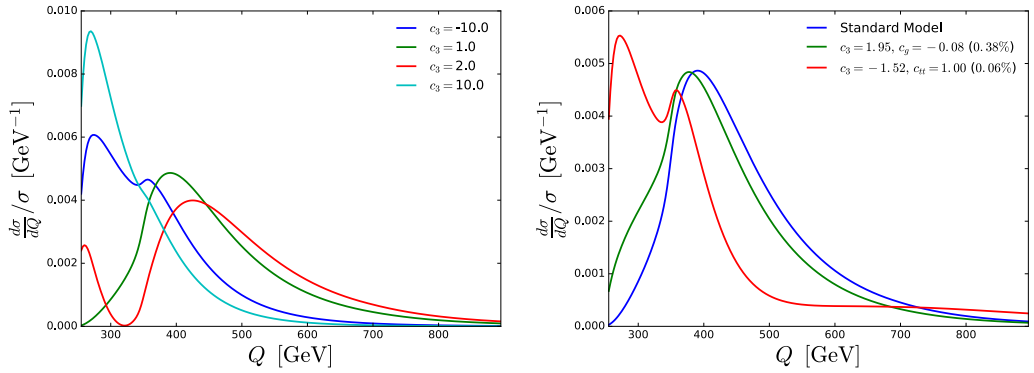

(a) (b)

Figure 3.4: Invariant mass distribution of the produced Higgs boson pair plotted for (a) different values of its self-coupling, and (b) different combinations of anomalous couplings that are degenerate with the SM. The relative deviation from the SM of the total cross section in (b) is specified between brackets on the label.

In this chapter we have analysed the impact of dimension 6 operators to Higgs pair production, in the context of the SMEFT, to NNLO accuracy in QCD in the heavy top approximation. These corrections have been combined in Ref. [47] with the NLO results with full top-quark mass dependence to provide the best predictions available so far for this kind of analysis. In the next chapter, we will focus on triple Higgs production, which is sensitive to the quartic Higgs boson self coupling, and compute the NNLO QCD corrections to the process in the HTL.

4

TRIPLE HIGGS BOSON PRODUCTION

In the SM, the triple and quartic self couplings of the Higgs, λ_3 and λ_4, are uniquely fixed by its mass m_H through the enforcement of gauge symmetries and renormalisability of the theory, namely $\lambda_3 = \lambda_4 = \lambda_{\text{SM}} = m_H^2/(2v^2)$, where $v \approx 246$ GeV is the Higgs vacuum expectation value. As discussed in the previous chapter, these couplings are directly accessible through double (for λ_3) and triple (for λ_4) Higgs boson production, although they might also be extracted indirectly from single Higgs production [16, 17, 76, 79–81] and precision electroweak observables [18, 82]. All of these measurements, however, are extremely challenging, and in particular already the determination of the triple self-coupling will prove very difficult at the high-luminosity phase of the LHC (see Ref. [83] for a review). Unfortunately, the much smaller triple-Higgs production rate makes the determination of λ_4 prohibitive at the LHC, and even challenging at future colliders [84, 85]. New physics effects, however, might change the prospects of measuring triple-Higgs production by inducing large enhancements of the cross section, and in this respect it is therefore desirable to provide precise predictions for the SM expectation.

As it occurs for single and double Higgs, the dominant triple Higgs production mechanism at hadron colliders is gluon fusion, mediated by a heavy-quark (mostly top quark) loop. This process, being gluon induced, is expected to present large QCD corrections. However, due to the massive loop appearing in the amplitude at Born level and the large number of external particles, the calculation of its higher order corrections is extremely challenging. As a consequence, the exact cross-section for triple Higgs production is only known at leading order (LO) in QCD [86, 87], while next-to-leading order (NLO) corrections are currently unknown. In order to provide precise predictions for triple Higgs production, approximate NLO corrections were calculated in Ref. [88] within the heavy top limit (HTL) for the virtual amplitudes, while keeping the exact dependence on the top mass m_t for the real emission diagrams (this approximation is denoted $\text{FT}_{\text{approx}}$). In Ref. [89] the NNLO virtual amplitudes where computed in the HTL, and the so-called soft-virtual approximation of the HTL NNLO corrections (NNLO_{SV}) was obtained [90]. Phenomenological results were presented by reweighting the NNLO_{SV} cross-section by the exact LO result (i.e. with full m_t dependence) [89], in what is known as the *Born-improved* (Bi) cross-section. In this chapter we improve on the results of Ref. [89] to go beyond the

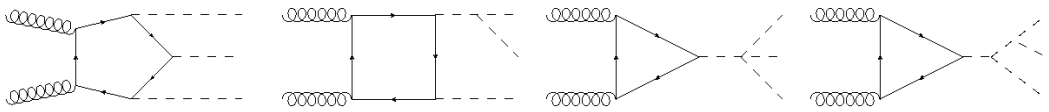

Figure 4.1: Diagrams that contribute to the LO triple Higgs production in the gluon fusion channel (modulo permutations of the final state bosons). We identify the pentagon $\mathcal{P}$ (left), box $\mathcal{B}$ (second from left) and triangles $\mathcal{T}_4$ and $\mathcal{T}_3$ (right) diagrams, respectively.

soft-virtual approximation, computing the complete set of NNLO QCD corrections for triple Higgs production within the HTL. In addition to that, we include partial finite-m_t effects by taking into account the NLO $\text{FT}_{\text{approx}}$ results of Ref. [88], thus providing a final estimate of the cross section that combines the most advanced results available to date.

The chapter is organised as follows. In Section 4.1 we examine the structure of the LO triple Higgs production cross-section and its dependence on λ_3 and λ_4. Then, in Section 4.2 we complete the calculation of the NNLO corrections in the HTL by adding the real emission corrections to the results presented in Ref. [89]. Then, in Section 4.3 we present the phenomenological results for triple Higgs production at the LHC and future hadron colliders. We estimate the dependence on the reweighting method by comparing the *Born-improved* result with a modified prescription (introduced in Ref. [46]), that we call *dynamically Born-improved*. Finally, we combine our result with the one presented in Ref. [88] to report our best prediction.

All of the results presented in this chapter have been published in Ref. [91].

4.1 THE AMPLITUDE AT LO

In this section we will examine the structure of the LO amplitude and cross-section. The Born amplitudes needed for the numerical calculation were obtained using RECOLA2 [92]. For the parton distribution functions we adopted the MMHT2014 [65] set interfaced via LHAPDF [69], while the CUBA [70] library was used to perform the numerical integration. The values implemented for the physical input parameters are $G_F = 1.16656 \times 10^{-5}$ GeV^{-2} for the Fermi constant, $m_H = 125$ GeV, $m_t = 173.2$ GeV and $\Gamma_H = \Gamma_t = 0$ for the masses and widths of the Higgs boson and the top quark, respectively, and $\alpha_S(m_Z) = 0.135$ for the strong coupling constant at LO, as provided by the MMHT2014 set. Throughout this work, the on-shell top quark mass scheme is used. All the plots in this section correspond to a collider centre of mass (CM) energy of 100 TeV, although we explicitly checked that all our conclusions also hold at 14 and 27 TeV.

For triple Higgs production, the relevant diagrams (modulo permutations of the final state particules) are shown in Figure 4.1. We can split them in four different categories: pentagons ($\mathcal{P}$), boxes ($\mathcal{B}$) and two triangle contributions ($\mathcal{T}_1$ and $\mathcal{T}_2$), each one of these with

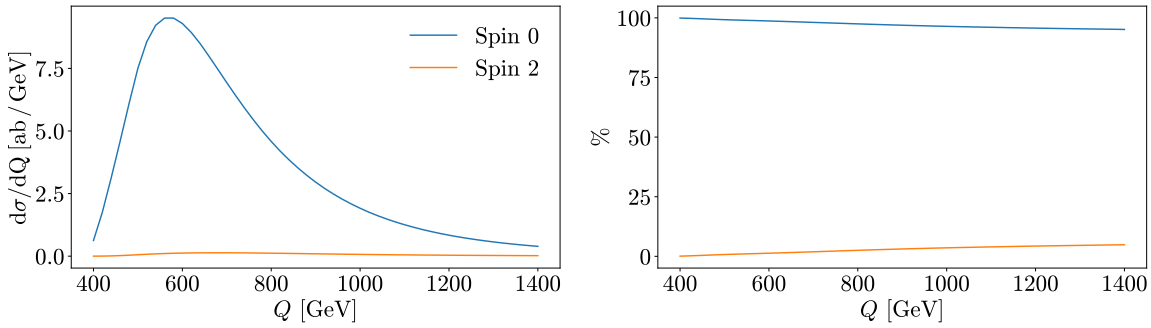

Figure 4.2: *Spin 0* ($\sim |\mathcal{M}_{++}|^2$) and *Spin 2* ($\sim |\mathcal{M}_{+-}|^2$) contributions to the invariant mass distribution of the triple Higgs system for collider CM energies of 100 TeV. The left plot shows the absolute contributions, while the right one shows the percentage.

a specific dependence on the parameters $\kappa_3 = \lambda_3/\lambda_{\text{SM}}$ and $\kappa_4 = \lambda_4/\lambda_{\text{SM}}$ that parametrise departures of the self couplings from the SM expectations,

$$\mathcal{M} = \mathcal{P} + \kappa_3\,\mathcal{B} + \kappa_3^2\,\mathcal{T}_3 + \kappa_4\,\mathcal{T}_4. \tag{4.1}$$

As in the case of double Higgs production [19], there are only two independent helicity configurations of the initial gluons, that we call

$$\mathcal{M}_{++} = \mathcal{M}_{--}, \qquad \text{“Spin 0"},$$
$$\mathcal{M}_{+-} = \mathcal{M}_{-+}, \qquad \text{“Spin 2"},$$

according to the value of total spin along the collision axis.

The *Spin 2* configuration vanishes in the limit $m_t \to \infty$, while the *Spin 0* configuration remains. We observe in Figure 4.2 that the contribution from the *Spin 2* piece is rather small (below 5% of the total cross-section). Also, we notice that triangle contributions $\mathcal{T}$ only contribute to the *Spin 0* helicity configuration, and therefore the *Spin 2* configuration is not sensitive to the quartic Higgs self coupling κ_4.

It is interesting to observe the share of the cross-section from each topological contribution and their corresponding interferences. In Figure 4.3 we show different contributions of the *Spin 0* component to the invariant mass distribution of the triple Higgs system. In the left panel we plot the interference structure between the $\mathcal{P}$ and the $\mathcal{B}$ diagrams, similar to the one usually presented for double Higgs production between the box and triangle contributions. This pattern can be better understood if we parametrise the amplitudes in terms of quark loop form factors (factoring out the Higgs boson couplings and propagators) and look at their behaviour in the HTL[1]:

$$\mathcal{T}_4 =: \frac{\alpha_s}{2\pi}\frac{Q^2}{3v^3}\,\frac{3m_H^2}{Q^2 - m_H^2}\,F_{\mathcal{T}}(Q^2)$$

1 Note that the normalization used in this chapter for $F_{\mathcal{T}}$ and $F_{\mathcal{B}}$ differs from the one used in chapter 3 for $F_{\triangle}$ and F_{box}.

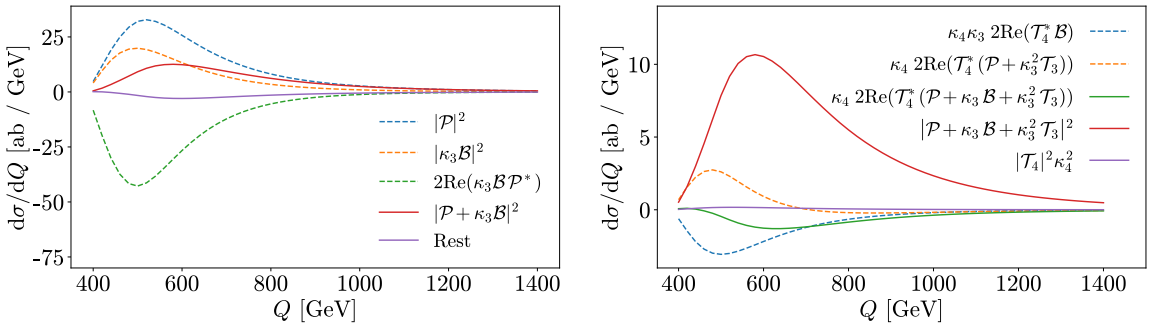

Figure 4.3: Different contributions to the *Spin 0* component of the invariant mass distribution. Left: In dashed lines we show the contributions from the pentagon and box diagrams, as well as their destructive interference, resulting in the red solid line. Right: The contributions separated by their κ_4 dependence. In dashed lines we show a similar destructive interference pattern, due to the sign difference between the box and the pentagon (and triangle) form factors, resulting in the green solid line.

$$
\begin{aligned}
\mathcal{T}_3 &=: \frac{\alpha_s}{2\pi}\frac{Q^2}{3v^3}\frac{\left(3m_H^2\right)^2}{Q^2-m_H^2}\sum_{(ij)}\frac{1}{s_{ij}-m_H^2}F_{\mathcal{T}}(s_{ij}) \\
\mathcal{B} &=: \frac{\alpha_s}{2\pi}\frac{Q^2}{3v^3}3m_H^2\sum_{(ij)}\frac{1}{s_{ij}-m_H^2}F_{\mathcal{B}}(Q^2,(p_i+p_j-p_1)^2,(p_i+p_j-p_2)^2,s_{ij},m_H^2) \\
\mathcal{P} &=: \frac{\alpha_s}{2\pi}\frac{Q^2}{3v^3}F_{\mathcal{P}}(p_1,p_2,p_3,p_4,p_5) \\
\implies \lim_{m_t\to\infty}F_{\mathcal{T}} &= \frac{1}{2}\lim_{m_t\to\infty}F_{\mathcal{P}} = -\lim_{m_t\to\infty}F_{\mathcal{B}} = 1,
\end{aligned}
\tag{4.2}
$$

where p_1 and p_2 is the four-momenta of the initial gluons, and p_i ($i=3,4,5$) the ones of the outgoing Higgs bosons, $Q^2=(p_1+p_2)^2$ and $s_{ij}=(p_i+p_j)^2$ are the squared invariant masses of the triple Higgs boson system and of the different pairs (ij), respectively, and $\sum_{(ij)}$ is a sum over the three different pairs $\{(34),(45),(53)\}$. The dominant contributions come from the pentagon and the box diagrams, as they are less suppressed by Higgs propagators, although the difference in sign between the $F_{\mathcal{P}}$ with $F_{\mathcal{B}}$ is responsible for a large negative interference between them. This effect is particularly strong at threshold, and therefore this region presents an enhanced sensitivity to any BSM effect that can alter the delicate cancellation between diagrams present in the SM.

In the right panel of Figure 4.3 we present, in solid lines, the contribution originated from different powers of κ_4. The quadratic dependence arises from the $\mathcal{T}_4$ triangle diagram, which is suppressed by a Higgs propagator ($\sim Q^{-2}$) making it negligible, with a contribution at the peak of $\sim 1.5\%$. The linear term has two contributions, plotted as dashed lines, that cancel each other to a large extent. This cancellation is due to the sign

difference of the form factors in Eq. (4.2), making the κ_4 linear contribution about a 15% of the κ_4-independent one.

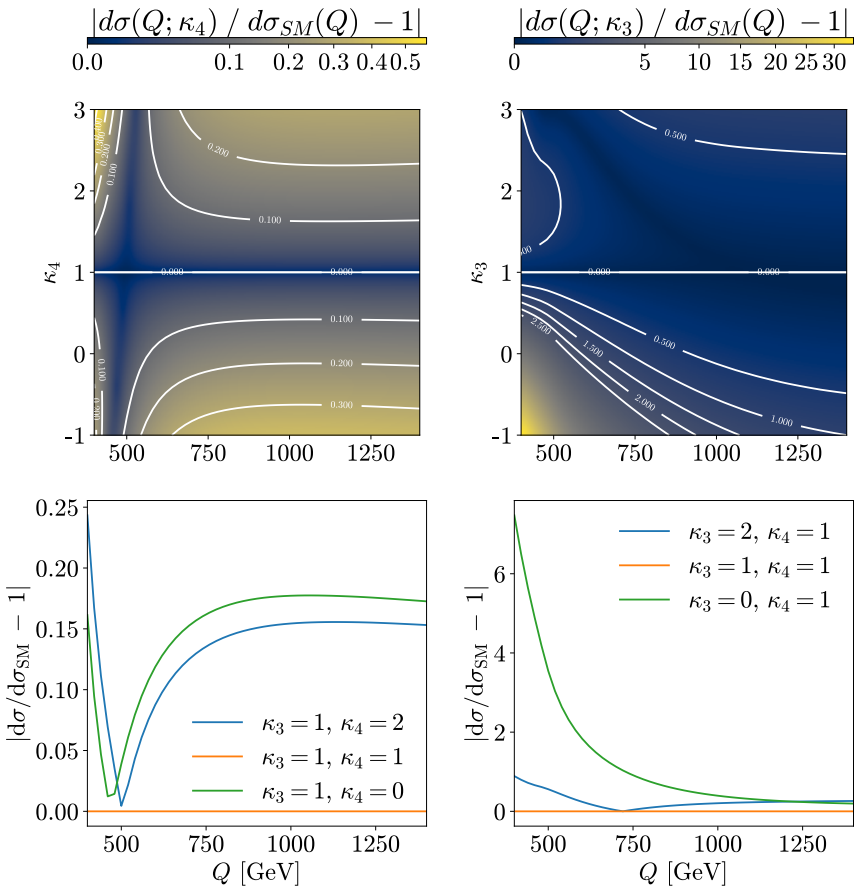

Figure 4.4: Departure from the SM of the triple Higgs boson invariant mass distribution for continuum (top) or discrete (bottom) values of κ_4 (left) and κ_3 (right). Due to the quadratic dependence of σ on the couplings, a nonlinear colormap is used for better visualisation.

Because of the different dependence on the self-couplings of the contributions presented in Eq. (4.1), a departure from the SM value $\kappa_{3,4} = 1$ might spoil the destructive interference patterns depicted in Figure 4.3. This can be seen clearly in Figure 4.4, where a large sensitivity to the κ_3 coupling is present particularly around the threshold, where the cross-section can be more than 30 times larger than the SM expectation. Indeed, deviations from $\kappa_3 = 1$ spoil the cancellation between the diagrams with most significant contributions, $\mathcal{P}$ and $\mathcal{B}$. In the case of κ_4, because it only affects the $2\mathrm{Re}((\mathcal{P}+\mathcal{B})\mathcal{T}_4^*)$ contribution, which is suppressed with respect to $|\mathcal{P}+\mathcal{B}|^2$, the regions of larger sensitivity are those in which the

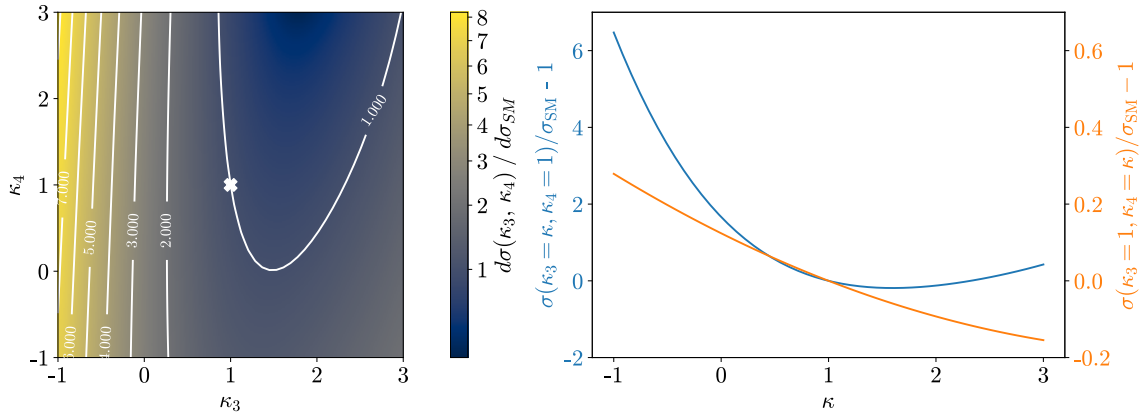

Figure 4.5: Departure of the inclusive cross-section as a function of κ_3 and κ_4 from its SM value. In the left plot the couplings are varied simultaneously and in the right one separately, keeping one fixed to the SM value. Due to the quadratic dependence of σ on the couplings, a nonlinear colormap is used for better visualisation.

latter is small, namely the production threshold (for $\kappa_3 = 1$) and the tail of the invariant mass distribution.

We can also analyse the dependence of the inclusive cross-section on the couplings $\kappa_{3,4}$, by performing variations with respect to the SM value, as shown in Figure 4.5. For illustrative purposes, both coupling modifiers are varied in the range $\kappa_i \in [-1; 3]$. While the dependence on κ_3 is large (e.g. $\sigma > 8\sigma_{\rm SM}$ for $\kappa_3 \sim -1$ and $\kappa_4 = 1$) and quadratic contributions become noticeable, the dependence on κ_4 is rather small (with departures of $|\sigma/\sigma_{\rm SM} - 1| < 28\%$ in the range under study), which is compatible with the right panel of Figure 4.3 that shows the $|\mathcal{T}_4|^2$ contribution to the invariant mass distribution.

4.2 NNLO CORRECTIONS

After discussing the different contributions to the LO cross-section in the previous section, we will present the results for the full NNLO corrections in the HTL.

As we discussed in the previous chapter, in the HTL the Higgs bosons couple directly to gluons via the effective Lagrangian

$$\mathcal{L}_{\rm eff} = -\frac{1}{4} G^a_{\mu\nu} G^{\mu\nu}_a \left(C_H \frac{h}{v} - C_{HH} \frac{h^2}{2v^2} + C_{HHH} \frac{h^3}{3v^3} + \dots \right), \tag{4.3}$$

where the matching coefficients can be expanded in powers of the strong coupling constant α_s as

$$C_X = -\frac{\alpha_s}{3\pi} \sum_{n \geq 0} C_X^{(n)} \left(\frac{\alpha_s}{\pi} \right)^n, \tag{4.4}$$

where the expansion is known up to fourth order for $X = H$, HH, HHH [32, 54–59].

The computation of the complete NLO corrections and of the virtual amplitudes up to NNLO, both in the HTL, was presented in Ref. [89]. The latter were used to construct the soft-virtual approximation (based on the results from Ref. [90]) to provide a phenomenological NNLO_{SV} cross-section. In the present work we computed the real emission amplitudes to obtain a full NNLO cross-section in the HTL, including all partonic channels in addition to gluon-fusion. To this end, we exploited the known relation between the single Higgs boson cross-section and some contributions to the multiple Higgs one. This is done in the same fashion as the calculation for double Higgs production discussed in chapter 3.

Contributions involving only one HTL operator at the amplitude level (i.e. a single effective vertex between Higgs bosons and gluons) are totally equivalent, apart for an overall normalization and the corresponding matching coefficient, to those from single Higgs production. In terms of the degree of difficulty, these contributions are *truly* at the NNLO level, but the results can be borrowed from single Higgs production, exploiting the above mentioned similarities. On the other hand, when considering diagrams with more than one HTL operator insertion (actually, their interference with the ones with just one insertion), as each of them carries an extra coupling $C_X = \mathcal{O}(\alpha_s)$, only tree level configurations can appear to NLO, while at NNLO accuracy the only possible contributions arise from one-loop and single real emission diagrams. Because of this simplification, their infrared divergences can actually be handled with standard NLO procedures.

In our calculation, the FeynArts [93] and FeynCalc [94, 95] packages were used to compute the amplitudes. The cancellation of their infrared singularities with the ones present in the virtual amplitudes presented in Ref. [89] and the absorption of the remaining ones into the evolution of the parton distribution functions was performed following the FKS [14, 15] approach described in section 2.3. In this work we neglect effects coming from the Higgs width, and set it equal to zero throughout the calculation.

We present below the final result with a notation suitable for the discussion on the reweighting following in Section 4.2.1. More details on the derivation can be found in Appendix B.

As discussed in section 2.2, the cross-section can be written as

$$\frac{\mathrm{d}\sigma}{\mathrm{d}Q^2} = \sum_{i,j} \int_0^1 \mathrm{d}x_1\, \mathrm{d}x_2\, f_{i/h_1}(x_1) f_{j/h_2}(x_2) \int_0^1 \mathrm{d}x\, \delta\left(x - \frac{Q^2}{x_1 x_2 s_H}\right) \frac{\mathrm{d}\hat{\sigma}_{ij}}{\mathrm{d}Q^2}, \tag{4.5}$$

where Q is the invariant mass of the triple Higgs system, $\sqrt{s_H}$ the collider centre of mass energy, and i, j are the labels for the massless partons inside the hadrons h_1 and h_2 with respective parton density $f_{(i,j)/(h_1,h_2)}$. Here the dependence on the factorisation and the renormalisation scales is implicitly understood.

The partonic cross-section $\hat{\sigma}$ is computed order by order as an expansion in the strong coupling α_S, such that up to NNLO we write it as

$$Q^2 \frac{\mathrm{d}\hat{\sigma}_{ij}}{\mathrm{d}Q^2} = \frac{1}{2Q^2 3!\, 2^2} \int \mathrm{dPS}_3 |\mathcal{M}_{3H}|^2 \left[\eta_{ij}^{(0)} + \left(\frac{\alpha_s}{2\pi}\right) \eta_{ij}^{(1)} + \left(\frac{\alpha_s}{2\pi}\right)^2 \eta_{ij}^{(2)} + \mathcal{O}(\alpha_s^3) \right], \quad (4.6)$$

where the LO amplitude $\mathcal{M}_{3H}$ can generically be written as

$$\mathcal{M}_{3H} = \left(\frac{\alpha_s}{2\pi}\right) \frac{Q^2}{3v^3} C_{\mathrm{LO}}^{3H}, \quad (4.7)$$

and

$$\begin{aligned} C_{\mathrm{LO}}^{3H}(p_1, p_2, p_3, p_4, p_5) =& F_{\mathcal{P}}(p_1, p_2, p_3, p_4, p_5) + F_{\mathcal{T}}(Q^2) \frac{3m_H^2 \kappa_4}{Q^2 - m_H^2} \\ &+ \sum_{(kl)} \frac{1}{s_{kl} - m_H^2} \Big[\frac{(3m_H^2 \kappa_3)^2}{Q^2 - m_H^2} F_{\mathcal{T}}(Q^2) + 3m_H^2 \kappa_3 \\ &\times F_{\mathcal{B}}(Q^2, (p_k + p_l - p_1)^2, (p_k + p_l - p_2)^2, s_{kl}, m_H^2) \Big]. \end{aligned} \quad (4.8)$$

The perturbative coefficients $\eta_{ij}^{(0,1,2)}$, within the HTL approximation and its extensions (reweightings) described in Section 4.2.1, are up to NNLO

$$\eta_{ij}^{(0)} = \eta_{ij}^{H\,(0)} = \delta(1-x)\delta_{ig}\delta_{jg}, \quad (4.9)$$

$$\eta_{ij}^{(1)} = 2\,\eta_{ij}^{H\,(1)} + \eta_{ij}^{H\,(0)} \frac{4}{3} \frac{\mathrm{Re}\left((C_{\mathrm{LO}}^{3H})^* \sum_{(kl)} C_{\mathrm{LO}}^{2H}(\{k,l\}) \right)}{|C_{\mathrm{LO}}^{3H}|^2}, \quad (4.10)$$

$$\begin{aligned} \eta_{ij}^{(2)} =& 4\,\eta_{ij}^{H\,(2)} + 4\eta_{ij}^{H\,(0)} \frac{2\,\mathrm{Re}\left((C_{\mathrm{LO}}^{3H})^* \left((C_{HHH}^{(2)} - C_H^{(2)})\mathcal{P} + (C_{HH}^{(2)} - C_H^{(2)})\kappa_3 \mathcal{B} \right) \right)}{|C_{\mathrm{LO}}^{3H}|^2} \\ &+ \eta_{ij}^{H\,(0)} \frac{\mathrm{Re}\left((C_{\mathrm{LO}}^{3H})^* (\mathcal{R}_{3H}^{(2)} + (C_{\mathrm{LO}}^{3H})^3\, \mathcal{T}_{3H}^{(2)}) \right) + \mathcal{V}_{3H}^{(2)} |C_{\mathrm{LO}}^{H}|^2}{|C_{\mathrm{LO}}^{3H}|^2} + \rho_{ij}^{(2)}, \end{aligned} \quad (4.11)$$

where $\eta_{ij}^{H,(n)}$, $n = 0, 1, 2$, are the corresponding QCD corrections for single Higgs production that can be found in Ref. [60] (and coincide with the results in Refs. [61, 62]), the renormalisation and factorisation scales were set to $\mu_F = \mu_R = Q$, k and l label the final state Higgs bosons, and $\sum_{(kl)}$ denotes the sum over distinct pairs of them. C_{LO}^{H} and C_{LO}^{2H} are (up to a normalisation factor) the LO amplitudes for single and double Higgs production

$$C_{\mathrm{LO}}^{H} = F_{\mathcal{T}}(m_H^2), \quad (4.12)$$

$$C_{\mathrm{LO}}^{2H}(\{k,l\}) = \frac{3m_H^2}{s_{kl} - m_H^2} F_{\mathcal{T}}(s_{kl}) + F_{\mathcal{B}}(\{k,l\}), \quad (4.13)$$

and the coefficients $\mathcal{R}_{3H}^{(2)}$, $\mathcal{T}_{3H}^{(2)}$ and $\mathcal{V}_{3H}^{(2)}$ are the finite remainders of the virtual corrections at NNLO presented in Ref. [89], with the only difference being that we use (as we will discuss later) the general definition of Eq. (4.2) for $C_{\rm LO}^{2H}$. If we express this coefficient in the HTL, the expressions are identical to those in Ref. [89].

The only missing ingredient, $\rho_{ij}^{(2)}$, corresponds to the finite remainder of the real emission corrections to the diagrams with more than one HTL operator insertion (the ones with a single HTL operator insertion are already included in $\eta_{ij}^{H(2)}$). These only contain diagrams with a single parton emission whose divergences were regulated using dimensional regularisation in $D = 4 - 2\epsilon$ dimensions in the FKS [14, 15] framework described in section 2.3. After subtracting the singularities, we can write the remainder as

$$\begin{aligned}\rho_{ij}^{(2)} = &\frac{4}{3}\frac{\mathrm{Re}\left((C_{\rm LO}^{3H})^* \sum_{(kl)} C_{\rm LO}^{2H}(\{k,l\})\right)}{|C_{\rm LO}^{3H}|^2}\rho_{ij}^{(sc)} \\ &+ \int_0^{2\pi} \mathrm{d}\phi \int_{-1}^{1} \mathrm{d}y \, \frac{1}{2}\left(\frac{1}{1-x}\right)_+ \left[\left(\frac{1}{1-y}\right)_+ + \left(\frac{1}{1+y}\right)_+\right] \rho_{ij}^{(r)}(x,y,\phi)\end{aligned} \tag{4.14}$$

that contains a soft-collinear term $\rho_{ij}^{(sc)}$ (arising from $\mathrm{d}\hat{\sigma}^{(sv)} + \mathrm{d}\hat{\sigma}^{(c+)} + \mathrm{d}\hat{\sigma}^{(c-)}$ defined in Eqs. (2.88) - (2.90)) and a regular term $\rho_{ij}^{(r)}$ (arising from $\mathrm{d}\hat{\sigma}^{(f)}$ in Eq. (2.91)) whose explicit expressions are given in Appendix B.

4.2.1 *Reweighting*

The results presented in this section complete the full NNLO corrections to triple Higgs production in the HTL when the quantities $F_{\mathcal{P}}$, $F_{\mathcal{B}}$ and $F_{\mathcal{T}}$ are expressed in this limit (see Eq. (4.2)). In order to retain part of the m_t dependence, this expression is usually reweighted by using the exact result for $\mathcal{M}_{3H}$ in Eq. (4.6), while keeping the coefficients $\eta_{ij}^{(0,1,2)}$ in the HTL. This procedure is usually referred to as the *Born-improved* (Bi) NNLO cross-section, and its accuracy has been studied for double Higgs production [27–29] at NLO finding that it overestimates the exact inclusive cross-section by a 32% at collider energies of 100 TeV (and around 16% at 14 TeV). This overestimation is enhanced in the tail of the Higgs pair invariant mass distribution.

In order to parametrise the dependence of the result on the reweighting procedure, we also considered the *dynamically-Born-improved* (dBi) NNLO cross-section, already used in chapter 3 in the context of double Higgs produciton, which we obtain by using the full dependence on the kinematics of the outgoing particles of $F_{\mathcal{T}}$, $F_{\mathcal{B}}$ and $F_{\mathcal{P}}$ in the definitions of $\mathcal{P}$, $\mathcal{B}$, $C_{\rm LO}^{H}$ and $C_{\rm LO}^{2H}$, and therefore also in the definitions of $\mathcal{R}_{3H}^{(2)}$,$\mathcal{T}_{3H}^{(2)}$, $\mathcal{V}_{3H}^{(2)}$ and $\rho_{ij}^{(2)}$. In this way, we reweight the HTL insertion operators with the respective LO amplitude diagram by diagram (e.g. the $(H)Hgg$ vertex with the (double) single Higgs production amplitude $\sim C_{\rm LO}^{(2)H}$). Different than in the previous chapter, for triple Higgs production the

reweight cannot be applied in a straightforward way, as the form factor $F_{\mathcal{B}}$ is not always defined for the kinematics characterising the HTL vertex. This happens in diagrams with two HTL vertices connected via an off-shell gluon (e.g. a box and a triangle loop). To fix this problem, we modify the kinematics in a way such that we preserve the momenta of the outgoing Higgs bosons, while redefining the momenta of the gluons entering the vertex to be on-shell.

For the triangle form factor $F_{\mathcal{T}}$, we evaluate it at the invariant mass of the outgoing Higgs boson, just as expressed in the Eqs. (4.12) and (4.13). For the box form factor $F_{\mathcal{B}}$ appearing in Eq. (4.13), we need to define a prescription that corrects the momenta of the initial gluons to compensate for the recoil of all other particles not involved in the HTL vertex. Lets recall we are labelling p_1 and p_2 as the momenta of the incoming partons, and $p_{(3,4,5)}$ the momenta of the outgoing Higgs Bosons. For the vertex with outgoing Higgses $\{i,j\}$, we define $q := p_i + p_j$, $M^2 := q^2$, and q_T^μ as the transverse component of q with respect to p_1 and p_2, and then define the momenta of the gluons entering the form factor as k_1 and $k_2 := q - k_1$ in the following way

$$F_{\mathcal{B}}(\{i,j\}) = F_{\mathcal{B}}((k_1+k_2)^2, (k_1-p_i)^2, (k_1-p_j)^2, m_H^2, m_H^2), \tag{4.15}$$

$$k_1^\mu := z_1 \frac{M^2}{2q\cdot p_1} p_1^\mu + \xi q_T^\mu + \frac{\xi \boldsymbol{q_T}^2}{z_1} \frac{q\cdot p_1}{M^2 p_1\cdot p_2} p_2^\mu, \qquad (q_T^\mu q_{T\mu} =: -\boldsymbol{q_T}^2), \tag{4.16}$$

$$z_1 := \frac{M^2 + 2\xi \boldsymbol{q_T}^2 + \sqrt{(M^2+2\xi\boldsymbol{q_T}^2)^2 - 4(M^2+\boldsymbol{q_T}^2)\xi^2\boldsymbol{q_T}^2}}{2M^2}, \tag{4.17}$$

where the different choices of $\xi \in [0, 1/2]$ define different consistent prescriptions to account for the Higgs pair recoil. This prescription corresponds to the one presented in Ref. [96] in the context of transverse-momentum resummation, if one chooses $\boldsymbol{k_{1T}} = \xi \boldsymbol{q_T}$ for the Eqs. (25) and (26) therein. In particular, if $\xi = 0$ the transverse recoil is compensated by one gluon ($\boldsymbol{k_{1T}} = 0, \boldsymbol{k_{2T}} = \boldsymbol{q_T}$) while if $\xi = 1/2$ it is equally compensated by both gluons ($\boldsymbol{k_{1T}} = \boldsymbol{k_{2T}} = \boldsymbol{q_T}/2$).

Let us emphasise that this prescription leaves unchanged the momenta of all the Higgs bosons involved, including their virtuality, and its main purpose is to redefine the momenta of the virtual gluons entering Box diagrams, so that these are on-shell and $F_{\mathcal{B}}$ is well defined.

With this prescription, the *dynamically Born improved* approximation is well defined and we will denote it as dBi_ξ. In particular, we will present results for dBi_0 and $\text{dBi}_{1/2}$ as benchmarks to show the dependence on the choice of ξ, and we will show that this dependence is numerically negligible at NLO and NNLO.

4.3 RESULTS

We present results for the NNLO cross-section for triple Higgs production, reweighted using the Bi, dBi_0 and $\text{dBi}_{1/2}$ prescriptions. The set-up is the same as the one used in

Section 4.1. We use the MMHT2014 [65] set of parton distributions, at the corresponding order in the strong coupling constant for each contribution (LO, NLO, NNLO). For phenomenological purposes, we compute this for collider energies of 100 TeV and 27 TeV that are relevant for physics at the Future Circular Collider and High-Energy LHC, respectively. To estimate the theoretical uncertainty arising from the missing higher orders in the perturbative series, we perform an independent variation of the factorisation and renormalisation scales in the range $[\mu_0/2, 2\mu_0]$, with the constrain $0.5 < \mu_R/\mu_F < 2$. The choice of the central values μ_0 used in this work were $\mu_0 = Q/2$ and $\mu_0 = Q$, where Q is the invariant mass of the triple Higgs system.

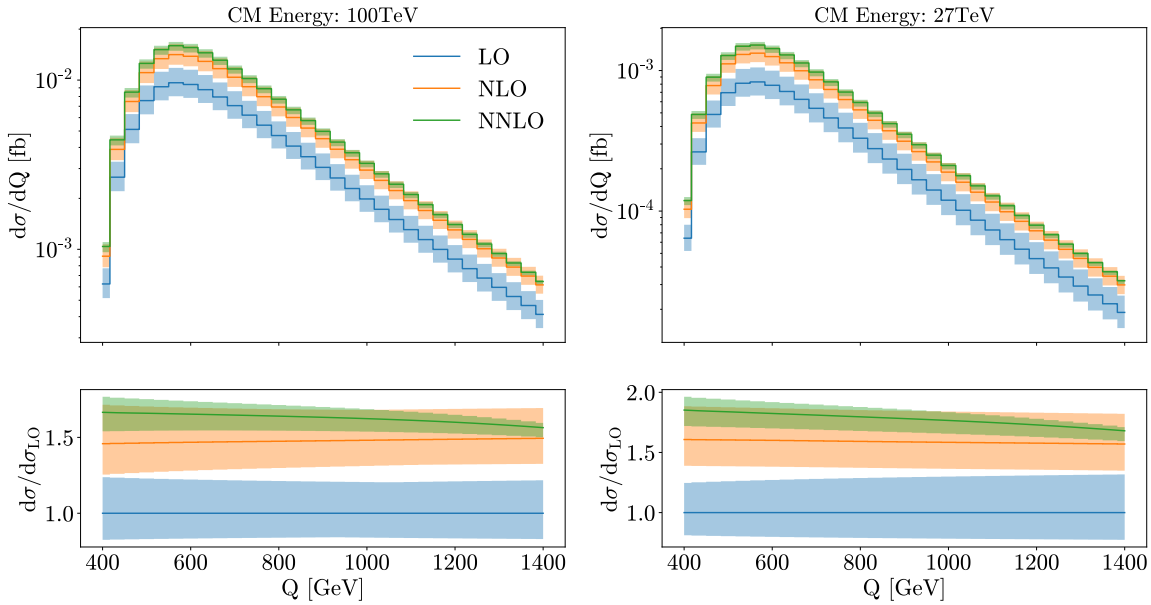

Figure 4.6: Invariant mass distribution of the triple Higgs system in the dBi approximation up to different orders (up) and corresponding K factor (down). The results are shown for a collider center of mass energy of 100 TeV (left) and 27 TeV (right). The shaded bands correspond to the uncertainty from the variation of scales from the central value of $\mu_0 = Q/2$.

In Figure 4.6 we see the cross-section computed in the dinamically Born improved approximation up to different orders, as well as the K factor defined as usual, $K = \mathrm{d}\sigma / \mathrm{d}\sigma_{\mathrm{LO}}$. As seen also within the soft-virtual approximation [89], the cross-section begins to stabilise only from NNLO. The K factors are rather flat at the peak of the invariant mass distribution, with values around 1.7 and 1.8 for collider CM energies of 100 and 27 TeV respectively, while the NNLO K factors present a suppression in the tail. Due to this suppression, the entire NNLO band falls inside the scale variation of the NLO, suggesting that the perturbative series is more stable in this region. The total scale uncertainty is reduced from 37% to 27% and to 11% when going from LO to NLO to NNLO, at 100 TeV

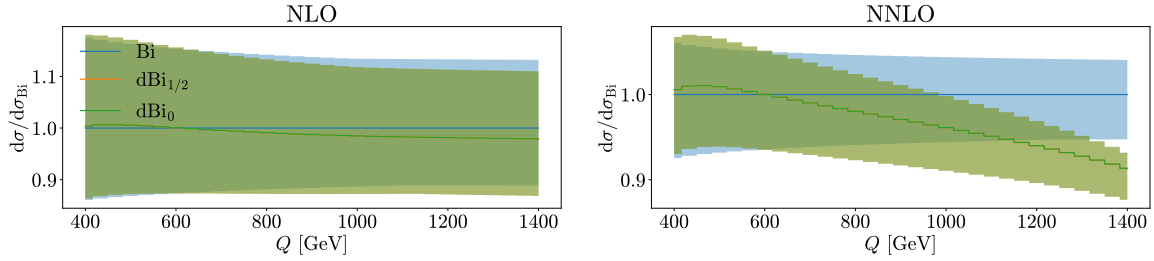

Figure 4.7: Comparison between the Bi, dBi_0 and $\mathrm{dBi}_{1/2}$ reweights to the triple Higgs boson invariant mass distribution. The result is shown at NLO (left) and NNLO (right) in the α_S expansion. There are no visible differences between the dBi_0 and $\mathrm{dBi}_{1/2}$ bands, as they overlap completely. The shaded bands correspond to the uncertainty from the variation of scales from the central value of $\mu_0 = Q/2$.

with a central scale choice of $\mu_0 = Q/2$. For 27 TeV the reduction is similar, from 48% to 30% and then to 12%.

To measure the effect of the reweighting, we can compare the different approximations Bi, dBi_0 and $\mathrm{dBi}_{1/2}$ and observe the corresponding effect on the invariant mass distribution. In Figure 4.7 we see that, although at NLO the three approximations are almost completely compatible, at NNLO there is a significant decrease in the tail of the distribution when using a $\mathrm{dBi}_{\tilde{\xi}}$ instead of the Bi approximation, a discrepancy that is even bigger than the scale variation in this region. We also notice that the dependence on $\tilde{\xi}$ of the $\mathrm{dBi}_{\tilde{\xi}}$ approximation is phenomenologically negligible. We know that for double Higgs production the Bi approximation overestimates the tail of the distribution at NLO respect to the exact calculation [27–29]. If this effect holds also for triple Higgs production, we can expect the dBi approximation to provide more reliable predictions, as it predicts a smaller tail of the distribution just by reweighting each contribution by the associated form factor instead of using the full amplitude.

In order to understand why the discrepancies in the tail of the invariant mass distribution between the Bi and dBi prescriptions arise only at NNLO, lets recall what are the main differences between the two reweighting procedures. The Bi reweights all amplitudes by the Born amplitude, including those that have more than one HTL vertex. The dBi only does this to amplitudes containing a single HTL vertex, while applying a different prescription for those amplitudes with more than one HTL vertex. In this way, the Bi reweighting procedure increases the relative significance of the amplitudes with many HTL vertices, respect to the dBi. At NLO such amplitudes appear only at tree level, due to the power counting of the HTL vertices, making the discrepancy phenomenologically negligible. At NNLO, such diagrams are enhanced by real emission corrections, making the discrepancy at the tail of the invariant mass distribution more noticeable.

In Table 4.1 we present the results for the inclusive cross-section obtained for different collider energies, choices of central scales μ_0, reweighting procedures and orders in the

$\mu_0 = Q$	14 TeV	27 TeV	100 TeV
LO	$0.0462^{+31\%}_{-22\%}$	$0.235^{+26\%}_{-19\%}$	$3.29^{+20\%}_{-15\%}$
NLO_{Bi}	$0.0833^{+18\%}_{-15\%}$	$0.408^{+16\%}_{-13\%}$	$5.12^{+14\%}_{-11\%}$
NLO_{dBi}	$0.0831^{+18\%}_{-15\%}$	$0.407^{+16\%}_{-13\%}$	$5.09^{+14\%}_{-12\%}$
NNLO_{Bi}	$0.105^{+8\%}_{-9\%}$	$0.503^{+7\%}_{-8\%}$	$6.11^{+6\%}_{-7\%}$
NNLO_{dBi}	$0.104^{+8\%}_{-9\%}$	$0.498^{+7\%}_{-8\%}$	$6.02^{+6\%}_{-7\%}$
$\mu_0 = Q/2$	14 TeV	27 TeV	100 TeV
LO	$0.0605^{+34\%}_{-24\%}$	$0.295^{+28\%}_{-20\%}$	$3.88^{+21\%}_{-16\%}$
NLO_{Bi}	$0.0983^{+18\%}_{-15\%}$	$0.473^{+16\%}_{-14\%}$	$5.75^{+15\%}_{-12\%}$
NLO_{dBi}	$0.0982^{+18\%}_{-15\%}$	$0.471^{+17\%}_{-14\%}$	$5.72^{+15\%}_{-12\%}$
NNLO_{Bi}	$0.114^{+5\%}_{-8\%}$	$0.540^{+5\%}_{-7\%}$	$6.47^{+5\%}_{-6\%}$
NNLO_{dBi}	$0.113^{+5\%}_{-8\%}$	$0.534^{+5\%}_{-7\%}$	$6.36^{+5\%}_{-6\%}$
$\text{NNLO}_{\text{Best}}$	$0.103^{+5\%}_{-8\%}$	$0.501^{+5\%}_{-7\%}$	$5.56^{+5\%}_{-6\%}$

Table 4.1: Results for the inclusive cross-section (in fb) of triple Higgs boson production for different collider energies, calculated at different orders and with the different reweighting procedures. The results are shown for central scale values of Q (top) and $Q/2$ (bottom). The dependence on ξ in the dBi_ξ reweight procedure is below the per-mill level and therefore omitted. The last row shows our best available prediction for the different collider energies. The uncertainties correspond to the scale variation.

perturbative expansion. The corresponding K factors for the dBi results are presented in Table 4.2. When comparing our results with the ones obtained in Ref. [89] in the soft-virtual approximation, we find that although the SV result differs only in about 1% from the full NNLO in the HTL, when using the Bi reweight the difference grows to a 2.5% and 4.4% increase in the inclusive cross-section at 14 TeV and 100 TeV, respectively. This larger difference is due to the fact that in the HTL the SV approximation is slightly smaller than the complete NNLO for small invariant masses, but compensates at large invariant masses, resulting in a small difference in the inclusive cross section. After the reweighting procedure, the region of large invariant masses is suppressed, and therefore this accidental compensation is reduced, increasing the difference in the inclusive cross sections between SV and complete NNLO.

The different reweighting procedures produce a small difference ranging from $\sim 0.7\%$ at 14 TeV up to $\sim 1.3\%$ at 100 TeV. Although in Figure 4.7 we see that the different reweights

$\mu_0 = Q$	14 TeV	27 TeV	100 TeV
K_{NLO}	1.80	1.732	1.56
K_{NNLO}	2.27	2.12	1.55
$\mu_0 = Q/2$	14 TeV	27 TeV	100 TeV
K_{NLO}	1.63	1.60	1.47
K_{NNLO}	1.87	1.81	1.64
$K_{\text{NNLO-Best}}$	1.70	1.70	1.43

Table 4.2: NLO and NNLO K factors for the inclusive triple Higgs boson production at different collider energies. These defined as the quotient between the dBi and the LO cross section. The results are shown for central scale values of Q (top) and $Q/2$ (bottom). The dependence on ξ in the $\text{dBi}_{\tilde{\xi}}$ reweight procedure is below the per-mill level and therefore omitted. The last row shows our best available prediction for the different collider energies.

lead to discrepancies larger than the theoretical uncertainties in the tail of the distribution, since this region has a small impact on the inclusive cross-section the results for the total cross-section are consistent within the theoretical uncertainties. Of course, this small difference at the total cross section level can only be a lower bound on the expected finite top mass effects, and from the results obtained at NLO within the $\text{FT}_{\text{approx}}$ (which are $\sim 10\%$ smaller than the dBi prediction) it is clear that they are expected to be much larger. What we can conclude from this exercise therefore, is that the systematic uncertainties related to the choice of the reweighting procedure (among the choices presented here) is expected to be marginal compared to the full size of the finite-m_t effects.

In order to provide the best possible estimate of the triple-Higgs production cross section, it becomes necessary to include the partial finite-m_t effects obtained in Ref. [88] within the $\text{FT}_{\text{approx}}$. To this end, we use the predictions presented therein and in Ref. [97] for the total cross section, and encode the finite mass effects in the parameter δ_t defined by

$$\sigma^{\text{NLO}}_{\text{FTapprox}} = \sigma^{\text{NLO}}_{\text{dBi}}(1+\delta_t)\,, \tag{4.18}$$

and we define our best prediction as

$$\sigma^{\text{NNLO}}_{\text{Best}} = \sigma^{\text{NNLO}}_{\text{dBi}} + \delta_t \sigma^{\text{NLO}}_{\text{dBi}}\,. \tag{4.19}$$

This procedure is similar to the prescription that was implemented in Ref. [97] for double-Higgs production. The values that we obtain for δ_t at the different collider energies are

δ_t = -0.107, -0.073 and -0.146 for 14, 27 and 100 TeV, respectively.[2] The corresponding cross sections and K factors are presented in Tables 4.1 and 4.2, respectively.

Before providing our final results, we address the issue of the remaining uncertainties associated to finite-m_t effects. There is in principle no reason to expect these effects to be smaller than the corresponding ones present in double Higgs production; in fact the typically larger invariant masses involved might point to the opposite direction. Of course, the more complicated structure of the triple Higgs production amplitudes, involving additional topologies, might lead to accidental cancellations of these effects that cannot be predicted at this point. In the absence of any prediction with full top mass dependence beyond the LO, one can only rely on approximated results in order to estimate the associated uncertainties at NNLO. The best available approximation at NLO, the $\text{FT}_{\text{approx}}$, differs from the Born-improved NLO at $\mathcal{O}(10\%)$ at 14 and 27 TeV, and $\mathcal{O}(15\%)$ at 100 TeV. The size of this difference can be a good estimation of the missing finite top mass effects, and indeed this is the case for the double-Higgs production cross section. In order to provide a conservative estimation, and having in mind the possibly worse situation in triple Higgs as compared to Higgs pair production, we estimate the uncertainty of our prediction to be of $\pm 15\%$ at 14 and 27 TeV, and $\pm 20\%$ at 100 TeV.

Given that the full dependence on the top mass is only retained at LO, it is not possible to perform a complete analysis on the top mass scheme uncertainty (which was found to be large at NLO in the case of double Higgs [29]). Nevertheless, a parametric variation of the default on-shell value $m_t = 173.2$ GeV used along this work to the correspondent one in the $\overline{\text{MS}}$ scheme, $\overline{m}_t(\overline{m}_t) = 163.6$ GeV (using a three-loop conversion between schemes), shows a decrease of about 25% in the cross section, which indicates an uncertainty in line with the one estimated for the finite top mass effects.

Compiling all the ingredients described in the last paragraphs, we arrive therefore to the following final prediction for the triple Higgs production cross section:

$$\sigma^{\text{NNLO}}_{\text{Best}} = 0.103^{+5\%}_{-8\%} \pm 15\%\,\text{fb}, \qquad K^{\text{NNLO}}_{\text{Best}} = 1.70, \qquad (14\ \text{TeV})$$

$$\sigma^{\text{NNLO}}_{\text{Best}} = 0.501^{+5\%}_{-7\%} \pm 15\%\,\text{fb}, \qquad K^{\text{NNLO}}_{\text{Best}} = 1.70, \qquad (27\ \text{TeV})$$

$$\sigma^{\text{NNLO}}_{\text{Best}} = 5.56^{+5\%}_{-6\%} \pm 20\%\,\text{fb}, \qquad K^{\text{NNLO}}_{\text{Best}} = 1.43. \qquad (100\ \text{TeV})$$

The results presented in this chapter correspond to the best predictions so far for triple Higgs production, which will become an important process in future hadronic colliders, as it will give direct access to the quartic self coupling of the Higgs boson. These results, together with the ones presented in previous chapter 3, conform the first part of this thesis. In the next part, we will focus on the associated production of a top-quark pair with a Higgs boson.

2 The value corresponding to 27 TeV was extracted from results of [88] computed at 33 TeV, which is the closest one in energy available in the literature.

Part II

ASSOCIATED PRODUCTION OF A TOP-QUARK PAIR AND A HIGGS BOSON

The NNLO computation of a $t\bar{t}h$ final state would allow for a precise determination of the Yukawa coupling of the top quark. In order to achieve such precision, a framework to handle its infrared divergences has to be developed. In this part, we will extend the q_T-subtraction framework to the associated production of a top quark pair with a colourless particle, and apply it to compute the NLO cross section and NNLO counter-terms of the $t\bar{t}h$ production process.

5

INTRODUCTION AND MOTIVATION

In the quest of determining the properties of the Higgs boson, and the ElectroWeak Symmetry Breaking scalar potential, the top quark plays a fundamental role. Being the heaviest particle in the Standard Model, it's the one with the largest coupling to the Higgs boson and a promising candidate to couple to new physics. In chapter 3 we considered deviations of the top Yukawa coupling y_t from its SM value in the context of double Higgs boson production, together with other effects of new physics in the context of EFT. Being mediated by a loop process, we saw that it is not straight forward to disentangle deviations in y_t from other new physics effects. A direct observation of y_t in a process that is tree-level at the lowest order would allow us to disentangle the different effects that could affect the ggH vertex. For other lighter particles particles like the bottom quark or the tau lepton, the Yukawa couplings y_b and y_τ have been inferred from the decay of the Higgs boson into a $b\bar{b}$ [98, 99] or $\tau\bar{\tau}$ [100, 101] pair, respectively. This strategy doesn't work for the top quark, as it's so massive that the decay of the Higgs boson into a top quark pair is kinematically forbidden. Instead, the more rare associated $t\bar{t}h$ production process, whose leading order diagrams are shown in Figure 5.1, has to be measured. In the recent years, the first observation of a top anti-top pair in association of a Higgs boson was made by both ATLAS [102] and CMS [103] detectors at the LHC, and since then the experimental accuracy has only improved [104, 105], providing an independent constrain on the Yukawa coupling of the top quark, y_t.

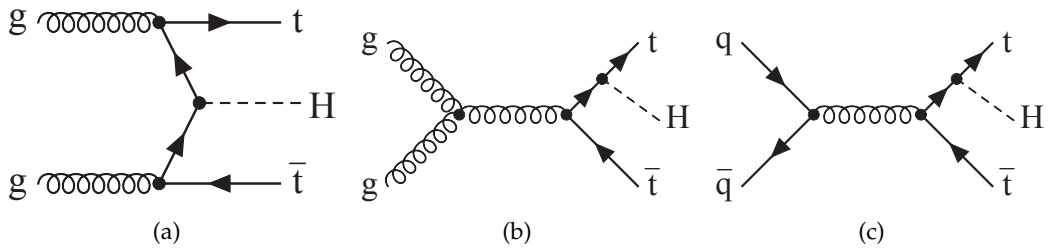

Figure 5.1: Tree level diagrams for $t\bar{t}h$ production in the gluon fusion (a-b) and quark annihilation (c) channels.

A significant effort has been made in the past years to improve the description of $t\bar{t}h$ production. The NLO QCD corrections were computed almost twenty years ago [106–109], and have been matched to parton showers in Refs. [110–112] and combined with NLO electroweak corrections in Refs. [113, 114]. So far, the main theoretical uncertainty comes from the variation of factorization and renormalization scales, which is an lower-bound estimate of the impact of higher-order QCD calculations. Soft gluon resummation effects have been computed at NLL [115] and NNLL [116–119], for selected differential cross sections, showing a significant decrease in the scale dependence, but a full NNLO calculation is not available at the moment.

In order to go further, one has to compute the NNLO QCD corrections. For this, several steps have to be taken: On one hand the two-loop five point amplitudes should be computed for the process, and on the other a framework to combine these with the one loop-real and tree level-double real emission amplitudes should be developed. This is necessary due to the intricate structure of infrared divergences that appear at intermediate steps of the calculation. Although for an Infrared Safe observable, such divergences cancel out and the cross section is finite, one has to do an analytical manipulation to make the cancellation explicit, before it is suitable for a numerical integration of the phase space. There are several formalisms to do such manipulations at NNLO order in QCD, which have been successfully applied to different processes [120–136].

In this part of the thesis we will make use of the q_T-subtraction method [136], which relies on the q_T-resummation formalism for colourless final states [137, 138] and have been successfully applied to a variety of processes [139–147], and its extension to massive colourful final states [148–152] which recently has been successfully applied in the computation of the fully differential cross section for $t\bar{t}$ production [153–155]. In order to extend the NNLO q_T-subtraction framework developed for $t\bar{t}$ to the production associated production of $t\bar{t}h$, we need to remove the kinematical restriction that forces the top quarks to be back-to-back at the lowest order of perturbation theory. This kinematical modification, although conceptually simple, makes the computation much more involved. In this part we will introduce the main ingredients and fully implement q_T-subtraction at NLO for a $t\bar{t}h$ and $t\bar{t}Z$ final states, and present the NNLO counter-terms that correctly cancel all infrared divergences in the real emission cross section.

This part is organised as follows: In chapter 6 we will present the theory background, including subtraction methods, the q_T-resummation and subtraction formalisms for colourless as well as massive colourful final states. In chapter 7 we present the for the first time an implementation of q_T-subtraction at NLO for a $t\bar{t}$ + colourless final state, and we make a numerical validation against the known results for $t\bar{t}h$ and $t\bar{t}Z$ production. Finally, in chapter 8 we present the NNLO counter-term for $t\bar{t}$ + colourless and show that it correctly cancels the infrared divergent behaviour of the real emission cross-section for $t\bar{t}h$ production. The work presented in this part is the subject of a publication which is currently in preparation [156].

6

THEORY BACKGROUND

In this section we will discuss the theory background in which our calculations were performed. As an introduction, let's go back to the FKS method, which we used in part I of this thesis.

6.1 SUBTRACTION SCHEMES FOR REGULARIZATION OF IR DIVERGENCES

Recall from section 2.3 that a NLO cross section can be written as

$$\frac{\mathrm{d}\sigma^{NLO}_{H_1,H_2}}{\mathrm{d}\Phi_n} = \frac{\mathrm{d}\sigma^{LO}_{H_1,H_2}}{\mathrm{d}\Phi_n} + \sum_{\substack{a_1\in H_1\\ a_2\in H_2}} \int_0^1 \mathrm{d}x_1\,\mathrm{d}x_2\, f_{a_1/H_1}(x_1) f_{a_2/H_2}(x_2) \left[\mathcal{V} + \int \frac{\mathrm{d}\Phi_{n+1}}{\mathrm{d}\Phi_n}\mathcal{R}\right], \quad (6.1)$$

where the initial state infrared divergences in the virtual amplitudes $\mathcal{V}$ have already been subtracted and absorbed into the parton distribution functions $f_{a_1/H_1}(x_1)$. In a similar way, we work with fully renormalized on-shell scattering amplitudes, regularized in the CDR scheme by analytic continuation in $D = 4 - 2\varepsilon$ dimensions, meaning that all UV divergences have been regularized. Therefore, all dependence on the factorization and renormalization scales, μ_F and μ_R, is implicitly understood.

Each term in the equation, the virtual and real emission contributions, is individually divergent. Now, we know that these divergences cancel out after the integration of unresolved radiation in the $\mathcal{R}$ term. We can, therefore, add and subtract a term $\mathcal{C}$, which we will call *counter-term*, that contains the same singularities as $\mathcal{R}$ so that we get the sum of two finite terms, as follows

$$\frac{\mathrm{d}\sigma^{NLO}_{H_1,H_2}}{\mathrm{d}\Phi_n} = \frac{\mathrm{d}\sigma^{LO}_{H_1,H_2}}{\mathrm{d}\Phi_n} + \sum_{\substack{a_1\in H_1\\ a_2\in H_2}} \int_0^1 \mathrm{d}x_1\,\mathrm{d}x_2\, f_{a_1/H_1}(x_1) f_{a_2/H_2}(x_2) \left[(\mathcal{V} + \int \mathcal{C}) + \int \frac{\mathrm{d}\Phi_{n+1}}{\mathrm{d}\Phi_n}(\mathcal{R} - \mathcal{C})\right]. \quad (6.2)$$

whenever we can perform the integration $\int \mathcal{C} = \int \frac{\mathrm{d}\Phi_{n+1}}{\mathrm{d}\Phi_n}\mathcal{C}$ analytically, we will be able to write down the NLO cross section as a sum of finite terms, and therefore suitable for

numerical computation of the convolution with any infrared-safe observable of interest. We've already seen the FKS method, which provides an explicit expression for $\mathcal{C}$:

$$\int \frac{\mathrm{d}\Phi_{n+1}}{\mathrm{d}\Phi_n}(\mathcal{R}-\mathcal{C}) = \frac{s}{16\pi^2}\iint \mathrm{d}\xi\,\mathrm{d}y\, f(\xi,y)\frac{1}{2}\left(\left(\frac{1}{1-y}\right)_+ + \left(\frac{1}{1+y}\right)_+\right)\left(\frac{1}{\xi}\right)_+ \tag{6.3}$$

$$\begin{aligned}\int \mathcal{C} = &\frac{(4\pi)^\varepsilon}{\Gamma(1-\varepsilon)}\frac{\Gamma(1-\varepsilon)^2}{\Gamma(1-2\varepsilon)}\frac{s^{1-\varepsilon}}{4}\int \frac{\mathrm{d}\phi}{(2\pi)^3}\sin(\phi)^{-2\varepsilon}\Big[-\frac{1}{2\varepsilon}\int \mathrm{d}y\, f(0,y)(1-y^2)^{-1-\varepsilon}\\ &-\frac{4^{-\varepsilon}}{2\varepsilon}\int \mathrm{d}\xi\left(\left(\frac{1}{\xi}\right)_+ - 2\varepsilon\left(\frac{\log(\xi)}{\xi}\right)_+\right)(f(\xi,1)+f(\xi,-1))\Big],\end{aligned} \tag{6.4}$$

where $f(\xi,y)=\xi^2(1-y^2)\mathcal{R}$ can be computed in the limits $\xi=0$, $y=\pm1$ in terms of $\mathcal{B}$ only, and after the analytical cancellation of the corresponding singularities in $\mathcal{V}$ we obtain a finite result in which we can set $\varepsilon=0$.

This method of constructing a counter-term to regulate divergences is what is known as a *subtraction* procedure. At NLO, the development of general-purpose subtraction frameworks allowed for the automation of NLO computations in software such as MadGraph, which implements FKS subtraction terms [14, 15], or matrix [157], which implements Catani-Seymour dipole subtraction terms [12, 158, 159].

At NNLO one could proceed in the same way, and write down the ingredients of the calculation, namely the double virtual $\mathcal{VV}$ (two loop-born interference and one loop squared amplitudes) that are defined in the n-particle phase space Φ_n, the real-virtual $\mathcal{RV}$ (one loop-born amplitude interferences that include the emission of an unresolved parton) defined in Φ_{n+1} and the double-real $\mathcal{RR}$ (tree level amplitudes squared that include the emission of two unresolved partons) defined in Φ_{n+2}:

$$\begin{aligned}\frac{\mathrm{d}\sigma^{NNLO}_{H_1,H_2}}{\mathrm{d}\Phi_n} = \frac{\mathrm{d}\sigma^{NLO}_{H_1,H_2}}{\mathrm{d}\Phi_n} + \sum_{\substack{a_1\in H_1\\ a_2\in H_2}}\int_0^1 \mathrm{d}x_1\,\mathrm{d}x_2\, f_{a_1/H_1}(x_1)f_{a_2/H_2}(x_2)\\ \Big[\mathcal{VV} + \int \frac{\mathrm{d}\Phi_{n+1}}{\mathrm{d}\Phi_n}\mathcal{RV} + \int \frac{\mathrm{d}\Phi_{n+2}}{\mathrm{d}\Phi_n}\mathcal{RR}\Big].\end{aligned} \tag{6.5}$$

As we can see, the structure of singularities will be much more involved. On one hand, in $\mathcal{RV}$ we have NLO-type of divergences (soft, collinear and soft-collinear) originating in the emitted radiation becoming unresolved, that should cancel singularities present in $\mathcal{VV}$. $\mathcal{RV}$ also contains singularities of virtual origin that partially cancels against the ones present in $\mathcal{RR}$, namely the ones originating from a single emitted parton becoming unresolved. The remaining singularities present in $\mathcal{RR}$ correspond to two partons becoming unresolved, which give rise to configurations double-soft, double-collinear, triple-collinear, soft-collinear, etc. These singularities should cancel against the ones present in $\mathcal{VV}$.

We can condense this complicated structure in two types of counter-terms: $\mathcal{C}_1$ (defined over Φ_{n+1}) accounting for the singularities in $\mathcal{RV}$, and $\mathcal{C}_2$ (defined over Φ_{n+2}) for the ones in $\mathcal{RR}$, and formally write the expression

$$\begin{aligned}\frac{\mathrm{d}\sigma^{NNLO}_{H_1,H_2}}{\mathrm{d}\Phi_n} =& \frac{\mathrm{d}\sigma^{NLO}_{H_1,H_2}}{\mathrm{d}\Phi_n} \\ &+ \sum_{\substack{a_1\in H_1\\ a_2\in H_2}} \int_0^1 \mathrm{d}x_1 \int_0^1 \mathrm{d}x_2\, f_{a_1/H_1}(x_1) f_{a_2/H_2}(x_2) \Bigg[\left(\mathcal{VV} + \int \mathcal{C}_1 + \iint \mathcal{C}_2\right) \\ &+ \int \frac{\mathrm{d}\Phi_{n+1}}{\mathrm{d}\Phi_n} \left(\mathcal{RV} - \mathcal{C}_1\right) + \int \frac{\mathrm{d}\Phi_{n+2}}{\mathrm{d}\Phi_n} \left(\mathcal{RR} - \mathcal{C}_2\right) \Bigg]. \end{aligned} \tag{6.6}$$

To build two such counter-terms in a way that is analytically integrable is highly non-trivial, but there are approaches that intend to do so: ColorFull subtraction [126, 127, 160–162] which can be thought of as an extension to NNLO of the Catani-Seymour dipole formula, Antenna Subtraction [120–125] which aims to reproduce the universal divergent behaviour of the amplitudes with analytically simpler expressions, and both Sector Decomposition [131, 132] and Nested Soft-Collinear Subtraction [163] which, inspired in FKS NLO subtraction scheme, aim to subtract the divergent points from the phase-space integration measure of the emitted radiation.

All the subtraction methods described above are *local*, in the sense that they allow us to evaluate the finite expressions throughout the entire phase space. One could, however, use a different approach in which the divergences are cancelled only after integration, what is called a *non-local* subtraction scheme. In the next section 6.2 we will describe one of such methods, which we'll use in through the rest of this thesis.

6.2 q_T-SUBTRACTION

The q_T subtraction method [136] was initially formulated to regulate the divergences of the QCD corrections to the hadroproduction of a colourless final state F, such as Drell-Yan [140] or Higgs boson production [139]. Following the nomenclature of the previous section, we consider

$$h_1(P_1) + h_2(P_2) \to F(q) + X \tag{6.7}$$

where $P_{1,2}$ is the momenta of the incoming Hadrons $h_{1,2}$ and q is the total momentum of the system F, which might be composed of several particles. We will define $\mathbf{q}_T$ as the component of the momentum q which is transversal to the axis defined by P_1 and P_2 in its the centre-of-mass frame. In this frame, the momentum of F, q, is completely specified by $\mathbf{q}_T$, the invariant mass squared $M^2 = q^2$ and the rapidity $y = \frac{1}{2}\ln\frac{q\cdot P_1}{q\cdot P_2}$. If the final system F is composed of several particles, there will be more independent variables that define the phase space Φ_n that we will generically call $\mathbf{\Omega}$.

At LO, there's no extra radiation emitted, and the final state has $\mathbf{q}_T = 0$. It is only at NLO that $\mathbf{q}_T \neq 0$ is allowed, and because the emitted radiation has a transverse momentum equal to $-\mathbf{q}_T$, in that case it cannot be neither collinear nor soft, meaning that the cross-section is free of divergences and can be treated as the LO calculation for the production of a final state comprised by F and a jet (i.e. $F +$ jet).

At NNLO we see a similar behaviour: In the phase-space region with $\mathbf{q}_T \neq 0$ there is least one of the unobserved emitted partons taking the recoil and therefore a finite transverse momentum, for this reason the singularities that can arise are just NLO-type (one parton becoming soft and/or collinear to P_1 or P_2, or collinear to the other parton). In this region, the cross section is just the NLO cross section for the production of $F +$ jet. We summarize this in the following formula:

$$\frac{\mathrm{d}\hat{\sigma}^{(N)NLO}_{a_1+a_2\to F}}{\mathrm{d}\mathbf{q}_T} = \mathrm{d}\hat{\sigma}^{(N)NLO}_{a_1+a_2\to F}\Big|_{\mathbf{q}_T=0}\delta(q_T) + \left.\frac{\mathrm{d}\hat{\sigma}^{(N)LO}_{a_1+a_2\to F+\text{jet}}}{\mathrm{d}\mathbf{q}_T}\right|_{\mathbf{q}_T\neq 0}. \tag{6.8}$$

In the NLO case, the second term can just be computed for a fixed $\mathbf{q}_T \neq 0$ by squaring the tree-level amplitude and integrating over the phase space without any inconvenience. In the NNLO case, the infrared structure of the second term for a fixed $\mathbf{q}_T \neq 0$ is that of a NLO calculation and therefore can be treated with any local subtraction scheme such as FKS or Catani-Seymour Dipole subtraction. All the pure NNLO singularities appear in the first term, at $\mathbf{q}_T = 0$, and they only cancel against the second term after an integration over q_T of the latter. This singular behaviour of the second term in the limit $\mathbf{q}_T \to 0$ manifests as large logarithms of the form $\ln^k(M^2/q_T^2)$. If we know the structure of such logarithms, we can construct a counter-term $\mathrm{d}\sigma_{CT}(\mathbf{q}_T)$ to cancel them, and write the cross section as a sum of two finite terms. Formally, we can write the expression

$$\begin{aligned}\mathrm{d}\hat{\sigma}^{(N)NLO}_{a_1+a_2\to F} = &\left[\mathrm{d}\hat{\sigma}^{(N)NLO}_{a_1+a_2\to F}\Big|_{\mathbf{q}_T=0} + \int \mathrm{d}\mathbf{q}_T\,\mathrm{d}\sigma_{CT}(\mathbf{q}_T)\right] \\ &+ \int \mathrm{d}\mathbf{q}_T \left[\left.\frac{\mathrm{d}\hat{\sigma}^{(N)LO}_{a_1+a_2\to F+\text{jet}}}{\mathrm{d}\mathbf{q}_T}\right|_{\mathbf{q}_T\neq 0} - \mathrm{d}\sigma_{CT}(\mathbf{q}_T)\right],\end{aligned} \tag{6.9}$$

and cancel analytically the singularities in the terms between the first pair brackets, while the ones between the last pair of brackets would only give a finite quantity after integration in $\mathbf{q}_T$. Because each of the terms inside the second pair of brackets is individually divergent when integrated, we introduce a technical *slicing* parameter $r_{cut} = q_T^2/M^2$ and perform the extrapolation given by the limit $r_{cut} \to 0$. Schematically, this is performed by doing replacing the integral in (6.9) by

$$\int \mathrm{d}\mathbf{q}_T \to \lim_{r_{cut}\to 0}\int_{M^2 r_{cut}} \mathrm{d}\mathbf{q}_T\,. \tag{6.10}$$

In practice, we will compute this integral for several finite values of r_{cut}, and perform a numerical extrapolation to get the value at $r_{cut} = 0$.

The structure of this divergent behaviour has been thoroughly studied in the context of q_T-resummation, of which we will review the main results.

6.2.1 *q_T-resummation formalism for a colour singlet final state*

In this subsection we will present the main results of the q_T-resummation formalism for a colour singlet final state [137]. Let's write the general fully differential cross section for the production of a colour-less system F as

$$\frac{\mathrm{d}\sigma_{h_1h_2\to F}}{\mathrm{d}^2\mathbf{q}_T\,\mathrm{d}M\,\mathrm{d}y\,\mathrm{d}\mathbf{\Omega}} = \left[\frac{\mathrm{d}\sigma_F}{\mathrm{d}\mathbf{q}_T}\right]^{(sing)} + \left[\frac{\mathrm{d}\sigma_F}{\mathrm{d}\mathbf{q}_T}\right]^{(reg)}, \tag{6.11}$$

where we grouped in $\left[\mathrm{d}\sigma_F/\mathrm{d}q_T^2\right]^{(sing)}$ the terms that are enhanced at $\mathbf{q}_T = 0$, i.e. those proportional to either $\delta(q_T^2)$ or $\ln^k(M^2/q_T^2)$, and in $\left[\mathrm{d}\sigma_F/\mathrm{d}q_T^2\right]^{(reg)}$ the ones which are regular in the limit $\mathbf{q}_T \to 0$. That is, by definition

$$\lim_{Q_T\to 0}\int_0^{Q_T^2}\mathrm{d}q_T^2\left[\frac{\mathrm{d}\sigma_F}{\mathrm{d}\mathbf{q}_T}\right]^{(reg)} = 0. \tag{6.12}$$

The main result of the q_T-resummation is encoded in the following resummation formula

$$\begin{aligned}\left[\frac{\mathrm{d}\sigma_F}{\mathrm{d}\mathbf{q}_T}\right]^{(sing)} =& \frac{M^2}{s}\int\frac{\mathrm{d}^2\mathbf{b}}{(2\pi)^2}e^{i\mathbf{b}\cdot\mathbf{q}_T}\sum_{\substack{a_1\in h_1\\ a_2\in h_2}}\int_{x_1}^1\frac{\mathrm{d}z_1}{z_1}\int_{x_2}^1\frac{\mathrm{d}z_2}{z_2}f_{a_1/h_1}\left(\frac{x_1}{z_1},\frac{b_0^2}{b^2}\right)f_{a_2/h_2}\left(\frac{x_2}{z_2},\frac{b_0^2}{b^2}\right)\\ &\times\sum_c\frac{\mathrm{d}\sigma^{(0)}_{c\bar{c}\to F}\left(x_1P_1,x_2P_2,M,\mathbf{\Omega}\right)}{\mathrm{d}M^2\,\mathrm{d}\mathbf{\Omega}}S_c(M,b)\left[H^FC_1C_2\right]_{c\bar{c};a_1a_2},\end{aligned} \tag{6.13}$$

where $x_{1,2} = \frac{M}{\sqrt{s}}e^{\pm y}$, and which describes the factorization of the singular part of the cross section into the leading order one ($\mathrm{d}\sigma^{(0)}_{c\bar{c}\to F}$), some process-independent factors ($S_c(M,b)$) and some process-dependent coefficients ($\left[H^FC_1C_2\right]_{c\bar{c};a_1a_2}$).

Let's describe the different ingredients shown in (6.13):

- First of all, we notice that the factorization is written in *impact parameter space* (or **b**-space), which means that we're taking a Fourier transform on the transverse momentum $\mathbf{q}_T$ and therefore mapping the singular region $q_T \ll M$ to $Mb \gg 1$.
- The factorization of the hadronic cross section into a partonic cross section is done in terms of the scaling variables $z_{1,2}$, which connect the invariant mass of the final system M to the partonic centre-of-mass energy $\sqrt{\hat{s}}$ ($M^2 = z_1z_2\hat{s}$).

- The parton distribution functions have been evolved from the factorization scale μ_F^2 to the transverse-momentum scale $(b_0/b)^2 \sim q_T^2$.
- The flavour corresponding to the partons entering the hard scattering $c\bar{c} \to F$ doesn't necessarily correspond to the ones of the partons coming out of the hadrons a_1, a_2, due to possible collinear splittings of these.
- The Sudakov factor $S_c(M, b)$ is universal and only depends on the flavour of the partons entering the hard scattering c. It resums all the logarithms originating soft and flavour conserving collinear emissions from the initial legs. Its expression is given by

$$S_c(M,b) = \exp\left\{ -\int_{b_0^2/b^2}^{M^2} \frac{\mathrm{d}q^2}{q^2} \left[A_c(\alpha_s(q^2)) \ln \frac{M^2}{q^2} + B_c(\alpha_s(q^2)) \right] \right\}, \tag{6.14}$$

  where the functions $A_c(\alpha_s)$ and $B_c(\alpha_s)$ admit a perturbative expansion

$$A_c(\alpha_s) = \sum_{n=1}^{\infty} \left(\frac{\alpha_s}{\pi}\right)^n A_c^{(n)} \tag{6.15}$$

$$B_c(\alpha_s) = \sum_{n=1}^{\infty} \left(\frac{\alpha_s}{\pi}\right)^n B_c^{(n)}. \tag{6.16}$$

- The factor $\left[H^F C_1 C_2\right]_{c\bar{c};a_1a_2}$ is process dependent and encodes the virtual corrections to the process (proportional to $\delta(\mathbf{q}_T)$), as well as the collinear flavour changing emissions from the initial legs. For quark-initiated hard processes ($c \neq g$), it can be explicitly written as

$$\begin{aligned}\left[H^F C_1 C_2\right]_{c\bar{c};a_1a_2} &= H_c^F(x_1P_1, x_2P_2; \mathbf{\Omega}; \alpha_s(M^2)) \\ &\quad \times C_{ca_1}(z_1; \alpha_s(b_0^2/b^2)) C_{ca_2}(z_2; \alpha_s(b_0^2/b^2))\end{aligned} \tag{6.17}$$

  where the functions H_c^F and C_{ab} admit a perturbative expansion:

$$H_c^F(x_1P_1, x_2P_2; \mathbf{\Omega}; \alpha_s) = 1 + \sum_{n=1}^{\infty} \left(\frac{\alpha_s}{\pi}\right)^n H_c^{F(n)}(x_1P_1, x_2P_2; \mathbf{\Omega}) \tag{6.18}$$

$$C_{ab}(z; \alpha_s) = \delta_{ab}\delta(z-1) + \sum_{n=1}^{\infty} \left(\frac{\alpha_s}{\pi}\right)^n C_{ab}^{(n)}(z). \tag{6.19}$$

  As we see, the coefficient H_c^F doesn't depend on the impact parameter b, which means that it's not enhanced by large logarithms, unlike the C_{ab} collinear functions. For gluon fusion processes ($c = g$), there is a similar structure, with the only difference being that the H_c^F and C_{ab} coefficients have Lorentz indices which are contracted among each other, and the C_{ab} functions not only depend on the modulus of the impact parameter $\mathbf{b}$ but also in it's direction, giving rise to non-trivial spin correlations [138]. This issue is addressed in Appendix C.1.

The formula (6.13) is invariant under a renormalization group transformation of the form

$$H_c^F(\alpha_s) \to H_c^F(\alpha_s)[h_c(\alpha_s)]^{-1}, \tag{6.20}$$

$$B_c(\alpha_s) \to B_c(\alpha_s) - \beta(\alpha_s)\frac{\mathrm{d}\ln h_c(\alpha_s)}{\mathrm{d}\ln \alpha_s}, \tag{6.21}$$

$$C_{ab}(\alpha_s) \to C_{ab}[h_c(\alpha_s)]^{1/2} \tag{6.22}$$

for an arbitrary function $h(\alpha_s) = 1 + \mathcal{O}(\alpha_s)$, where $\beta(\alpha_s)$ is the QCD β-function. Because of this invariance, the expressions for H_c^F, C_{ab} and B_c will depend on the *resummation scheme*. The expressions presented above correspond to the *hard* scheme, which is characterized by the fact that all the process dependence of $\left[H^F C_1 C_2\right]_{c\bar{c};a_1a_2}$ is encoded in H_c^F, while C_{ab} are universal and process independent. To be precise, this is the scheme in which, order by order in perturbation theory, the functions $C_{ab}^{(n)}(z)$ don't contain any $\delta(1-z)$ terms.

In the hard scheme, the collinear functions C_{ab} are known up to, at least, second order in α_s. The first order coefficients have the following form

$$C_{qq}^{(1)}(z) = \frac{1}{2}C_F(1-z), \tag{6.23}$$

$$C_{gq}^{(1)}(z) = \frac{1}{2}C_F z, \tag{6.24}$$

$$C_{qg}^{(1)}(z) = \frac{1}{2}z(1-z), \tag{6.25}$$

$$C_{gg}^{(1)}(z) = C_{q\bar{q}}^{(1)}(z) = C_{qq'}^{(1)}(z) = C_{q\bar{q}'}^{(1)}(z) = 0, \tag{6.26}$$

where $C_F = \frac{4}{3}$ and $C_A = 3$ are colour factors. The second order coefficients $C_{ab}^{(2)}$ can be found in Ref. [137], and the third order coefficients for the quark channels have been recently computed in Ref. [164]. The $B_c^{(n)}$ coefficients in equation (6.15) are resummation scheme dependent for $n \geq 2$, while $B_c^{(1)}$ and $A_c^{(n\geq 1)}$ are scheme-independent. The first order coefficients read [165, 166]

$$A_g^{(1)} = C_A, \qquad A_q^{(1)} = A_{\bar{q}}^{(1)} = C_F, \tag{6.27}$$

$$B_g^{(1)} = -\frac{1}{6}(11C_a - 2n_f), \qquad B_q^{(1)} = B_{\bar{q}}^{(1)} = -\frac{3}{2}C_F, \tag{6.28}$$

while the second order ones, $A^{(2)}$ and $B^{(2)}$, can be found in Refs. [165, 166] and [137], respectively.

The H_c^F can be written in terms of the finite part of the loop amplitudes. In order to do so, lets define $\mathcal{M}_{c\bar{c}\to F}$ the $\overline{\text{MS}}$ renormalized on-shell scattering amplitude, regularized in the CDR scheme by analytic continuation in $D = 4 - 2\varepsilon$ dimensions. This amplitude admits a perturbative expansion in α_s:

$$\mathcal{M}_{c\bar{c}\to F} = \sum_{n=0}^{\infty}\left(\frac{\alpha_s}{2\pi}\right)^n \mathcal{M}_{c\bar{c}\to F}^{(n)} \tag{6.29}$$

Order by order in α_s, the amplitude $\mathcal{M}_{c\bar{c}\to F}$ contains poles of IR origin which follow a universal structure that has been studied at one loop [12, 167–169] and two loops [167, 170, 171]. We can therefore define the hard-virtual amplitude as the finite remainder after the subtraction of these divergences [137]

$$\widetilde{\mathcal{M}}_{c\bar{c}\to F}(p_1, p_2, M, \mathbf{\Omega}) = \left[1 - \widetilde{\mathcal{I}}_c(\varepsilon, M)\right] \mathcal{M}_{c\bar{c}\to F}(p_1, p_2, M, \mathbf{\Omega}), \tag{6.30}$$

with

$$\widetilde{\mathcal{I}}_c(\varepsilon, M) = \sum_{n=1}^{\infty} \left(\frac{\alpha_s(\mu_R)}{2\pi}\right)^n \widetilde{\mathcal{I}}_c^{(n)}(\varepsilon, M^2/\mu_R^2) \tag{6.31}$$

The process-independent *insertion operator* $\tilde{I}_c$ has poles in ε fixed to match the IR divergent structure of $\mathcal{M}_{c\bar{c}\to F}$, making the $\left[1 - \tilde{I}_c(\varepsilon, M)\right]$ operator responsible for the subtraction of the IR poles in the amplitude $\mathcal{M}_{c\bar{c}\to F}$ (plus some IR finite part).

With these definitions, the Hard-virtual resummation coefficient H_c^F can then be written in the hard-scheme in terms of $\tilde{M}_{c\bar{c}\to F}$ as

$$H_c^F = \frac{\left|\widetilde{\mathcal{M}}_{c\bar{c}\to F}(x_1P_1, x_2P_2, M, \mathbf{\Omega})\right|^2}{\left|\mathcal{M}^{(0)}_{c\bar{c}\to F}(x_1P_1, x_2P_2, M, \mathbf{\Omega})\right|^2}. \tag{6.32}$$

The explicit form for this operator is known up to $\mathcal{O}(\alpha_s^2)$, which allows for the computation of the resummed Next-to-Next-to-Leading Logarithmic matched to NNLO cross sections (NNLL+NNLO) for the production of colourless final states, provided the corresponding two-loop amplitudes to the process are known.

6.2.2 *q_T-resummation formalism for massive colourful final state*

So far, we have described the q_T-resummation formalism for a colourless final state F. When we consider a colourful final state, the structure of the IR divergences is more rich, as we have to consider also the emission of partons from the final state coloured legs. If in addition to the colourless final state F we produce a pair of a heavy quarks $Q\bar{Q}$, we will have divergences originating from the emission of soft gluons from heavy quark legs[1]. The case of q_T-resummation in heavy quark hadroproduction has been studied in Ref. [150], and the resummation formula is the same as in (6.13) but with the replacement $H^F \to \mathbf{H\Delta}$, that is

$$\left[\frac{\mathrm{d}\sigma_F}{\mathrm{d}\mathbf{q}_T}\right]^{(sing)} = \frac{M^2}{s} \int \frac{\mathrm{d}^2\mathbf{b}}{(2\pi)^2} e^{i\mathbf{b}\cdot\mathbf{q}_T} \sum_{\substack{a_1\in h_1\\ a_2\in h_2}} \int_{x_1}^1 \frac{\mathrm{d}z_1}{z_1} \int_{x_2}^1 \frac{\mathrm{d}z_2}{z_2} f_{a_1/h_1}\left(\frac{x_1}{z_1}, \frac{b_0^2}{b^2}\right) f_{a_2/h_2}\left(\frac{x_2}{z_2}, \frac{b_0^2}{b^2}\right)$$

1 The collinear emission from a massive quark doesn't generate any IR divergences, as these are regulated by the quark's mass.

$$\times \sum_c \frac{\mathrm{d}\sigma^{(0)}_{c\bar{c}\to F}\left(x_1P_1, x_2P_2, M, \mathbf{\Omega}\right)}{\mathrm{d}M^2\,\mathrm{d}\mathbf{\Omega}} S_c(M,b)\left[(\mathbf{H\Delta})C_1C_2\right]_{c\bar{c};a_1a_2}. \tag{6.33}$$

The $\mathbf{\Delta}$ embodies the new contributions due to soft emission of gluons from the final state, which means that by setting $\mathbf{\Delta} = 1$ we get the expression for the colourless final state. The bold font is used to denote that it is a colour operator. That is, if we define a colour basis and then write the amplitude $\mathcal{M}_{c\bar{c}\to Q\bar{Q}F}$ as a vector $\left|\mathcal{M}_{c\bar{c}\to Q\bar{Q}F}\right\rangle$ in colour-space, then the $\mathbf{\Delta}$ operator takes the form of a matrix. In the hard scheme, the $\mathbf{H\Delta}$ coefficient takes the form [150]

$$\left[(\mathbf{H\Delta})C_1C_2\right]_{c\bar{c};a_1a_2} = (\mathbf{H\Delta})_{c\bar{c}}C_{ca_1}(z_1;\alpha_s(b_0^2/b^2))C_{ca_2}(z_2;\alpha_s(b_0^2/b^2)) \tag{6.34}$$

$$(\mathbf{H\Delta})_{c\bar{c}} = \frac{\left\langle\widetilde{\mathcal{M}}_{c\bar{c}\to Q\bar{Q}F}\right|\mathbf{\Delta}\left|\widetilde{\mathcal{M}}_{c\bar{c}\to Q\bar{Q}F}\right\rangle}{|\mathcal{M}^{(0)}_{c\bar{c}\to Q\bar{Q}F}(x_1P_1, x_2P_2;\mathbf{\Omega})|^2}, \tag{6.35}$$

where the auxiliar hard-virtual amplitude $\left|\widetilde{\mathcal{M}}\right\rangle$ is defined analogous to Eq. (6.30) as

$$\left|\widetilde{\mathcal{M}}_{c\bar{c}\to Q\bar{Q}F}\right\rangle = \left[1 - \widetilde{\mathbf{I}}_{c\bar{c}\to Q\bar{Q}F}(\varepsilon, M)\right]\left|\mathcal{M}_{c\bar{c}\to Q\bar{Q}F}\right\rangle. \tag{6.36}$$

Just like in the case of a colour singlet final state, in gluon fusion processes the coefficients $(\mathbf{H\Delta})_{gg}$ and C_{ga} contain Lorentz indices, and their contraction give rise to non-trivial spin correlations due to the dependence of C_{ga} on both the modulus and direction of the impact parameter $\mathbf{b}$. In the case of a massive coloured final state, these spin correlations are enriched by the structure of the $\mathbf{\Delta}$ colour operator [150]. This is discussed in more detail in Appendix C.1.

The insertion operator $\widetilde{\mathbf{I}}_c$ can be rewritten in terms of a piece that is identical to $\widetilde{\mathcal{I}}_c$ from the colour-singlet case, plus some new piece $\widetilde{\mathbf{I}}_{Q\bar{Q}F}$ that encodes all the soft emissions from the final state. For example, at NLO it can be written as follows [150]

$$\widetilde{\mathbf{I}}^{(1)}_{c\bar{c}\to Q\bar{Q}F}(\varepsilon, M) = \widetilde{\mathcal{I}}^{(1)}_c(\varepsilon, M) + \widetilde{\mathbf{I}}^{(1)}_{Q\bar{Q}F} \tag{6.37}$$

$$= \widetilde{\mathcal{I}}^{(1)}_c(\varepsilon, M) + \frac{1}{\varepsilon}\mathbf{\Gamma}^{(1)}_Q + \mathbf{F}_Q + \mathcal{O}(\varepsilon), \tag{6.38}$$

where $\mathbf{\Gamma}^{(1)}_Q$ is the first order soft anomalous dimension operator for a massive quark Q, and $\mathbf{F}_Q$ is a finite remainder. That the difference respect to the colour-singlet case only has a single pole in ε is related to the fact that, for a massive quark, there are no collinear divergences at NLO, thus neither soft-collinear that could give rise to double poles.

In general, the expression for the $\mathbf{\Delta}$ factor will be

$$\mathbf{\Delta} = \mathbf{V}(b; M, \mathbf{\Omega})\mathbf{D}(\mathbf{b}; M, \mathbf{\Omega})\mathbf{V}^\dagger(b; M, \mathbf{\Omega}) \tag{6.39}$$

where the factor

$$\mathbf{V} = \overline{P}_q \exp\left\{ - \int_{b_0^2/b^2}^{M^2} \frac{\mathrm{d}q^2}{q^2} \mathbf{\Gamma}_Q(\alpha_s(q^2); M, \mathbf{\Omega}) \right\}, \tag{6.40}$$

resums all logarithmic enhanced terms $\alpha_s(M^2)^n \ln(Mb)^k$ (with $k \leq n$) originating from soft emissions on the massive quarks Q, from a scale $b_0/b \sim q_T$ up to M. The symbol $\overline{P}_q$ means that the matrix exponentiation is anti-path ordered with respect to the integration variable q^2.

The factor $\mathbf{D}$ which depends on the angles of $\mathbf{b}$, encodes azimuthal correlations and, thanks to renormalization group invariance, it can be always chosen in such a way that at all orders

$$\langle \mathbf{D} \rangle_{\phi(\mathbf{b})} = 1, \tag{6.41}$$

where $\langle \rangle_{\phi(\mathbf{b})}$ denotes the azimuthal average over $\mathbf{b}$.

Therefore, the only extra ingredients needed in the case where there's a massive quark Q in the final state are the soft anomalous dimension operator $\mathbf{\Gamma}_Q$, the Insertion operator $\widetilde{\mathbf{I}}_{Q\bar{Q}F}$ and the new spin-correlations discussed in Appendix C.1.

6.2.3 *q_T-subtraction formalism massive colourful final state*

Now that we have all the ingredients to describe the region of $q_T \to 0$, we can write down the expressions for the subtraction formula (6.9). Let's focus on the process

$$h_1 h_2 \to Q\bar{Q}F + X, \tag{6.42}$$

where Q is a massive quark, such as the top quark, and F is a colourless final state, such as a Higgs or a Z boson, and X denotes any other unobserved final state. The expression for the (N)NLO cross section given by (6.9) can be written down as a sum of two finite terms, thanks to the knowledge of the behaviour at $q_T \to 0$ given by the q_T-resummation formalism. The q_T-subtraction formula for the partonic cross section of the process $a_1 a_2 \to Q\bar{Q}F + X$ takes the form [152]

$$\mathrm{d}\hat{\sigma}^{(N)NLO}_{a_1 a_2 \to Q\bar{Q}F} = \mathcal{H}^{Q\bar{Q}F;(N)NLO}_{a_1 a_2 \to c\bar{c}} \otimes \mathrm{d}\hat{\sigma}^{LO}_{c\bar{c} \to Q\bar{Q}F} + \left[\mathrm{d}\hat{\sigma}^{(N)LO}_{a_1 a_2 \to Q\bar{Q}F+\text{jet}} - \mathrm{d}\hat{\sigma}^{CT,(N)NLO}_{a_1 a_2 \to Q\bar{Q}F} \right], \tag{6.43}$$

where the counter-term is defined as

$$\mathrm{d}\hat{\sigma}^{CT,NLO}_{a_1 a_2 \to Q\bar{Q}F} = \sum_c \frac{\alpha_s}{\pi} \Sigma^{Q\bar{Q}F(1)}_{a_1 a_2 \to c\bar{c}} \left(z_1, z_2; \frac{q_T}{M} \right) \frac{\mathrm{d}q_T^2}{M^2} \otimes \mathrm{d}\hat{\sigma}^{LO}_{c\bar{c} \to Q\bar{Q}F} \tag{6.44}$$

$$\mathrm{d}\hat{\sigma}^{CT,NNLO}_{a_1 a_2 \to Q\bar{Q}F} = \sum_c \left(\frac{\alpha_s}{\pi} \right)^2 \Sigma^{Q\bar{Q}F(2)}_{a_1 a_2 \to c\bar{c}} \left(z_1, z_2; \frac{q_T}{M} \right) \frac{\mathrm{d}q_T^2}{M^2} \otimes \mathrm{d}\hat{\sigma}^{LO}_{c\bar{c} \to Q\bar{Q}F} \tag{6.45}$$

and the $\otimes$ denotes a convolution with respect to the z_1 and z_2 longitudinal momentum fractions of the incoming partons in $\mathrm{d}\hat{\sigma}^{LO}_{c\bar{c}\to Q\bar{Q}F}$, c and $\bar{c}$, respectively. The coefficients $\Sigma^{Q\bar{Q}F(1)}(z_1,z_2,r)$ and $\Sigma^{Q\bar{Q}F(2)}(z_1,z_2,r)$ encode the logarithmic dependence on $r = q_T/M$, which can be factorised in the following way

$$\Sigma^{Q\bar{Q}F(1)}_{a_1a_2\to c\bar{c}}(z_1,z_2;r) = \sum_{n=1}^{2} \Sigma^{Q\bar{Q}F(1;n)}_{a_1a_2\to c\bar{c}}(z_1,z_2)\tilde{I}_n(r), \tag{6.46}$$

$$\Sigma^{Q\bar{Q}F(2)}_{a_1a_2\to c\bar{c}}(z_1,z_2;r) = \sum_{n=1}^{4} \Sigma^{Q\bar{Q}F(2;n)}_{a_1a_2\to c\bar{c}}(z_1,z_2)\tilde{I}_n(r). \tag{6.47}$$

The functions $\tilde{I}_n(r)$, when Fourier-transformed to $\mathbf{b}$-space, correspond to the $\ln^n(b^2/b_0^2+1) \overset{b\gg b_0}{\sim} \ln(b^2/b_0^2)$ that behave logarithmically at small q_T[2]

$$\begin{aligned}\tilde{I}_n\left(\frac{q_T}{M}\right) =& M^2\int \frac{\mathrm{d}^2\mathbf{b}}{4\pi} e^{i\mathbf{b}\cdot\mathbf{q}_T} \ln^n\left(\frac{M^2b^2}{b_0^2}+1\right)\\ =& \left(\frac{q_T}{M}\right)^{-2}\int_0^\infty \mathrm{d}x\,\frac{x}{2}J_0(x)\ln^n\left(\frac{x^2}{b_0^2}\left(\frac{q_T}{M}\right)^{-2}+1\right),\end{aligned} \tag{6.48}$$

where in the last step we used that the function only depends on the modulus of $\mathbf{b}$ to write the integral in terms of the 0th-order Bessel function J_0. This functions are computed in Ref. [172].

At NLO, the functions $\Sigma^{Q\bar{Q}F(k;n)}_{a_1a_2\to c\bar{c}}(z_1,z_2)$ and $\mathcal{H}^{Q\bar{Q}F;(N)NLO}_{a_1a_2\to c\bar{c}}(z_1,z_2)$ read

$$\Sigma^{Q\bar{Q}F(1;2)}_{a_1a_2\to c\bar{c}}(z_1,z_2) = -\frac{1}{2}A_c^{(1)}\delta_{ca_1}\delta_{\bar{c}a_2}\delta(1-z_1)\delta(1-z_2), \tag{6.49}$$

$$\begin{aligned}\Sigma^{Q\bar{Q}F(1;1)}_{a_1a_2\to c\bar{c}}(z_1,z_2) =& -\left[\delta_{ca_1}\delta_{\bar{c}a_2}B_c^{(1)}\delta(1-z_1)\delta(1-z_2)+\delta_{ca_1}P_{\bar{c}a_2}(z_2)+\delta_{\bar{c}a_2}P_{ca_1}(z_2)\right]\\ &-\delta_{ca_1}\delta_{\bar{c}a_2}\delta(1-z_1)\delta(1-z_2)\frac{\left\langle\widetilde{\mathcal{M}}^{(0)}_{c\bar{c}\to Q\bar{Q}F}\right|\left(\mathbf{\Gamma}_Q^{(1)}+\mathbf{\Gamma}_Q^{(1)\dagger}\right)\left|\widetilde{\mathcal{M}}^{(0)}_{c\bar{c}\to Q\bar{Q}F}\right\rangle}{\left|\mathcal{M}^{(0)}_{c\bar{c}\to Q\bar{Q}F}\right|^2},\end{aligned} \tag{6.50}$$

$$\begin{aligned}\mathcal{H}^{Q\bar{Q}F;NLO}_{a_1a_2\to c\bar{c}}(z_1,z_2) =& -\delta_{ca_1}\delta_{\bar{c}a_2}\left[H_c^{Q\bar{Q}F(1)}\delta(z_1)\delta(z_2)-k\beta_0\ell_R\right]\\ &+\delta_{ca_1}\delta(1-z_1)C^{(1)}_{\bar{c}a_2}(z_2)+\delta_{\bar{c}a_2}\delta(1-z_2)C^{(1)}_{ca_1}(z_1)\\ &+\ell_F\left[\delta_{ca_1}\delta(1-z_1)P^{(1)}_{\bar{c}a_2}(z_2)+\delta_{\bar{c}a_2}\delta(1-z_2)P^{(1)}_{ca_1}(z_1)\right],\end{aligned} \tag{6.51}$$

where k represents the power of α_s of the LO partonic process, (i.e. $|\mathcal{M}^{(0)}_{c\bar{c}\to Q\bar{Q}F}|^2 = \mathcal{O}(\alpha_s^k)$), we defined

$$\ell_R = \ln\frac{M^2}{\mu_R^2} \qquad \text{and} \qquad \ell_F = \ln\frac{M^2}{\mu_F^2}, \tag{6.52}$$

2 The modification $\ln(b^2/b_0^2) \to \ln^n(b^2/b_0^2+1)$ ensures that the expressions for the counter-terms don't introduce spurious logarithmic enhancements in regions of high q_T ($b\to 0$), and therefore preserve unitarity.

and $P_{ab}^{(1)}$ first order Altarelli-Parisi splitting function $P_{ab}(z)$, with an $\frac{\alpha_s}{\pi}$ normalization, i.e.

$$P_{ab}(z) = \sum_{n=1}^{\infty} \left(\frac{\alpha_s}{\pi}\right)^n P_{ab}^{(n)}(z) \,. \tag{6.53}$$

At NNLO, the coefficients can be expressed in a more compact form in Mellin space[3], and they read

$$\Sigma^{Q\bar{Q}F(2;4)}_{a_1a_2\to c\bar{c},\,(N_1,N_2)} = \frac{1}{8} A_c^{(1)\,2} \delta_{ca_1}\delta_{\bar{c}a_2}, \tag{6.54}$$

$$\Sigma^{Q\bar{Q}F(2;3)}_{a_1a_2\to c\bar{c},\,(N_1,N_2)} = -A_c^{(1)} \left[\frac{1}{3}\beta_0 \delta_{ca_1}\delta_{\bar{c}a_2} + \Sigma^{Q\bar{Q}F(1;1)}_{a_1a_2\to c\bar{c},\,(N_1,N_2)}\right], \tag{6.55}$$

$$\begin{aligned}
\Sigma^{Q\bar{Q}F(2;2)}_{a_1a_2\to c\bar{c},\,(N_1,N_2)} =& -\frac{1}{2} A_c^{(1)} \left[\mathcal{H}^{Q\bar{Q}F;\,NLO}_{a_1a_2\to c\bar{c},\,(N_1,N_2)} - \beta_0 \delta_{ca_1}\delta_{\bar{c}a_2}\ell_R\right] \\
& -\frac{1}{2}\sum_{b_1,b_2}\left(\delta_{b_1a_1}\gamma^{(1)}_{b_2a_2,N_2} + \gamma^{(1)}_{b_1a_1,N_1}\delta_{b_2a_2}\right) \\
& \quad \times \left[\Sigma^{Q\bar{Q}F(1;1)}_{b_1b_2\to c\bar{c},\,(N_1,N_2)} - \delta_{cb_1}\delta_{\bar{c}b_2}\frac{\left\langle \widetilde{\mathcal{M}}^{(0)}_{c\bar{c}\to Q\bar{Q}F}\right| \mathbf{\Gamma}_t^{(1)} + \mathbf{\Gamma}_t^{(1)\dagger} \left|\widetilde{\mathcal{M}}^{(0)}_{c\bar{c}\to Q\bar{Q}F}\right\rangle}{\left|\mathcal{M}^{(0)}_{c\bar{c}\to Q\bar{Q}F}\right|^2}\right] \\
& -\frac{1}{2}\left[A_c^{(2)}\delta_{ca_1}\delta_{\bar{c}a_2} + (B_c^{(1)} - \beta_0)\Sigma^{Q\bar{Q}F(1;1)}_{b_1b_2\to c\bar{c},\,(N_1,N_2)}\right] \\
& +\frac{1}{2}\delta_{ca_1}\delta_{\bar{c}a_2}B_c^{(1)}\frac{\left\langle \widetilde{\mathcal{M}}^{(0)}_{c\bar{c}\to Q\bar{Q}F}\right| \mathbf{\Gamma}_t^{(1)} + \mathbf{\Gamma}_t^{(1)\dagger} \left|\widetilde{\mathcal{M}}^{(0)}_{c\bar{c}\to Q\bar{Q}F}\right\rangle}{\left|\mathcal{M}^{(0)}_{c\bar{c}\to Q\bar{Q}F}\right|^2} \\
& +\frac{1}{2}\delta_{cb_1}\delta_{\bar{c}b_2}\frac{\left\langle \widetilde{\mathcal{M}}^{(0)}_{c\bar{c}\to Q\bar{Q}F}\right| \left(\mathbf{\Gamma}_t^{(1)} + \mathbf{\Gamma}_t^{(1)\dagger}\right)^2 \left|\widetilde{\mathcal{M}}^{(0)}_{c\bar{c}\to Q\bar{Q}F}\right\rangle}{\left|\mathcal{M}^{(0)}_{c\bar{c}\to Q\bar{Q}F}\right|^2},
\end{aligned} \tag{6.56}$$

$$\begin{aligned}
\Sigma^{Q\bar{Q}F(2;1)}_{a_1a_2\to c\bar{c},\,(N_1,N_2)} =& -\Sigma^{Q\bar{Q}F(1;1)}_{a_1a_2\to c\bar{c},\,(N_1,N_2)}\beta_0\ell_R \\
& -\sum_{b_1b_2}\mathcal{H}^{Q\bar{Q}F;\,NLO}_{a_1a_2\to c\bar{c},\,(N_1,N_2)}\left[\delta_{b_1a_1}\delta_{b_2a_2}B_c^{(1)} + \delta_{b_1a_1}\gamma^{(1)}_{b_2a_2,N_2} + \gamma^{(1)}_{b_1a_1,N_1}\delta_{b_2a_2}\right] \\
& -\delta_{ca_1}\delta_{\bar{c}a_2}B_c^{(2)} + \beta_0\left(\delta_{ca_1}C^{(1)}_{\bar{c}a_2,N_2} + C^{(1)}_{ca_1,N_1}\delta_{\bar{c}a_2}\right) - \left(\delta_{ca_1}\gamma^{(2)}_{\bar{c}a_2,N_2} + \gamma^{(2)}_{ca_1,N_1}\delta_{\bar{c}a_2}\right) \\
& -\delta_{ca_1}\delta_{\bar{c}a_2}\left[\frac{\left\langle \widetilde{\mathcal{M}}^{(0)}_{c\bar{c}\to Q\bar{Q}F}\right| \mathbf{\Gamma}_t^{(1)} + \mathbf{\Gamma}_t^{(1)\dagger} \left|\widetilde{\mathcal{M}}^{(1)}_{c\bar{c}\to Q\bar{Q}F}\right\rangle}{\left|\mathcal{M}^{(1)}_{c\bar{c}\to Q\bar{Q}F}\right|^2} + \text{h.c.}\right]
\end{aligned}$$

3 The (N_1, N_2) moments respect to the variables z_1 and z_2 is defined by the Mellin transform

$$f_{(N1,N2)} = \int_0^1 \mathrm{d}z_1 \int_0^1 \mathrm{d}z_2\, z_1^{N_1-1} z_2^{N_2-1} f(z_1, z_2).$$

$$
\begin{aligned}
&-\delta_{ca_1}\delta_{\bar{c}a_2}\frac{\left\langle\widetilde{\mathcal{M}}^{(0)}_{c\bar{c}\to Q\bar{Q}F}\right|\mathbf{\Gamma}^{(2)}_t+\mathbf{\Gamma}^{(2)\dagger}_t\left|\widetilde{\mathcal{M}}^{(0)}_{c\bar{c}\to Q\bar{Q}F}\right\rangle}{\left|\mathcal{M}^{(0)}_{c\bar{c}\to Q\bar{Q}F}\right|^2}\\
&-\frac{\left\langle\widetilde{\mathcal{M}}^{(0)}_{c\bar{c}\to Q\bar{Q}F}\right|\mathbf{\Gamma}^{(1)}_t+\mathbf{\Gamma}^{(1)\dagger}_t\left|\widetilde{\mathcal{M}}^{(0)}_{c\bar{c}\to Q\bar{Q}F}\right\rangle}{\left|\mathcal{M}^{(0)}_{c\bar{c}\to Q\bar{Q}F}\right|^2}\Bigg[\delta_{ca_1}C^{(1)}_{\bar{c}a_2,N_2}+C^{(1)}_{ca_1,N_1}\delta_{\bar{c}a_2}\\
&\quad+\ell_F\left(\delta_{b_1a_1}\gamma^{(1)}_{b_2a_2,N_2}+\gamma^{(1)}_{b_1a_1,N_1}\delta_{b_2a_2}\right)-\ell_R\beta_0\delta_{ca_1}\delta_{\bar{c}a_2}\Bigg],
\end{aligned}
\tag{6.57}
$$

$$
\begin{aligned}
\mathcal{H}^{Q\bar{Q}F;NNLO}_{a_1a_2\to c\bar{c},\,(N_1,N_2)}=&\delta_{ca_1}\delta_{\bar{c}a_2}H^{Q\bar{Q}F(2)}_c+\delta_{ca_1}C^{(2)}_{\bar{c}a_2,N_2}+C^{(2)}_{ca_1,N_1}\delta_{\bar{c}a_2}+C^{(1)}_{ca_1,N_1}C^{(1)}_{\bar{c}a_2,N_2}\\
&+H^{Q\bar{Q}F(1)}_c\left(\delta_{ca_1}C^{(1)}_{\bar{c}a_2,N_2}+C^{(1)}_{ca_1,N_1}\delta_{\bar{c}a_2}\right)+\frac{\ell_F^2}{2}\beta_0\left(\delta_{ca_1}\gamma^{(1)}_{\bar{c}a_2,N_2}+\gamma^{(1)}_{ca_1,N_1}\delta_{\bar{c}a_2}\right)\\
&+\left(\delta_{ca_1}\gamma^{(2)}_{\bar{c}a_2,N_2}+\gamma^{(2)}_{ca_1,N_1}\delta_{\bar{c}a_2}\right)\ell_F-\mathcal{H}^{Q\bar{Q}F;NLO}_{a_1a_2\to c\bar{c},\,(N_1,N_2)}\beta_0\ell_R\\
&+\frac{1}{2}\sum_{b_1,b_2}\left[\mathcal{H}^{Q\bar{Q}F;NLO}_{b_1b_2\to c\bar{c},\,(N_1,N_2)}+\delta_{cb_1}\delta_{\bar{c}b_2}H^{Q\bar{Q}F(1)}_c+\delta_{ca_1}C^{(1)}_{\bar{c}a_2,N_2}+C^{(1)}_{ca_1,N_1}\delta_{\bar{c}a_2}\right]\\
&\quad\times\left[\left(\delta_{b_1a_1}\gamma^{(1)}_{b_2a_2,N_2}+\gamma^{(1)}_{b_1a_1,N_1}\delta_{b_2a_2}\right)\ell_F-\delta_{b_1a_1}\delta_{b_2a_2}k\beta_0\ell_R\right]\\
&-\delta_{ca_1}\delta_{\bar{c}a_2}k\left(\frac{1}{2}\beta_0^2\ell_R^2+\beta_1\ell_R\right),
\end{aligned}
\tag{6.58}
$$

where $\gamma^{(n)}_{ab,N}$ is the N moment of the n-order Altarelli-Parisi splitting function $P_{ab}(z)$, i.e.

$$
\gamma_{ab,N}=\int_0^1 \mathrm{d}z\, z^(N-1)P_{ab}(z)=\sum_{n=1}^{\infty}\left(\frac{\alpha_s}{\pi}\right)^n\gamma^{(n)}_{ab,N}\,. \tag{6.59}
$$

As mentioned before, in gluon initiated processes ($c=g$), the azimuthal correlations arising at small q_T don't vanish upon averaging in $\phi(b)$ and they give an extra contribution to the two-loop soft function, encoded in the following replacement

$$
\mathcal{H}^{Q\bar{Q}F;NNLO}_{a_1a_2\to gg,\,(N_1,N_2)}\longrightarrow\mathcal{H}^{Q\bar{Q}F;NNLO}_{a_1a_2\to gg,\,(N_1,N_2)}+H^{Q\bar{Q}F}_G G^{(1)}_{ga_1,N_1}G^{(1)}_{ga_2,N_2} \tag{6.60}
$$

$$
+H^{Q\bar{Q}F}_{\mathbf{D}G}\left(G^{(1)}_{ga_1,N_1}\delta_{ga_2}+\delta_{ga_1}G^{(1)}_{ga_2,N_2}\right), \tag{6.61}
$$

where the functions $G^{(1)}_{ab}$ are universal, and the coefficients $H^{Q\bar{Q}F}_G$ and $H^{Q\bar{Q}F}_{\mathbf{D}G}$ are process-dependent spin correlations, with a non-trivial colour structure for the latter. Their expressions can be found in Appendix C.1. Their calculation involves complicated $\mathbf{b}$-space integrals which have only been computed for the production of a $t\bar{t}$ pair [152–154], and are currently unknown for $t\bar{t}h$ hadroproduction.

This concludes the general formulation of q_T-subtraction for the hadroproduction of a heavy quark pair in association with a colourless final state. At NLO, to compute the

counter-term we need the soft anomalous dimension operator $\mathbf{\Gamma}_Q^{(1)}$, while for the soft function $\mathcal{H}_{a_1a_2\to c\bar{c}}^{(1)}$ we also need the finite part of the insertion operator $\widetilde{\mathbf{I}}^{(1)}$ that is new for the colourful final state, i.e. $\mathbf{F}_Q$. At NNLO the counter-term depends on these two quantities plus the second order soft anomalous dimension operator $\mathbf{\Gamma}_Q^{(2)}$. To compute the soft function $\mathcal{H}_{a_1a_2\to c\bar{c}}^{(2)}$ one would need the second order insertion operator $\widetilde{\mathbf{I}}^{(2)}$ as well as the spin correlations $H_G^{Q\bar{Q}F}$ and $H_{\mathbf{D}G}^{Q\bar{Q}F}$ appearing in $\mathcal{H}_{a_1a_2\to gg}^{(2)}$. While all of these ingredients are known for the $t\bar{t}$ production, allowing for a fully differential NNLO computation of hadroproduction of a top pair, the extension to the case in which the quark pair is no longer back-to-back (at LO), such as $t\bar{t}h$ or $t\bar{t}Z$, has not been performed yet mainly due to the more complicated kinematical structure.

In the following chapter 7 we will present the soft function $\mathcal{H}_{t\bar{t}h}^{(1)}$ for the first time and implement the q_T-subtraction method for $t\bar{t}h$ and $t\bar{t}Z$ production at NLO. Afterwards, in chapter 7, we will present the implementation of the NNLO counter-terms for $t\bar{t}h$.

7

NLO RESULTS

In this chapter we present the work done to implement q_T subtraction at NLO for the $t\bar{t}h$ hadro-production. We will start in section 7.1 by showing the necessary ingredients, this is the NLO soft-anomalous dimension operator $\mathbf{\Gamma}_t^{(1)}$ and the final-state originated piece of the NLO insertion operator $\widetilde{\mathbf{I}}_{t\bar{t}h}^{(1)}$, computed from the NLO amplitude in the eikonal approximation. Afterwards, in section 7.2 we will briefly discuss the numerical setup and present the results, validated against other available generators, for the $t\bar{t}$, $t\bar{t}h$ and $t\bar{t}Z$ hadroproduction processes.

7.1 INGREDIENTS

In order to implement the q_T-subtraction formalism at NLO for $t\bar{t}h$, we need the insertion operator $\widetilde{\mathbf{I}}_{c\bar{c}\to t\bar{t}h}^{(1)}(\varepsilon, M)$, which we write as the sum of $\widetilde{\mathcal{I}}_c^{(1)}(\varepsilon, M)$ which describes all the initial state divergences and $\widetilde{\mathbf{I}}_{t\bar{t}h}$ which describes all the new divergences arising from final state radiation. Because the coloured legs in the final state are top quarks, all collinear divergences are regulated by the mass of the top m_t and the only ones contributing to the insertion operator originate in the emission of soft gluons. These soft emissions are described at amplitude level by the eikonal approximation:

$$\begin{aligned}\sum_{\text{pol}\, g} |\mathcal{M}_{a_1a_2\to t\bar{t}hg}^{(\text{tree})}|^2 \overset{k\to 0}{\approx} -4\pi\alpha_s(\mu_R)\mu_R^{2\varepsilon} \sum_{i=1}^{4} \frac{p_i\cdot p_j}{(k\cdot p_i)(k\cdot p_j)} \left\langle \mathcal{M}_{a_1a_2\to t\bar{t}h}^{(\text{tree})} \right| \mathbf{T}_i\cdot\mathbf{T}_j \left| \mathcal{M}_{a_1a_2\to t\bar{t}h}^{(\text{tree})} \right\rangle \\ = \left\langle \mathcal{M}_{a_1a_2\to t\bar{t}h}^{(\text{tree})} \right| 4\pi\alpha_s(\mu_R)\mu_R^{2\varepsilon}\mathbf{T}_{\text{soft}} \left| \mathcal{M}_{a_1a_2\to t\bar{t}h}^{(\text{tree})} \right\rangle, \end{aligned} \tag{7.1}$$

where the sum runs over the polarizations of the emitted gluon of momentum k, $\{p_i\}_{i=1,\dots,4}$ denote the momentum of the coloured legs $\{a_1, a_2, t, \bar{t}\}$ (in that order) and $\mathcal{T}_i$ denote the colour operator of the leg coloured i. We can rewrite this $\mathbf{T}_{\text{soft}}$ in terms of the one appearing for a colourless final state plus the new final state and final-initial interferences

$$\mathbf{T}_{\text{soft}} = -\sum_{i,j=1}^{4} \frac{p_i\cdot p_j}{k\cdot p_i k\cdot p_j}\mathbf{T}_i\cdot\mathbf{T}_j = \frac{2p_1\cdot p_2}{p_1\cdot k\,(p_1+p_2)\cdot k}\mathbf{T}_1^2 + \frac{2p_1\cdot p_2}{p_2\cdot k\,(p_1+p_2)\cdot k}\mathbf{T}_2^2$$

$$
\begin{aligned}
&- \Bigg[\frac{p_3^2}{(p_3\cdot k)^2}\mathbf{T}_3^2 + \frac{p_4^2}{(p_4\cdot k)^2}\mathbf{T}_4^2 + \frac{2p_3\cdot p_4}{p_3\cdot k\, p_4\cdot k}\mathbf{T}_3\cdot\mathbf{T}_4 \\
&\quad + 2\sum_{i=1}^{2}\sum_{j=3}^{4}\left(\frac{p_i\cdot p_j}{p_j\cdot k} - \frac{p_1\cdot p_2}{(p_1+p_2)\cdot k}\right)\frac{\mathbf{T}_i\cdot\mathbf{T}_j}{p_i\cdot k}\Bigg].
\end{aligned}
\tag{7.2}
$$

The first line contributes to $\widetilde{\mathcal{I}}_c^{(1)}(\varepsilon, M)$ (together with the collinear initial state divergences), while the last two lines (which are only non-zero for a colourful final state) give rise to the new piece $\widetilde{\mathbf{I}}_{t\bar{t}h}$.

After we approximate the amplitude in the soft region as (7.1) we can integrate over the phase-space of the extra radiation for a fixed q_T

$$
\begin{aligned}
&\int \mathrm{d}^D k\, \delta_+(k^2)\delta^{(D-2)}(q_T + k_T) \sum_{\text{pol}\, g} |\mathcal{M}^{(\text{tree})}_{a_1a_2\to t\bar{t}hg}|^2 \\
&\quad \supset -4\pi\alpha_s(\mu_R)\mu_R^{2\varepsilon}\left\langle \mathcal{M}^{(\text{tree})}_{a_1a_2\to t\bar{t}h}\right| \int \mathrm{d}^D k\, \delta_+(k^2)\delta^{D-2}(\mathbf{q}_T + \mathbf{k}_T) \\
&\qquad \Bigg[\frac{p_3^2}{(p_3\cdot k)^2}\mathbf{T}_3^2 + \frac{p_4^2}{(p_4\cdot k)^2}\mathbf{T}_4^2 + \frac{2p_3\cdot p_4}{p_3\cdot k\, p_4\cdot k}\mathbf{T}_3\cdot\mathbf{T}_4 \\
&\qquad + 2\sum_{i=1}^{2}\sum_{j=3}^{4}\left(\frac{p_i\cdot p_j}{p_j\cdot k} - \frac{p_1\cdot p_2}{(p_1+p_2)\cdot k}\right)\frac{\mathbf{T}_i\cdot\mathbf{T}_j}{p_i\cdot k}\Bigg] \left|\mathcal{M}^{(\text{tree})}_{a_1a_2\to t\bar{t}h}\right\rangle \\
&\quad = -4\pi\alpha_s(\mu_R)\mu_R^{2\varepsilon} \\
&\qquad \left\langle \mathcal{M}^{(\text{tree})}_{a_1a_2\to t\bar{t}h}\right| I_{33}\mathbf{T}_3^2 + I_{44}\mathbf{T}_4^2 + I_{34}\mathbf{T}_3\cdot\mathbf{T}_4 + \sum_{\substack{i=1,2\\ j=3,4}} I_{ij}\mathbf{T}_i\cdot\mathbf{T}_j \left|\mathcal{M}^{(\text{tree})}_{a_1a_2\to t\bar{t}h}\right\rangle
\end{aligned}
\tag{7.3}
$$

where we only considered the terms in $\mathbf{T}_{\text{soft}}$ which contribute to $\widetilde{\mathbf{I}}_{t\bar{t}h}$, namely the last two lines of (7.2), and we defined the scalar integrals I_{ij} as

$$
I_{ij} = \int \mathrm{d}^D k\, \delta_+(k^2)\delta^{D-2}(\mathbf{q}_T + \mathbf{k}_T) f_{ij}(k) \tag{7.4}
$$

$$
f_{ij} = \begin{cases} \frac{p_j^2}{(p_j\cdot k)^2} & \text{if } i = j \in \{3,4\} \\ 2\frac{p_i\cdot p_j}{p_i\cdot k\, p_j\cdot k} & \text{if } i = 3,\ j = 4 \\ \frac{2}{p_i\cdot k}\left(\frac{p_i\cdot p_j}{p_j\cdot k} - \frac{p_1\cdot p_2}{(p_1+p_2)\cdot k}\right) & \text{if } i \in \{1,2\},\ j \in \{3,4\} \end{cases} \tag{7.5}
$$

We can factor out the dependence on q_T^2 by rescaling the integration momentum k. This dependence encodes the divergent behaviour, which becomes an explicit pole in ε when we go to impact parameter space (operating with $\int \mathrm{d}^{D-2}\mathbf{q}_T\, e^{-i\mathbf{b}\cdot\mathbf{q}_T}$):

$$
\left(\frac{q_T^2}{M^2}\right)^{-1-\varepsilon} \xrightarrow{\mathbf{b}\text{-space}} \frac{1}{\varepsilon}\left(\frac{b^2M^2}{b_0^2}\right)^{\varepsilon}. \tag{7.6}
$$

After factorizing the dependence on q_T^2, the integrals will only retain a dependence on the unit vector $\mathbf{q}_T/q_T$ that will disappear upon azimuthal integration.

The integrals appearing in (7.4), although unpublished, were computed in b-space in the context of A. Torre's doctoral thesis [173], which allow us to write down their explicit expressions

$$\left\langle \tilde{I}_{jj}(\mathbf{b}) \right\rangle_{\phi_{\mathbf{q}_T}} = \frac{\mathcal{N}}{(4\pi)^2} \left(\frac{b^2}{b_0^2}\right)^{\varepsilon} \left[\frac{1}{\varepsilon} + \ln\left(1 + \frac{p_{j,T}^2}{p_j^2}\right) + \mathcal{O}(\varepsilon)\right], \tag{7.7}$$

$$\left\langle \tilde{I}_{ij}(\mathbf{b}) \right\rangle_{\phi_{\mathbf{q}_T}} = \frac{\mathcal{N}}{(4\pi)^2} \left(\frac{b^2}{b_0^2}\right)^{\varepsilon} \left[\frac{1}{\varepsilon} \ln\left(\frac{4(p_i \cdot p_j)^2}{(p_1+p_2)^2 p_j^2}\right) - \mathrm{Li}_2\left(-\frac{p_{j,T}^2}{p_j^2}\right) + \mathcal{O}(\varepsilon)\right], \tag{7.8}$$

$$\left\langle \tilde{I}_{34}(\mathbf{b}) \right\rangle_{\phi_{\mathbf{q}_T}} = \frac{\mathcal{N}}{(4\pi)^2} \left(\frac{b^2}{b_0^2}\right)^{\varepsilon} \frac{1}{\beta_{34}} \left[\frac{1}{\varepsilon} \ln\left(\frac{1+\beta_{34}}{1-\beta_{34}}\right) + L_{34} + \mathcal{O}(\varepsilon)\right], \tag{7.9}$$

where $j \in \{3,4\}$, $i \in \{1,2\}$,

$$\mathcal{N} = -8\pi^2 \Gamma(1-\varepsilon)^2 \Omega_{(d-2)} e^{-2\gamma_E \varepsilon}$$

is a normalization constant proportional to the total solid angle $\Omega_{(d-2)} = \frac{2\pi}{\pi^{\varepsilon}\Gamma(1-\varepsilon)}$, $p_{j,T}$ denotes the transverse component of momentum p_j respect to the axis defined by $p_1$in the partonic centre of mass. We denote by $\langle\rangle_{\phi_{\mathbf{q}_T}}$ the azimuthal average in the direction of $\mathbf{q}_T$, and use a tilde to denote that the integrals are written in impact parameter space. The following quantities were also defined

$$\beta_{34} = \sqrt{1 - \frac{p_3^2 p_4^2}{(p_3 \cdot p_4)^2}}, \tag{7.10}$$

$$\begin{aligned} L_{34} = {} & \frac{1}{2} \ln\left(\frac{1+\beta_{34}}{1-\beta_{34}}\right) \ln\left[\left(1 + \frac{p_{3,T}^2}{p_3^2}\right)\left(1 + \frac{p_{4,T}^2}{p_4^2}\right)\right] - 2\mathrm{Li}_2\left(\frac{2\beta_{34}}{1+\beta_{34}}\right) \\ & - \frac{1}{4} \ln^2\left(\frac{1+\beta_{34}}{1-\beta_{34}}\right) + \left\{\left[\mathrm{Li}_2\left(1 - \sqrt{\frac{1-\beta_{34}}{1+\beta_{34}}} r\right) + \mathrm{Li}_2\left(1 - \sqrt{\frac{1-\beta_{34}}{1+\beta_{34}}} \frac{1}{r}\right)\right.\right. \\ & \left.\left. + \frac{1}{2} \ln^2(r)\right] + (r \to \bar{r})\right\}, \end{aligned} \tag{7.11}$$

where $r = \frac{p_1 \cdot p_3}{p_1 \cdot p_4}$ and $\bar{r} = \frac{p_2 \cdot p_3}{p_2 \cdot p_4}$.

After we transform Eq. (7.3) to impact parameter space, take the azimuthal average and plug in the results in Eqs. (7.7) - (7.9), we obtain

$$\int \mathrm{d}^D k\, \delta_+(k^2) e^{i\mathbf{b}\cdot\mathbf{k}_T} \sum_{\mathrm{pol}\, g} |\mathcal{M}^{(\mathrm{tree})}_{a_1 a_2 \to t\bar{t}hg}|^2$$

$$\supset \mathcal{N}\left(\frac{b^2M^2}{b_0^2}\right)^{\varepsilon}\left\langle \mathcal{M}^{(\text{tree})}_{a_1a_2\to t\bar{t}h}\right|\text{Re}\,\widetilde{\mathbf{I}}_{t\bar{t}h}+\mathcal{O}(\varepsilon)\left|\mathcal{M}^{(\text{tree})}_{a_1a_2\to t\bar{t}h}\right\rangle, \tag{7.12}$$

$$\widetilde{\mathbf{I}}_{t\bar{t}h}=-\frac{1}{2}\frac{\alpha_s(\mu_R)}{2\pi}\left(\frac{\mu_R^2}{M^2}\right)^{\varepsilon}\left[-\frac{4}{\varepsilon}\mathbf{\Gamma}_t+\mathbf{F}_t\right]+\mathcal{O}(\alpha_s^2), \tag{7.13}$$

$$\begin{aligned}\mathbf{\Gamma}_t=&-\frac{1}{4}\Bigg[\sum_{j=3,4}(1-i\pi)\mathbf{T}_j^2+\mathbf{T}_4^2+\mathbf{T}_3\cdot\mathbf{T}_4\frac{1}{\beta_{34}}\left(\ln\left(\frac{1+\beta_{34}}{1-\beta_{34}}\right)-i2\pi(1+\beta_{34})\right)\\&+\sum_{\substack{i=1,2\\j=3,4}}\mathbf{T}_i\cdot\mathbf{T}_j\ln\left(\frac{4(p_i\cdot p_j)^2}{(p_1+p_2)^2p_j^2}\right)\Bigg],\end{aligned} \tag{7.14}$$

$$\mathbf{F}_t=\sum_{j=3,4}\mathbf{T}_j^2\ln\left(1+\frac{p_{j,T}^2}{p_j^2}\right)+\mathbf{T}_3\cdot\mathbf{T}_4L_{34}-\sum_{\substack{i=1,2\\j=3,4}}\mathbf{T}_i\cdot\mathbf{T}_j\text{Li}_2\left(-\frac{p_{j,T}^2}{p_j^2}\right). \tag{7.15}$$

We can see that the pole is described by the anomalous dimension operator $\mathbf{\Gamma}_t$, which multiplied by the factor $\left(\frac{b^2M^2}{b_0^2}\right)^{\varepsilon}=1+\varepsilon\ln\frac{b^2M^2}{b_0^2}+\mathcal{O}(\varepsilon^2)$ gives a finite contribution logarithmic in $b^2M^2\sim M^2/q_T^2$. This is the origin of the $\mathbf{\Gamma}_t$ contribution to $\Sigma^{Q\bar{Q}F(1;1)}_{a_1a_2\to c\bar{c}}$ in Eq. (6.49). The $\mathbf{F}_t$ operator is the finite part of the insertion operator, which is independent of b (i.e. proportional to $\delta(q_T)$), and contributes to the first order hard coefficient

$$\begin{aligned}H_c^{Q\bar{Q}F(1)}=&2\text{Re}\frac{\left\langle\widetilde{\mathcal{M}}^{(1)}_{c\bar{c}\to t\bar{t}h}\right|\widetilde{\mathcal{M}}^{(0)}_{c\bar{c}\to t\bar{t}h}\rangle}{\left|\mathcal{M}^{(0)}_{c\bar{c}\to t\bar{t}h}\right|^2}\\=&2\text{Re}\frac{\left\langle\mathcal{M}^{(1)}_{c\bar{c}\to t\bar{t}h}\right|\mathcal{M}^{(0)}_{c\bar{c}\to t\bar{t}h}\rangle-\left\langle\mathcal{M}^{(0)}_{c\bar{c}\to t\bar{t}h}\right|\widetilde{\mathbf{I}}^{(1)}_{c\bar{c}\to t\bar{t}h}\left|\mathcal{M}^{(0)}_{c\bar{c}\to t\bar{t}h}\right\rangle}{\left|\mathcal{M}^{(0)}_{c\bar{c}\to t\bar{t}h}\right|^2}.\end{aligned} \tag{7.16}$$

When restricted to $t\bar{t}$ kinematics in which the heavy quarks are back to back (that is, $\mathbf{p}_{T,3}=-\mathbf{p}_{T,4}=\mathbf{p}_T$), this coefficient reduces to the known result [150]

$$\begin{aligned}\mathbf{F}_t=&(\mathbf{T}_3^2+\mathbf{T}_4^2)\ln\left(1+\frac{p_T^2}{m_t^2}\right)+(\mathbf{T}_3+\mathbf{T}_4)^2\text{Li}_2\left(-\frac{p_T^2}{m_t^2}\right)+\mathbf{T}_3\cdot\mathbf{T}_4\\&\times\frac{1}{\beta_{34}}\Bigg\{\ln\left(\frac{1+\beta_{34}}{1-\beta_{34}}\right)\ln\left(1+\frac{p_T^2}{m_t^2}\right)-2\text{Li}_2\left(\frac{2\beta_{34}}{1+\beta_{34}}\right)-\frac{1}{4}\ln^2\left(\frac{1+\beta_{34}}{1-\beta_{34}}\right)\\&+2\left[\text{Li}_2\left(1-\sqrt{\frac{1-\beta_{34}}{1+\beta_{34}}}e^{y_{34}}\right)+\text{Li}_2\left(1-\sqrt{\frac{1-\beta_{34}}{1+\beta_{34}}}e^{-y_{34}}\right)+\frac{1}{2}y_{34}^2\right]\Bigg\},\end{aligned} \tag{7.17}$$

where $y_{34}=y_3-y_4$ is the rapidity difference between the quarks t and $\bar{t}$.

With the results for $\mathbf{F}_t^{(1)}$ and $\mathbf{\Gamma}_t^{(1)}$ presented in Eq. (7.12) we are able to perform q_T subtraction at NLO for a generic final state $Q\bar{Q}F$, in particular for $t\bar{t}h$ and $t\bar{t}Z$ that will be presented in the following section 7.2.

7.2 RESULTS AND VALIDATION

In this section we present some of the numerical results used to validate the NLO implementation of q_T subtraction for a massive coloured final state. For this purposes, we have implemented all the formulae presented in the previous section 7.1 in a private Fortran code. All tree and one-loop level amplitudes, as well as colour-correlators, were computed using the OpenLoops library [174]. The MMHT 2014 [65] sets of parton distribution functions are used, interpolated by LHAPDF [69]. Multi-dimensional integration is performed using the CUBA library [70]. All phase-space generation routines were adapted from the ones present in MCFM [175].

For validation purposes, we compared our results for $pp \to t\bar{t}h$ against the ones obtained by MadGraph [176]. For $pp \to t\bar{t}$ we also compared against MCFM [175, 177] and Top++ [178]. The following values were used for the physical parameters: $m_t = 173.3\text{GeV}$ and $m_H = 125\text{GeV}$ for the masses of the top quark and the Higgs boson, whose widths were neglected $\Gamma_t = \Gamma_H = 0$, and the Fermi electroweak scheme was used with $m_Z = 91.1876\text{GeV}$ and $m_W = 80.3850\text{GeV}$ for the masses of the weak bosons W and Z, and $G_F = 1.16656 \times 10^{-5}\text{GeV}^{-2}$ for the Fermi coupling constant. All results were computed for a hadronic centre of mass energy of 13TeV.

As anticipated in eq (6.10), we compute the counter-term and the real emission cross sections for finite values of $r_{cut} = q^2_{T,min}/M^2$, therefore our cross section $\sigma(r_{cut})$ is r_{cut}-dependent. Afterwards, a numerical extrapolation to $r_{cut} = 0$ is performed. This is done using the algorithm defined in [157], which we will briefly describe: A series of linear fits are performed on the results for $r_{cut} \in [r_{min}, r_{max}]$, where r_{min} is the minimum value of r_{cut} for which the cross section is computed (typically $r_{min} \sim 0.2\%$ and r_{max} is varied in the interval $[0.5\%, 1\%]$). The fit which has the minimum χ^2 is used as the best fit, and its intercept is the reported value $\sigma(r_{cut} = 0)$. In order to be conservative about the systematic uncertainty introduced by the extrapolation, we sum quadratically the uncertainty of the intercept inherent to the linear fit $\Delta\sigma_{fit}$ with half the distance between the extrapolated value $\sigma(r_{cut} = 0)$ and the closest computed value $\sigma(r_{cut} = r_{min})$. That is,

$$\Delta\sigma^2 = \sqrt{\Delta\sigma^2_{fit} + \left(\frac{\sigma(r_{cut} = 0) - \sigma(r_{cut} = r_{min})}{2}\right)^2}. \tag{7.18}$$

7.2.1 *Validation: Top pair production*

We first validated our implementation in $pp \to t\bar{t}$ production. First of all, we compared numerically in several random points of the phase space that the counter-term, as well as the different coefficients that comprises it, coincides with the previous known result as implemented in [152]. Then, we compared our result with the ones provided by MadGraph, MCFM and Top++. The renormalization and factorization scales were fixed to $\mu_R = \mu_F = m_t = 173.3\text{GeV}$. The result as a function of r_{cut}, along with its extrapolation

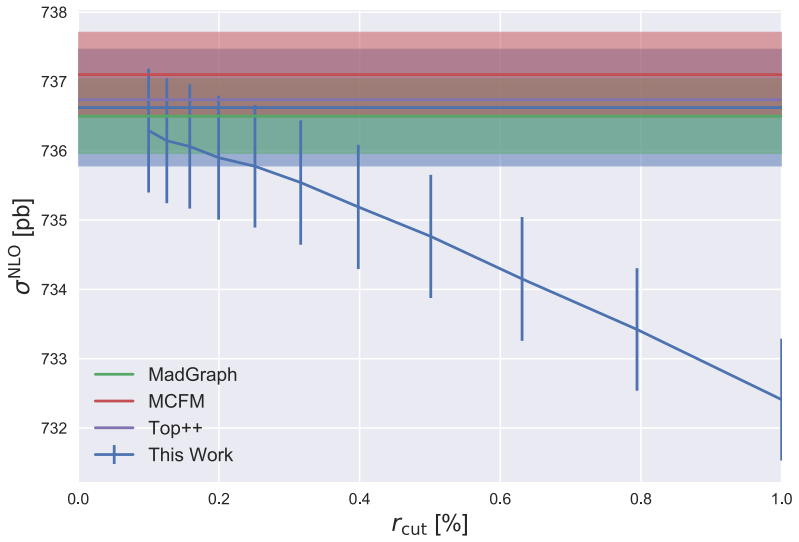

Figure 7.1: Inclusive cross section for $t\bar{t}$ production at NLO, plotted for different values of the technical parameter $r_{cut} = q^2_{T,min}/M^2$. In shaded bands we plot the extrapolated value to $r_{cut} = 0$, as well as the values computed by MadGraph, MCFM and Top++.

to $r_{cut} = 0$, is shown in Figure 7.1 and the numerical values are reported in Table 7.1. We notice that the cross section converges smoothly in r_{cut}, and the extrapolation to $r_{cut} = 0$ is consistent with all the other results below the permill level.

METHOD	$\sigma^{(NLO)}_{t\bar{t}}(pb)$
Top++	736.737
MCFM	737.1 ± 0.6
MadGraph	736.5 ± 0.5
This Work	736.6 ± 0.8

Table 7.1: Numerical results for the inclusive cross section to $t\bar{t}$ production at NLO, as provided by different packages.

7.2.2 *Top pair production in association with a massive boson*

Once we crossed-checked our implementation in the $t\bar{t}$ case, we computed the NLO cross section for $t\bar{t}h$ for the first time in the q_T-subtraction framework. Because this implementation should work for the production of any $t\bar{t}$ + colourless final state, we also computed the cross section for the similar $t\bar{t}Z$ production process. To validate our result,

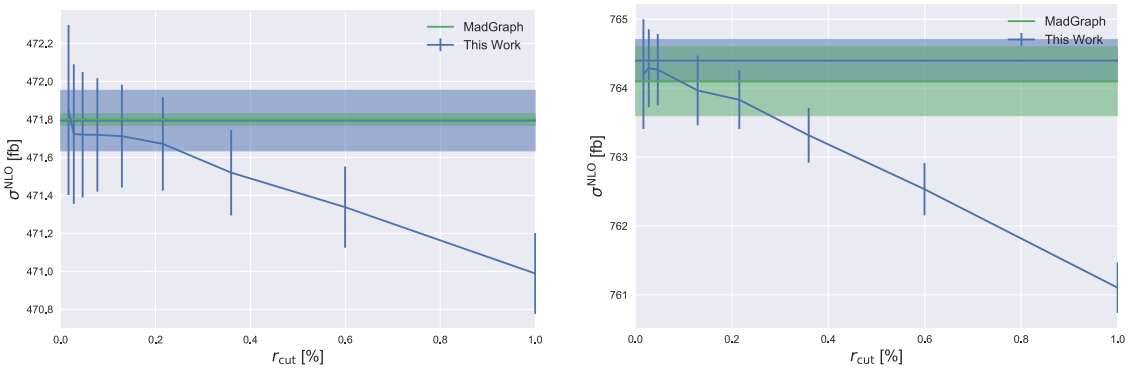

(a) $t\bar{t}h$ (b) $t\bar{t}Z$

Figure 7.2: Inclusive cross section for $t\bar{t}h$ (a) and $t\bar{t}Z$ (b) production at NLO, plotted for different values of the technical parameter $r_{cut} = q^2_{T,min}/M^2$. In shaded bands we plot the extrapolated value to $r_{cut} = 0$, as well as the values computed by MadGraph.

we compared it with the one provided by MadGraph. For a separate validation of the two scale-dependent pieces, we chose different renormalization and factorization scales, which were fixed to $\mu_R = 2\mu_F = 2m_t + m_H = 471.6$GeV. The result as a function of r_{cut}, along with its extrapolation to $r_{cut} = 0$, is shown in Figure 7.2 and the numerical values are reported in Table 7.2. We notice that the cross section converges smoothly in r_{cut}, and the extrapolation to $r_{cut} = 0$ is consistent with all the other results below the per mill level, with a relative difference of (0.03 ± 0.4)‰.

METHOD	$\sigma^{(NLO)}_{t\bar{t}h}(fb)$	$\sigma^{(NLO)}_{t\bar{t}Z}(fb)$
MadGraph	471.80 ± 0.03	764.1 ± 0.5
This Work	471.79 ± 0.16	764.4 ± 0.3

Table 7.2: Numerical results for the inclusive cross section to $t\bar{t}h$ production at NLO, computed for the first time with the q_T-subtraction method and computed by MadGraph.

We also validated our result by comparing single-differential distributions with MadGraph. For this purpose, we used a fixed value for $r_{cut} = 0.1\%$, as from Figure 7.2 we see at this point we should expect good agreement and is much more computationally cheap than performing a bin-wise extrapolation. We found agreement at the few percent level, compatible with the numerical error bars of each bin. Some examples of differential distributions are shown in Figure 7.3.

Having applied q_T-subtraction to $t\bar{t}h(Z)$ production and successfully recovered the known NLO results, we will start the discussion on the NNLO implementation of q_T-subtraction in the following chapter.

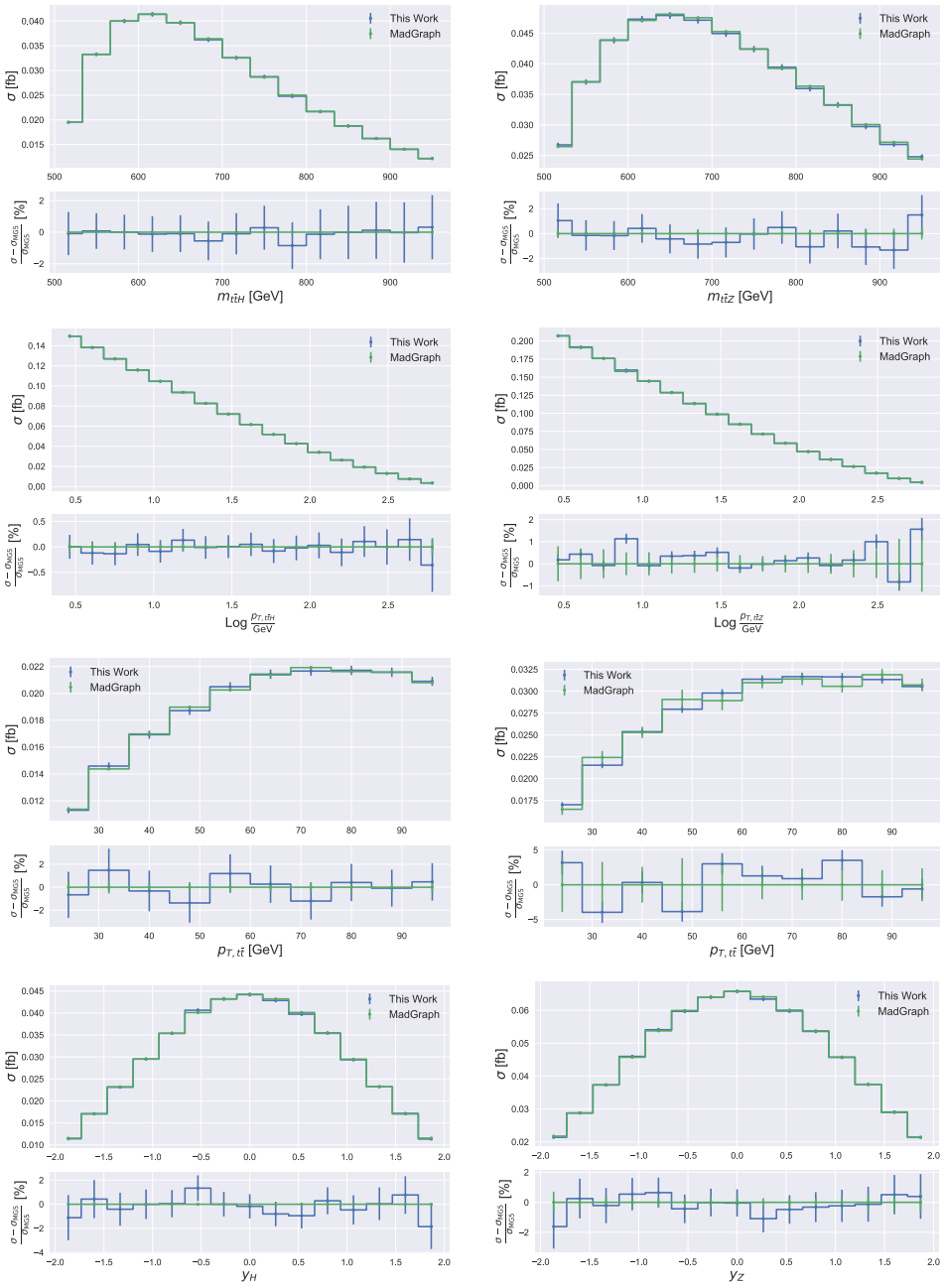

Figure 7.3: Single differential distributions $t\bar{t}h$ (left) and $t\bar{t}Z$ (right) production at NLO computed with the q_T-subtraction implementation of this work and with MadGraph. In the bottom subplots we see the relative difference between our result and the one of MadGraph, finding agreement for a numerical precision at the percent level.

8

NNLO RESULTS

In this chapter we present the implementation of the NNLO counter-term of q_T-subtraction for $t\bar{t}h$ production. We will start in section 8.1 by presenting the necessary ingredients to go from NLO to NNLO, namely the NNLO soft-anomalous dimension operator $\mathbf{\Gamma}_t^{(2)}$. Then, we will discuss the numerical setup and present the results in section 8.2.

8.1 INGREDIENTS

In order to compute the NNLO counter-terms, we need the second order soft anomalous dimension $\mathbf{\Gamma}^{(2)}$ which is known in general form up to two loops [179]. In the case of two coloured massive legs in the final state, and after subtracting the initial state piece, we can write it in the following form

$$\begin{aligned}\mathbf{\Gamma}_t = &\left[(\mathbf{T}_3+\mathbf{T}_4)^2 i\pi - \sum_{\substack{i=1,2\\j=3,4}} \mathbf{T}_i\cdot\mathbf{T}_j \ln\frac{(2p_i\cdot p_j)^2}{(p_1+p_2)^2 p_j^2}\right]\frac{\gamma_{\text{cusp}}(\alpha_s)}{4} + \gamma^Q(\alpha_s)\\ &-\frac{\mathbf{T}_3\cdot\mathbf{T}_4}{2}\gamma_{\text{cusp}}(\alpha_s,\beta_{34}) - \left(\frac{\alpha_s}{\pi}\right)^2\frac{1}{4}\left(\pi\beta_0\mathbf{F}_t^{(1)} + \left[\mathbf{\Gamma}_t^{(1)},\mathbf{F}_t^{(1)}\right]\right)\\ &+\left(\frac{\alpha_s}{\pi}\right)^2\sum_{i=1,2}\frac{if^{abc}\mathbf{T}_3^a\mathbf{T}_4^b\mathbf{T}_i^c}{4}g(\beta_{34})\ln\frac{p_3\cdot p_i}{p_4\cdot p_i},\end{aligned} \tag{8.1}$$

where

$$\gamma^Q(\alpha_s) = -\frac{\alpha_s}{\pi}\frac{C_F}{2} + \left(\frac{\alpha_s}{\pi}\right)^2\left[\frac{C_F C_A}{16}\left(\frac{2}{3}\pi^2 - \frac{98}{9} - 4\zeta_3\right) + \frac{40}{9}\frac{T_F C_F n_f}{16}\right] + \mathcal{O}(\alpha_s^3), \tag{8.2}$$

$$\gamma_{\text{cusp}}(\alpha_s) = \frac{\alpha_s}{\pi} + \left(\frac{\alpha_s}{\pi}\right)^2\left[\left(\frac{67}{36} - \frac{\pi^2}{12}\right)C_A - \frac{5}{9}T_F n_f\right] + \mathcal{O}(\alpha_s^3), \tag{8.3}$$

$$\gamma_{\text{cusp}}(\alpha_s,\beta) = \gamma_{\text{cusp}}(\alpha_s)\frac{1}{\beta}\left[\frac{1}{2}\ln^2\left(\frac{1+\beta}{1-\beta}\right) - i\pi\right] + \left(\frac{\alpha_s}{\pi}\right)^2\frac{C_A}{2}\left\{\right.$$

$$
\begin{aligned}
&\frac{1}{4}\ln^2\left(\frac{1+\beta}{1-\beta}\right) - \frac{5}{6}\pi^2 + \zeta_3 - i\pi\ln\left(\frac{1+\beta}{1-\beta}\right) + \frac{1}{\beta^2}\Bigg[\mathrm{Li}_3\left(\frac{1-\beta}{1+\beta}\right)\\
&+\frac{1}{2}\ln\left(\frac{1+\beta}{1-\beta}\right)\mathrm{Li}_2\left(\frac{1-\beta}{1+\beta}\right) + \frac{1}{24}\ln^3\left(\frac{1+\beta}{1-\beta}\right) - \frac{5}{12}\pi^2\ln\left(\frac{1+\beta}{1-\beta}\right)\\
&-\zeta_3 + i\pi\left(-\mathrm{Li}_2\left(\frac{1-\beta}{1+\beta}\right) - \frac{1}{4}\ln^2\left(\frac{1+\beta}{1-\beta}\right) + \frac{\pi^2}{6}\right)\Bigg]\\
&+\frac{1}{\beta}\Bigg[-\frac{1}{24}\ln^3\left(\frac{1+\beta}{1-\beta}\right) + \mathrm{Li}_2\left(\frac{1-\beta}{1+\beta}\right) - \frac{1}{4}\ln^2\left(\frac{1+\beta}{1-\beta}\right)\\
&-\ln\left(\frac{1+\beta}{1-\beta}\right)\ln\left(\frac{2}{1+\beta}\right) + \frac{5}{12}\pi^2\ln\left(\frac{1+\beta}{1-\beta}\right) + \frac{5}{6}\pi^2\\
&+i\pi\left(\frac{1}{4}\ln^2\left(\frac{1+\beta}{1-\beta}\right) + \ln\left(\frac{1+\beta}{1-\beta}\right) + 2\ln\left(\frac{2}{1+\beta}\right) - \frac{\pi^2}{6}\right)\Bigg]\Bigg\}\\
&+\mathcal{O}(\alpha_s^3),
\end{aligned}
\tag{8.4}
$$

and $\zeta_3 = 1.202\ldots$ is the Riemann zeta function evaluated in 3, and

$$
\mathrm{Li}_3(z) = -\int_0^z \frac{\mathrm{d}t}{t}\ln(t)\ln(1-zt)
$$

is the third degree polylogarithm function. The g function that appears in the last line of Eq. (8.1) can be written as

$$
\begin{aligned}
g(\beta) =& i\pi\left[\ln\left(\frac{1+\beta}{1-\beta}\right) - \frac{1}{\beta}\left(2\ln\left(\frac{2}{1+\beta}\right) + \ln\left(\frac{1+\beta}{1-\beta}\right)\right)\right] - \frac{1}{4}\ln^2\left(\frac{1+\beta}{1-\beta}\right) + \frac{5}{6}\pi^2\\
&+\frac{1}{\beta}\left[-\mathrm{Li}_2\left(\frac{1-\beta}{1+\beta}\right) + \frac{1}{4}\ln^2\left(\frac{1+\beta}{1-\beta}\right) + \ln\left(\frac{2}{1+\beta}\right)\ln\left(\frac{1+\beta}{1-\beta}\right) - \frac{5}{6}\pi^2\right]
\end{aligned}
\tag{8.5}
$$

With these definitions, we have the first two orders of the anomalous dimension operator

$$
\mathbf{\Gamma}_t = \frac{\alpha_s}{\pi}\mathbf{\Gamma}_t^{(1)} + \left(\frac{\alpha_s}{\pi}\right)^2\mathbf{\Gamma}_t^{(2)} + \mathcal{O}(\alpha_s^3).
$$

We note that we recover equation (7.14) for the first order coefficient $\mathbf{\Gamma}_t^{(1)}$. For the second order, we note that more complicated colour structures appear

- Four colour-correlations appear due to the term

$$
\left[\mathbf{\Gamma}_t^{(1)}, \mathbf{F}_t^{(1)}\right] = -\frac{1}{2}\left(\frac{1}{\beta_{34}}L_{34}(\beta_{34}) + \mathrm{Li}_2\left(-\frac{p_{3,T}^2}{p_3^2}\right) + \mathrm{Li}_2\left(-\frac{p_{4,T}^2}{p_4^2}\right)\right)
$$

$$\times \ln\left(\frac{(p_1\cdot p_3)(p_2\cdot p_4)}{(p_1\cdot p_4)(p_2\cdot p_3)}\right)[\mathbf{T}_1\cdot\mathbf{T}_3,\ \mathbf{T}_3\cdot\mathbf{T}_4]\,. \tag{8.6}$$

But because the expression that enters the NNLO counter-term is $\mathbf{\Gamma}_t^{(2)}+\mathbf{\Gamma}_t^{(2)\dagger}$, we are only interested in $\left[\mathbf{\Gamma}_t^{(1)},\mathbf{F}_t^{(1)}\right]+\left[\mathbf{\Gamma}_t^{(1)},\mathbf{F}_t^{(1)}\right]^\dagger$. As for the $c\bar{c}\to t\bar{t}h$ kinematics, the prefactor in Eq. (8.6) is real and, due to the antihermiticity of the commutation operator $[\mathbf{T}_1\cdot\mathbf{T}_3,\ \mathbf{T}_3\cdot\mathbf{T}_4]+[\mathbf{T}_1\cdot\mathbf{T}_3,\ \mathbf{T}_3\cdot\mathbf{T}_4]^\dagger=0$, this four colour-correlator term does not contribute to the NNLO counter-term.

- Triple colour-correlations appear in the last term of Eq. (8.1). First of all, we can simplify the sum using the colour conservation ($\sum_{k=1,4}\mathbf{T}_k=0$) and the antisymmetry of f^{abc}, which implies that $if^{abc}\mathbf{T}_3^a\mathbf{T}_4^b\mathbf{T}_1^c=-if^{abc}\mathbf{T}_3^a\mathbf{T}_4^b\mathbf{T}_2^c$. Then, we can use the antihermiticity of the operator $if^{abc}\mathbf{T}_3^a\mathbf{T}_4^b\mathbf{T}_1^c$ to write the contribution of this term to the counter-term, that is to $\left\langle\widetilde{\mathcal{M}}^{(0)}\right|\mathbf{\Gamma}_t^{(2)}+\mathbf{\Gamma}_t^{(2)\dagger}\left|\widetilde{\mathcal{M}}^{(0)}\right\rangle$, in the following way

$$\left\langle\widetilde{\mathcal{M}}^{(0)}\right|if^{abc}\mathbf{T}_3^a\mathbf{T}_4^b\mathbf{T}_1^c\left|\widetilde{\mathcal{M}}^{(0)}\right\rangle\frac{2i\mathrm{Im}\ g(\beta_{34})}{4}\ln\frac{(p_3\cdot p_1)(p_4\cdot p_2)}{(p_4\cdot p_1)(p_3\cdot p_2)}. \tag{8.7}$$

At variance with the four colour-correlator, the prefactor $g(\beta_{34})$ has an imaginary part and therefore the antihermiticity of the colour operator will not be enough for this contribution to vanish. Nevertheless, there are several cases in which this term will not contribute:

1. In pair production, e.g. in the $t\bar{t}$ case, because the massive quarks are back to back $p_i\cdot p_3=-p_i\cdot p_4$ the logarithm evaluates to $\ln(1)=0$. In this particular kinematics, this term will not contribute.
2. Whenever the LO amplitude $\widetilde{\mathcal{M}}^{(0)}$ doesn't contain non-trivial complex phases, the contraction $\left\langle\widetilde{\mathcal{M}}^{(0)}\right|if^{abc}\mathbf{T}_3^a\mathbf{T}_4^b\mathbf{T}_1^c\left|\widetilde{\mathcal{M}}^{(0)}\right\rangle$ will vanish [180, 181]. This is the case of both $t\bar{t}$ and $t\bar{t}h$, but in cases like $t\bar{t}Z$ due to the axial coupling that introduces a complex phase in the LO amplitude, there will be a contribution of this three colour-correlators. In this three particular cases, we have cross-checked this argument numerically.

With this ingredients, plus the NLO result, we can implement all the counter-terms in equations (6.54)-(6.58) as well as the soft function for the off-diagonal channels. Before presenting these results, we will make a brief comment on the numerical implementation of colour-correlators at NNLO using OpenLoops.

8.1.1 *Three and four colour correlators with* OpenLoops

As in the previous chapter, we get our amplitudes from the OpenLoops library. While there is an interface to compute any two colour-correlators, it also provides the amplitude

as a colour-vector, which we can use to compute any correlator we need. In order to do this, we have to write down the colour-operators as a matrices in colour space, in the same basis that OpenLoops uses. For the $t\bar{t}h$ production, at LO we have two channels: The gluon initiated $gg \to t\bar{t}h$ and the quark anti-quark channel $q\bar{q} \to t\bar{t}h$. The basis used by OpenLoops in these two processes are

$$\left|c_1^{gg}\right\rangle = (T^{a_1}T^{a_2})_{i_3}^{\bar{j}_4}, \qquad \left|c_2^{gg}\right\rangle = (T^{a_2}T^{a_1})_{i_3}^{\bar{j}_4}, \tag{8.8}$$

$$\left|c_1^{q\bar{q}}\right\rangle = \delta_{i_3}^{\bar{i}_1}\delta_{j_2}^{\bar{j}_4}, \qquad \left|c_2^{q\bar{q}}\right\rangle = \delta_{i_3}^{\bar{j}_4}\delta_{j_2}^{\bar{i}_1}, \tag{8.9}$$

where T^a are the generators of $SU(3)$ in the adjoint representation, the indices i, j and a refer to the colour indices of a quark, an anti-quark and a gluon, respectively, and the subindices refer to the leg being considered. The indices i and j transform in the fundamental representation of $SU(3)$, $\bar{i}$ and $\bar{j}$ in the anti-fundamental, and a in the adjoint representation.

If we write the amplitude in this basis $|\mathcal{M}\rangle = \mathcal{M}_1 |c_1\rangle + \mathcal{M}_2 |c_2\rangle$, for any colour-operator $\mathbf{O}$ have that

$$\langle\mathcal{M}|\,\mathbf{O}\,|\mathcal{M}\rangle = \sum_{l,m=1,2} \mathcal{M}_l^* \mathcal{M}_m \langle c_l|\,\mathbf{O}\,|c_l\rangle\,. \tag{8.10}$$

The coefficient $\mathcal{M}_1$ and $\mathcal{M}_2$ are provided by OpenLoops, so, we only need to compute the colour-matrices $\langle c_l|\,\mathbf{O}\,|c_l\rangle$ in the basis (8.8) and (8.9), for the operators $\mathbf{O}$ we need. We will denote this colour-matrix as $[\mathbf{O}]$.

For q_T subtraction at NNLO, we need $\mathbf{\Gamma}^{(n)} + \mathbf{\Gamma}^{(n)\dagger}$ for $n = 1, 2$, as well as $\left(\mathbf{\Gamma}^{(1)} + \mathbf{\Gamma}^{(1)\dagger}\right)^2$, both of which can be written in terms of the two, three and four colour-correlators $\mathbf{T}_i \cdot \mathbf{T}_j$, $if^{abc}\mathbf{T}_3^a\mathbf{T}_4^b\mathbf{T}_1^c$ and $\mathbf{T}_i \cdot \mathbf{T}_j\mathbf{T}_k \cdot \mathbf{T}_l$. Let's recall that the colour operator $\mathbf{T}_i$ describe the emission of a gluon of colour a from the leg i

$$\mathbf{T}_i = if^{bac}, \qquad \text{if leg } i \text{ is a gluon} \tag{8.11}$$

$$\mathbf{T}_i = (T^a)_i^{\bar{j}}, \qquad \text{if leg } i \text{ is a final state quark or initial state anti-quark.} \tag{8.12}$$

With these definitions we can compute all the colour matrices, which for the two-colour correlators read

$$[\mathbf{T}_1^2]_{gg} = [\mathbf{T}_2^2]_{gg} = C_A\frac{C_F}{2}\begin{pmatrix} 2C_AC_F & -1 \\ -1 & 2C_AC_F \end{pmatrix}, \tag{8.13}$$

$$[\mathbf{T}_3^2]_{gg} = [\mathbf{T}_4^2]_{gg} = C_F\frac{C_F}{2}\begin{pmatrix} 2C_AC_F & -1 \\ -1 & 2C_AC_F \end{pmatrix}, \tag{8.14}$$

$$[\mathbf{T}_1 \cdot \mathbf{T}_2]_{gg} = -\frac{1}{4}C_A^3C_F\begin{pmatrix} 1 & 0 \\ 0 & 1 \end{pmatrix}, \tag{8.15}$$

$$[\mathbf{T}_3 \cdot \mathbf{T}_4]_{gg} = -\frac{1}{4} C_F (C_A - 2C_F) \begin{pmatrix} 1 & C_A^2 + 1 \\ C_A^2 + 1 & 1 \end{pmatrix}, \tag{8.16}$$

$$[\mathbf{T}_1 \cdot \mathbf{T}_3]_{gg} = [\mathbf{T}_2 \cdot \mathbf{T}_4]_{gg} = \frac{1}{4} C_A C_F \begin{pmatrix} -2C_A C_F & 1 \\ 1 & 1 \end{pmatrix}, \tag{8.17}$$

$$[\mathbf{T}_1 \cdot \mathbf{T}_4]_{gg} = [\mathbf{T}_2 \cdot \mathbf{T}_3]_{gg} = \frac{1}{4} C_A C_F \begin{pmatrix} 1 & 1 \\ 1 & -2C_A C_F \end{pmatrix} \tag{8.18}$$

for the gluon fusion channel, while for the quark annihilation we have

$$[\mathbf{T}_1^2]_{q\bar{q}} = [\mathbf{T}_2^2]_{q\bar{q}} = [\mathbf{T}_3^2]_{q\bar{q}} = [\mathbf{T}_4^2]_{q\bar{q}} = C_F \begin{pmatrix} C_A^2 & C_A \\ C_A & C_A^2 \end{pmatrix}, \tag{8.19}$$

$$[\mathbf{T}_1 \cdot \mathbf{T}_2]_{q\bar{q}} = [\mathbf{T}_3 \cdot \mathbf{T}_4]_{q\bar{q}} = -C_A C_F \begin{pmatrix} 0 & 1 \\ 1 & C_A \end{pmatrix}, \tag{8.20}$$

$$[\mathbf{T}_1 \cdot \mathbf{T}_3]_{q\bar{q}} = [\mathbf{T}_2 \cdot \mathbf{T}_4]_{q\bar{q}} = -C_A C_F \begin{pmatrix} C_A & 1 \\ 1 & 0 \end{pmatrix}, \tag{8.21}$$

$$[\mathbf{T}_1 \cdot \mathbf{T}_4]_{q\bar{q}} = [\mathbf{T}_2 \cdot \mathbf{T}_3]_{q\bar{q}} = C_A C_F \begin{pmatrix} 0 & 1 \\ 1 & 0 \end{pmatrix}. \tag{8.22}$$

As for the colour matrix of the triple correlator, it reads

$$[i f^{abc} \mathbf{T}_3^a \mathbf{T}_4^b \mathbf{T}_1^c]_{gg} = -\frac{1}{4} C_A^2 C_F \begin{pmatrix} 0 & 1 \\ -1 & 0 \end{pmatrix}, \tag{8.23}$$

$$[i f^{abc} \mathbf{T}_3^a \mathbf{T}_4^b \mathbf{T}_1^c]_{q\bar{q}} = \frac{1}{2} C_A^2 C_F \begin{pmatrix} 0 & 1 \\ -1 & 0 \end{pmatrix}, \tag{8.24}$$

which also means that $\langle \mathcal{M} | \, i f^{abc} \mathbf{T}_3^a \mathbf{T}_4^b \mathbf{T}_1^c \, | \mathcal{M} \rangle = 2i \, \mathrm{Im}(\mathcal{M}_1^* \mathcal{M}_2)$. For processes where the $\mathcal{M}_1^* \mathcal{M}_2$ interference is real, such as $t\bar{t}h$, this correlator will vanish.

In a similar way, we can also compute the colour matrices for the four-colour correlator. This we have done it with the help of the FeynCalc package [94, 95], and the results are listed in Appendix C.2.

8.2 RESULTS

In this section we present the numerical results for the computation of the NNLO counter-terms to $t\bar{t}h$ production in the q_T subtraction framework. For this purposes, we have implemented the formulae corresponding to the counter-term presented in the previous section 8.1 in a private Fortran code, the same described in section 7.2 for the NLO

results. For the double real and real-virtual emission corrections, we used the MUNICH [1] code which provides a fully automated implementation of the NLO Catani-Seymour dipole-subtraction formalism. For validation purposes, we also obtained the NNLO cross section for $t\bar{t}$ production from the MATRIX code [157], which implements q_T-subtraction for colourless final states and has recently incorporated the results for $t\bar{t}$ [153, 154].

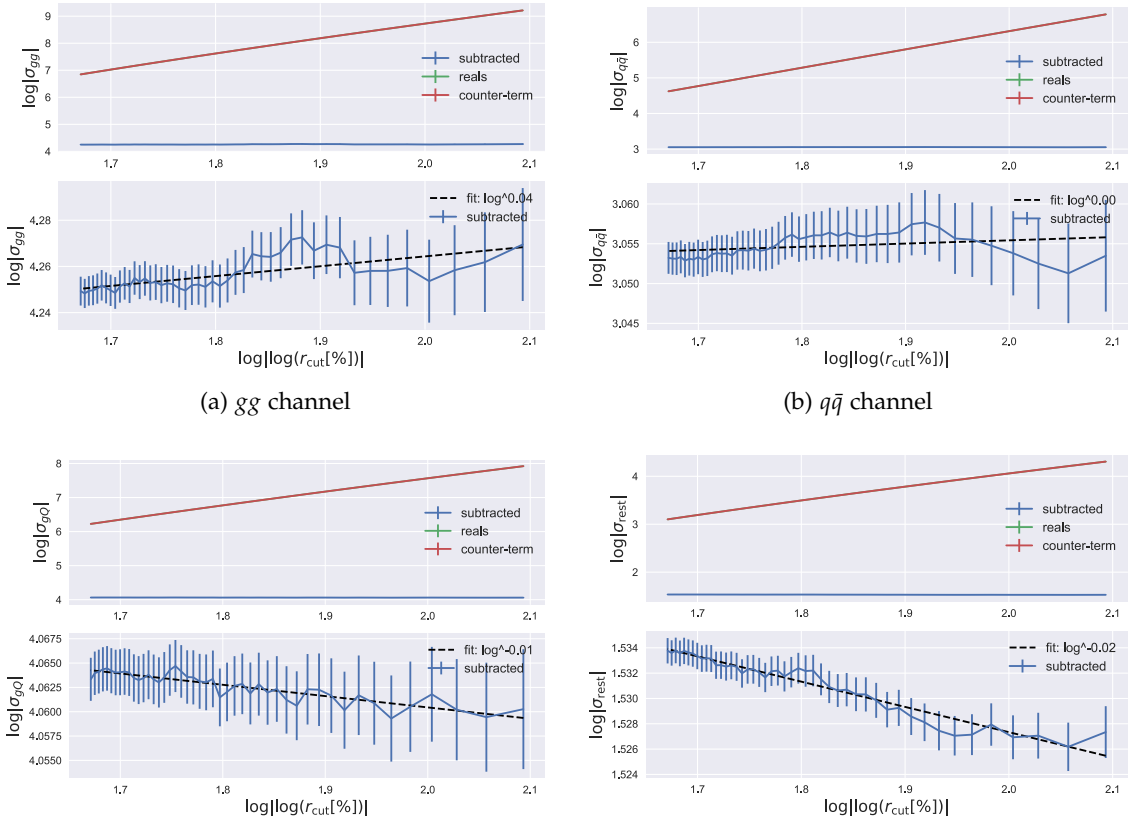

(a) gg channel

(b) $q\bar{q}$ channel

(c) gQ channel

(d) *rest* channel

Figure 8.1: Double log plots of the NNLO cross section as a function of $\ln r_{cut}$ for the four different partonic channels. In this scale, the logarithmic behaviour is seen as a straight line whose slope is the power of the leading log. For each partonic channel we plot individually the real emission NNLO cross section and its counter-term, as well as the subtraction of the two (upper plot). A zoom into the subtracted cross section is shown together with a linear fit shown in dashed line (bottom plot). The real emission cross section is obtained from MUNICH, while the corresponding counter-term is the one implemented in this work.

1 MUNICH is the abbreviation of "MUlti-chaNnel Integrator at Swiss (CH) precision", an automated parton-level NLO generator by S. Kallweit

In all the results shown in this section, the top quark and the higgs have masses $m_t = 173.3\text{GeV}$ and $m_H = 125\text{GeV}$, respectively, and their widths are neglected ($\Gamma_t = \Gamma_H = 0$). The factorization and renormalizations scales are fixed at the mass of the top quark $\mu_F = \mu_R = m_t$. The Fermi Electroweak scheme is used, whose inputs are the masses of the Z and W bosons and the Fermi coupling constant, set to the values $m_Z = 91.1876\text{GeV}$, $m_W = 80.3850\text{GeV}$ and $G_F = 1.166390 \times 10^{-5}\text{GeV}^{-2}$, respectively. For the parton distribution functions, the NNPDF 3.1 [182] set with a strong coupling constant of $\alpha_s(m_Z) = 0.118$. The hadronic centre of mass energy is set at 13TeV.

With no two-loop amplitudes nor soft-function available at the moment, as well as the spin-correlations appearing in the hard scattering of gluons, only the counter-term was implemented leaving the completion of the Hard Collinear factor as future work.

In order to validate our implementation, first we made checked numerically that the coefficients of the counter-term for $t\bar{t}$ production are identical to those computed by MATRIX. For $t\bar{t}h$, the validity of the formalism is tested in the cancellation of all the logarithmic behaviour of the cross section in the limit $r_{cut} \to 0$. Because the Hard-Collinear term is independent of r_{cut}, this can be tested by subtracting the counter-term to the double real and real-virtual emission cross section computed by MUNICH, and analyse its behaviour as $r_{cut} \to 0$. We will call this the *subtracted real emission* cross section

$$\sigma_S^{(NNLO)} = \sigma_{t\bar{t}h+\text{jet}}^{(NLO)} - \sigma_{CT}^{(NNLO)}.$$

CHANNEL	$\sigma_s^{(NNLO)}(fb)$
gg	-71.0 ± 0.3
$q\bar{q}$	-21.26 ± 0.04
gQ	$+58.01 \pm 0.07$
rest	-4.607 ± 0.002
All channels	-38.7 ± 0.3

Table 8.1: Numerical results for the extrapolation to $r_{cut} \to 0$ of the subtracted real emission cross section at NNLO for $t\bar{t}h$ production. The result is shown for the different partonic channels individually, as well as for the total cross section.

Because the divergent behaviour of the real emission cross section is logarithmic $\sigma \sim \ln(r_{cut})^n$, we can numerically estimate the power of the leading logarithmic divergence with the slope of curve

$$\ln(\sigma) \sim n \ln|\ln(r_{cut})|$$

as a function of $\ln|\ln(r_{cut})|$. In Figure 8.1 we plot this for the four distinct partonic channels:

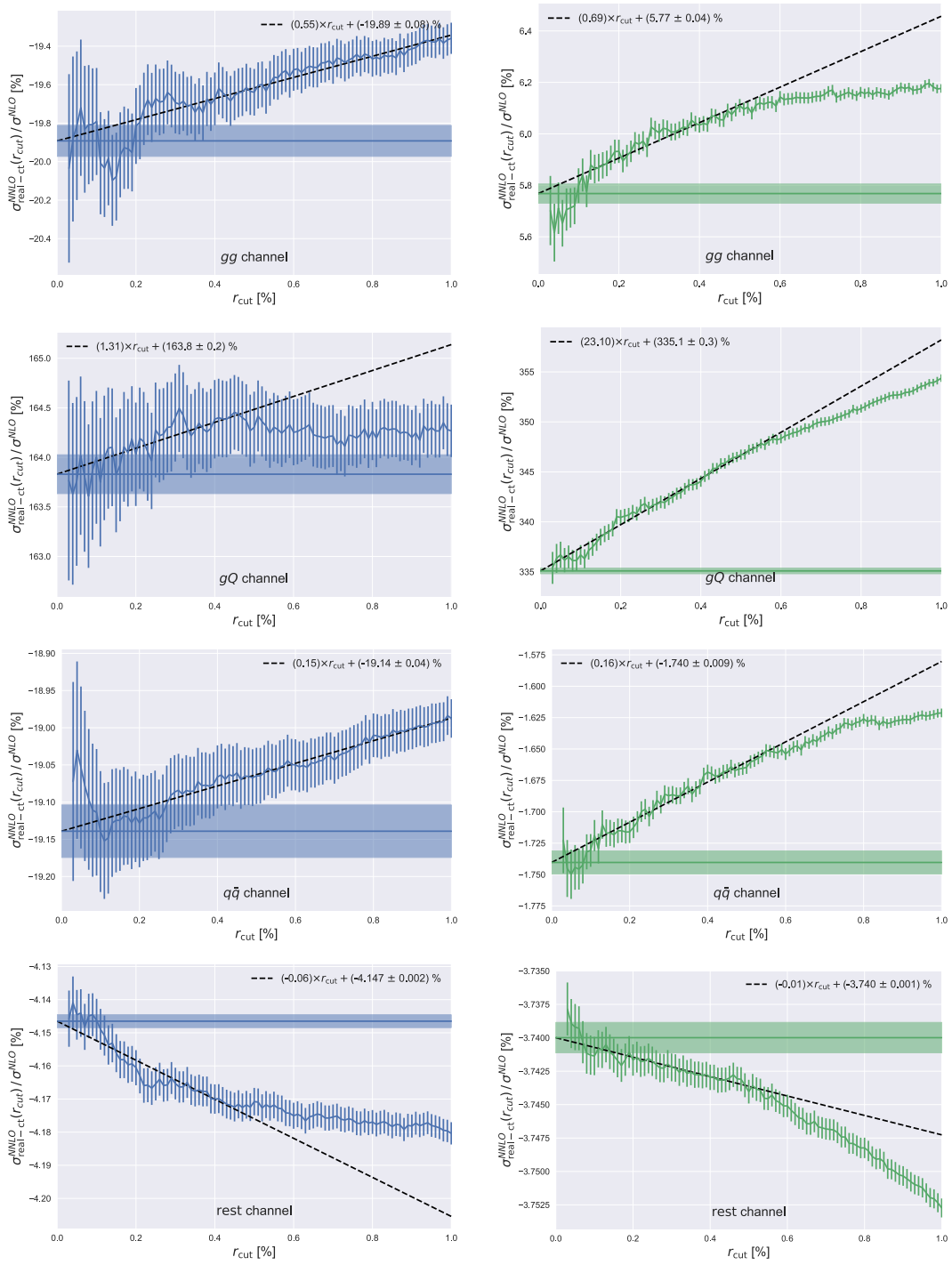

Figure 8.2: Subtracted real emission NNLO cross section as a function of r_{cut} for the four different partonic channels, normalized by the corresponding NLO contribution, for $t\bar{t}h$ production (left) and $t\bar{t}$ production (right). In the *rest* channel, the $q\bar{q}$ NLO contribution is used for normalization. The linear fit used for the extrapolation to $r_{cut} = 0$ is plotted in dashed line, and its slope is written in the label. The $t\bar{t}h$ computation uses the counterterm implemented in this work, while the $t\bar{t}$ is obtained with MATRIX. All real emissions are obtained by MUNICH, with the same statistics for both final states on each partonic channel.

- gg: The gluon initiated process $gg \to t\bar{t}h + X$, which contributes at LO and diverges as $\sim \ln^4(r_{cut})$.
- $q\bar{q}$: The quark-antiquark initiated process$q\bar{q} \to t\bar{t}h + X$ for $q \in Q = \{u, \bar{u}, d, \bar{d}, c, \bar{c}, s, \bar{s}, b\}$, which also contributes at LO and diverges as $\sim \ln^4(r_{cut})$.
- gQ: The gluon-quark initiated processes $gq \to t\bar{t}h$ and $qg \to t\bar{t}h$ for $q \in Q$. This starts to contribute only at NLO, and diverges as $\sim \ln^3(r_{cut})$
- *rest*: The off-diagonal quark initiated processes $qq' \to t\bar{t}h$ for $q, q' \in Q$ and $q' \neq \bar{q}$. This channel only starts to contribute at NNLO, and therefore only contains NLO-like divergences $\sim \ln^2(r_{cut})$.

We see that after subtracting the counter-term to the real-emission cross section, we're left with a curve of slope ~ 0. The reason why it is not exactly 0 is due to power corrections of $\mathcal{O}(r_{cut}^n)$ that vanish in the limit $r_{cut} \to 0$. Lets note that in Figure 8.1, the limit $r_{cut} \to 0$ corresponds to $\ln|\ln r_{cut}| \to \infty$ in the horizontal axis.

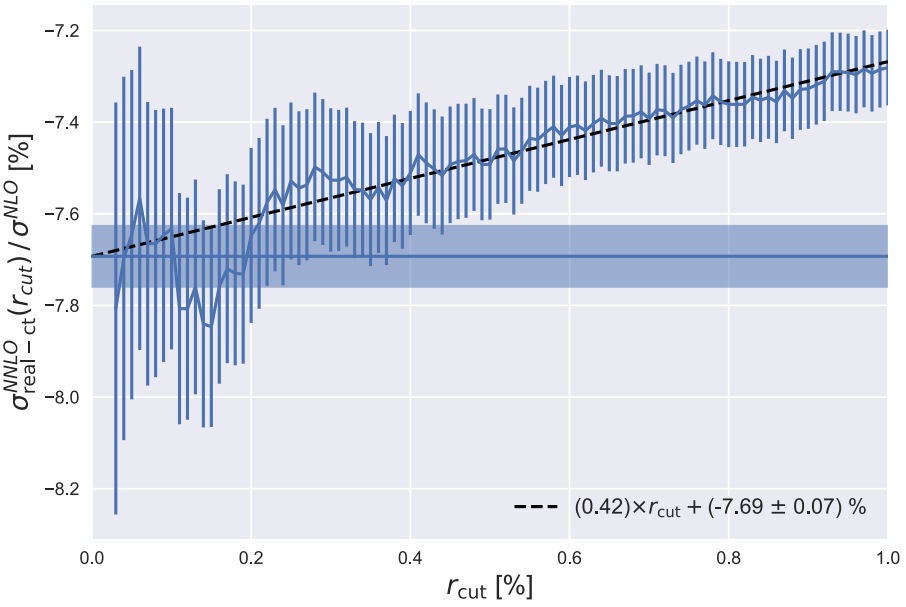

Figure 8.3: Subtracted real emission NNLO cross section for $t\bar{t}h$ production as a function of r_{cut}, normalized by the NLO cross section. The linear fit used for the extrapolation to $r_{cut} = 0$ is plotted in dashed line. The counter-term is computed with the implementation presented in this work, the real emission amplitudes are obtained from MUNICH.

The remaining dependence on r_{cut} is finite in the limit $r_{cut} \to 0$, and is shown in the left plots of Figure 8.2. To compare the stability[2] of this remaining dependence on r_{cut} to

2 By *stability on* r_{cut} we mean the dependence of the subtracted result on r_{cut}, which have an influence on the computational cost needed to get a reliable extrapolation to $r_{cut} \to 0$.

the $t\bar{t}$ case, we normalise each partonic channel to the corresponding NLO contribution and examine the slope of the linear fit defined by the extrapolation algorithm (described in section 7.2). The reason for this normalisation is that the size of the extrapolation to $r_{cut} \to 0$ is meaningless without the corresponding Hard-Collinear function. For the *rest* channel, whose NLO contribution is null, we normalised by the $q\bar{q}$ NLO contribution. We can see that in both diagonal partonic channels, gg and $q\bar{q}$, the relative dependence on r_{cut} is slightly smaller. The greatest improvement in stability is seen in the gQ channel, where this dependence is reduced by an order of magnitude. The only channel where the stability is worsened the *rest*, but as this is a subdominant channel, the overall inclusive production cross section is slightly more stable for $t\bar{t}h$ than for $t\bar{t}$.

Finally, the total subtracted real emission cross section is shown (normalised to the NLO result) in Figure 8.3, and its values are presented in Table 8.1.

With these results we close the second part of this thesis. Motivated by the need of NNLO precision for the $t\bar{t}h$ hadroproduction, we have tackled the extension of the q_T-subtraction framework for handling IR divergences to processes with final states consisting in a heavy quark pair plus some colourless final state. We presented in chapter 7 all of the necessary ingredients for a NLO implementation, and numerically crossed checked it against known results for $t\bar{t}h$ and $t\bar{t}Z$ production. At NNLO all the ingredients for the implementation of the counter-term have been worked out in 8, and for $t\bar{t}h$ production we have numerically checked that all NNLO IR singularities are cancelled from the real emission cross section. In order to have a full NNLO implementation, the two-loop soft function and the NLO spin-correlations have to be computed for a general kinematics. This, along with the corresponding two-loop amplitudes, would allow for the computation of the NNLO corrections to $t\bar{t}h$ production, which in turn would result in more accurate determinations of the top-quark Yukawa coupling.

9

CONCLUSIONS

Although BSM physics in the near future might not be available for direct detection in resonant searches, physics at a higher energy scale can be accessed through precision measurements of the Higgs boson couplings. The triple and quartic self-couplings are of particular interest because they provide insight into the electroweak symmetry breaking mechanism, and multiple Higgs boson production results in a sensitive channel for these studies, as it provides tree-level access to such couplings. Another coupling of interest is the top-quark Yukawa. Being the heaviest particle in the standard model, the top-quark has the strongest coupling to the Higgs boson and the value of its Yukawa drives the evolution of the Higgs self-coupling. Any deviations from the SM values of the observed Higgs self couplings will be intertwined with deviations of the top-quark Yukawa, as the main production channel for the Higgs is gluon fusion through a top quark loop. An independent and direct measurement of the Yukawa coupling can be performed through the observation of the $t\bar{t}h$ associated production.

In this context of precision measurements of the couplings in the Higgs-top sector, accurate theory predictions need to include Next-to-Next-to Leading Order QCD corrections to keep up with the continuously increasing experimental accuracy. In this thesis we have worked in three different processes: In part I we focused on the double and triple Higgs boson production, while in part II we moved to the associated production of a top-quark pair with a Higgs boson. The first two are particularly sensitive to the triple and quartic self couplings of the Higgs boson, respectively, while the third provides tree-level access to the top-quark Yukawa.

After having provided a general introduction in chapters 1 and 2, in chapter 3 we computed the cross section for Higgs boson pair production, both inclusive and differential in the invariant mass of the produced pair, including all terms up to $\mathcal{O}(\alpha_S^4)$ (NNLO in QCD) and considering all relevant dimension 6 operators in the SM EFT. The EFT approach supplies a model independent way of addressing deviations from the SM due to heavy BSM physics, by the addition of these higher dimensional effective operators. In order to be consistent one must include all operators that modify the Higgs boson couplings relevant for the process, and for Higgs boson pair production through gluon fusion there are five relevant dimension 6 operators. These modify the coupling between the Higgs boson

and the top quark, as well as the Higgs triple self-coupling, and they add new contact interactions between the Higgs and the gluon field. The calculation was performed in the heavy top limit, and a proper rescaling prescription was implemented to approximate the effects of the finite top quark mass on the result. Then, a comprehensive study of the phenomenology introduced by the anomalous couplings was carried out, from which we would like to emphasize the following points:

- The K-factor as a function of the couplings was found to be rather flat, within a 16% deviation from its SM value. The exception is in regions of the anomalous couplings space where the cross section is minimized and radiative corrections turn out to be significant, reaching values for the K-factor as high as 4.07 (84% higher than the SM) and as low as 0.76 (34% of the SM value).

- The degeneracies of the inclusive cross section with respect to the anomalous couplings were studied, showing that radiative corrections do not substantially alter its shape. Also, it was shown that even in the case of a measurement compatible with the SM inclusive cross section expectation, it is possible to have large deviations from the SM couplings that render the same value.

- The differential invariant mass distribution of the produced Higgs boson pair was studied, showing that it encodes enough information to disentangle between combinations of anomalous couplings that are degenerate in the inclusive cross section. The reason for this high sensitivity is the destructive interference between triangle and box diagrams, that renders a small cross section near threshold in the SM. This cancellation, and the corresponding large deviation from it in BSM scenarios, provides a powerful tool for the discovery of new physics that couples to the Higgs boson.

Some comments must be held about the limitations of this calculation, in which we are including the contributions from amplitudes mediated by dimension 6 operators, both from their interference with the SM as well as from their square modulus. The latter is *a priori* expected to be of the same order as the interference between amplitudes originated from dimension 8 operators and the SM. While in some cases (e.g. strongly coupled theories) the dimension 8 operators can be ignored, in general one should either perform a global analysis including them, or restrict the validity of the calculation to deviations from the SM far smaller than the current experimental bounds. Regarding the dimension 6 operators not included in this analysis, some of them, such as the chromomagnetic dipole-moment, despite being constrained by top quark pair production and representing a higher order correction on the top quark Yukawa coupling, could still result in a significant contribution to the Higgs boson pair production cross section. In order to consistently include this operator into the analysis one should consider several other QCD operators that are mixed with it through Renormalization Group flow (see Ref. [48]).

The work presented in chapter 3 has been published in Ref. [46], and recently a combination with the NLO computation with full dependence on the top-quark mass has been performed in Ref. [47], providing the most accurate prediction so far for this kind of EFT analysis.

In chapter 4 we presented the complete set of NNLO corrections to triple Higgs boson production at hadron colliders in the heavy top limit. To partially retain finite top mass effects two different reweighting procedures have been implemented: The usual Born-improved approximation (Bi), and a procedure that we call dynamically Born improved approximation (dBi), which is an extension of the reweight performed in chapter 3 adapted to the new kinematical configuration. Both procedures coincide at LO, and from their difference at higher orders we infer the dependence of the result upon the reweighting procedure. Overall, we found that the invariant mass distribution is sensitive to the reweighting procedure only in the tail, where the cross-section is already small, while for the inclusive cross-section the dependence on this procedure is $\mathcal{O}(1\%)$, which falls inside the scale variation uncertainties of $\mathcal{O}(7\%)$. In order to provide a prediction based on the most advanced results available in the literature, we combined our dBi-reweighted NNLO results with the NLO predictions obtained within the $\text{FT}_{\text{approx}}$. From the differences between the available NLO approximations we estimated the size of the missing finite top mass effects. The work presented in this chapter has been published in Ref. [91].

Finally, in part II of the thesis we focused on the associated production of a top-quark pair with a Higgs boson. With the experimental precision getting closer to the theory uncertainty, NNLO accurate predictions are needed. In order to perform such a computation, we tackled the extension of the q_T-subtraction framework to handle the infrared singularities of the process. This framework, which was established in the context of transverse-momentum resummation, was originally developed for colour-singlet final states and has recently been extended to heavy-quark pair production. Nevertheless, in order to implement it for a process such as $t\bar{t}h$ all of its ingredients have to be computed for a general kinematics, in which the heavy quarks are no longer back to back (in the lowest order configuration). In particular, the soft anomalous dimension operator has to be used in its general form, and the soft function becomes much more involved. After providing an introduction to transverse momentum resummation and q_T-subtraction in chapters 5 and 6, in chapter 7 we presented for the first time the NLO implementation of q_T-subtraction to a process whose final state consist of a heavy-quark pair and a colourless particle. We numerically computed the inclusive and single-differential cross section for $t\bar{t}h$ and $t\bar{t}Z$ production and crossed checked the result against the MadGraph generator. Then, in chapter 8, we presented the NNLO counter-term needed to cancel the IR divergences of the real emission cross section. In particular, triple-colour correlators that didn't contribute for $t\bar{t}$ production, start to contribute for more general kinematics ($t\bar{t}X$) whenever complex phases appear in the LO cross section, which would be the case of $t\bar{t}Z$, for example. We checked numerically that for $t\bar{t}h$ production, the counter-terms successfully cancel the

NNLO IR singularities in the real-emission cross section. Regarding the stability of the computation with the technical slicing parameter on the transverse momentum, r_{cut}, we compared the dependence of the inclusive cross section between the $t\bar{t}h$ and $t\bar{t}$ cases, relative to the NLO cross section, finding that it is slightly more stable. This improvement in stability would enhance the numerical precision of the extrapolation to $r_{cut} \to 0$, and its physical origin remains to be investigated. The work presented part II is the subject of a publication which is currently in preparation [156].

In order to have a fully NNLO implementation of q_T-subtraction for $t\bar{t}h$ production, further work is needed towards the generalisation to a general kinematics of the two-loop soft function and the spin-correlations appearing in gluon fusion processes. This, together with the computation of the relevant two-loop amplitudes, would allow for a complete NNLO prediction for $t\bar{t}h$ production, as well as similar processes such as $t\bar{t}Z$ and $t\bar{t}W^{\pm}$.

Part III

APPENDIX

A

REAL EMISSION CORRECTIONS IN DOUBLE HIGGS PRODUCTION

In this appendix we present the expressions for the renormalized real emission contributions to the NNLO cross section. Namely $\hat{\sigma}_{ij}^{(c+)}$, $\hat{\sigma}_{ij}^{(c-)}$ and $\hat{\sigma}_{ij}^{(f)}$, that appear in Eqs. (3.17) – (3.21) for the different partonic subprocesses $ij \to HH + X$.

The expressions for the SM are presented in Ref. [33] and are calculated in the HTL and then reweighted by the Born cross section following Eq. (3.23). For the contributions under consideration, this implies that the HTL real correction is multiplied by the factor $\frac{\mathrm{Re}(C_{LO})}{|C_{LO}^{HTL}|^2}$. As discussed at the end of section 3.1.2, we use a different prescription to avoid the numerically dangerous division by $|C_{LO}^{HTL}|^2$ and directly introduce the exact LO amplitude as $\mathrm{Re}(C_{LO}^* V_{\mathrm{eff}}^2)$, also taking into account the reweighting of the effective vertex between gluons and the Higgs of Eq. (3.22). The results are the same as the presented in Ref. [33], but making the following replacements

$$\Delta_{LO} \to 1\,, \tag{A.1}$$

$$\mathrm{Re}(C_{LO}) \to \mathrm{Re}\left(C_{LO}^* V_{\mathrm{eff}}^2\right)\,, \tag{A.2}$$

$$\frac{\hat{\sigma}_{LO}}{|C_{LO}|^2} \to \int_{t_-}^{t_+} dt \frac{G_F^2\,\alpha_s^2}{512(2\pi)^3}\,, \tag{A.3}$$

and then using the definition for C_{LO} given in Eq. (3.13).

For completeness, we present the resulting expressions once these replacements are performed. These can be written (for $\mu_R = \mu_F = Q$) as

$$\begin{aligned}
\hat{\sigma}_{gg}^{(c+)} &= \hat{\sigma}_{gg}^{(c-)} = \int_{t_-}^{t_+} dt \frac{G_F^2\,\alpha_s^2}{512(2\pi)^3} \left(\frac{\alpha_s}{2\pi}\right)^2 8\left[1-(1-x)x\right]^2 \\
&\times \left[2\left(\frac{\log(1-x)}{1-x}\right)_+ - \frac{\log x}{1-x}\right] \mathrm{Re}\left(C_{LO}^* V_{\mathrm{eff}}^2\right)\,, \\
\hat{\sigma}_{gg}^{(f)} &= \int d\cos\theta_1\, d\theta_2\, dy\, \frac{\sqrt{x(x-4M_H^2/Q^2)}}{1024\,\pi^4} \left(\frac{1}{1-x}\right)_+ \\
&\times \left[\left(\frac{1}{1-y}\right)_+ + \left(\frac{1}{1+y}\right)_+\right] f_{gg}(x,y,\theta_1,\theta_2)\,,
\end{aligned}$$

$$
\begin{aligned}
\hat{\sigma}^{(c+)}_{qg} &= \hat{\sigma}^{(c-)}_{gq} = \int_{t_-}^{t_+} dt \frac{G_F^2\,\alpha_s^2}{512(2\pi)^3}\left(\frac{\alpha_s}{2\pi}\right)^2 \frac{16}{9}\Big\{\left[1+(1-x)^2\right] \\
&\times \left[2\log(1-x)-\log x\right]+x^2\Big\}\,\mathrm{Re}\left(C_{LO}^* V_{\rm eff}^2\right)\,, \\
\hat{\sigma}^{(f)}_{qg} &= \int d\cos\theta_1\, d\theta_2\, dy\, \frac{\sqrt{x(x-4M_H^2/Q^2)}}{512\,\pi^4}\left(\frac{1}{1-y}\right)_+ f_{qg}(x,y,\theta_1,\theta_2)\,, \\
\hat{\sigma}^{(f)}_{gq} &= \int d\cos\theta_1\, d\theta_2\, dy\, \frac{\sqrt{x(x-4M_H^2/Q^2)}}{512\,\pi^4}\left(\frac{1}{1+y}\right)_+ f_{gq}(x,y,\theta_1,\theta_2)\,, \\
\hat{\sigma}^{(f)}_{q\bar{q}} &= \int d\cos\theta_1\, d\theta_2\, dy\, \frac{\sqrt{x(x-4M_H^2/Q^2)}}{512\,\pi^4}\, f_{q\bar{q}}(x,y,\theta_1,\theta_2)\,,
\end{aligned}
\tag{A.4}
$$

where the integration variable t is defined in Eq. (3.16) with limits $t_\pm = t\,(\cos\theta_1 = \pm 1)$, G_F is the Fermi coupling, and the plus distributions are those defined in (2.39) and (2.70), which we repeat below for completness

$$
\int_0^1 dx\, G_+(x)\, f(x) = \int_0^1 dx\, G(x)\,[f(x)-f(1)]\,, \tag{A.5}
$$

$$
\int_{-1}^1 dy\, f(y)\left(\frac{1}{1\pm y}\right)_+ = \int_{-1}^1 dy\, \frac{f(y)-f(\mp 1)}{1\pm y}\,. \tag{A.6}
$$

The functions $f_{ij}(x,y,\theta_1,\theta_2)$ are defined as

$$
\begin{aligned}
f_{gg}(x,y,\theta_1,\theta_2) &= \frac{\alpha_s^4 G_F^2 \mathrm{Re}\left(C_{LO}^* V_{\rm eff}^2\right)}{576\pi^2 s} s(1-x)^2(1-y^2) \\
&\times \Big[F(s,q_1,q_2,t_k,u_k)+F(s,\hat{q}_1,\hat{q}_2,t_k,u_k)+F(s,q_2,q_1,u_k,t_k) \\
&+ F(s,\hat{q}_2,\hat{q}_1,u_k,t_k)+F(t_k,q_1,w_2,s,u_k)+F(t_k,\hat{q}_1,w_1,s,u_k)\Big]\,, \\
f_{qg}(x,y,\theta_1,\theta_2) &= \frac{\alpha_s^4 G_F^2 \mathrm{Re}\left(C_{LO}^* V_{\rm eff}^2\right)}{648\pi^2 s} s(1-x)(1-y) \\
&\times \left[h(s,q_1,q_2,t_k,u_k)+h(s,\hat{q}_1,\hat{q}_2,t_k,u_k)\right]\,, \\
f_{gq}(x,y,\theta_1,\theta_2) &= \frac{\alpha_s^4 G_F^2 \mathrm{Re}\left(C_{LO}^* V_{\rm eff}^2\right)}{648\pi^2 s} s(1-x)(1+y) \\
&\times \left[h(s,\hat{q}_2,\hat{q}_1,u_k,t_k)+h(s,q_2,q_1,u_k,t_k)\right]\,, \\
f_{q\bar{q}}(x,y,\theta_1,\theta_2) &= -\frac{\alpha_s^4 G_F^2 \mathrm{Re}\left(C_{LO}^* V_{\rm eff}^2\right)}{243\pi^2 s} s(1-x) \\
&\times \left[h(t_k,q_1,w_2,s,u_k)+h(t_k,\hat{q}_1,w_1,s,u_k)\right]\,,
\end{aligned}
\tag{A.7}
$$

and the function F is defined as follows

$$
F(s,q_1,q_2,t_k,u_k) = f_1(s,q_1,q_2,t_k,u_k)+f_2(s,q_1,q_2,t_k,u_k)\,. \tag{A.8}
$$

The invariants used [183] are defined in terms of Q^2, x, y, θ_1 and θ_2 as

$$\begin{aligned}
s &= Q^2 \,, \\
t_k &= -\tfrac{1}{2}s(1-x)(1-y) \,, \\
u_k &= -\tfrac{1}{2}s(1-x)(1+y) \,, \\
q_1 &= M_H^2 - \tfrac{1}{2}(s+t_k)(1-\beta_x \cos\theta_1) \,, \\
q_2 &= M_H^2 - \tfrac{1}{2}(s+u_k)(1+\beta_x \cos\theta_2 \sin\theta_1 \sin\psi + \beta_x \cos\theta_1 \cos\psi) \,, \\
\hat{q}_1 &= (p_1-k_2)^2 = 2M_H^2 - s - t_k - q_1 \,, \\
\hat{q}_2 &= (p_2-k_1)^2 = 2M_H^2 - s - u_k - q_2 \,, \\
w_1 &= (k+k_1)^2 = M_H^2 - q_1 + q_2 - t_k \,, \\
w_2 &= (k+k_2)^2 = M_H^2 + q_1 - q_2 - u_k \,,
\end{aligned} \tag{A.9}$$

where the coefficients β_x and ψ defined as

$$\begin{aligned}
\beta_x &= \sqrt{1 - \frac{4M_H^2}{x\,s}} \,, \\
\cos\psi &= 1 - \frac{8x}{(1+x)^2 - (1-x)^2 y^2} \,.
\end{aligned} \tag{A.10}$$

Finally, the expressions for the functions f_1, f_2 and h that complete the presentation of the real emission contributions are the following

$$\begin{aligned}
f_1(s,q_1,q_2,t_k,u_k) = \frac{1}{q_1 s\, t_k (M_H^2+q_1-q_2-u_k)u_k} \Big[& s t_k(-q_2^2(2s-3t_k)(s+t_k) + q_1 q_2 \\
& (6s^2+3st_k+2t_k^2+q_2(s+t_k)) - q_1^2(q_2 s + 4(s^2+st_k+t_k^2))) + (2(q_1-q_2)s^2 \\
& (2q_1^2 - 2q_1q_2 + q_2^2 + s^2) + s(-q_1^2 s + q_2(-3q_2^2 + 2q_2 s - 8s^2) + q_1(6q_2^2 + 3q_2 s + 14s^2))t_k \\
& + (-8q_1^2 s - q_2(q_2^2 - 3q_2 s + 7s^2) + q_1(q_2^2 + 10q_2 s + 17s^2))t_k^2 + (-4q_1^2 + 6q_1(q_2+s) \\
& + q_2(q_2+4s))t_k^3)u_k + (2s(2q_1^3 - 2q_1^2(q_2+s) - 2q_2 s(q_2+s) + q_1(q_2+s)(q_2+3s)) \\
& + (q_1(q_1-q_2)q_2 + (11q_1 - 6q_2)q_2 s + 2(11q_1 - 3q_2)s^2 - 2s^3)t_k + (-4q_1^2 + 7q_1q_2 - 3q_2^2 \\
& + 23q_1 s + q_2 s - 6s^2)t_k^2 + (6q_1 + 2q_2 + s)t_k^3)u_k^2 + (-4s(q_1^2 + q_2 s - q_1(q_2+2s)) \\
& - (3q_1^2 - 13q_1 s + s(7q_2+4s))t_k + (6q_1 - 3q_2 - 2s)t_k^2 + t_k^3)u_k^3 + (q_1 - t_k)(4s+t_k)u_k^4 \\
& - M_H^6 s(t_k+u_k)(t_k+2u_k) + M_H^4(s t_k((-q_1+q_2)s + (q_1+2q_2-2s)t_k + 3t_k^2) \\
& + (2(q_1-q_2)s^2 + 3(2q_1+q_2)s t_k + (q_1 - q_2 + 9s)t_k^2 + 5t_k^3)u_k + (q_1(6s+t_k) \\
& + t_k(-q_2+9s+6t_k))u_k^2 + t_k u_k^3) + M_H^2(s t_k((q_1-q_2)(q_1+q_2-2s)s + (-q_2(2q_1+q_2) \\
& + (q_1+q_2)s)t_k + 2(q_1-3q_2)t_k^2) - (4q_1(q_1-q_2)s^2 + s(-3q_2(-4q_1+q_2) + (q_1+3q_2)s \\
& - 2s^2)t_k + 2(-q_2^2 + 6q_2 s - 4s^2 + q_1(q_2+s))t_k^2 + 2(q_1+3q_2+2s)t_k^3)u_k - (2s(4q_1^2 \\
& - 2q_1q_2 + q_2^2 + s^2) + (q_1^2 - q_2(q_2-3s) + 11q_1 s)t_k + (3(q_1+q_2)+8s)t_k^2 + 6t_k^3)u_k^2
\end{aligned}$$

$$+(-4s(q_2+s)-6st_k-5t_k^2+2q_1(2s+t_k))u_k^3-(4s+t_k)u_k^4)\Big]\,, \tag{A.11}$$

$$f_2(s,q_1,q_2,t_k,u_k)=\frac{1}{q_2 s\, t_k^2 u_k}\Big[st_k(4q_2s^3-s((M_H^2+3q_1-4q_2)(q_1-q_2)$$
$$+(4M_H^2+q_1-11q_2)s)t_k-((M_H^2+3q_1-4q_2)(M_H^2-q_2)+(7M_H^2+2q_1$$
$$-11q_2)s)t_k^2+4(-M_H^2+q_2)t_k^3)-(4(q_1-q_2)^2s^3+s^2(4(M_H^2-q_2)(q_1-q_2)$$
$$+5(q_1-3q_2)s)t_k+s(5M_H^4+6q_1^2+5q_2(q_2-5s)+q_1(-6q_2+s)$$
$$+M_H^2(-6q_1-4q_2+4s))t_k^2+((M_H^2-q_2)(4M_H^2-3q_1-q_2)+3(3M_H^2+2q_1-5q_2)s$$
$$+s^2)t_k^3+(M_H^2-q_2+4s)t_k^4)u_k-(-8(M_H^2-q_1)(q_1-q_2)s^2+s(4(M_H^2-q_1)$$
$$\times(M_H^2-q_2)+(-5M_H^2+8q_1-15q_2)s)t_k+((M_H^2-q_1)(4M_H^2-3q_1-q_2)+(M_H^2$$
$$-q_1-20q_2)s+5s^2)t_k^2+2(M_H^2+2q_1-4q_2)t_k^3+t_k^4)u_k^2+(-4(M_H^2-q_1)^2s$$
$$+(3M_H^2-3q_1+10q_2)st_k+(-5M_H^2+q_1+10q_2+s)t_k^2+t_k^3)u_k^3+4q_2t_ku_k^4\Big]\,, \tag{A.12}$$

$$h(s,q_1,q_2,t_k,u_k)=\frac{1}{t_k^2q_2}\Big[2(-M_H^4t_k^2-q_2^2(s^2+st_k+t_k^2)+M_H^2t_k(-M_H^2+t_k)u_k$$
$$-(M_H^2-t_k)^2u_k^2-q_1^2(s+u_k)^2+q_1(s(-M_H^2t_k+q_2(2s+t_k))+(2(M_H^2+q_2)s$$
$$+(M_H^2-q_2-2s)t_k)u_k+2(M_H^2-t_k)u_k^2)+q_2(-t_k(s^2+u_k(t_k+u_k))$$
$$+M_H^2(s(t_k-2u_k)+t_k(2t_k+u_k))))\Big]\,. \tag{A.13}$$

B

REAL EMISSION CORRECTIONS IN TRIPLE HIGGS PRODUCTION

In this appendix we present the results for the corrections arising from real emission in diagrams with more than one HTL insertion operator.

Because each HTL operator insertion carries a α_s factor, tree level diagrams with two operator insertions are already NLO, so their real radiation corrections correspond to a single parton emission. In the same way, diagrams with three operator insertions appear only at NNLO and their real emission corrections are of higher order, and therefore not considered. The single real emission amplitudes present divergences when the emitted parton becomes unresolved, some of which will cancel against the divergences present in the corresponding loop corrections calculated in Ref. [89] and the rest have to be absorbed in the NLO evolution of the parton distribution functions. In order to perform such cancellations, we used an FKS approach in $D = 4 - 2\epsilon$ dimensions, which is presented in section 2.3.

The explicit expressions for the finite remainder of the real emission contribution for each channel are given below,

$$\rho_{gg}^{(sc)} = 2\pi^2\delta(1-x) + 12\,(1-(1-x)x)^2\left(2\mathcal{D}_1(x) - \frac{\log(x)}{1-x}\right), \tag{B.1}$$

$$\rho_{qg}^{(sc)} = \rho_{gq}^{(sc)} = \frac{4}{3}\left(x^2 + (2\log(1-x) - \log(x))(1+(1-x)^2)\right), \tag{B.2}$$

$$\rho_{ij}^{(r)}(x,y,\phi) = \frac{1}{2\pi s^2}\sum_{(kl)}\frac{\mathrm{Re}\left((C_{\mathrm{LO}}^{3H})^* C_{\mathrm{LO}}^{2H}(\{k,l\})\right)}{|C_{\mathrm{LO}}^{3H}|^2} f_{ij}(\{k,l\}), \tag{B.3}$$

where $\sum_{(kl)}$ denotes a sum over the three distinct combinations of pair of Higgs bosons that we label $\{k,l\}$, and the $f(\{k,l\})$ functions are defined for each channel as

$$f_{gg}(\{k,l\}) = \mathcal{G}(s,t_k,u_k,q_1,q_2,s_{kl},m_H^2) + \mathcal{G}(s,t_k,u_k,\hat{q}_1,\hat{q}_2,m_H^2,s_{kl}) \tag{B.4}$$

$$f_{qg}(\{k,l\}) = \frac{-2}{9}(1-x)(1+y)\,\mathcal{Q}(s,t_k,u_k,q_1,q_2,s_{kl},m_H^2) \tag{B.5}$$

$$f_{gq}(\{k,l\}) = \frac{-2}{9}(1-x)(1-y)\,\mathcal{Q}(s,u_k,t_k,\hat{q}_2,\hat{q}_1,s_{kl},m_H^2) \tag{B.6}$$

$$f_{qq}(\{k,l\}) = \frac{-8}{27}(1-x)^2(1-y^2)\,\mathcal{Q}(t_k, s, u_k, q_1, q_1 - q_2 + s_{kl} - u_k, s_{kl}, m_H^2). \tag{B.7}$$

The invariants entering as arguments of f are defined for each $\{k,l\}$ pair. For a given $\{k,l\}$, we call p_1 and p_2 the four-momenta of the incoming partons, $p_{hh} = p_k + p_l$ the sum of the four-momenta of the outgoing Higgs bosons labelled k and l, p_h the four-momenta of the other Higgs and k the one of the emitted parton. Then we define the invariants as

$$\begin{aligned}
s &= (p_1 + p_2)^2 = xQ^2, & q_1 &= (p_1 - p_h)^2,\\
t_k &= (p1 - k)^2 = -\frac{s}{2}(1-x)(1-y), & q_2 &= (p_2 - p_{hh})^2,\\
u_k &= (p2 - k)^2 = -\frac{s}{2}(1-x)(1+y), & \hat{q}_1 &= (p_1 - p_{hh})^2 = m_H^2 - q_1 - s + s_{kl} - t_k,\\
s_{kl} &= p_{kl}^2, & \hat{q}_2 &= (p_2 - p_h)^2 = m_H^2 - q_2 - s + s_{kl} - u_k.
\end{aligned} \tag{B.8}$$

The functions $\mathcal{G}$ and $\mathcal{Q}$ are regular in the limits $x \to 1$ and $y \to \pm 1$. From the expressions in Equations (A9-A12) we can see explicitly that soft divergences appear only in the gg channel, as all others f_{ij} vanish in this limit. The gg channel also shows divergent behaviour in both collinear $y \to \pm 1$ limits. The qg and gq channels only have singularities in $y \to 1$ and $y \to -1$ respectively, while the qq channel is completely regular and free of any divergences.

The analytic expressions for $\mathcal{G}$ and $\mathcal{Q}$ are

$$\begin{aligned}
\mathcal{G}(s,t,u,q_1,q_2,m_1^2,m_2^2) &= \frac{g_1(s,t,u,q_1,q_2,m_1^2,m_2^2)}{s(m_2^2 - q_1 + q_2 - t)} + \frac{g_2(s,t,u,q_1,q_2,m_1^2,m_2^2)}{q_1 q_2}\\
&\quad + \frac{g_3(s,t,u,q_1,q_2,m_1^2,m_2^2)}{q_2 tu(q_1 + s + t - m_1^2 - m_2^2)},\\
\mathcal{Q}(s,t,u,q_1,q_2,m_1^2,m_2^2) &= \frac{-4}{t(m_2^2 - q_2 - s + m_1^2 - u)}\\
&\quad \times \Bigg(m_1^2 s^2 t + m_2^2 s^2 t - s^3 t + m_1^4 t^2 - m_1^2 s t^2 + s^2 t^2 + q_2^2(s^2 + st + t^2)\\
&\quad + m_1^2 m_2^2 tu - m_2^2 stu - s^2 tu - 2m_1^2 t^2 u + st^2 u + m_2^4 u^2 + m_1^2 tu^2\\
&\quad - stu^2 + t^2 u^2 - tu^3 + q_1^2(s+u)^2 - q_2(2s^2 t + s(m_1^2 t - t^2 - 2m_2^2 u\\
&\quad - tu) + t(2m_1^2 t + u(m_2^2 - 2t + u))) + q_1(s^2 t + u(-(m_1^2 t) - 2m_2^2 u\\
&\quad + tu) + s(m_1^2 t - 2m_2^2 u + 2tu) - q_2(2s^2 - tu + s(t + 2u)))\Bigg)\\
&\quad - \frac{4}{tq_2}\Bigg(m_1^4 t^2 + q_2^2(s^2 + st + t^2) + m_1^2 m_2^2 tu - m_1^2 t^2 u + m_2^4 u^2 - 2m_2^2 tu^2\\
&\quad + t^2 u^2 + q_1^2(s+u)^2 + q_2(s^2 t + s(-(m_1^2 t) + 2m_2^2 u) + t(-2m_1^2 t
\end{aligned} \tag{B.9}$$

$$+ u(-m_2^2 + t + u))) - q_1(u(m_1^2 t + 2m_2^2 u - 2tu) - s(m_1^2 t - 2m_2^2 u + 2tu) + q_2(2s^2 - tu + s(t + 2u)))\Bigg), \tag{B.10}$$

with g_1, g_2 and g_3 being the following polynomials:

$$\begin{aligned}
&g_1(s,t,u,q_1,q_2,m_1^2,m_2^2) = \\
&\quad 4m_1^2 q_2 s^3 t - 4q_2^2 s^3 t + q_2 s^4 t - 4m_1^4 s^2 t^2 + 8m_1^2 q_2 s^2 t^2 - 4q_2^2 s^2 t^2 \\
&\quad + m_1^2 s^3 t^2 + 9q_2 s^3 t^2 - 2s^4 t^2 - 2m_1^2 s^2 t^3 + 12q_2 s^2 t^3 - 8s^3 t^3 + 4q_2 s t^4 \\
&\quad - 10s^2 t^4 - 4s t^5 + m_1^2 q_2 s^3 u - q_2^2 s^3 u + 4q_2 s^4 u + m_1^4 s^2 t u - 2m_1^2 q_2 s^2 t u \\
&\quad - 5q_2^2 s^2 t u + 2m_1^2 s^3 t u + 14q_2 s^3 t u - 8s^4 t u + 4m_1^2 q_2 s t^2 u - 4q_2^2 s t^2 u \\
&\quad + 8m_1^2 s^2 t^2 u + 25q_2 s^2 t^2 u - 19s^3 t^2 u - 4m_1^4 t^3 u + 8m_1^2 q_2 t^3 u - 4q_2^2 t^3 u \\
&\quad - m_1^2 s t^3 u + 11q_2 s t^3 u - 24s^2 t^3 u - 10s t^4 u + 9q_2 s^3 u^2 + 25q_2 s^2 t u^2 \\
&\quad - 12s^3 t u^2 + 5m_1^2 s t^2 u^2 + 11q_2 s t^2 u^2 - 34s^2 t^2 u^2 + 8m_1^2 t^3 u^2 - 8q_2 t^3 u^2 \\
&\quad - 19s t^3 u^2 + 10q_2 s^2 u^3 + 10q_2 s t u^3 - 11s^2 t u^3 - 15s t^2 u^3 - 4t^3 u^3 \\
&\quad + 4q_2 s u^4 - 4s t u^4 + m_2^4(s^2(t - 4u)u - 4t u^3) - q_1^2(4s t u^2 + 4t u^3 \\
&\quad + s^3(t + 4u) + s^2 u(5t + 4u)) + m_2^2(m_1^2 s^2 t^2 + 2s^3 t^2 + 6s^2 t^3 + 4s t^4 \\
&\quad - 8m_1^2 s^2 t u + 7s^3 t u + 17s^2 t^2 u + 10s t^3 u + m_1^2 s^2 u^2 + 4s^3 u^2 + 28s^2 t u^2 \\
&\quad - 8m_1^2 t^2 u^2 + 19s t^2 u^2 + 7s^2 u^3 + 15s t u^3 + 8t^2 u^3 + 4s u^4 + q_1(-2s^2(t \\
&\quad - 4u)u + 4s t u^2 + 8t u^3 + s^3(t + 4u)) - q_2(4s t u^2 - 8t^2 u^2 + s^3(t + 4u) \\
&\quad + s^2(t^2 - 8t u + u^2))) + q_1(8t^2(m_1^2 - u)u^2 - s^4(t + 4u) - s^3(10t^2 \\
&\quad + 23t u + 11u^2 + m_1^2(4t + u)) - s(4t^4 + 10t^3 u + 15t u^3 + 4u^4 + t^2 u(4m_1^2 \\
&\quad + 23u)) - s^2(10t^3 + 30t^2 u + 33t u^2 + 11u^3 + m_1^2(t^2 - 8t u + u^2)) \\
&\quad + q_2(-8t^2 u^2 + 5s^3(t + u) + 4s t u(t + u) + s^2(t^2 + 4t u + u^2))),
\end{aligned} \tag{B.11}$$

$$\begin{aligned}
&g_2(s,t,u,q_1,q_2,m_1^2,m_2^2) = \\
&\quad q_2 s(3s - 2t)t(-(m_1^2 t) + q_2(s + t)) + (q_2^3(s + t)(s + 2t) \\
&\quad + q_2^2(s^2(-m_1^2 + s) + 3s(-2m_1^2 + s)t + 2(-3m_1^2 + s)t^2) - 2m_1^2 t^2(m_1^4 \\
&\quad + (s + t)^2) + q_2 t(2s^3 - s^2(m_1^2 - 9t) + 2t(3m_1^4 + t^2) + s(3m_1^4 - 2m_1^2 t \\
&\quad + 4t^2)))u - 2m_2^6 t u^2 + t(2t(-m_1^2 + s + t)^2 + q_2^2(3s + 2t) + q_2(5s^2 \\
&\quad + 4t(-m_1^2 + t) + s(-3m_1^2 + 10t)))u^2 + 2t(q_2(2s + t) + t(-m_1^2 \\
&\quad + 2s + 2t))u^3 + 2t^2 u^4 + q_1^3 t(s + u)(s + 2u) + q_1^2(st(s^2 + m_1^2 t \\
&\quad - q_2(2s + t)) + (s^2(-m_1^2 + q_2 + 3s) + 3s(-q_2 + s)t + (-2m_1^2 + 2q_2 \\
&\quad + 3s)t^2)u + (s(-m_1^2 + q_2 + s) + 2st + 2t^2)u^2 - 2su^3) + m_2^2(-((q_1 \\
&\quad - q_2)st(q_1 s + m_1^2 t - q_2(s + t))) - (-4q_2 s^3 + s(6q_1(q_1 - q_2)
\end{aligned}$$

$$
\begin{aligned}
&+ (q_1 - 5q_2)s)t + (q_2 s + q_1(-4m_1^2 + 4q_2 + 3s))t^2)u - (q_2(m_1^2 \\
&- q_2 - 7s)s + q_1 s(-m_1^2 + q_2 + 3s) + 2(m_1^4 + 3q_1^2 - 2m_1^2 q_2 + q_2^2 + q_1 s \\
&- 3q_2 s + s^2)t + 4(q_1 + s)t^2 + 2t^3)u^2 + 2(q_1 s + q_2 s - 2t(s \\
&+ t))u^3 - 2tu^4) + q_1(st(q_2^2(s + t) + m_1^2(4s^2 + 7st + 2t^2) \\
&- q_2(8s^2 + 5st + t(m_1^2 + 2t))) + s(-2q_2 s(-m_1^2 + q_2 + 4s) + (-3m_1^4 \\
&+ 6m_1^2 q_2 - 3q_2^2 + 5m_1^2 s - 14q_2 s + 2s^2)t + (6m_1^2 - 5q_2 + 5s)t^2 + 4t^3)u \\
&+ (q_2(m_1^2 - q_2 - 5s)s + (2m_1^4 + 2q_2^2 - 5q_2 s + 9s^2 - m_1^2(4q_2 + s))t \\
&+ 10st^2 + 2t^3)u^2 + 2(-(q_2 s) + 2t(s + t))u^3 + 2tu^4) + m_2^4 tu(-3q_2 s \\
&- 2m_1^2 t + 2q_2 t + 2tu + 3q_1(s + 2u)),
\end{aligned}
\tag{B.12}
$$

$$
\begin{aligned}
&g_3(s, t, u, q_1, q_2, m_1^2, m_2^2) = \\
&- (q_1^3 u(s + u)^2(3t^2 + 4su)) + q_2^3 t(s + t)^2(4st + 3u^2) + q_2^2(-4s^4 u^2 \\
&+ s^3 u(-5t^2 + 4(m_1^2 + m_2^2)u - 10tu) + t^2 u^2(m_2^2(t - 3u) + t(-6m_1^2 \\
&+ t + 5u)) + s^2 t(u(8m_2^2 t + 4m_2^2 u - 11tu + u^2) + m_1^2(-8t^2 \\
&+ 4tu + 5u^2)) + st(-(m_1^2 t(8t^2 - 4tu + u^2)) + u(5t^3 - 4t^2 u + 3m_2^2 u^2 \\
&+ tu(5m_2^2 + 6u)))) + q_1^2(q_2(-3t^3 u^2 + st^2 u(3t + 11u) + 4s^3(t^2 + 2u^2) \\
&+ s^2 u(11t^2 + 8tu + 8u^2)) + u(-4s^4 u - s^3(4t^2 + 9tu - 4(m_1^2 \\
&- 2u)u) + t^2 u(u(-7t + u) + 3m_1^2(t + u)) - s^2(5t^3 + 7t^2 u + 16tu^2 \\
&+ 4u^3 + m_1^2(-3t^2 + 4tu - 8u^2)) + 2m_2^2(s + u)(2s^2 u + 5t^2 u + s(t^2 \\
&+ 6u^2)) + s(-(tu(12t^2 + 2tu + 7u^2)) + m_1^2(-3t^3 + 6t^2 u + 4tu^2 \\
&+ 4u^3)))) + u(m_2^6 u(-(st^2) + 4t^2 u + 4su^2) + m_2^2 t(s^3(4m_1^2 t + u(t \\
&+ 5u)) + s^2(m_1^2(6t^2 + 4tu - 9u^2) + u(5t^2 + 10tu + 3u^2)) \\
&+ tu(4m_1^4 t + 2t(3t - u)u + m_1^2(-3t^2 + 2tu + 5u^2)) + s(tu(7t^2 \\
&+ 5tu + u^2) + m_1^4(t^2 + 6tu + 4u^2) + m_1^2(3t^3 + 5t^2 u - 3tu^2 \\
&- 3u^3))) + m_2^4(-(s^2 u^2(5t + 4u)) + t^2 u(u(-9t + u) + 4m_1^2(t \\
&+ u)) + s(-(tu(2t^2 + 4tu + 7u^2)) + m_1^2(t^3 - t^2 u + 4tu^2 + 4u^3))) \\
&- t^2(4m_1^2 s^4 + s^3(-4m_1^4 + u(t + 5u) + m_1^2(11t + 5u)) + s^2(m_1^4(-7t \\
&+ u) + m_1^2(11t^2 + 16tu - 4u^2) + u(5t^2 + 5tu - u^2)) + (-m_1^2 \\
&+ t)u(t(t - u)u + m_1^2(t^2 + 7tu + 4u^2)) + s(-6m_1^6 u + tu(4t^2 + tu \\
&- 2u^2) - m_1^4(4t^2 + 6tu + u^2) + m_1^2(4t^3 + 9t^2 u + 8tu^2 + 5u^3)))) \\
&+ q_2(8s^5 tu + s^4 tu(-8m_1^2 - 8m_2^2 + 29t + 25u) - s^3 u(t(21m_1^2 t \\
&- 52t^2 + 17m_1^2 u - 76tu - 23u^2) + m_2^2(20t^2 + 25tu + 8u^2)) \\
&+ tu(3m_1^4 t^2 u - m_2^4 tu(4t + u) - 2m_1^2(2t^4 + 4t^3 u + 8t^2 u^2 \\
&+ 5tu^3 + 2u^4) + t(4t^4 + 11t^3 u + 18t^2 u^2 + 14tu^3 + 4u^4) - m_2^2(4t^4
\end{aligned}
$$

$$+ 7t^3u + 4u^4 + tu^2(-3m_1^2 + 14u) + t^2u(5m_1^2 + 17u))) - s^2u(m_2^4(t^2$$
$$- 8u^2) + t(-45t^3 + 4m_1^4u - 103t^2u - 63tu^2 - 12u^3 + m_1^2(26t^2$$
$$+ 27tu + 17u^2)) + m_2^2(m_1^2(t^2 + 4tu - 8u^2) + t(29t^2 + 66tu + 29u^2)))$$
$$+ st(m_1^4t(4t^2 - 4tu - 13u^2) - m_1^2u(19t^3 + 22t^2u + 28tu^2$$
$$+ 10u^3 + m_2^2(t^2 + 4tu + 3u^2)) + u(18t^4 + 57t^3u + 58t^2u^2 + 29tu^3$$
$$+ 4u^4 - m_2^4(t^2 - 14tu + 4u^2) - m_2^2(13t^3 + 56t^2u + 35tu^2$$
$$+ 11u^3)))) - q_1(q_2^2(-3t^2u^3 + stu^2(11t + 3u) + 4s^3(2t^2 + u^2)$$
$$+ s^2t(8t^2 + 8tu + 11u^2)) - q_2(8s^4u(t + u) + s^3u(29t^2 + 39tu$$
$$+ 8u(-m_1^2 - m_2^2 + u)) + tu(4t^4 + 8t^3u + 4u^4 + tu^2(-3m_1^2$$
$$+ m_2^2 + 14u) + t^2u(3m_1^2 + 7m_2^2 + 18u)) + stu(-3m_1^2t^2 + 17t^3$$
$$+ 14m_1^2tu + 53t^2u + 3m_1^2u^2 + 37tu^2 + 11u^3 - 2m_2^2(t^2 + 13tu$$
$$- 2u^2)) + s^2(4tu(10t^2 + 17tu + 7u^2) - 2m_2^2u(5t^2 + 2tu + 8u^2)$$
$$+ m_1^2(8t^3 - 7t^2u - tu^2 - 8u^3))) + u(m_2^4(11t^2u^2 - s^2(t^2 - 8u^2)$$
$$+ s(5t^2u + 12u^3)) - m_2^2(s^3u(5t + 8u) + t^2u(2(8t - u)u - 7m_1^2(t + u))$$
$$+ s^2(t^3 + 8t^2u + 21tu^2 + 8u^3 + m_1^2(t^2 + 4tu - 8u^2)) + s(tu(15t^2$$
$$+ 6tu + 14u^2) + 2m_1^2(t^3 - 3t^2u - 4tu^2 - 4u^3))) + t(s^4(t$$
$$+ 5u) + s^3(3m_1^2t + 3t^2 - m_1^2u + 6tu + 8u^2) + s^2(2t^3 - 4m_1^4u$$
$$+ 8t^2u + 12tu^2 + 3u^3 + 4m_1^2(2t^2 + 2tu - 3u^2)) + tu(3m_1^4t$$
$$+ t(5t - 2u)u + m_1^2(-2t^2 + 3tu + 5u^2)) + s(tu(10t^2 + 3tu + u^2)$$
$$+ m_1^4(-3t^2 + 6tu + 4u^2) + m_1^2(7t^3 + 3t^2u - 2tu^2 - 3u^3))))). \tag{B.13}$$

C

TOP-PAIR ASSOCIATED PRODUCTION WITH A HIGGS BOSON

C.1 SPIN CORRELATIONS IN GLUON FUSION PROCESSES

$\mathbf{q}_T$-subtraction was first developed in the context of Drell-Yan production, which is mainly dominated by the $q\bar{q}$ channel, but was afterwards applied to processes in which gluon fusion is the dominant channel, such as Higgs boson production. Later works found that the transverse-momentum resummation in the gluon fusion channel has a richer structure, due to a spin correlation of the collinear splitting functions. In this section we want to discuss the treatment of gluon fusion amplitudes in the context of q_t-subtraction, and write down the main results.

The main result of the q_T-resummation formalism is the factorization formula of Eq. (6.33)

$$\left[\frac{\mathrm{d}\sigma_F}{\mathrm{d}\mathbf{q}_T}\right]^{(sing)} = \frac{M^2}{s}\int \frac{\mathrm{d}^2\mathbf{b}}{(2\pi)^2} e^{i\mathbf{b}\cdot\mathbf{q}_T} \sum_{\substack{a_1\in h_1\\ a_2\in h_2}} \int_{x_1}^1 \frac{\mathrm{d}z_1}{z_1}\int_{x_2}^1 \frac{\mathrm{d}z_2}{z_2} f_{a_1/h_1}\left(\frac{x_1}{z_1}, \frac{b_0^2}{b^2}\right) f_{a_2/h_2}\left(\frac{x_2}{z_2}, \frac{b_0^2}{b^2}\right)$$
$$\times \sum_c \frac{\mathrm{d}\sigma^{(0)}_{c\bar{c}\to F}\left(x_1P_1, x_2P_2, M, \mathbf{\Omega}\right)}{\mathrm{d}M^2\,\mathrm{d}\mathbf{\Omega}} S_c(M,b)\left[(\mathbf{H\Delta})C_1C_2\right]_{c\bar{c};a_1a_2},$$

whose different components were discussed in sections 6.2.1 and 6.2.2 for colourless and massive colourful final states, respectively.

For quark-annihilation processes, the Hard Collinear factor reads

$$\left[(\mathbf{H\Delta})C_1C_2\right]_{c\bar{c};a_1a_2} = (\mathbf{H\Delta})_{c\bar{c}} C_{ca_1}(z_1;\alpha_s(b_0^2/b^2))C_{ca_2}(z_2;\alpha_s(b_0^2/b^2))$$
$$(\mathbf{H\Delta})_{c\bar{c}} = \frac{\left\langle \widetilde{\mathcal{M}}_{c\bar{c}\to Q\bar{Q}F}\right| \mathbf{\Delta} \left|\widetilde{\mathcal{M}}_{c\bar{c}\to Q\bar{Q}F}\right\rangle}{|\mathcal{M}^{(0)}_{c\bar{c}\to Q\bar{Q}F}(x_1P_1, x_2P_2;\mathbf{\Omega})|^2},$$

where the polarization spinors of the amplitude are contained inside $\mathcal{M}$ and the sum over polarization turns the coefficient $\left\langle \widetilde{\mathcal{M}}_{c\bar{c}\to Q\bar{Q}F}\right| \mathbf{\Delta} \left|\widetilde{\mathcal{M}}_{c\bar{c}\to Q\bar{Q}F}\right\rangle$ into a scalar.

In the case of gluon fusion processes, we can write the amplitude for incoming gluon polarizations λ_1 and λ_2 as

$$\mathcal{M} = \mathcal{M}^{\mu_1\mu_2}\epsilon^{\lambda_1}_{\mu_1}(p_1)\epsilon^{\lambda_2}_{\mu_2}(p_2), \tag{C.1}$$

where $\epsilon^\lambda_\mu(p)$ is the polarization vector transversal to momentum p^μ. In this way, the squared matrix element summed over polarizations read s

$$|\mathcal{M}|^2 = (\mathcal{M}^{\mu_1\mu_2})^\dagger \mathcal{M}_{\nu_1\nu_2} d_{\mu_1\nu_1} d_{\mu_2\nu_2}, \tag{C.2}$$

where $d_{\mu\nu} = \sum_\lambda (\epsilon^\lambda_\mu(p))^* \epsilon^\lambda_\nu(p)$ is the polarization tensor. We can work in the physical gauge in which p_1 is the reference vector for $\epsilon^\lambda_2(p_2)$ and viceversa, as both $p_1^2 = p_2^2 = 0$ and $p_1 \cdot p_2 = \hat{s}/2 \neq 0$ (where $\hat{s}$ is the partonic centre-of-mass energy). In this gauge, the polarization tensor reads

$$d^{\mu\nu}(p_1, p_2) = -g^{\mu\nu} + \frac{p_1^\mu p_2^\nu + p_2^\mu p_1^\nu}{p_1 \cdot p_2}. \tag{C.3}$$

Some properties to note is that it's symmetric (on both $p_1 \leftrightarrow p_2$ and $\mu \leftrightarrow \nu$), has a null trace ($g_{\mu\nu} d^{\mu\nu} = 0$) and is transversal to both p_1^μ and p_2^μ ($p_i^\mu d_{\mu\nu} = 0$ for $i = 1, 2$).

For gluon fusion processes, the Hard Collinear factor reads

$$\begin{aligned}\left[(\mathbf{H\Delta}) C_1 C_2\right]_{gg;a_1a_2} =& (\mathbf{H\Delta})_{gg;\mu_1\nu_1,\mu_2\nu_2} \\ &\times C^{\mu_1\nu_1}_{ga_1}(z_1; p_1, p_2, \mathbf{b}; \alpha_s(b_0^2/b^2))\; C^{\mu_2\nu_2}_{ga_2}(z_2; p_1, p_2, \mathbf{b}; \alpha_s(b_0^2/b^2))\end{aligned} \tag{C.4}$$

$$(\mathbf{H\Delta})_{gg;\mu_1\nu_1,\mu_2\nu_2} = \frac{\left\langle \widetilde{\mathcal{M}}^{\mu_1'\mu_2'}_{gg\to Q\bar{Q}F} \middle| \mathbf{\Delta} \middle| \widetilde{\mathcal{M}}^{\nu_1'\nu_2'}_{gg\to Q\bar{Q}F} \right\rangle d_{\mu_1'\mu_1} d_{\mu_2'\mu_2} d_{\nu_1'\nu_1} d_{\nu_2'\nu_2}}{|\mathcal{M}^{(0)}_{gg\to Q\bar{Q}F}(x_1P_1, x_2P_2; \mathbf{\Omega})|^2}. \tag{C.5}$$

In this case, we see that the universal Collinear functions $C^{\mu\nu}_{ga}$ have Lorentz indices, and they depend on both the modulus and the direction of the impact parameter $\mathbf{b}$. This are consequences of the collinear factorization properties of gluonic amplitudes. They can be decomposed as

$$C^{\mu\nu}_{ga}(z; p_1, p_2, \mathbf{b}; \alpha_s) = d^{\mu\nu}(p_1, p_2) C_{ga}(z; \alpha_s) + D^{\mu\nu}(p1, p2; \mathbf{b}) G_{ga}(z; \alpha_s), \tag{C.6}$$

where all of the dependence on the direction of $\mathbf{b}$ is encoded in the tensor

$$D^{\mu\nu}(p1, p2; \mathbf{b}) = d^{\mu\nu}(p1, p2) - 2\frac{b^\mu b^\nu}{\mathbf{b}^2}, \tag{C.7}$$

with $\mathbf{b}^2 = -b^\mu b_\mu$. The impact parameter vector in four-dimensional notation $b^\mu = (0, \mathbf{b}, 0)$ lies in the plane transversal to p_1 and p_2.

The gluonic coefficient function $C_{ga}(z; \alpha_s)$ is the same as the one introduced in Eq. (6.17) and its expansion in α_s starts at $\mathcal{O}(1)$. The coefficient $G_{ga}(z; \alpha_s)$, on the other hand, starts at $\mathcal{O}(\alpha_s)$, that is

$$G_{ag}(z; \alpha_s) = \sum_{n=1}^{\infty} \left(\frac{\alpha_s}{\pi}\right)^n G^{(n)}_{ga}(z) \tag{C.8}$$

with the first order coefficients $G^{(1)}_{gg}$ and $G^{(1)}_{gq}$ differing only in a colour factor [138]

$$G^{(1)}_{gg}(z) = C_A \frac{1-z}{z}, \tag{C.9}$$

$$G^{(1)}_{gq}(z) = G^{(1)}_{g\bar{q}}(z) = C_F \frac{1-z}{z}. \tag{C.10}$$

If we plug Eq. (C.6) in Eq. (C.4), we get three different kind of contributions:

$$\begin{aligned}
[(\mathbf{H\Delta})C_1C_2]_{gg;a_1a_2} =& (\mathbf{H\Delta})_{gg;\mu_1\nu_1,\mu_2\nu_2}\; d^{\mu_1\nu_1}\; d^{\mu_2\nu_2}\; C_{ga_1}(z_1)C_{ga_2}(z_2) \\
&+(\mathbf{H\Delta})_{gg;\mu_1\nu_1,\mu_2\nu_2} \\
&\quad\times\Big[\, d^{\mu_1\nu_1}\; D^{\mu_2\nu_2}\; C_{ga_1}(z_1)G_{ga_2}(z_2) + D^{\mu_1\nu_1}\; d^{\mu_2\nu_2}\; G_{ga_1}(z_1)C_{ga_2}(z_2)\Big] \\
&+(\mathbf{H\Delta})_{gg;\mu_1\nu_1,\mu_2\nu_2}\; D^{\mu_1\nu_1}\; D^{\mu_2\nu_2}\; G_{ga_1}(z_1)G_{ga_2}(z_2),
\end{aligned} \tag{C.11}$$

with $\mathbf{\Delta} = \mathbf{V}^\dagger\mathbf{D}\mathbf{V}$ and $\mathbf{D} = 1 + \mathcal{O}(\alpha_s)$.

The first term in Eq. (C.11), which we can call *collinear-collinear*, has the same structure as the corresponding one in $q\bar{q}$ annihilation, and all of the treatment of section 6.2.2 can be applied straight forward, with the Hard-virtual resummation coefficient $H_g^{Q\bar{Q}F}$ taking the following form

$$H_g^{Q\bar{Q}F} = \frac{\left(\widetilde{\mathcal{M}}^{\mu_1\mu_2}_{gg\to Q\bar{Q}F}(x_1P_1, x_2P_2, M, \mathbf{\Omega})\right)^\dagger \widetilde{\mathcal{M}}^{\nu_1\nu_2}_{gg\to Q\bar{Q}F}(x_1P_1, x_2P_2, M, \mathbf{\Omega})}{\left|\mathcal{M}^{(0)}_{c\bar{c}\to F}(x_1P_1, x_2P_2, M, \mathbf{\Omega})\right|^2} d_{\mu_1\nu_1}d_{\mu_2\nu_2}. \tag{C.12}$$

In particular, it is still true that the average over azimuth of $\mathbf{b}$, $\langle\rangle_{\phi(\mathbf{b})}$, corresponds to set $\mathbf{D} \to 1$.

The terms in the second line of Eq. (C.11), which we can call *soft-collinear*, contains interference of the final-state soft factor $\mathbf{\Gamma} = \mathbf{V}^\dagger\mathbf{D}\mathbf{V}$ with either one of the initial legs. The term with $\mathbf{D} = 1$ vanishes upon azimuthal average in $\mathbf{b}$, leaving only a contribution of $\mathbf{D} - 1 = \mathcal{O}(\alpha_s)$. For this reason, this term only contributes in the presence of a coloured final state, while it vanishes for a colour singlet final state. Also, because the coefficient G starts at $\mathcal{O}(\alpha_s)$, this term starts to contribute at NNLO with a coefficient $H^{Q\bar{Q}F}_{\mathbf{D}G}$.

The last line of Eq. (C.11) corresponds to the interference of the soft factor $\mathbf{\Gamma}$ with both initial legs. Because it has two factors $G_{ga} = \mathcal{O}(\alpha_s)$, its first contribution is at NNLO with $\mathbf{D} = 1$, which also means that it has the same expression as for a colour singlet final state. We will denote this contribution as $H_G^{Q\bar{Q}F}$.

After integration over $\mathbf{b}$, with all azimuthal correlations integrated out, this contributions have to be added to the Hard-Collinear function $\mathcal{H}^{(NNLO)_{a_1a_2\to gg}}$ presented in section 6.2.3

$$\mathcal{H}^{Q\bar{Q}F;NNLO}_{a_1a_2\to gg,\,(N_1,N_2)} \longrightarrow \mathcal{H}^{Q\bar{Q}F;NNLO}_{a_1a_2\to gg,\,(N_1,N_2)} + H_G^{Q\bar{Q}F} G^{(1)}_{ga_1,N_1} G^{(1)}_{ga_2,N_2} \tag{C.13}$$

$$+H_{\mathbf{D}G}^{Q\bar{Q}F}\left(G_{ga_1,N_1}^{(1)}\delta_{ga_2}+\delta_{ga_1}G_{ga_2,N_2}^{(1)}\right), \tag{C.14}$$

with

$$H_G^{Q\bar{Q}F}=\int\frac{\mathrm{d}\phi_b}{2\pi}D_{\mu_1\nu_1}(\mathbf{b})D_{\mu_2\nu_2}(\mathbf{b})\frac{\left\langle\mathcal{M}_{gg\to Q\bar{Q}F}^{(0)\mu_1\mu_2}\middle|\,\mathcal{M}_{gg\to Q\bar{Q}F}^{(0)\nu_1\nu_2}\right\rangle}{\left|\mathcal{M}_{c\bar{c}\to F}^{(0)}(x_1P_1,x_2P_2,M,\mathbf{\Omega})\right|^2}, \tag{C.15}$$

$$H_{\mathbf{D}G}^{Q\bar{Q}F}=\int\frac{\mathrm{d}\phi_b}{2\pi}d_{\mu_1\nu_1}D_{\mu_2\nu_2}(\mathbf{b})\frac{\left\langle\mathcal{M}_{gg\to Q\bar{Q}F}^{(0)\mu_1\mu_2}\middle|\,\mathbf{D}^{(1)}(\mathbf{b})\,\middle|\mathcal{M}_{gg\to Q\bar{Q}F}^{(0)\nu_1\nu_2}\right\rangle}{\left|\mathcal{M}_{c\bar{c}\to F}^{(0)}(x_1P_1,x_2P_2,M,\mathbf{\Omega})\right|^2}. \tag{C.16}$$

In $H_G^{Q\bar{Q}F}$ the integration over ϕ_b is simpler, the coefficient reduces to spin correlations of the LO amplitude and it contributes (due to the G_{ga} function attached to each leg) to all partonic channels. $H_{\mathbf{D}G}^{Q\bar{Q}F}$, on the other hand, only contributes to gQ and gg partonic channels, and its computation requires the evaluation of complicated **b**-space integrals, due to the dependence on **b** of the **D** colour operator. The result will contain not only spin correlations of the LO amplitude, but also of its two-colour correlators, making its calculation highly non-trivial.

These contributions have been only computed for the $t\bar{t}$ final state [151, 152], and its extension to more general process such as $t\bar{t}h$ is currently under progress.

C.2 COLOUR CORRELATORS MATRICES FOR OPENLOOPS

In this section we present the matrix representation of the two- and four-colour correlators in the basis used by OpenLoops for the processes $t\bar{t}$, $t\bar{t}H$ and $t\bar{t}Z$.

If we fix a colour basis $\{|c_i\rangle\}_i$, we can write an amplitude as $\mathcal{M}$ as a vector in colour space

$$|\mathcal{M}\rangle=\sum_i\mathcal{M}_i\,|c_i\rangle\,, \tag{C.17}$$

and therefore any colour operator **O** has an expectation value given by the expression

$$\langle\mathcal{M}|\,\mathbf{O}\,|\mathcal{M}\rangle=\sum_{i,j}\mathcal{M}_i^\dagger M_j\,[\mathbf{O}]_{ij} \tag{C.18}$$

where we defined the matrix representation of the colour operator **O** as

$$[\mathbf{O}]_{ij}=\langle c_i|\,\mathbf{O}\,|c_j\rangle\,. \tag{C.19}$$

OpenLoops provides for any amplitude $\mathcal{M}$ the vector representation in colour-space $(M_1,\cdots,M_i,\cdots)$, and the basis it uses for the production of $t\bar{t}$, $t\bar{t}h$ and $t\bar{t}Z$ is

$$\left|c_1^{gg}\right\rangle=(T^{a_1}T^{a_2})_{i_3}^{\bar{j}_4},\qquad\left|c_2^{gg}\right\rangle=(T^{a_2}T^{a_1})_{i_3}^{\bar{j}_4},\qquad\text{for gluon fusion processes} \tag{C.20}$$

$$\left|c_1^{q\bar{q}}\right\rangle = \delta_{i_3}^{\bar{i}_1}\delta_{j_2}^{\bar{j}_4} \qquad \left|c_2^{q\bar{q}}\right\rangle = \delta_{i_3}^{\bar{j}_4}\delta_{j_2}^{\bar{i}_1}, \qquad \text{for quark annihilation processes.} \tag{C.21}$$

With these definitions we can compute all the two and four-colour correlators needed. In order to write their results, first we can notice that thanks to colour-conservation, not all the combinations are independent. First of all, any squared colour-operator T is proportional to the identity, so $T_i^2 = \mathbf{1}C_i$ with $C_i = C_A$ if the leg i is a gluon or C_F if is a quark. Having this in mind, we only have to consider distinct combinations of $T_i \cdot T_{j\neq i}$. Thanks to colour-conservation, that is

$$\mathbf{T}_1 + \mathbf{T}_2 + \mathbf{T}_3 + \mathbf{T}_4 = 0, \tag{C.22}$$

any combination of the form $T_i \cdot T_4$ can be written as a linear combination of $T_i \cdot T_j$, with $i, j \in \{1, 2, 3\}$. We're left only with three distinct combinations $\{\mathbf{T}_1 \cdot \mathbf{T}_2, \mathbf{T}_2 \cdot \mathbf{T}_3, \mathbf{T}_1 \cdot \mathbf{T}_3\}$ out of which, one can be written in terms of the other two plus the Cassimir coefficients, using that

$$\mathbf{1}C_4 = \mathbf{T}_4^2 = (\mathbf{T}_1 + \mathbf{T}_2 + \mathbf{T}_3)^2 = (C_1 + C_2 + C_3)\mathbf{1} + 2(\mathbf{T}_1 \cdot \mathbf{T}_2 + \mathbf{T}_2 \cdot \mathbf{T}_3 + \mathbf{T}_1 \cdot \mathbf{T}_3) \tag{C.23}$$

In this way, is enough to compute the colour matrices $[\mathbf{1}]$, $[\mathbf{T}_1 \cdot \mathbf{T}_2]$ and $[\mathbf{T}_1 \cdot \mathbf{T}_3]$ and any other two-colour correlator can be written as a linear combination of these three. Using the same arguments, for the four colour-correlators is enough to compute $\left[(\mathbf{T}_1 \cdot \mathbf{T}_2)^2\right]$, $[(\mathbf{T}_1 \cdot \mathbf{T}_2)(\mathbf{T}_1 \cdot \mathbf{T}_3)]$, $[(\mathbf{T}_1 \cdot \mathbf{T}_3)(\mathbf{T}_1 \cdot \mathbf{T}_2)]$ and $\left[(\mathbf{T}_1 \cdot \mathbf{T}_3)^2\right]$. The matrix representation of any other four-colour correlator can be written as a linear combination of these four matrices, the matrices of the two-colour correlators and the one of the identity.

Below we write the expressions for

$$\Big\{ [\mathbf{1}], [\mathbf{T}_1 \cdot \mathbf{T}_2], [\mathbf{T}_1 \cdot \mathbf{T}_3], \left[(\mathbf{T}_1 \cdot \mathbf{T}_2)^2\right], \left[(\mathbf{T}_1 \cdot \mathbf{T}_3)^2\right], [(\mathbf{T}_1 \cdot \mathbf{T}_2)(\mathbf{T}_1 \cdot \mathbf{T}_3)], \\ [(\mathbf{T}_1 \cdot \mathbf{T}_3)(\mathbf{T}_1 \cdot \mathbf{T}_2)] \Big\} \tag{C.24}$$

in the basis specified in (C.20) (for $gg \to t\bar{t}(H/Z)$ processes) and (C.21) (for $q\bar{q} \to t\bar{t}(H/Z)$ processes). We denote which basis is being used as a subscript, either $[\mathbf{O}]_{gg}$ or $[\mathbf{O}]_{q\bar{q}}$.

For the gluon fusion processes we have,

$$[\mathbf{1}]_{gg} = \frac{C_F}{2}\begin{pmatrix} 2C_AC_F & -1 \\ -1 & 2C_AC_F \end{pmatrix}, \tag{C.25}$$

$$[\mathbf{T}_1 \cdot \mathbf{T}_2]_{gg} = -\frac{1}{4}C_A^3C_F\begin{pmatrix} 1 & 0 \\ 0 & 1 \end{pmatrix}, \tag{C.26}$$

$$[\mathbf{T}_1 \cdot \mathbf{T}_3]_{gg} = \frac{1}{4} C_A C_F \begin{pmatrix} -2C_A C_F & 1 \\ 1 & 1 \end{pmatrix}, \tag{C.27}$$

$$[(\mathbf{T}_1 \cdot \mathbf{T}_2)^2]_{gg} = \frac{1}{8} C_A^2 C_F \begin{pmatrix} C_A^2 + 2 & 2 \\ 2 & C_A^2 + 2 \end{pmatrix}, \tag{C.28}$$

$$[(\mathbf{T}_1 \cdot \mathbf{T}_3)^2]_{gg} = \frac{1}{8} C_A^2 C_F \begin{pmatrix} 2C_A C_F & -1 \\ -1 & 1 \end{pmatrix}, \tag{C.29}$$

$$[(\mathbf{T}_1 \cdot \mathbf{T}_2)(\mathbf{T}_1 \cdot \mathbf{T}_3)]_{gg} = \frac{1}{8} C_A^2 C_F \begin{pmatrix} C_A^2 & -2 \\ 0 & -2 \end{pmatrix}, \tag{C.30}$$

$$[(\mathbf{T}_1 \cdot \mathbf{T}_3)(\mathbf{T}_1 \cdot \mathbf{T}_2)]_{gg} = \frac{1}{8} C_A^2 C_F \begin{pmatrix} C_A^2 & 0 \\ -2 & -2 \end{pmatrix}, \tag{C.31}$$

while for the quark annihilation processes

$$[\mathbf{1}]_{q\bar{q}} = \begin{pmatrix} C_A^2 & C_A \\ C_A & C_A^2 \end{pmatrix}, \tag{C.32}$$

$$[\mathbf{T}_1 \cdot \mathbf{T}_2]_{q\bar{q}} = -\, C_A C_F \begin{pmatrix} 0 & 1 \\ 1 & C_A \end{pmatrix}, \tag{C.33}$$

$$[\mathbf{T}_1 \cdot \mathbf{T}_3]_{q\bar{q}} = -\, C_A C_F \begin{pmatrix} C_A & 1 \\ 1 & 0 \end{pmatrix}, \tag{C.34}$$

$$[(\mathbf{T}_1 \cdot \mathbf{T}_2)^2]_{q\bar{q}} = \frac{1}{2} C_A C_F \begin{pmatrix} 1 & 2C_F \\ 2C_F & 2C_A C_F \end{pmatrix}, \tag{C.35}$$

$$[(\mathbf{T}_1 \cdot \mathbf{T}_3)^2]_{q\bar{q}} = \frac{1}{2} C_A C_F \begin{pmatrix} 2C_A C_F & 2C_F \\ 2C_F & 1 \end{pmatrix}, \tag{C.36}$$

$$[(\mathbf{T}_1 \cdot \mathbf{T}_2)(\mathbf{T}_1 \cdot \mathbf{T}_3)]_{q\bar{q}} = \frac{1}{2} C_F \begin{pmatrix} 0 & -1 \\ 2C_A C_F & 0 \end{pmatrix}, \tag{C.37}$$

$$[(\mathbf{T}_1 \cdot \mathbf{T}_3)(\mathbf{T}_1 \cdot \mathbf{T}_2)]_{q\bar{q}} = \frac{1}{2} C_F \begin{pmatrix} 0 & 2C_A C_F \\ -1 & 0 \end{pmatrix}, \tag{C.38}$$

and the corresponding Cassimir for each process are

$$C_1 = C_2 = \begin{cases} C_A & \text{for } gg \text{ processes} \\ C_F & \text{for } q\bar{q} \text{ processes} \end{cases} \qquad \text{and} \qquad C_3 = C_4 = C_F. \tag{C.39}$$

BIBLIOGRAPHY

[1] Peter W. Higgs. "Broken symmetries, massless particles and gauge fields." In: *Phys. Lett.* 12 (1964), pp. 132–133. DOI: 10.1016/0031-9163(64)91136-9.

[2] Peter W. Higgs. "Broken Symmetries and the Masses of Gauge Bosons." In: *Phys. Rev. Lett.* 13 (1964), pp. 508–509. DOI: 10.1103/PhysRevLett.13.508.

[3] F. Englert and R. Brout. "Broken Symmetry and the Mass of Gauge Vector Mesons." In: *Phys. Rev. Lett.* 13 (1964), pp. 321–323. DOI: 10.1103/PhysRevLett.13.321.

[4] Georges Aad et al. "Observation of a new particle in the search for the Standard Model Higgs boson with the ATLAS detector at the LHC." In: *Phys. Lett.* B716 (2012), pp. 1–29. DOI: 10.1016/j.physletb.2012.08.020. arXiv: 1207.7214 [hep-ex].

[5] Serguei Chatrchyan et al. "Observation of a new boson at a mass of 125 GeV with the CMS experiment at the LHC." In: *Phys. Lett.* B716 (2012), pp. 30–61. DOI: 10.1016/j.physletb.2012.08.021. arXiv: 1207.7235 [hep-ex].

[6] Georges Aad et al. "Measurements of the Higgs boson production and decay rates and constraints on its couplings from a combined ATLAS and CMS analysis of the LHC pp collision data at $\sqrt{s} = 7$ and 8 TeV." In: *JHEP* 08 (2016), p. 045. DOI: 10.1007/JHEP08(2016)045. arXiv: 1606.02266 [hep-ex].

[7] Gerard 't Hooft. "Renormalizable Lagrangians for Massive Yang-Mills Fields." In: *Nucl. Phys.* B35 (1971), pp. 167–188. DOI: 10.1016/0550-3213(71)90139-8.

[8] Gerard 't Hooft and M. J. G. Veltman. "Regularization and Renormalization of Gauge Fields." In: *Nucl. Phys.* B44 (1972), pp. 189–213. DOI: 10.1016/0550-3213(72)90279-9.

[9] F. Bloch and A. Nordsieck. "Note on the Radiation Field of the electron." In: *Phys. Rev.* 52 (1937), pp. 54–59. DOI: 10.1103/PhysRev.52.54.

[10] T. Kinoshita. "Mass singularities of Feynman amplitudes." In: *J. Math. Phys.* 3 (1962), pp. 650–677. DOI: 10.1063/1.1724268.

[11] T.D. Lee and M. Nauenberg. "Degenerate Systems and Mass Singularities." In: *Phys. Rev.* 133 (1964). Ed. by G. Feinberg, B1549–B1562. DOI: 10.1103/PhysRev.133.B1549.

[12] S. Catani and M.H. Seymour. "A General algorithm for calculating jet cross-sections in NLO QCD." In: *Nucl. Phys. B* 485 (1997). [Erratum: Nucl.Phys.B 510, 503–504 (1998)], pp. 291–419. DOI: 10.1016/S0550-3213(96)00589-5. arXiv: hep-ph/9605323.

[13] Stefano Catani and Massimiliano Grazzini. "Infrared factorization of tree level QCD amplitudes at the next-to-next-to-leading order and beyond." In: *Nucl. Phys. B* 570 (2000), pp. 287–325. DOI: 10.1016/S0550-3213(99)00778-6. arXiv: hep-ph/9908523.

[14] S. Frixione, Z. Kunszt, and A. Signer. "Three jet cross-sections to next-to-leading order." In: *Nucl. Phys.* B467 (1996), pp. 399–442. DOI: 10.1016/0550-3213(96)00110-1. arXiv: hep-ph/9512328 [hep-ph].

[15] S. Frixione. "A General approach to jet cross-sections in QCD." In: *Nucl. Phys.* B507 (1997), pp. 295–314. DOI: 10.1016/S0550-3213(97)00574-9. arXiv: hep-ph/9706545 [hep-ph].

[16] Giuseppe Degrassi, Pier Paolo Giardino, Fabio Maltoni, and Davide Pagani. "Probing the Higgs self coupling via single Higgs production at the LHC." In: *JHEP* 12 (2016), p. 080. DOI: 10.1007/JHEP12(2016)080. arXiv: 1607.04251 [hep-ph].

[17] Wojciech Bizon, Martin Gorbahn, Ulrich Haisch, and Giulia Zanderighi. "Constraints on the trilinear Higgs coupling from vector boson fusion and associated Higgs production at the LHC." In: (2016). arXiv: 1610.05771 [hep-ph].

[18] Giuseppe Degrassi, Marco Fedele, and Pier Paolo Giardino. "Constraints on the trilinear Higgs self coupling from precision observables." In: (2017). arXiv: 1702.01737 [hep-ph].

[19] E. W. Nigel Glover and J. J. van der Bij. "Higgs boson pair production via gluon fusion." In: *Nucl. Phys.* B309 (1988), pp. 282–294. DOI: 10.1016/0550-3213(88)90083-1.

[20] Oscar J. P. Eboli, G. C. Marques, S. F. Novaes, and A. A. Natale. "Twin Higgs boson production." In: *Phys. Lett.* B197 (1987), pp. 269–272. DOI: 10.1016/0370-2693(87)90381-9.

[21] T. Plehn, M. Spira, and P. M. Zerwas. "Pair production of neutral Higgs particles in gluon-gluon collisions." In: *Nucl. Phys.* B479 (1996). [Erratum: Nucl. Phys.B531,655(1998)], pp. 46–64. DOI: 10.1016/0550-3213(96)00418-X,10.1016/S0550-3213(98)00406-4. arXiv: hep-ph/9603205 [hep-ph].

[22] C. J. C. Burges and Howard J. Schnitzer. "Virtual Effects of Excited Quarks as Probes of a Possible New Hadronic Mass Scale." In: *Nucl. Phys.* B228 (1983), pp. 464–500. DOI: 10.1016/0550-3213(83)90555-2.

[23] Chung Ngoc Leung, S. T. Love, and S. Rao. "Low-Energy Manifestations of a New Interaction Scale: Operator Analysis." In: *Z. Phys.* C31 (1986), p. 433. DOI: 10.1007/BF01588041.

[24] W. Buchmuller and D. Wyler. "Effective Lagrangian Analysis of New Interactions and Flavor Conservation." In: *Nucl. Phys.* B268 (1986), pp. 621–653. DOI: 10.1016/0550-3213(86)90262-2.

[25] B. Grzadkowski, M. Iskrzynski, M. Misiak, and J. Rosiek. "Dimension-Six Terms in the Standard Model Lagrangian." In: *JHEP* 10 (2010), p. 085. DOI: 10.1007/JHEP10(2010)085. arXiv: 1008.4884 [hep-ph].

[26] Rodrigo Alonso, Elizabeth E. Jenkins, Aneesh V. Manohar, and Michael Trott. "Renormalization Group Evolution of the Standard Model Dimension Six Operators III: Gauge Coupling Dependence and Phenomenology." In: *JHEP* 04 (2014), p. 159. DOI: 10.1007/JHEP04(2014)159. arXiv: 1312.2014 [hep-ph].

[27] S. Borowka, N. Greiner, G. Heinrich, S. P. Jones, M. Kerner, J. Schlenk, U. Schubert, and T. Zirke. "Higgs Boson Pair Production in Gluon Fusion at Next-to-Leading Order with Full Top-Quark Mass Dependence." In: *Phys. Rev. Lett.* 117.1 (2016). [Erratum: Phys. Rev. Lett.117,no.7,079901(2016)], p. 012001. DOI: 10.1103/PhysRevLett.117.079901,10.1103/PhysRevLett.117.012001. arXiv: 1604.06447 [hep-ph].

[28] S. Borowka, N. Greiner, G. Heinrich, S. P. Jones, M. Kerner, J. Schlenk, and T. Zirke. "Full top quark mass dependence in Higgs boson pair production at NLO." In: *JHEP* 10 (2016), p. 107. DOI: 10.1007/JHEP10(2016)107. arXiv: 1608.04798 [hep-ph].

[29] Julien Baglio, Francisco Campanario, Seraina Glaus, Margarete Mühlleitner, Michael Spira, and Juraj Streicher. "Gluon fusion into Higgs pairs at NLO QCD and the top mass scheme." In: *Eur. Phys. J.* C79.6 (2019), p. 459. DOI: 10.1140/epjc/s10052-019-6973-3. arXiv: 1811.05692 [hep-ph].

[30] S. Dawson, S. Dittmaier, and M. Spira. "Neutral Higgs boson pair production at hadron colliders: QCD corrections." In: *Phys. Rev.* D58 (1998), p. 115012. DOI: 10.1103/PhysRevD.58.115012. arXiv: hep-ph/9805244 [hep-ph].

[31] Daniel de Florian and Javier Mazzitelli. "Two-loop virtual corrections to Higgs pair production." In: *Phys. Lett.* B724 (2013), pp. 306–309. DOI: 10.1016/j.physletb.2013.06.046. arXiv: 1305.5206 [hep-ph].

[32] Jonathan Grigo, Kirill Melnikov, and Matthias Steinhauser. "Virtual corrections to Higgs boson pair production in the large top quark mass limit." In: *Nucl. Phys.* B888 (2014), pp. 17–29. DOI: 10.1016/j.nuclphysb.2014.09.003. arXiv: 1408.2422 [hep-ph].

[33] Daniel de Florian and Javier Mazzitelli. "Higgs Boson Pair Production at Next-to-Next-to-Leading Order in QCD." In: *Phys. Rev. Lett.* 111 (2013), p. 201801. DOI: 10.1103/PhysRevLett.111.201801. arXiv: 1309.6594 [hep-ph].

[34] Daniel de Florian, Massimiliano Grazzini, Catalin Hanga, Stefan Kallweit, Jonas M. Lindert, Philipp Maierhöfer, Javier Mazzitelli, and Dirk Rathlev. "Differential Higgs Boson Pair Production at Next-to-Next-to-Leading Order in QCD." In: *JHEP* 09 (2016), p. 151. DOI: 10.1007/JHEP09(2016)151. arXiv: 1606.09519 [hep-ph].

[35] Long-Bin Chen, Hai Tao Li, Hua-Sheng Shao, and Jian Wang. "Higgs boson pair production via gluon fusion at N^{3}LO in QCD." In: *Phys. Lett. B* 803 (2020), p. 135292. DOI: 10.1016/j.physletb.2020.135292. arXiv: 1909.06808 [hep-ph].

[36] Long-Bin Chen, Hai Tao Li, Hua-Sheng Shao, and Jian Wang. "The gluon-fusion production of Higgs boson pair: N^{3}LO QCD corrections and top-quark mass effects." In: *JHEP* 03 (2020), p. 072. DOI: 10.1007/JHEP03(2020)072. arXiv: 1912.13001 [hep-ph].

[37] Florian Goertz, Andreas Papaefstathiou, Li Lin Yang, and José Zurita. "Higgs boson pair production in the D=6 extension of the SM." In: *JHEP* 04 (2015), p. 167. DOI: 10.1007/JHEP04(2015)167. arXiv: 1410.3471 [hep-ph].

[38] Alex Pomarol and Francesco Riva. "Towards the Ultimate SM Fit to Close in on Higgs Physics." In: *JHEP* 01 (2014), p. 151. DOI: 10.1007/JHEP01(2014)151. arXiv: 1308.2803 [hep-ph].

[39] Adam Falkowski and Francesco Riva. "Model-independent precision constraints on dimension-6 operators." In: *JHEP* 02 (2015), p. 039. DOI: 10.1007/JHEP02(2015)039. arXiv: 1411.0669 [hep-ph].

[40] John Ellis, Veronica Sanz, and Tevong You. "The Effective Standard Model after LHC Run I." In: *JHEP* 03 (2015), p. 157. DOI: 10.1007/JHEP03(2015)157. arXiv: 1410.7703 [hep-ph].

[41] Beranger Dumont, Sylvain Fichet, and Gero von Gersdorff. "A Bayesian view of the Higgs sector with higher dimensional operators." In: *JHEP* 07 (2013), p. 065. DOI: 10.1007/JHEP07(2013)065. arXiv: 1304.3369 [hep-ph].

[42] Adam Falkowski. "Effective field theory approach to LHC Higgs data." In: *Pramana* 87.3 (2016), p. 39. DOI: 10.1007/s12043-016-1251-5. arXiv: 1505.00046 [hep-ph].

[43] Anja Butter, Oscar J. P. Éboli, J. Gonzalez-Fraile, M. C. Gonzalez-Garcia, Tilman Plehn, and Michael Rauch. "The Gauge-Higgs Legacy of the LHC Run I." In: *JHEP* 07 (2016), p. 152. DOI: 10.1007/JHEP07(2016)152. arXiv: 1604.03105 [hep-ph].

[44] Ramona Grober, Margarete Muhlleitner, Michael Spira, and Juraj Streicher. "NLO QCD Corrections to Higgs Pair Production including Dimension-6 Operators." In: *JHEP* 09 (2015), p. 092. DOI: 10.1007/JHEP09(2015)092. arXiv: 1504.06577 [hep-ph].

[45] G. Buchalla, M. Capozi, A. Celis, G. Heinrich, and L. Scyboz. "Higgs boson pair production in non-linear Effective Field Theory with full m_t-dependence at NLO QCD." In: *JHEP* 09 (2018), p. 057. DOI: 10.1007/JHEP09(2018)057. arXiv: 1806.05162 [hep-ph].

[46] Daniel de Florian, Ignacio Fabre, and Javier Mazzitelli. "Higgs boson pair production at NNLO in QCD including dimension 6 operators." In: *JHEP* 10 (2017), p. 215. DOI: 10.1007/JHEP10(2017)215. arXiv: 1704.05700 [hep-ph].

[47] Daniel de Florian, Ignacio Fabre, Gundrum Heinrich, and Javier Mazzitelli. "Improved NNLO Higgs pair production with EFT effects." In: *11th Les Houches Workshop on Physics at TeV Colliders: PhysTeV Les Houches*. Mar. 2020. arXiv: 2003.01700 [hep-ph].

[48] Fabio Maltoni, Eleni Vryonidou, and Cen Zhang. "Higgs production in association with a top-antitop pair in the Standard Model Effective Field Theory at NLO in QCD." In: *JHEP* 10 (2016), p. 123. DOI: 10.1007/JHEP10(2016)123. arXiv: 1607.05330 [hep-ph].

[49] Diogo Buarque Franzosi and Cen Zhang. "Probing the top-quark chromomagnetic dipole moment at next-to-leading order in QCD." In: *Phys. Rev.* D91.11 (2015), p. 114010. DOI: 10.1103/PhysRevD.91.114010. arXiv: 1503.08841 [hep-ph].

[50] J. Baglio, A. Djouadi, R. Gröber, M.M. Mühlleitner, J. Quevillon, and M. Spira. "The measurement of the Higgs self-coupling at the LHC: theoretical status." In: *JHEP* 04 (2013), p. 151. DOI: 10.1007/JHEP04(2013)151. arXiv: 1212.5581 [hep-ph].

[51] Roberto Contino, Christophe Grojean, Mauro Moretti, Fulvio Piccinini, and Riccardo Rattazzi. "Strong Double Higgs Production at the LHC." In: *JHEP* 05 (2010), p. 089. DOI: 10.1007/JHEP05(2010)089. arXiv: 1002.1011 [hep-ph].

[52] G. F. Giudice, C. Grojean, A. Pomarol, and R. Rattazzi. "The Strongly-Interacting Light Higgs." In: *JHEP* 06 (2007), p. 045. DOI: 10.1088/1126-6708/2007/06/045. arXiv: hep-ph/0703164 [hep-ph].

[53] Roberto Contino, Margherita Ghezzi, Christophe Grojean, Margarete Muhlleitner, and Michael Spira. "Effective Lagrangian for a light Higgs-like scalar." In: *JHEP* 07 (2013), p. 035. DOI: 10.1007/JHEP07(2013)035. arXiv: 1303.3876 [hep-ph].

[54] K. G. Chetyrkin, Bernd A. Kniehl, and M. Steinhauser. "Hadronic Higgs decay to order α_s^4." In: *Phys. Rev. Lett.* 79 (1997), pp. 353–356. DOI: 10.1103/PhysRevLett.79.353. arXiv: hep-ph/9705240 [hep-ph].

[55] K. G. Chetyrkin, Johann H. Kuhn, and Christian Sturm. "QCD decoupling at four loops." In: *Nucl. Phys.* B744 (2006), pp. 121–135. DOI: 10.1016/j.nuclphysb.2006.03.020. arXiv: hep-ph/0512060 [hep-ph].

[56] Michael Kramer, Eric Laenen, and Michael Spira. "Soft gluon radiation in Higgs boson production at the LHC." In: *Nucl. Phys.* B511 (1998), pp. 523–549. DOI: 10.1016/S0550-3213(97)00679-2. arXiv: hep-ph/9611272 [hep-ph].

[57] Y. Schroder and M. Steinhauser. "Four-loop decoupling relations for the strong coupling." In: *JHEP* 01 (2006), p. 051. DOI: 10.1088/1126-6708/2006/01/051. arXiv: hep-ph/0512058 [hep-ph].

[58] A. Djouadi, M. Spira, and P. M. Zerwas. "Production of Higgs bosons in proton colliders: QCD corrections." In: *Phys. Lett.* B264 (1991), pp. 440–446. DOI: 10.1016/0370-2693(91)90375-Z.

[59] Michael Spira. "Effective Multi-Higgs Couplings to Gluons." In: *JHEP* 10 (2016), p. 026. DOI: 10.1007/JHEP10(2016)026. arXiv: 1607.05548 [hep-ph].

[60] Charalampos Anastasiou and Kirill Melnikov. "Higgs boson production at hadron colliders in NNLO QCD." In: *Nucl. Phys.* B646 (2002), pp. 220–256. DOI: 10.1016/S0550-3213(02)00837-4. arXiv: hep-ph/0207004 [hep-ph].

[61] Robert V. Harlander and William B. Kilgore. "Next-to-next-to-leading order Higgs production at hadron colliders." In: *Phys. Rev. Lett.* 88 (2002), p. 201801. DOI: 10.1103/PhysRevLett.88.201801. arXiv: hep-ph/0201206 [hep-ph].

[62] V. Ravindran, J. Smith, and W. L. van Neerven. "NNLO corrections to the total cross-section for Higgs boson production in hadron hadron collisions." In: *Nucl. Phys.* B665 (2003), pp. 325–366. DOI: 10.1016/S0550-3213(03)00457-7. arXiv: hep-ph/0302135 [hep-ph].

[63] Jon Butterworth et al. "PDF4LHC recommendations for LHC Run II." In: *J. Phys.* G43 (2016), p. 023001. DOI: 10.1088/0954-3899/43/2/023001. arXiv: 1510.03865 [hep-ph].

[64] Sayipjamal Dulat, Tie-Jiun Hou, Jun Gao, Marco Guzzi, Joey Huston, Pavel Nadolsky, Jon Pumplin, Carl Schmidt, Daniel Stump, and C. P. Yuan. "New parton distribution functions from a global analysis of quantum chromodynamics." In: *Phys. Rev.* D93.3 (2016), p. 033006. DOI: 10.1103/PhysRevD.93.033006. arXiv: 1506.07443 [hep-ph].

[65] L. A. Harland-Lang, A. D. Martin, P. Motylinski, and R. S. Thorne. "Parton distributions in the LHC era: MMHT 2014 PDFs." In: *Eur. Phys. J.* C75.5 (2015), p. 204. DOI: 10.1140/epjc/s10052-015-3397-6. arXiv: 1412.3989 [hep-ph].

[66] Richard D. Ball et al. "Parton distributions for the LHC Run II." In: *JHEP* 04 (2015), p. 040. DOI: 10.1007/JHEP04(2015)040. arXiv: 1410.8849 [hep-ph].

[67] Stefano Carrazza, José I. Latorre, Juan Rojo, and Graeme Watt. "A compression algorithm for the combination of PDF sets." In: *Eur. Phys. J.* C75 (2015), p. 474. DOI: 10.1140/epjc/s10052-015-3703-3. arXiv: 1504.06469 [hep-ph].

[68] G. Watt and R. S. Thorne. "Study of Monte Carlo approach to experimental uncertainty propagation with MSTW 2008 PDFs." In: *JHEP* 08 (2012), p. 052. DOI: 10.1007/JHEP08(2012)052. arXiv: 1205.4024 [hep-ph].

[69] Andy Buckley, James Ferrando, Stephen Lloyd, Karl Nordström, Ben Page, Martin Rüfenacht, Marek Schönherr, and Graeme Watt. "LHAPDF6: parton density access in the LHC precision era." In: *Eur. Phys. J.* C75 (2015), p. 132. DOI: 10.1140/epjc/s10052-015-3318-8. arXiv: 1412.7420 [hep-ph].

[70] T. Hahn. "CUBA: A Library for multidimensional numerical integration." In: *Comput. Phys. Commun.* 168 (2005), pp. 78–95. DOI: 10.1016/j.cpc.2005.01.010. arXiv: hep-ph/0404043 [hep-ph].

[71] Aleksandr Azatov, Roberto Contino, Giuliano Panico, and Minho Son. "Effective field theory analysis of double Higgs boson production via gluon fusion." In: *Phys. Rev.* D92.3 (2015), p. 035001. DOI: 10.1103/PhysRevD.92.035001. arXiv: 1502.00539 [hep-ph].

[72] CMS Collaboration. "Precise determination of the mass of the Higgs boson and studies of the compatibility of its couplings with the standard model." In: (2014).

[73] Aleksandr Azatov, Roberto Contino, Camila S. Machado, and Francesco Riva. "Helicity Selection Rules and Non-Interference for BSM Amplitudes." In: (2016). arXiv: 1607.05236 [hep-ph].

[74] Alexandra Carvalho, Martino Dall'Osso, Tommaso Dorigo, Florian Goertz, Carlo A. Gottardo, and Mia Tosi. "Higgs Pair Production: Choosing Benchmarks With Cluster Analysis." In: *JHEP* 04 (2016), p. 126. DOI: 10.1007/JHEP04(2016)126. arXiv: 1507.02245 [hep-ph].

[75] Massimiliano Grazzini, Agnieszka Ilnicka, Michael Spira, and Marius Wiesemann. "Modeling BSM effects on the Higgs transverse-momentum spectrum in an EFT approach." In: (2016). arXiv: 1612.00283 [hep-ph].

[76] Stefano Di Vita, Christophe Grojean, Giuliano Panico, Marc Riembau, and Thibaud Vantalon. "A global view on the Higgs self-coupling." In: (2017). arXiv: 1704.01953 [hep-ph].

[77] S. Dawson, A. Ismail, and Ian Low. "What's in the loop? The anatomy of double Higgs production." In: *Phys. Rev.* D91.11 (2015), p. 115008. DOI: 10.1103/PhysRevD.91.115008. arXiv: 1504.05596 [hep-ph].

[78] Duane A. Dicus, Chung Kao, and Wayne W. Repko. "Interference effects and the use of Higgs boson pair production to study the Higgs trilinear self coupling." In: *Phys. Rev.* D92.9 (2015), p. 093003. DOI: 10.1103/PhysRevD.92.093003. arXiv: 1504.02334 [hep-ph].

[79] Matthew McCullough. "An Indirect Model-Dependent Probe of the Higgs Self-Coupling." In: *Phys. Rev.* D90.1 (2014). [Erratum: Phys. Rev.D92,no.3,039903(2015)], p. 015001. DOI: 10.1103/PhysRevD.90.015001, 10.1103/PhysRevD.92.039903. arXiv: 1312.3322 [hep-ph].

[80] Martin Gorbahn and Ulrich Haisch. "Indirect probes of the trilinear Higgs coupling: $gg \to h$ and $h \to \gamma\gamma$." In: *JHEP* 10 (2016), p. 094. DOI: 10.1007/JHEP10(2016)094. arXiv: 1607.03773 [hep-ph].

[81] Fabio Maltoni, Davide Pagani, Ambresh Shivaji, and Xiaoran Zhao. "Trilinear Higgs coupling determination via single-Higgs differential measurements at the LHC." In: *Eur. Phys. J.* C77.12 (2017), p. 887. DOI: 10.1140/epjc/s10052-017-5410-8. arXiv: 1709.08649 [hep-ph].

[82] Graham D. Kribs, Andreas Maier, Heidi Rzehak, Michael Spannowsky, and Philip Waite. "Electroweak oblique parameters as a probe of the trilinear Higgs boson self-interaction." In: *Phys. Rev.* D95.9 (2017), p. 093004. DOI: 10.1103/PhysRevD.95.093004. arXiv: 1702.07678 [hep-ph].

[83] J. Alison et al. "Higgs Boson Pair Production at Colliders: Status and Perspectives." In: *Double Higgs Production at Colliders Batavia, IL, USA, September 4, 2018-9, 2019*. Ed. by B. Di Micco, M. Gouzevitch, J. Mazzitelli, and C. Vernieri. 2019. arXiv: 1910.00012 [hep-ph]. URL: https://lss.fnal.gov/archive/2019/conf/fermilab-conf-19-468-e-t.pdf.

[84] Andreas Papaefstathiou and Kazuki Sakurai. "Triple Higgs boson production at a 100 TeV proton-proton collider." In: *JHEP* 02 (2016), p. 006. DOI: 10.1007/JHEP02(2016)006. arXiv: 1508.06524 [hep-ph].

[85] Andreas Papaefstathiou, Gilberto Tetlalmatzi-Xolocotzi, and Marco Zaro. "Triple Higgs boson production to six *b*-jets at a 100 TeV proton collider." In: *Eur. Phys. J.* C79.11 (2019), p. 947. DOI: 10.1140/epjc/s10052-019-7457-1. arXiv: 1909.09166 [hep-ph].

[86] Tilman Plehn and Michael Rauch. "The quartic higgs coupling at hadron colliders." In: *Phys. Rev.* D72 (2005), p. 053008. DOI: 10.1103/PhysRevD.72.053008. arXiv: hep-ph/0507321 [hep-ph].

[87] T. Binoth, S. Karg, N. Kauer, and R. Ruckl. "Multi-Higgs boson production in the Standard Model and beyond." In: *Phys. Rev.* D74 (2006), p. 113008. DOI: 10.1103/PhysRevD.74.113008. arXiv: hep-ph/0608057 [hep-ph].

[88] F. Maltoni, E. Vryonidou, and M. Zaro. "Top-quark mass effects in double and triple Higgs production in gluon-gluon fusion at NLO." In: *JHEP* 11 (2014), p. 079. DOI: 10.1007/JHEP11(2014)079. arXiv: 1408.6542 [hep-ph].

[89] Daniel de Florian and Javier Mazzitelli. "Two-loop corrections to the triple Higgs boson production cross section." In: *JHEP* 02 (2017), p. 107. DOI: 10.1007/JHEP02(2017)107. arXiv: 1610.05012 [hep-ph].

[90] Daniel de Florian and Javier Mazzitelli. "A next-to-next-to-leading order calculation of soft-virtual cross sections." In: *JHEP* 12 (2012), p. 088. DOI: 10.1007/JHEP12(2012)08,10.1007/JHEP12(2012)088. arXiv: 1209.0673 [hep-ph].

[91] Daniel de Florian, Ignacio Fabre, and Javier Mazzitelli. "Triple Higgs production at hadron colliders at NNLO in QCD." In: *JHEP* 03 (2020), p. 155. DOI: 10.1007/JHEP03(2020)155. arXiv: 1912.02760 [hep-ph].

[92] Ansgar Denner, Jean-Nicolas Lang, and Sandro Uccirati. "Recola2: REcursive Computation of One-Loop Amplitudes 2." In: *Comput. Phys. Commun.* 224 (2018), pp. 346–361. DOI: 10.1016/j.cpc.2017.11.013. arXiv: 1711.07388 [hep-ph].

[93] Thomas Hahn. "Generating Feynman diagrams and amplitudes with FeynArts 3." In: *Comput. Phys. Commun.* 140 (2001), pp. 418–431. DOI: 10.1016/S0010-4655(01)00290-9. arXiv: hep-ph/0012260 [hep-ph].

[94] R. Mertig, M. Bohm, and Ansgar Denner. "FEYN CALC: Computer algebraic calculation of Feynman amplitudes." In: *Comput. Phys. Commun.* 64 (1991), pp. 345–359. DOI: 10.1016/0010-4655(91)90130-D.

[95] Vladyslav Shtabovenko, Rolf Mertig, and Frederik Orellana. "New Developments in FeynCalc 9.0." In: *Comput. Phys. Commun.* 207 (2016), pp. 432–444. DOI: 10.1016/j.cpc.2016.06.008. arXiv: 1601.01167 [hep-ph].

[96] Stefano Catani, Daniel de Florian, Giancarlo Ferrera, and Massimiliano Grazzini. "Vector boson production at hadron colliders: transverse-momentum resummation and leptonic decay." In: *JHEP* 12 (2015), p. 047. DOI: 10.1007/JHEP12(2015)047. arXiv: 1507.06937 [hep-ph].

[97] D. de Florian et al. "Handbook of LHC Higgs Cross Sections: 4. Deciphering the Nature of the Higgs Sector." In: (2016). DOI: 10.2172/1345634, 10.23731/CYRM-2017-002. arXiv: 1610.07922 [hep-ph].

[98] Morad Aaboud et al. "Observation of $H \to b\bar{b}$ decays and VH production with the ATLAS detector." In: *Phys. Lett. B* 786 (2018), pp. 59–86. DOI: 10.1016/j.physletb.2018.09.013. arXiv: 1808.08238 [hep-ex].

[99] A. M. Sirunyan et al. "Observation of Higgs boson decay to bottom quarks." In: *Phys. Rev. Lett.* 121.12 (2018), p. 121801. DOI: 10.1103/PhysRevLett.121.121801. arXiv: 1808.08242 [hep-ex].

[100] Albert M Sirunyan et al. "Observation of the Higgs boson decay to a pair of τ leptons with the CMS detector." In: *Phys. Lett. B* 779 (2018), pp. 283–316. DOI: 10.1016/j.physletb.2018.02.004. arXiv: 1708.00373 [hep-ex].

[101] Morad Aaboud et al. "Cross-section measurements of the Higgs boson decaying into a pair of τ-leptons in proton-proton collisions at $\sqrt{s} = 13$ TeV with the ATLAS detector." In: *Phys. Rev. D* 99 (2019), p. 072001. DOI: 10.1103/PhysRevD.99.072001. arXiv: 1811.08856 [hep-ex].

[102] M. Aaboud et al. "Observation of Higgs boson production in association with a top quark pair at the LHC with the ATLAS detector." In: *Phys. Lett. B* 784 (2018), pp. 173–191. DOI: 10.1016/j.physletb.2018.07.035. arXiv: 1806.00425 [hep-ex].

[103] Albert M Sirunyan et al. "Observation of $t\bar{t}H$ production." In: *Phys. Rev. Lett.* 120.23 (2018), p. 231801. DOI: 10.1103/PhysRevLett.120.231801. arXiv: 1804.02610 [hep-ex].

[104] "Analysis of $t\bar{t}H$ and $t\bar{t}W$ production in multilepton final states with the ATLAS detector." In: (Oct. 2019).

[105] Albert M Sirunyan et al. "Measurements of $t\bar{t}H$ production and the CP structure of the Yukawa interaction between the Higgs boson and top quark in the diphoton decay channel." In: (Mar. 2020). arXiv: 2003.10866 [hep-ex].

[106] W. Beenakker, S. Dittmaier, M. Kramer, B. Plumper, M. Spira, and P.M. Zerwas. "Higgs radiation off top quarks at the Tevatron and the LHC." In: *Phys. Rev. Lett.* 87 (2001), p. 201805. DOI: 10.1103/PhysRevLett.87.201805. arXiv: hep-ph/0107081.

[107] W. Beenakker, S. Dittmaier, M. Kramer, B. Plumper, M. Spira, and P.M. Zerwas. "NLO QCD corrections to t anti-t H production in hadron collisions." In: *Nucl. Phys. B* 653 (2003), pp. 151–203. DOI: 10.1016/S0550-3213(03)00044-0. arXiv: hep-ph/0211352.

[108] L. Reina and S. Dawson. "Next-to-leading order results for t anti-t h production at the Tevatron." In: *Phys. Rev. Lett.* 87 (2001), p. 201804. DOI: 10.1103/PhysRevLett.87.201804. arXiv: hep-ph/0107101.

[109] S. Dawson, C. Jackson, L.H. Orr, L. Reina, and D. Wackeroth. "Associated Higgs production with top quarks at the large hadron collider: NLO QCD corrections." In: *Phys. Rev. D* 68 (2003), p. 034022. DOI: 10.1103/PhysRevD.68.034022. arXiv: hep-ph/0305087.

[110] Rikkert Frederix, Stefano Frixione, Valentin Hirschi, Fabio Maltoni, Roberto Pittau, and Paolo Torrielli. "Scalar and pseudoscalar Higgs production in association with a top–antitop pair." In: *Phys. Lett. B* 701 (2011), pp. 427–433. DOI: 10.1016/j.physletb.2011.06.012. arXiv: 1104.5613 [hep-ph].

[111] M.V. Garzelli, A. Kardos, C.G. Papadopoulos, and Z. Trocsanyi. "Standard Model Higgs boson production in association with a top anti-top pair at NLO with parton showering." In: *EPL* 96.1 (2011), p. 11001. DOI: 10.1209/0295-5075/96/11001. arXiv: 1108.0387 [hep-ph].

[112] Heribertus B. Hartanto, Barbara Jager, Laura Reina, and Doreen Wackeroth. "Higgs boson production in association with top quarks in the POWHEG BOX." In: *Phys. Rev. D* 91.9 (2015), p. 094003. DOI: 10.1103/PhysRevD.91.094003. arXiv: 1501.04498 [hep-ph].

[113] S. Frixione, V. Hirschi, D. Pagani, H.S. Shao, and M. Zaro. "Weak corrections to Higgs hadroproduction in association with a top-quark pair." In: *JHEP* 09 (2014), p. 065. DOI: 10.1007/JHEP09(2014)065. arXiv: 1407.0823 [hep-ph].

[114] Yu Zhang, Wen-Gan Ma, Ren-You Zhang, Chong Chen, and Lei Guo. "QCD NLO and EW NLO corrections to $t\bar{t}H$ production with top quark decays at hadron collider." In: *Phys. Lett. B* 738 (2014), pp. 1–5. DOI: 10.1016/j.physletb.2014.09.022. arXiv: 1407.1110 [hep-ph].

[115] Anna Kulesza, Leszek Motyka, Tomasz Stebel, and Vincent Theeuwes. "Soft gluon resummation for associated $t\bar{t}H$ production at the LHC." In: *JHEP* 03 (2016), p. 065. DOI: 10.1007/JHEP03(2016)065. arXiv: 1509.02780 [hep-ph].

[116] Alessandro Broggio, Andrea Ferroglia, Ben D. Pecjak, Adrian Signer, and Li Lin Yang. "Associated production of a top pair and a Higgs boson beyond NLO." In: *JHEP* 03 (2016), p. 124. DOI: 10.1007/JHEP03(2016)124. arXiv: 1510.01914 [hep-ph].

[117] Alessandro Broggio, Andrea Ferroglia, Ben D. Pecjak, and Li Lin Yang. "NNLL resummation for the associated production of a top pair and a Higgs boson at the LHC." In: *JHEP* 02 (2017), p. 126. DOI: 10.1007/JHEP02(2017)126. arXiv: 1611.00049 [hep-ph].

[118] Alessandro Broggio, Andrea Ferroglia, Rikkert Frederix, Davide Pagani, Benjamin D. Pecjak, and Ioannis Tsinikos. "Top-quark pair hadroproduction in association with a heavy boson at NLO+NNLL including EW corrections." In: *JHEP* 08 (2019), p. 039. DOI: 10.1007/JHEP08(2019)039. arXiv: 1907.04343 [hep-ph].

[119] Anna Kulesza, Leszek Motyka, Daniel Schwartländer, Tomasz Stebel, and Vincent Theeuwes. "Associated top quark pair production with a heavy boson: differential cross sections at NLO+NNLL accuracy." In: *Eur. Phys. J. C* 80.5 (2020), p. 428. arXiv: 2001.03031 [hep-ph].

[120] David A. Kosower. "Antenna factorization of gauge theory amplitudes." In: *Phys. Rev. D* 57 (1998), pp. 5410–5416. DOI: 10.1103/PhysRevD.57.5410. arXiv: hep-ph/9710213.

[121] David A. Kosower. "Multiple singular emission in gauge theories." In: *Phys. Rev. D* 67 (2003), p. 116003. DOI: 10.1103/PhysRevD.67.116003. arXiv: hep-ph/0212097.

[122] David A. Kosower. "Antenna factorization in strongly ordered limits." In: *Phys. Rev. D* 71 (2005), p. 045016. DOI: 10.1103/PhysRevD.71.045016. arXiv: hep-ph/0311272.

[123] A. Gehrmann-De Ridder, T. Gehrmann, and E.W.Nigel Glover. "Antenna subtraction at NNLO." In: *JHEP* 09 (2005), p. 056. DOI: 10.1088/1126-6708/2005/09/056. arXiv: hep-ph/0505111.

[124] A. Daleo, T. Gehrmann, and D. Maitre. "Antenna subtraction with hadronic initial states." In: *JHEP* 04 (2007), p. 016. DOI: 10.1088/1126-6708/2007/04/016. arXiv: hep-ph/0612257.

[125] James Currie, E.W.N. Glover, and Steven Wells. "Infrared Structure at NNLO Using Antenna Subtraction." In: *JHEP* 04 (2013), p. 066. DOI: 10.1007/JHEP04(2013)066. arXiv: 1301.4693 [hep-ph].

[126] Gabor Somogyi, Zoltan Trocsanyi, and Vittorio Del Duca. "Matching of singly- and doubly-unresolved limits of tree-level QCD squared matrix elements." In: *JHEP* 06 (2005), p. 024. DOI: 10.1088/1126-6708/2005/06/024. arXiv: hep-ph/0502226.

[127] Vittorio Del Duca, Claude Duhr, Gábor Somogyi, Francesco Tramontano, and Zoltán Trócsányi. "Higgs boson decay into b-quarks at NNLO accuracy." In: *JHEP* 04 (2015), p. 036. DOI: 10.1007/JHEP04(2015)036. arXiv: 1501.07226 [hep-ph].

[128] M. Czakon. "A novel subtraction scheme for double-real radiation at NNLO." In: *Phys. Lett. B* 693 (2010), pp. 259–268. DOI: 10.1016/j.physletb.2010.08.036. arXiv: 1005.0274 [hep-ph].

[129] M. Czakon. "Double-real radiation in hadronic top quark pair production as a proof of a certain concept." In: *Nucl. Phys. B* 849 (2011), pp. 250–295. DOI: 10.1016/j.nuclphysb.2011.03.020. arXiv: 1101.0642 [hep-ph].

[130] M. Czakon and D. Heymes. "Four-dimensional formulation of the sector-improved residue subtraction scheme." In: *Nucl. Phys. B* 890 (2014), pp. 152–227. DOI: 10.1016/j.nuclphysb.2014.11.006. arXiv: 1408.2500 [hep-ph].

[131] T. Binoth and G. Heinrich. "An automatized algorithm to compute infrared divergent multiloop integrals." In: *Nucl. Phys. B* 585 (2000), pp. 741–759. DOI: 10.1016/S0550-3213(00)00429-6. arXiv: hep-ph/0004013.

[132] Charalampos Anastasiou, Kirill Melnikov, and Frank Petriello. "A new method for real radiation at NNLO." In: *Phys. Rev. D* 69 (2004), p. 076010. DOI: 10.1103/PhysRevD.69.076010. arXiv: hep-ph/0311311.

[133] Radja Boughezal, Christfried Focke, Xiaohui Liu, and Frank Petriello. "*W*-boson production in association with a jet at next-to-next-to-leading order in perturbative QCD." In: *Phys. Rev. Lett.* 115.6 (2015), p. 062002. DOI: 10.1103/PhysRevLett.115.062002. arXiv: 1504.02131 [hep-ph].

[134] Radja Boughezal, Xiaohui Liu, and Frank Petriello. "*N*-jettiness soft function at next-to-next-to-leading order." In: *Phys. Rev. D* 91.9 (2015), p. 094035. DOI: 10.1103/PhysRevD.91.094035. arXiv: 1504.02540 [hep-ph].

[135] Jonathan Gaunt, Maximilian Stahlhofen, Frank J. Tackmann, and Jonathan R. Walsh. "N-jettiness Subtractions for NNLO QCD Calculations." In: *JHEP* 09 (2015), p. 058. DOI: 10.1007/JHEP09(2015)058. arXiv: 1505.04794 [hep-ph].

[136] Stefano Catani and Massimiliano Grazzini. "An NNLO subtraction formalism in hadron collisions and its application to Higgs boson production at the LHC." In: *Phys. Rev. Lett.* 98 (2007), p. 222002. DOI: 10.1103/PhysRevLett.98.222002. arXiv: hep-ph/0703012.

[137] Stefano Catani, Leandro Cieri, Daniel de Florian, Giancarlo Ferrera, and Massimiliano Grazzini. "Universality of transverse-momentum resummation and hard factors at the NNLO." In: *Nucl. Phys. B* 881 (2014), pp. 414–443. DOI: 10.1016/j.nuclphysb.2014.02.011. arXiv: 1311.1654 [hep-ph].

[138] Stefano Catani and Massimiliano Grazzini. "QCD transverse-momentum resummation in gluon fusion processes." In: *Nucl. Phys. B* 845 (2011), pp. 297–323. DOI: 10.1016/j.nuclphysb.2010.12.007. arXiv: 1011.3918 [hep-ph].

[139] Massimiliano Grazzini. "NNLO predictions for the Higgs boson signal in the H —> WW —> lnu lnu and H —> ZZ —> 4l decay channels." In: *JHEP* 02 (2008), p. 043. DOI: 10.1088/1126-6708/2008/02/043. arXiv: 0801.3232 [hep-ph].

[140] Stefano Catani, Leandro Cieri, Giancarlo Ferrera, Daniel de Florian, and Massimiliano Grazzini. "Vector boson production at hadron colliders: a fully exclusive QCD calculation at NNLO." In: *Phys. Rev. Lett.* 103 (2009), p. 082001. DOI: 10.1103/PhysRevLett.103.082001. arXiv: 0903.2120 [hep-ph].

[141] Giancarlo Ferrera, Massimiliano Grazzini, and Francesco Tramontano. "Associated WH production at hadron colliders: a fully exclusive QCD calculation at NNLO." In: *Phys. Rev. Lett.* 107 (2011), p. 152003. DOI: 10.1103/PhysRevLett.107.152003. arXiv: 1107.1164 [hep-ph].

[142] Giancarlo Ferrera, Massimiliano Grazzini, and Francesco Tramontano. "Associated ZH production at hadron colliders: the fully differential NNLO QCD calculation." In: *Phys. Lett. B* 740 (2015), pp. 51–55. DOI: 10.1016/j.physletb.2014.11.040. arXiv: 1407.4747 [hep-ph].

[143] Stefano Catani, Leandro Cieri, Daniel de Florian, Giancarlo Ferrera, and Massimiliano Grazzini. "Diphoton production at hadron colliders: a fully-differential QCD calculation at NNLO." In: *Phys. Rev. Lett.* 108 (2012). [Erratum: Phys.Rev.Lett. 117, 089901 (2016)], p. 072001. DOI: 10.1103/PhysRevLett.108.072001. arXiv: 1110.2375 [hep-ph].

[144] Massimiliano Grazzini, Stefan Kallweit, Dirk Rathlev, and Alessandro Torre. "$Z\gamma$ production at hadron colliders in NNLO QCD." In: *Phys. Lett. B* 731 (2014), pp. 204–207. DOI: 10.1016/j.physletb.2014.02.037. arXiv: 1309.7000 [hep-ph].

[145] F. Cascioli, T. Gehrmann, M. Grazzini, S. Kallweit, P. Maierhöfer, A. von Manteuffel, S. Pozzorini, D. Rathlev, L. Tancredi, and E. Weihs. "ZZ production at hadron colliders in NNLO QCD." In: *Phys. Lett. B* 735 (2014), pp. 311–313. DOI: 10.1016/j.physletb.2014.06.056. arXiv: 1405.2219 [hep-ph].

[146] T. Gehrmann, M. Grazzini, S. Kallweit, P. Maierhöfer, A. von Manteuffel, S. Pozzorini, D. Rathlev, and L. Tancredi. "W^+W^- Production at Hadron Colliders in Next to Next to Leading Order QCD." In: *Phys. Rev. Lett.* 113.21 (2014), p. 212001. DOI: 10.1103/PhysRevLett.113.212001. arXiv: 1408.5243 [hep-ph].

[147] Massimiliano Grazzini, Stefan Kallweit, and Dirk Rathlev. "$W\gamma$ and $Z\gamma$ production at the LHC in NNLO QCD." In: *JHEP* 07 (2015), p. 085. DOI: 10.1007/JHEP07(2015)085. arXiv: 1504.01330 [hep-ph].

[148] Hua Xing Zhu, Chong Sheng Li, Hai Tao Li, Ding Yu Shao, and Li Lin Yang. "Transverse-momentum resummation for top-quark pairs at hadron colliders." In: *Phys. Rev. Lett.* 110.8 (2013), p. 082001. DOI: 10.1103/PhysRevLett.110.082001. arXiv: 1208.5774 [hep-ph].

[149] Hai Tao Li, Chong Sheng Li, Ding Yu Shao, Li Lin Yang, and Hua Xing Zhu. "Top quark pair production at small transverse momentum in hadronic collisions." In: *Phys. Rev. D* 88 (2013), p. 074004. DOI: 10.1103/PhysRevD.88.074004. arXiv: 1307.2464 [hep-ph].

[150] Stefano Catani, Massimiliano Grazzini, and A. Torre. "Transverse-momentum resummation for heavy-quark hadroproduction." In: *Nucl. Phys. B* 890 (2014), pp. 518–538. DOI: 10.1016/j.nuclphysb.2014.11.019. arXiv: 1408.4564 [hep-ph].

[151] Stefano Catani, Massimiliano Grazzini, and Hayk Sargsyan. "Transverse-momentum resummation for top-quark pair production at the LHC." In: *JHEP* 11 (2018), p. 061. DOI: 10.1007/JHEP11(2018)061. arXiv: 1806.01601 [hep-ph].

[152] Roberto Bonciani, Stefano Catani, Massimiliano Grazzini, Hayk Sargsyan, and Alessandro Torre. "The q_T subtraction method for top quark production at hadron colliders." In: *Eur. Phys. J. C* 75.12 (2015), p. 581. DOI: 10.1140/epjc/s10052-015-3793-y. arXiv: 1508.03585 [hep-ph].

[153] Stefano Catani, Simone Devoto, Massimiliano Grazzini, Stefan Kallweit, Javier Mazzitelli, and Hayk Sargsyan. "Top-quark pair hadroproduction at next-to-next-to-leading order in QCD." In: *Phys. Rev. D* 99.5 (2019), p. 051501. DOI: 10.1103/PhysRevD.99.051501. arXiv: 1901.04005 [hep-ph].

[154] Stefano Catani, Simone Devoto, Massimiliano Grazzini, Stefan Kallweit, and Javier Mazzitelli. "Top-quark pair production at the LHC: Fully differential QCD predictions at NNLO." In: *JHEP* 07 (2019), p. 100. DOI: 10.1007/JHEP07(2019)100. arXiv: 1906.06535 [hep-ph].

[155] Stefano Catani, Simone Devoto, Massimiliano Grazzini, Stefan Kallweit, and Javier Mazzitelli. "Top-quark pair hadroproduction at NNLO: differential predictions with the MSbar mass." In: (May 2020). arXiv: 2005.00557 [hep-ph].

[156] Ignacio Fabre, Massimiliano Grazzini, and Stefan Kallweit. *$t\bar{t}H$ production at NNLO: The off-diagonal channels*. (In preparation).

[157] Massimiliano Grazzini, Stefan Kallweit, and Marius Wiesemann. "Fully differential NNLO computations with MATRIX." In: *Eur. Phys. J. C* 78.7 (2018), p. 537. DOI: 10.1140/epjc/s10052-018-5771-7. arXiv: 1711.06631 [hep-ph].

[158] S. Catani and M.H. Seymour. "The Dipole formalism for the calculation of QCD jet cross-sections at next-to-leading order." In: *Phys. Lett. B* 378 (1996), pp. 287–301. DOI: 10.1016/0370-2693(96)00425-X. arXiv: hep-ph/9602277.

[159] Stefano Catani, Stefan Dittmaier, Michael H. Seymour, and Zoltan Trocsanyi. "The Dipole formalism for next-to-leading order QCD calculations with massive partons." In: *Nucl. Phys. B* 627 (2002), pp. 189–265. DOI: 10.1016/S0550-3213(02)00098-6. arXiv: hep-ph/0201036.

[160] Gabor Somogyi, Zoltan Trocsanyi, and Vittorio Del Duca. "A Subtraction scheme for computing QCD jet cross sections at NNLO: Regularization of doubly-real emissions." In: *JHEP* 01 (2007), p. 070. DOI: 10.1088/1126-6708/2007/01/070. arXiv: hep-ph/0609042.

[161] Vittorio Del Duca, Claude Duhr, Adam Kardos, Gábor Somogyi, and Zoltán Trócsányi. "Three-Jet Production in Electron-Positron Collisions at Next-to-Next-to-Leading Order Accuracy." In: *Phys. Rev. Lett.* 117.15 (2016), p. 152004. DOI: 10.1103/PhysRevLett.117.152004. arXiv: 1603.08927 [hep-ph].

[162] Vittorio Del Duca, Claude Duhr, Adam Kardos, Gábor Somogyi, Zoltán Sz˝ or, Zoltán Trócsányi, and Zoltán Tulipánt. "Jet production in the CoLoRFulNNLO method: event shapes in electron-positron collisions." In: *Phys. Rev. D* 94.7 (2016), p. 074019. DOI: 10.1103/PhysRevD.94.074019. arXiv: 1606.03453 [hep-ph].

[163] Fabrizio Caola, Kirill Melnikov, and Raoul Röntsch. "Nested soft-collinear subtractions in NNLO QCD computations." In: *Eur. Phys. J. C* 77.4 (2017), p. 248. DOI: 10.1140/epjc/s10052-017-4774-0. arXiv: 1702.01352 [hep-ph].

[164] Ming-xing Luo, Tong-Zhi Yang, Hua Xing Zhu, and Yu Jiao Zhu. "Quark Transverse Parton Distribution at the Next-to-Next-to-Next-to-Leading Order." In: *Phys. Rev. Lett.* 124.9 (2020), p. 092001. DOI: 10.1103/PhysRevLett.124.092001. arXiv: 1912.05778 [hep-ph].

[165] Jiro Kodaira and Luca Trentadue. "Single Logarithm Effects in electron-Positron Annihilation." In: *Phys. Lett. B* 123 (1983), pp. 335–338. DOI: 10.1016/0370-2693(83)91213-3.

[166] S. Catani, E. D'Emilio, and L. Trentadue. "The Gluon Form-factor to Higher Orders: Gluon Gluon Annihilation at Small Q^-transverse." In: *Phys. Lett. B* 211 (1988), pp. 335–342. DOI: 10.1016/0370-2693(88)90912-4.

[167] Stefano Catani. "The Singular behavior of QCD amplitudes at two loop order." In: *Phys. Lett. B* 427 (1998), pp. 161–171. DOI: 10.1016/S0370-2693(98)00332-3. arXiv: hep-ph/9802439.

[168] W.T. Giele and E.W.Nigel Glover. "Higher order corrections to jet cross-sections in e+ e- annihilation." In: *Phys. Rev. D* 46 (1992), pp. 1980–2010. DOI: 10.1103/PhysRevD.46.1980.

[169] Zoltan Kunszt, Adrian Signer, and Zoltan Trocsanyi. "Singular terms of helicity amplitudes at one loop in QCD and the soft limit of the cross-sections of multiparton processes." In: *Nucl. Phys. B* 420 (1994), pp. 550–564. DOI: 10.1016/0550-3213(94)90077-9. arXiv: hep-ph/9401294.

[170] Robert V. Harlander. "Virtual corrections to g g —> H to two loops in the heavy top limit." In: *Phys. Lett. B* 492 (2000), pp. 74–80. DOI: 10.1016/S0370-2693(00)01042-X. arXiv: hep-ph/0007289.

[171] V. Ravindran, J. Smith, and W.L. van Neerven. "Two-loop corrections to Higgs boson production." In: *Nucl. Phys. B* 704 (2005), pp. 332–348. DOI: 10.1016/j.nuclphysb.2004.10.039. arXiv: hep-ph/0408315.

[172] Giuseppe Bozzi, Stefano Catani, Daniel de Florian, and Massimiliano Grazzini. "Transverse-momentum resummation and the spectrum of the Higgs boson at the LHC." In: *Nucl. Phys. B* 737 (2006), pp. 73–120. DOI: 10.1016/j.nuclphysb.2005.12.022. arXiv: hep-ph/0508068.

[173] S. Catani, M. Grazzini, and A. Torre. (Unpublished).

[174] Federico Buccioni, Jean-Nicolas Lang, Jonas M. Lindert, Philipp Maierhöfer, Stefano Pozzorini, Hantian Zhang, and Max F. Zoller. "OpenLoops 2." In: *Eur. Phys. J. C* 79.10 (2019), p. 866. DOI: 10.1140/epjc/s10052-019-7306-2. arXiv: 1907.13071 [hep-ph].

[175] John M. Campbell, R. Keith Ellis, and Walter T. Giele. "A Multi-Threaded Version of MCFM." In: *Eur. Phys. J. C* 75.6 (2015), p. 246. DOI: 10.1140/epjc/s10052-015-3461-2. arXiv: 1503.06182 [physics.comp-ph].

[176] J. Alwall, R. Frederix, S. Frixione, V. Hirschi, F. Maltoni, O. Mattelaer, H. S. Shao, T. Stelzer, P. Torrielli, and M. Zaro. "The automated computation of tree-level and next-to-leading order differential cross sections, and their matching to parton shower simulations." In: *JHEP* 07 (2014), p. 079. DOI: 10.1007/JHEP07(2014)079. arXiv: 1405.0301 [hep-ph].

[177] John M. Campbell, R.Keith Ellis, and Ciaran Williams. "Vector boson pair production at the LHC." In: *JHEP* 07 (2011), p. 018. DOI: 10.1007/JHEP07(2011)018. arXiv: 1105.0020 [hep-ph].

[178] Michal Czakon and Alexander Mitov. "Top++: A Program for the Calculation of the Top-Pair Cross-Section at Hadron Colliders." In: *Comput. Phys. Commun.* 185 (2014), p. 2930. DOI: 10.1016/j.cpc.2014.06.021. arXiv: 1112.5675 [hep-ph].

[179] Andrea Ferroglia, Matthias Neubert, Ben D. Pecjak, and Li Lin Yang. "Two-loop divergences of massive scattering amplitudes in non-abelian gauge theories." In: *JHEP* 11 (2009), p. 062. DOI: 10.1088/1126-6708/2009/11/062. arXiv: 0908.3676 [hep-ph].

[180] Jeffrey R. Forshaw, Michael H. Seymour, and Andrzej Siodmok. "On the Breaking of Collinear Factorization in QCD." In: *JHEP* 11 (2012), p. 066. DOI: 10.1007/JHEP11(2012)066. arXiv: 1206.6363 [hep-ph].

[181] M. Czakon and P. Fiedler. "The soft function for color octet production at threshold." In: *Nucl. Phys. B* 879 (2014), pp. 236–255. DOI: 10.1016/j.nuclphysb.2013.12.008. arXiv: 1311.2541 [hep-ph].

[182] Richard D. Ball et al. "Parton distributions from high-precision collider data." In: *Eur. Phys. J. C* 77.10 (2017), p. 663. DOI: 10.1140/epjc/s10052-017-5199-5. arXiv: 1706.00428 [hep-ph].

[183] Stefano Frixione. "A Next-to-leading order calculation of the cross-section for the production of W+ W- pairs in hadronic collisions." In: *Nucl. Phys.* B410 (1993), pp. 280–324. DOI: 10.1016/0550-3213(93)90435-R.

LIST OF PUBLICATIONS AND PRESENTATIONS

During the period of the PhD, the following publications have been produced:

[1] Daniel de Florian, Ignacio Fabre, and Javier Mazzitelli. "Higgs boson pair production at NNLO in QCD including dimension 6 operators." In: *JHEP* 10 (2017), p. 215. DOI: 10.1007/JHEP10(2017)215. arXiv: 1704.05700 [hep-ph].

[2] Daniel de Florian, Manuel Der, and Ignacio Fabre. "QCD⊕QED NNLO corrections to Drell Yan production." In: *Phys. Rev. D* 98.9 (2018), p. 094008. DOI: 10.1103/PhysRevD.98.094008. arXiv: 1805.12214 [hep-ph].

[3] Daniel de Florian, Ignacio Fabre, and Javier Mazzitelli. "Triple Higgs production at hadron colliders at NNLO in QCD." In: *JHEP* 03 (2020), p. 155. DOI: 10.1007/JHEP03(2020)155. arXiv: 1912.02760 [hep-ph].

[4] Daniel de Florian, Ignacio Fabre, Gundrum Heinrich, and Javier Mazzitelli. "Improved NNLO Higgs pair production with EFT effects." In: *11th Les Houches Workshop on Physics at TeV Colliders: PhysTeV Les Houches*. Mar. 2020. arXiv: 2003.01700 [hep-ph].

[5] Ignacio Fabre, Massimiliano Grazzini, and Stefan Kallweit. *$t\bar{t}H$ production at NNLO: The off-diagonal channels*. (In preparation).

and the following oral presentations have been given at international conferences and workshops:

[1] Ignacio Fabre and Daniel de Florian. "Higgs Pair Production." PH-Institute at ICAS (UNSAM), Argentina. 2017. URL: https://indico.cern.ch/event/655608/contributions/2735963/.

[2] Ignacio Fabre. "Multiple Higgs Production at the LHC." Pheno-Exp at ICAS (UNSAM), Argentina. 2018. URL: https://indico.cern.ch/event/703922/contributions/2981588/.

[3] Ignacio Fabre. "Mixed QCDxQED corrections to Drell-Yan Z boson Production." High Precision for Hard Proceses at Freiburg U., Germany. 2018. URL: https://indico.cern.ch/event/694599/contributions/3142649/.

[4] Ignacio Fabre. "Mixed QCDxQED corrections to Drell-Yan Z boson Production." Radcor at Avignon, France. 2019. URL: https://indico.cern.ch/event/783212/contributions/3512601/.